THE UNIVERSITY
of EDINBURGH

The Role of the LINC00961 Locus in Vascular Endothelial Cell Function

Rachel Louise Sanders

Submitted for the degree of Doctor of Philosophy

The University of Edinburgh

2021

Declaration

I declare that the work presented in this thesis is entirely my own work, except where explicitly stated by reference to or acknowledgment of other persons such as my colleagues in the Baker lab who contributed to parts of this work. This work has not been submitted for any other degree.

Rachel Louise Sanders

January 2021

Acknowledgments

First and foremost, I would like to say thanks to my main supervisor Professor Andrew Baker for giving me the amazing opportunity to come to Edinburgh, join his group, and complete my PhD. To my second supervisor Dr Mairi Brittan, who together with Andy helped direct this project and provided support and guidance. To my third supervisor Dr Andrea Caporali, who kindly donated samples and his time when we needed another perspective on the direction of this work.

I would like to acknowledge and thank the British Heart Foundation for awarding me the studentship which funded this research and my time in Edinburgh.

A huge thanks to all the past and present members of the Baker lab who offered their time, support, expertise, and moral support. Thanks to Dr. Helen Spencer, Dr. Mounia Boulberdaa and Dr. Julie Rodor for laying down the foundation for this project, especially Julie for having to put up with my repetitive questions only she and her bioinformatics knowledge could answer. To Dr. Marco Meloni for his expertise in mouse *in vivo* work and surgical skills used through this work.

My gratitude also goes to many of the wonderful people I met during my time in Edinburgh: To Dr. Laura Denby for solid scientific advice whenever needed and top-notch banter particularly around our shared love of Pokémon. To Dr. James O'Sullivan for our much-needed coffee breaks which kept us both sane. To Dr. Amy Cochrane who at times was the only other person alive who understood exactly my frustrations throughout this project, who provided help and support at a moment's notice even after moving into a new lab group, and who helped to cultivate my love of the Netherlands, dank je vel.

To Dr. Ana-Mishel Spiroski, the most amazing post doc and friend who possesses knowledge on almost every subject known to man and who helped further my understanding of and love for rodents.

A huge thank you to all the animal facilities staff whose knowledge and work have made every aspect of the animal work possible. To the LF2 staff, particularly Jon Henderson and Will Mungall who taught me a lot of my rodent handling and dissection skills, and who also helped cultivate my love for rodents and *in vivo* experiments.

To the students in the Baker lab who I shared this journey with, Dr. Francesca Vacante (lab BFF), Dr. Joe Monteiro (Mo-Jo Joe-Joe), John Hung (Dr John), the CVS PhD student cohort and lastly to my office friends, particularly Dr. Andrea Lovdel and Dr. David Mellis for helping to make the hard times bearable, which I will never forget.

To my partner Kevin, who provided me with the much-needed support in the never-ending writing of this thesis, my quest to become a PhD, and who kind of helped to distract the cat (Wilson/Pancake) who always wanted my attention when I sat down to write! Ik hou van jou. Lastly, a thank you to my family who supported the crazy notion that I could become a scientist.

Abstract

Over 17 million yearly deaths are caused by cardiovascular diseases worldwide, and up to 80% are due to heart attacks and strokes caused by atherosclerosis: fatty plaque build-up within artery walls restricting blood flow. Atherosclerotic plaque can also build up in arteries supplying the extremities such as the arms and legs; this is called peripheral arterial disease and is the 3rd most common atherosclerotic disease following that of the coronary arteries and cerebral arteries. With no cure for chronic ischemic diseases, clinical management includes reducing risk factors and utilising drug therapies to help with ailments that exacerbate disease such as diabetes and hypertension. Surgical intervention is a last resort with a high number of peripheral arterial disease patients requiring limb amputation. To avoid this, many clinical trials have attempted to increase patients' blood flow by targeting endothelial cells and stimulating angiogenesis, the development of new blood vessels from pre-existing vessels. However, none of these attempts have led to a curative therapy yet. To prevent ischemic disease from escalating to amputation, heart attacks, or strokes, it is vital we find a way to combat them at early stages. Endothelial dysfunction, the aberrant or extended activation of adaptive endothelial behaviours, is an early event in atherosclerotic development, hence further understanding of endothelial molecular mechanisms is required.

Long non-coding RNAs (lncRNAs) regulate many cell functions but are not well characterised and are poorly understood due to their previous categorisation as 'junk DNA'. Several lncRNAs have been identified in aspects of cardiovascular pathophysiology, however, the human genome is estimated to possess ~ 270,000 lncRNAs, ergo many remain undiscovered. High-throughput RNA-sequencing in a human embryonic stem cell to endothelial cell differentiation protocol identified the lncRNA LINC00961 as endothelial enriched. This locus houses a micropeptide, small peptide of amino acid regulation (SPAAR), and has a mouse homologue; unique factors suggesting an important and evolutionary conserved function. Therefore, this project sought to investigate the role of the LINC00961 locus in the endothelium.

Knock down of LINC00961 expression by ~90% was achieved in human umbilical vein endothelial cells which significantly reduced several endothelial functions; tubule

formation, proliferation, adhesion, migration, and barrier integrity. The LINC00961 locus knock out mouse line showed no lethality; however, a foetal growth restriction like phenotype was identified in male LINC00961$^{-/-}$ animals; these offspring were significantly smaller and lighter with an increased brain weight to body ratio at 9 weeks of age. Cardiac ultrasound at 8 weeks of age found no differences in cardiac output between female LINC00961$^{-/-}$ and wildtype controls. However, reduced left ventricular wall diameter, slower mitral valve deceleration, and isovolumetric contraction time were observed in these mice. This restricted heart filling and compromised myocardial relaxation indicates the early stages of diastolic dysfunction.

Adult male LINC00961$^{-/-}$ and wild type control mice underwent surgically induced hind limb ischemia. Comparable to *in vitro* data, LINC00961 deletion caused transient changes to capillary number during early hypoxic injury, and a lack of mature α-smooth muscle actin vessels at baseline, indicating underlying issues with vessel physiology. Crucially, lentiviral overexpression cassettes showed LINC00961 acted independently of SPAAR in human umbilical vein endothelial cells, and LINC00961 and SPAAR were linked to the actin binding proteins thymosin β-4 and SYNE1, respectively.

LINC00961 and SPAAR are encoded by the same locus but have opposing effects on angiogenesis. Reduction of locus expression also affected other endothelial behaviours; thus, this locus contributes to maintaining proper endothelial function. This refinement of angiogenic control may be in part due to actin cytoskeletal regulation via thymosin β-4 and SYNE1 interactions. Murine LINC00961 contributes to blood vessel physiology and may also have a role in heart physiology given the altered parameters in LINC00961$^{-/-}$ hearts. Therefore, this locus has important roles in several aspects of cardiovascular biology and is a potential novel target for therapeutic regulation of angiogenesis in patients with compromised blood flow.

Lay summary

The human cardiovascular system comprises the heart and blood vessels and is a vast complex system whose main function is to pump blood from the heart to the rest of the body delivering the vital oxygen and nutrients our tissues require. Over 17 million yearly deaths are caused by cardiovascular diseases worldwide, particularly from atherosclerotic disease, which is the build-up of fatty plaques within artery walls that can calcify and stiffen causing restricted blood flow. When atherosclerotic plaques occur in the coronary and cerebral arteries, they can lead to heart attacks and strokes respectively, collectively accounting for up to 80% of yearly worldwide deaths caused by cardiovascular disease. Peripheral arterial disease is the third most common atherosclerotic disease and is the formation of plaques in arteries supplying the arms and legs, subsequently causing restricted blood flow in the extremities, which can lead to limb amputation, especially in patients with further compromised vessels such as diabetic and hypertensive patients. With no cure for these chronic ischemic diseases, clinical management includes reducing risk factors, utilising drug therapies, and as a last resort, surgical intervention to attempt to either bypass a blocked artery (e.g., coronary artery by-pass graph), or potentially amputate limbs if peripheral arterial disease has progressed to end stage disease. To avoid these measures, many clinical trials have attempted to revascularize tissue and increase patients' blood flow by targeting endothelial cells which line the luminal side of blood vessels, to stimulate angiogenesis, the development of new blood vessels from pre-existing vessels. However, none of these attempts have led to a curative therapy yet.

The endothelium has many important functions besides angiogenesis, such as forming a barrier for larger molecules, interactions with the immune system, and communication with the surrounding smooth muscle in larger vessels to modulate contraction and relaxation. Under normal physiological conditions, endothelial cells are quiescent (non- proliferative), and adhere tightly to each other. However, when stimulated, they become activated and adapt their behaviour according to the stimulus. When endothelial cells become aberrantly activated or activation is prolonged beyond what is needed, their function is referred to as dysfunctional. This dysfunction is an initial step in the development of systemic vascular diseases such as atherosclerosis and therefore better understanding of endothelial biology can aid in the discovery of therapeutic agents to combat ischemic disease.

Ribonucleic acid (RNA) is an intermediate molecule involved in turning information in the DNA of genes into functional proteins. Long non-coding RNAs (lncRNAs) are RNA molecules that lack this protein coding potential of genes and are poorly understood. LncRNAs have previously been discarded as unimportant and arising from 'junk DNA', however, in recent years their importance in biological functions has come to light and they offer novel mechanisms of cellular functions, and therefore the potential to develop new therapeutics for disease treatment, especially considering there is estimated to be up to 270,000 lncRNAs in the human genome.

This project investigated the function of an endothelial enriched lncRNA, LINC00961, which also encodes a small protein termed SPAAR. Depletion of this transcript in human primary endothelial cells resulted in a myriad of defects including failure of the endothelium to form capillary vessel like networks, reduced cell-cell adherence, reduced cell proliferation, and disruption of the endothelial barrier. LINC00961 has a mouse homologue, a rare feature of lncRNAs suggesting a conserved evolutionary function: We therefore generated a LINC00961 locus knock out (KO) mouse and utilised the murine hind limb ischaemia model, to mimic human peripheral arterial disease, and investigated the effects of this deletion on angiogenesis, which is a vital process in response to ischaemia and regeneration after injury. The KO offspring were viable; however, male LINC00961 KO animals were significantly smaller and lighter with an increased brain weight to body ratio at 9 weeks of age. This indicates they have a foetal growth restriction like phenotype affecting their development in utero which could affect their risk of cardiovascular diseases such as a heart attack or stroke, later in life. Cardiac ultrasound at 8 weeks of age found no differences in cardiac output between female LINC00961 KO and wildtype controls. However, reduced left ventricular wall diameter, slower mitral valve deceleration and isovolumetric contraction time were observed in these KO mice. These data show that they have restricted heart filling and compromised heart muscle relaxation indicating the early stages of diastolic dysfunction and suggesting they may have an increased risk for heart problems later in life.

Adult male LINC00961 KO and wildtype mice underwent surgery to induced hind limb ischemia, which is lack of blood flow to the back leg. This was achieved by blocking one of the femoral arteries, which are the largest arteries supplying blood to the legs.

LINC00961 deletion caused a lack of mature larger vessels at baseline and transient changes to capillary number during hypoxic injury, indicating underlying issues with vessels in the muscle of the mouse leg. Crucially, separate overexpression experiments showed LINC00961 acted independently of its micropeptide SPAAR; LINC00961 was shown to be anti-angiogenic, and SPAAR pro-angiogenic, although their precise regulation requires further investigation. The actin cytoskeleton provides important cellular structure allowing cells to dynamically change shape (required in angiogenesis) among having many other functions. Interestingly, both LINC00961 and SPAAR likely exert their effects through pathways that involve interactions with actin-binding proteins as LINC00961 and SPAAR were found to bind to thymosin β-4 and SYNE1 respectively, although further investigation into these specific pathways is required.

In conclusion, this project identified a functional role for the LINC00961 locus in human and mouse. LINC00961 and SPAAR are encoded by the same locus but have opposing effects on blood vessel growth and function on angiogenesis. Reduction of locus expression also affected other endothelial behaviours; thus, this locus is important in maintaining proper endothelial function. This refinement of angiogenic control may be in part due to actin cytoskeletal regulation via thymosin β-4 and SYNE1 interactions. Mouse LINC00961 contributes to blood vessel physiology, and may also have a role in heart physiology, given the altered parameters in young LINC00961 KO hearts. Therefore, this locus has important roles in several aspects of cardiovascular biology and is a potential novel target for therapeutic regulation of angiogenesis in patients with compromised blood flow.

Abbreviations

ACE	Angiotensin-converting-enzyme
ANOVA	Analysis of variance
ANG-1	Angiopoietin 1
BAT	Brown adipose tissue
bEND3	Immortalised mouse brain microvascular endothelial cell line
BMEC	Brain microvascular endothelial cells
BMP	Bone morphogenic protein
bp	Base pairs
BPD	Biparietal diameter
BrPM	Beat rhythm per minute
CAD	Coronary artery disease
cDNA	Complementary DNA
chr	Chromosome
CLI	Critical limb ischemia
CO_2	Carbon dioxide
COSHH	Control of substances hazardous to health
CRLS1	Cardiolipin synthase 1
CTX	Cardiotoxin
DCM	Dilated cardiomyopathy
DMEM	Dulbecco’s modified eagle medium
DNA	Deoxyribonucleic acid
EB	Embryoid bodies
EC	Endothelial cell
ECM	Extracellular matrix
EDRF	Endothelial-derived relaxing factors
EdU	5-ethynyl-2'-deoxyuridine
EGFL7	EGF like domain multiple 7
EGM-2	Endothelial cell basal media plus supplements
EHT	Endothelial to haematopoietic transition
EMT	Epithelial to mesenchymal transition
ENCODE	The encyclopaedia of DNA elements
EndoMT	Endothelial to mesenchymal transition
eNOS	Endothelial nitric oxide synthase
ERG	ETS Transcription Factor ERG

ESC	Embryonic stem cell
FACS	Fluorescence- activated cell sorting
FBS	Foetal bovine serum
FGF	Fibroblast growth factor
FGR	Foetal growth restriction
FISH	Fluorescent *in situ* hybridisation
FLI1	Friend leukaemia integration 1
FPKM	Fragments per kilobase of transcript per million mapped reads
GAPDH	Gylceraldehdye-3 dehydrogenase
GFP	Green fluorescent protein
gRNA	Guide RNA
gWAT	Gonadal white adipose tissue
HA	Hemagglutinin
HCC	Hepatocellular carcinoma
hEGF	Human erythroid growth factor
hES	Human embryonic stem cells
HLD	High density lipoprotein
HF	Heart failure
hFGF-B2	Human recombinant fibroblast growth factor
HIF1-α	Hypoxia inducible factor 1α
HLI	Hind limb ischaemia
HOTAIR	Hox antisense intergenic RNA
HOTTIP	HOXA transcript at the distal tip
HRE	Hypoxia response element
HRG	Hypoxia responsive gene
HSVEC	Human saphenous vein endothelial cells
HUVEC	Human umbilical vein endothelial cells
ICAM1	Intercellular adhesion molecule 1
IFN	Interferon
IP1B	Immortalised endothelial mouse cell line
iWAT	Inguinal white adipose tissue
Kb	Kilobase
KD	Knock down
KLF2	Krüppel-like factor 4
KO	Knock out

LDL	Low density lipoprotein
LDPI	Laser Doppler perfusion imaging
lincRNA	Long intergenic non-coding RNA
lncRNA	Long non-coding RNA
MCEC	Immortalised mouse cardiovascular endothelial cell line
MDRL	Mitochondrial dynamic related lncRNA
MEG3	Maternally expressed gene 3
MI	Myocardial infarction
miRNA	MicroRNA
mM	Millimolar
modRNA	Modified RNA (synthetic)
MOI	Multiplicity of infection
MP	Micropeptide
MRI	Magnetic resonance imaging
mRNA	Messenger RNA
mTOR	Mammalian target of rapamycin
ncRNA	Non-coding RNA
NF-κB	Nuclear factor Kappa β
nM	Nanomolar
NO	Nitric oxide
NORAD	Non-coding RNA activated by DNA damage
NPDC1	Neural proliferation, differentiation and control 1
NS	Not significant
ORF	Open reading frame
OxLDL	Oxidated low density lipoprotein
PAD	Peripheral arterial disease
PAF	Platelet activating factor
PBS	Phosphate buffered saline
PCA	Principal Component analysis
PCR	Polymerase chain reaction
PDGF	Platelet derived growth factor
PDGFR	Platelet derived growth factor receptor
pen/strep	Penicillin/streptomycin
PFA	Paraformaldehyde
PI3K	Phosphatidylinositol-4,5-biphosphate 3-kinase
PLAR	Pipeline for lncRNA annotation from RNA-seq data

PLX-PAD	Placental-derived adherent stromal cells
POLII	RNA polymerase II
PRC2	Polycomb repressive complex 2
pre-miRNA	Premature miRNA
pri- miRNA	Primary miRNA
pWAT	Peri-renal white adipose tissue
qRT-PCT	Quantitative real-time PCR
RACE	Rapid amplification of cDNA ends
RCC	Renal cell carcinoma
RISC	RNA induced silencing complex
RNA	Ribonucleic acid
RNAi	RNA silencing
RNA-seq	RNA sequencing
ROS	Reactive oxygen species
SEM	Standard error of the mean
SENCR	Smooth muscle and endothelial cell enriched migration/differentiation associated LncRNA
siRNA	Short interfering RNA/ silencing RNA
SHEP1	SH2 Domain-Containing Eph Receptor-Binding
SMC	Smooth muscle cell
SMILR	Smooth muscle induced LncRNA enhances replication
SPAAR	Small regulatory polypeptide of amino acid regulation
STAT1	Signal transducer and activator of transcription 1
SVEC4-10	Immortalised mouse lymphatic endothelial cell line
TERRA	Long noncoding telomeric repeat-containing RNAs
TMSB4X	Thymosin beta-4X
UBC	Ubiquitin C
UTR	Untranslated region
VECAM-1	Vascular cell adhesion protein 1
VE Cadherin	Vascular endothelial cadherin (CD144, Cadherin 5)
VEGF	Vascular endothelial growth factor
VEGFA	Vascular endothelial growth factor A
VEGFC	Vascular endothelial growth factor C
VSMC	Vascular smooth muscle cell
WHO	World Health Organisation
WT	Wild type

Xist	X- inactive specific transcript
α-SMA	Alpha smooth muscle actin
µg	Microgram
µl	Microliter

Table of Contents

List of Figures

List of Tables

Chapter 1 Introduction

1.1 Cardiovascular disease

1.1.1 Atherosclerosis

Over 17 million yearly deaths are caused by cardiovascular diseases worldwide, and up to 80% are due to heart attacks and strokes caused by atherosclerosis; fatty plaque build-up within artery walls which narrows the lumen and restricts blood flow (http://www.who.int/cardiovascular_diseases/en/). At the molecular and cellular levels atherosclerosis is a complex disease involving endothelial cells (ECs), leukocytes, and smooth muscle cells (SMCs) in the artery wall [1]. In atherosclerosis, an artery wall develops a lipid rich plaque containing leukocytes and high amounts of low-density lipoproteins (LDL) and pathological oxidised-LDL [2]. As a plaque develops and increases in size, it narrows the lumen which restricts blood flow and causes vessel remodelling; SMCs in the artery wall proliferate, and chronic inflammation in the vessel wall develops [1, 3, 4]. Ultimately the plaque can develop a thin fibrous cap on the luminal side which can be prone to rupture causing thrombi to form, completely blocking blood flow [5]. Alternatively, an unruptured or stable plaque can become so large that it completely blocks the lumen, preventing blood flow.

Due to anatomical location, disrupted shear stress (blood flow), such as that found in a branched or curved vessel, and cell lineage, atherosclerotic plaques notoriously develop in known lesion prone areas and consequently cause disease [6]. Notably, the inner arch of the ascending aorta is lesion prone [7] as well as atherosclerotic plaque development in the Circle of Willis in the brain which has been linked to the development of Alzheimer's disease (Beach 2007); plaques in the coronary arteries which can lead to myocardial infarction (MI); plaques in the carotid or cerebral arteries which can lead to ischaemic strokes; and plaques in the arteries of the limbs which can cause peripheral arterial disease (PAD), as shown in Figure 1.1. With no cure for chronic ischaemic diseases, clinical management includes reducing risk factors and utilising drug therapies to help with ailments that exacerbate disease such as diabetes and hypertension. Therefore, arterial development, anatomy, and growth and repair after injury have been intensely studied to understand the biology of healthy and diseased vessels [8]. It is vital we find a way to combat plaque and disease development at early stages to prevent ischaemic disease from escalating to heart

attacks, strokes or amputations, therefore, we need to understand the molecular underpinnings of disease initiation and development.

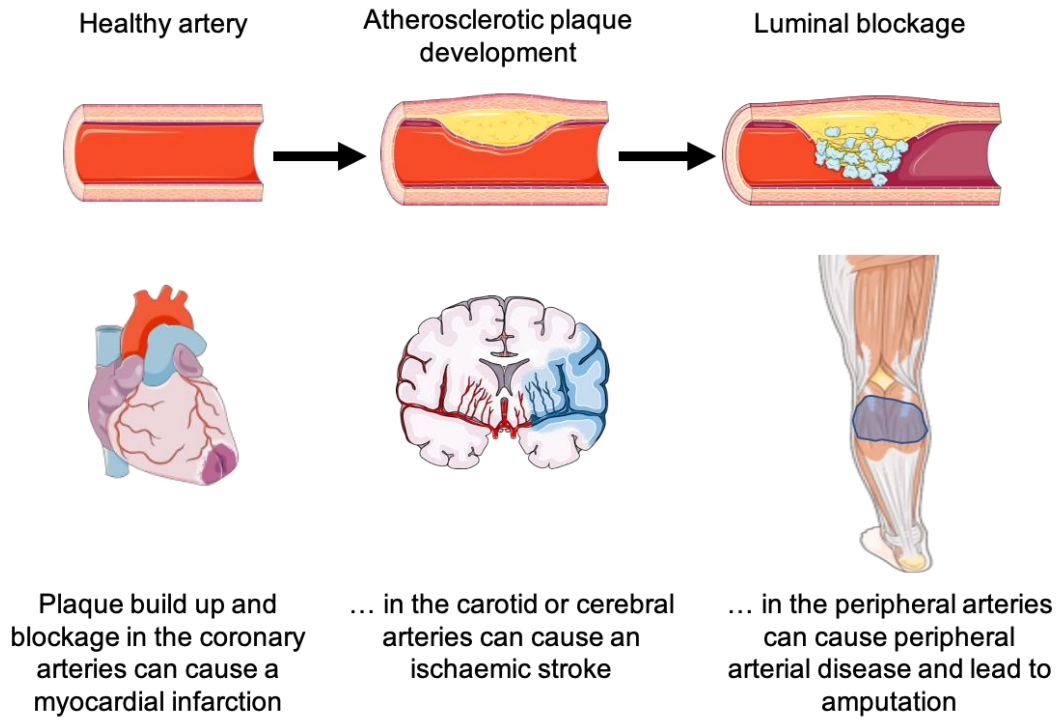

Figure 1.1 Atherosclerotic plaque progression and disease outcomes.

Schematic showing a healthy artery developing an atherosclerotic plaque over time, eventually leading to blood flow blockage and fibrous cap development, causing a pro-thrombotic environment, and the main ischaemic events that can occur due to atherosclerotic disease, myocardial infarction, stroke, and peripheral arterial disease.

1.1.2 Peripheral Arterial Disease

Atherosclerosis in the systemic circulation can cause peripheral arterial disease (PAD) (Refer to Figure 1.1), the 3rd most common atherosclerotic disease following that of the coronary and cerebral arteries [9]. It was estimated in 2010 that PAD affects 202 million people worldwide [10]. Ultimately, prolonged arterial occlusion leads to hypoxia and tissue necrosis termed critical limb ischaemia (CLI) which can result in amputation [10]. Currently, around a quarter of CLI patients require amputation every year [11]. A recent study showed that although the prevalence of PAD has decreased in Europe and the USA since 1990, concerningly, mortality rates related to PAD have actually increased [12] despite the advancement in surgical procedures. Therefore, there is a need to develop therapeutics for disease intervention [13]. Occlusion in the abdominal aorta can cause claudication in the buttocks, thighs, and calf muscles, causing bilateral PAD, whereas occlusion in the popliteal, common iliac, common femoral, and superficial femoral arteries can cause unilateral PAD [14]. Symptoms of PAD can vary depending on the severity of disease at presentation, for example intermittent claudication (aching muscle) can occur in the above muscles and disappear with rest. Other symptoms can include pain during exercise or rest, ulceration, paralysis, a cold foot/limb, and gangrene. However, patients can be asymptomatic in later stages of the disease [14]; this is especially of concern for diabetic PAD patients as nerve damage caused by diabetic neuropathy contributes to the number of asymptomatic patients who presents at a later stage of disease [15]. As such diagnosis relies on clinical guidelines which include an ankle-brachial index (ABI) ≤ 0.9; this refers to the ratio of blood pressure in the ankle compared to blood pressure in the arm. An ABI < 0.9 is also an indicator of systemic atherosclerosis [14]. This is important as PAD is already recognised as a disease reflecting generalised atherosclerosis within the vascular system and therefore its presence/diagnosis increases the risk of other cardiovascular events and complications [15, 16]. However, a recent study revealed that measuring atherosclerotic plaque deposition in a patient's arteries does not help predict PAD patient mortality rates. Interestingly, this study did show that cardiac troponin T levels negatively correlated with PAD patient survival [17]. Recently, Chevalier & colleagues (2020) uncovered a role for endothelial-to-mesenchymal transition (EndoMT) in the microvasculature of patients with CLI which is a further pathophysiology contributing to luminal blockage and ischaemia, besides the initial development of atherosclerotic plaques [18], further indicating the complexities of this disease.

1.1.3 Myocardial infarction

Atherosclerotic plaque build-up in the coronary arteries is the main cause of an MI (Figure 1.1). Severe luminal narrowing or rupture of an unstable plaque can lead to blood clots and vessel blockage resulting in ischaemic heart tissues [19]. Prolonged lack of blood flow, and therefore oxygen, to a portion of heart muscle ultimately results in necrosis of ischaemic muscle and formation of a fibrotic scar. Clinicians differentiate MI patients into ST elevation MI (STEMI), based on alterations to the ST wave on a patients' electrocardiogram (ECG), or non-STEMI patients, the latter of which is considered less severe [20]. STEMI patients present with one of their coronary arteries completely blocked, develop larger infarcts with a larger portion of the heart muscle at risk from becoming infarcted, and have less collateral blood supply [20]. Although MI survival rates are at their highest, factors such as an increasing population and life expectancy increases ultimately increase the disease burden of MI, especially when we consider the increasing survival rates of MI patients and their increased risk for future cardiovascular events such as another MI or other complications from atherosclerotic disease such as stroke; these patients are also at an increased risk for all-cause mortality (death by any cause) [21] [22] and ultimately having an MI shortens a patient's life expectancy by >16 years [23] [24]. It is therefore important that we increase our knowledge of the underlying mechanisms contributing to the development of MI in order to guide both preventative measures and treatment post MI to further improve morbidity and mortality rates and patient quality of life post MI.

Clinically, in-stent restenosis (development of a second blockage in an artery having previously undergone angioplasty to remove a blockage) is estimated to occur in up to 10% of patients having undergone coronary angioplasties despite the advances in surgical interventions such as drug coated stents to try to avoid this [25]. Half of all saphenous vein bypass grafts also fail within 10 years due to neointimal formation (blockage of the lumen caused by SMC hyperplasia); the pathophysiology of which also includes prolonged EC activation and dysfunction [26]. EC dysfunction has also been reported in coronary artery disease (CAD), diabetes, hypertensive patients, hypercholesterolemia, pulmonary arterial hypertension, lupus, and in smokers [27, 28], further validating the need to understand and find ways to modulate EC dysfunction.

1.2 Endothelial Cells

The endothelium regulates homeostasis of the vasculature and represents a monolayer barrier between the vessel wall and blood. ECs play important roles in regulating shear stress, permeable barrier maintenance, leukocyte extravasation, blood clotting, inflammation, vascular tone, extracellular matrix (ECM) deposition, and vasoconstriction and vasodilation [7, 29] [27] [30]. They respond and adapt to changes in blood flow and blood components, and although usually maintaining a physiological state of anti-inflammation, anti-thrombosis, vessel dilation, and maintenance of tight junctions, activation of these cells produces an environment adapted for blood coagulation, inflammation, and vasoconstriction which are necessary for wound healing and repair of vessel wall injury [29]. Mature blood vessel ECs are in a quiescent state with a low baseline turnover rate [31] and upon activation such as responding to damage or stimuli to undergo angiogenesis, adapt their behaviour accordingly. However, aberrant or uncontrolled activation leads to EC dysfunction which is an early event in atherosclerotic development [29]. Upon activation, ECs produce platelet activating factor (PAF) causing platelets and neutrophils to adhere to the endothelium. This, alongside the release of von Willebrand factor (vWF) from the endothelium, creates a pro-coagulation environment and potentiates leukocyte adherence. Vessel permeabilization is increased with endothelial activation and leads to leaky blood vessels and a proinflammatory environment [30].

Despite creating a continuous layer throughout the vascular system, ECs are heterogeneous in nature and different vascular beds such as arterial and venous ECs and have differing spatiotemporal gene expression profiles [30] [32]. Maladaptive EC behaviour differs across vascular beds which parallels the development of atherosclerosis in plaque prone regions. Factors such as local hemodynamics/blood pressure, shear stress, genetics, and local immunological reactions affect ECs and vascular beds can respond differently to insults such as hypercholesterolaemia, injury, and oxidative stress [6, 32]. Ultimately, endothelial dysfunction can lead to de-deendothelialised areas of arterial wall plaques exposing sub-endothelial components and facilitating platelet attachment to the plaque [33].

1.2.1 Angiogenesis

Angiogenesis is the process by which new blood vessels (capillaries) arise from pre-existing capillaries, for example, in the adult during wound healing and in female reproductive health [34]. This contrasts with vasculogenesis, the process whereby blood vessels first develop during embryogenesis. Once this primary network is established, angiogenesis expands and remodels the circulation, and continues to repair vessels upon damage [35]. During angiogenesis ECs undergo sprouting, proliferation, migration, and anastomose to form new capillaries in the microvasculature [36]. Sprouting angiogenesis includes quiescent EC activation, proliferation, migration, and tubule formation. Here, ECs can return to quiescence [37]. For ECs to migrate, partial degradation of the ECM is required to allow movement of the cells along a gradient of proangiogenic factors such as vascular endothelial cell growth factor (VEGF) [38] demonstrated in Figure 1.2 with VEGF as a stimulant binding to VEGF receptors (VEGFR) on ECs and endothelial release of platelet derived growth factor (PDGF) signalling to the supporting cells in the stroma [39]. Capillaries are also supported by the presence of contractile, mesenchymal plastic mural cells called pericytes which extend projections into the basement membrane to interact with ECs [40] [41]. Pericytes are classed as EC regulators; they detach from capillaries during angiogenic sprouting and interact with ECs to stabilise maturing vessels in later stages of angiogenesis, however, their other functions remain poorly understood [41, 42].

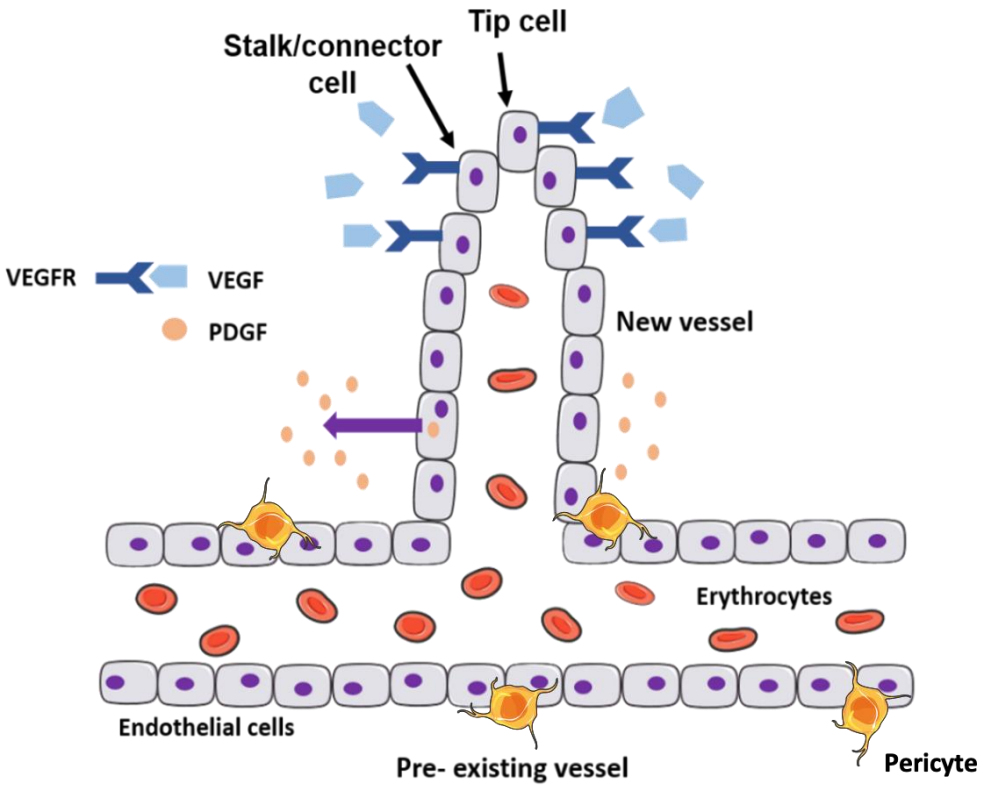

Figure 1.2 Angiogenesis.

New blood vessels sprout from pre-existing vessels and elongate in the direction from which they receive an angiogenic stimuli e.g., Vascular endothelial growth factor (VEGF). Endothelial cells secrete platelet derived growth factor (PDGF) which acts in an autocrine manner on the endothelium promoting angiogenesis. Pericytes are recruited to support mature capillaries.

The most investigated and characterised of the pro-angiogenic molecules is VEGF-A (referred to here as VEGF), although the collective VEGF family also includes VEGF-B, -C -D, and placental growth factor [43]. Additionally, many other pro-angiogenic molecules have been identified such as PDGF, fibroblast growth factor (FGF), and angiopoietin 1 (ANG-1). In contrast, anti-angiogenic molecules include ANG-2, endostatin, interferon (IFN) α and β, and monocyte chemoattractant protein (MCP-1) [44] [45].

Endogenously, upregulation of VEGF and thereby angiogenesis is regulated by hypoxia, a lack of oxygen in body tissues, which stimulates VEGF tissue upregulation signalling via its receptors on the endothelium to initiate angiogenesis [45]. The transcription of VEGF and other hypoxia responsive genes (HRGs) (such as VEGFR1 and 2, endoglin, endothelin-1, endothelial nitric oxide synthase (eNOS), and erythropoietin) [45] is controlled by the hypoxia inducible factor (HIF) regulatory pathway, orchestrated by the transcription factors HIF1-α, responsible for EC hypoxic gene regulation in acute hypoxia, and HIF2-α, responsible for hypoxic gene regulation in prolonged hypoxia in ECs [46]. Currently, over 100 genes have been reported to be regulated by hypoxia [47, 48], the molecular mechanism of which is HIF stabilisation. Under normoxic conditions HIFs are degraded in an oxygen dependent pathway [49], however, when oxygen levels are low HIFs are not degraded and instead translocate to the nucleus where they control gene expression by binding to DNA elements called HIF responsive elements (HRE), consequently inducing hypoxic gene profiles [46].

Endothelial progenitor cells (EPCs) have been defined as cells similar to ECs which circulate in the blood, are capable of adhering to the endothelium, can contribute to new vessel growth and restore EC coverage [50].There have been several hypotheses as to the origins of EPCs such as suggestions that they originate from the bone marrow [51]. Although a large number of circulating ECs have been shown to be apoptotic [52] a portion may be terminally differentiated ECs which have become detached from the endothelium and retain the ability to form colonies by clonal expansion [53, 54] and protocols have been designed to isolate EPCs from patient peripheral blood and culture the ones which form colonies for research purposes [52, 55]. The presence of vascular injury and vascular regeneration has been correlated to an increase in the number of EPCs in the circulation [31]. EPCs have been reported to express a variety of different markers and characteristics, and as such no definitive

panel of cell surface markers has been agreed upon which identifies these cells [50], never-the-less, these cells have been proven to be important to endothelial homeostasis and vessel repair. Interestingly, they have been shown to decline in number with age and a lower number of circulating EPCs has been identified as a predictor of atherosclerosis progression [56], likely reflecting a decreased ability for angiogenesis and increased endothelial dysfunction.

1.2.2 Arteriogenesis

In contrast to expansion of capillary networks, arteriogenesis is the expansion and remodelling of larger vessels such as arterioles, and it is the combination of angiogenesis and arteriogenesis which successfully enhances perfusion [57]. Arteriogenesis generates new collateral vessels 20-100 μm in diameter in humans that are surrounded by a layer of SMCs and whose functions include vasodilation and vasoconstriction to regulate blood flow [58] [59, 60]. The formation of these collateral vessels is necessary to potentiate blood flow to downstream newly formed microvasculature (capillaries formed through angiogenesis) [57]. Increased shear stress in the pre-existing collateral vessels is the stimulus which triggers arteriogenesis; this can be caused by increased blood flow which has been diverted from a blocked vessel from an acute blockage, or from a slow increase in diverted flow over time as blood flow will naturally take the path of least resistance [61]. Increased fluid shear stress against the vessel wall stimulates the mechanisms required to increase luminal diameter [62]. These remodelled collaterals are usually located distally from the ischaemic tissue in instances of PAD [63] [61].

ECs typically align themselves with the axis of laminar flow of blood; this high shear stress on the endothelial wall is promotive of EC survival and quiescence [64]. Disrupted flow can cause EC disorganisation [6] and ECs are equipped to sense mechanical strain on the vessel wall and respond to increased shear stress via biochemical signalling [65]. Shear-stress responsive elements (SSRE) similar to HREs, are present in arteriogenesis associated gene promoter regions and regulate their transcription in the now activated endothelium [61]. They increase their adhesion molecules and secrete chemokines and growth factors. The chemokine CCL2 attracts monocytes and macrophages that further support arteriogenesis by secreting growth factors such as the mitogenic FGF to stimulate EC and SMC proliferation and contribute to ECM remodelling by the secretion of matrix metalloproteinases as well

as fibronectin and proteoglycans [61, 65-68]. MCP1 secreted by ECs also contributes to attracting lymphocytes and local inflammation [63] [67]. Diabetic patients represent a high percentage of CLI, and MI patients and the endothelial dysfunction associated with diabetes negatively affects the endothelium's ability to orchestrate arteriogenesis giving rise to poor collateral vessel development systemically [69]. Individuals vary in the degree of collateralisation they can achieve, and Seiler & colleagues (2013) found that up to a third of CAD patients have adequate endogenous collaterals to partly conserve flow to the heart which can even prevent an MI from occurring [70] [71], thus leaving 2 thirds of those patients at a higher risk for progressing towards an MI.

The behaviour of SMCs in collateral vessels is important as SMCs normally possess a contractile phenotype allowing them to function in vessel dilation and contraction. For example, SMC relaxation causes vessel dilation in response to endothelial released nitric oxide (eNO) which diffuses to the SMCs. SMCs can also dilate in an endothelial independent manner, for example, sodium nitroprusside is a NO donor; it can provide NO to the SMCs directly, by-passing the need for eNO release [72]. A limitation of remodelled collateral arteries is that they cannot withstand quite the same high pressure as the original blocked main arteries [61]. The number of and diameter of collateral vessels in the heart, brain and peripheral vascular has been reported to vary widely amongst healthy individuals which is attributed to natural polymorphisms within populations that contribute to differences in cellular properties [73, 74]. For example, the glutamate to aspartate (Glu298Asp) polymorphism present in the endothelial nitric oxide synthase gene has been associated with diminished collaterals in the hearts of CAD patients, especially those with diabetes [75, 76]. Similarly, a proline to serine (Pro582Ser) polymorphism in the HIF-1α gene has been found to be more prevalent in CAD patients who lack collaterals [77]. Other polymorphisms such as cysteine to threonine (Cys1772Thr) in HIF-1α has also been associated with fewer coronary collaterals [78].

1.3 Human embryonic stem cell differentiation into endothelial cells

Human embryonic stem cells (hESCs) were first isolated from human blastocysts in 1998 [79] and since then protocols have even been established to create induced pluripotent stem cells (iPSCs) from terminally differentiated adult cells [80]. These cells are pluripotent and continue to grow and replicate in culture indefinitely unlike primary donor cells which are terminally differentiated and become exhausted after

several passages in culture with the inability to continue replicating, termed replicative senescence [79]. These hESC lines have been used to produce desired cell types by manipulating their differentiation; this technique has become a vital tool in the identification of novel transcript profiles, understanding the mechanisms of cellular differentiation, generating *in vitro* models of disease with patient specific mutations, developing and testing new drugs, and has the potential to generate cells for therapeutic application [81]. Levenberg & colleagues (2002) were the first to report of their success in deriving ECs from hESCs, they did this by isolating the ECs from embryoid bodies which are groups of cells spontaneously differentiated from hESCs which typically include cells of different types [82]. Recently, the Baker lab used single cell RNA-seq on hESC derived ECs to identify novel transcripts involved in the commitment and maturation of ECs, where the study concluded that transcriptional architecture of these hESCs derived ECs differed to that of freshly isolated mature and foetal ECs [83]. The GMP compliant method used here also resulted in a high yield of 60% ECs [83, 84]. ECs derived from this protocol have also been shown by MacAskill & colleagues (2018) to improve perfusion following murine HLI when injected at the time of surgery [85], indicating their potential to promote therapeutic angiogenesis in PAD and MI patients by injection of these cells to the injury site, though these are not yet ready for human clinical trials.

1.4 Therapeutic treatments for peripheral arterial disease

Treatment of PAD focuses on prevention via lowering risk factors, management of symptoms, and surgical intervention, but at present there is no cure. Pharmacological agents are prescribed to reduce deformities in red blood cells, decrease platelet aggregation, decrease inflammation, and induce vasodilation, to prevent blockages and improve blood flow [86]. Administration of pain relief and implementing lifestyle changes such as diet improvement, weight loss, exercise, and quitting smoking are typically recommended. Surgical options include angioplasty, stenting, and bypass grafts that attempt to re-vascularise the limb [87]. Complications in finding treatments lie in the fact that PAD and atherosclerosis are complex diseases which encompass many abnormalities such as EC dysfunction, vessel damage and impaired angiogenesis, vessel remodelling, changes in lipid profile, activation of platelets, SMC activation and phenotype switching, disturbances in the ECM, inflammation, and

systemic risk factors such as diabetes [13, 88, 89]. For example, diabetic patients are at a 4- fold increased risk of developing CLI [11]. Surgical intervention in CLI is a last resort, to avoid this, many clinical trials have attempted to increase patients' blood flow by targeting ECs and stimulating angiogenesis. However, none of these attempts have led to a curative therapy as of yet. In fact, data from CLI patients shows a significant increase in pro-angiogenic factors such as VEGF and FGF are already upregulated endogenously and it Is likely their downstream signalling pathways which are impaired [90].

Similar to MI clinical trials, intramuscular injection of VEGF into the affected limbs of CLI patients has been attempted by several groups. Early experiments by Baumgartner & colleagues (1998) used intramuscular injection of 4000 μg of naked human VEGF plasmid DNA into the affected limbs. They reported improved ABI scores, new vessels visible during contrast angiography, improved distal flow in 80% of patient limbs, improved healing of ulcers, and finally, the rescue of blood flow in 3 patients' limbs who had been due to receive amputation [91]. Despite these positive results, a study by the same group in 2000 which administered increasing doses of a human VEGF encoding plasmid (2-8 mg) reported several incidences of oedema in the affected limb, although improvements in pain, ulcer healing, and ABI index were also seen, indicating the potential benefit of VEGF therapy when an optimised dose is used [92]. Reports in the literature show that prolonged VEGF exposure is detrimental to ECs and vessel integrity, resulting in blood vessels that are 'leaky' leading to tissue oedema [93], similar to that reported in by Baumgartner & colleagues (2000). Since then, work such as that of Kusumanto & colleagues (2006), who also administered intramuscular VEGF to the affected limb, disappointingly found no decrease in amputation rate, however, over 50% of patients reported small improvements in skin ulcers, pain reduction, and some improvements in peripheral blood flow [94, 95]. Interestingly, Masaki & colleagues (2002) showed that a 5-fold overexpression of VEGF in a murine hind limb ischaemia (HLI) model actually resulted in a hastening to amputation, indicating that doses that are too high can have disastrous consequences [96]. Therefore, finding the optimal therapeutic dose of VEGF has been difficult and these studies highlight the inconsistency of VEGF therapy and the need for further research in the control of therapies in modulating angiogenesis and limb reperfusion, and finding alternate or conjunctive therapies. Interestingly, as dietary changes are being viewed as a tool to combat the

development of cardiovascular and other disease, Zhang & colleagues (2019) reported that 1000mg/kg dose of curcumin can increase angiogenesis both *in vitro* in mouse cells and in murine HLI. They showed that these effects were, at least in part, due to an increase in microRNA (miR) -93 (known to be pro-angiogenic) being viewed as a tool to combat the development of cardiovascular and other disease [97].

Models of animal HLI have been established in several species which take a surgical approach in order to recapitulate the tissue ischaemia seen in human PAD/CLI. Rabbits, rats, and mice have been extensively used to investigate vascular and muscular regeneration and involve permanent ligation of one or both femoral arteries. The procedure can also include ligation of the femoral vein and nerve in some instances [8, 98-100]], with the murine unilateral HLI model being the gold standard which most researchers use today [98] [8] [99]. However, unlike human PAD and CLI which are chronic conditions, murine HLI induces a transient and resolving phenotype. The recovery processes post HLI induction have been extensively studied to uncover potential reparative pathways for both angiogenesis and myogenesis, as muscle regeneration after injury is dependent on an adequate blood flow, in an attempt to modulate angiogenesis and muscle regeneration with therapeutic agents [101] [86]. Despite many preclinical studies showing positive results, failure of these methods in clinical trials is likely because these data are from a transient ischaemia model not a chronic disease model, and thus not all aspects of the disease were present. Although the results are valid and likely translatable to humans, the overall therapy effectiveness has many other obstacles to overcome in human disease like co-morbidities that are often present in patients with PAD such as hyperlipidaemia, hypercholesterolemia, diabetes, oxidative stress, age-related decline in reparative mechanisms, chronic inflammation, and the presence of other diseases [102], a lot of which are lacking in the various HLI models [103]. Other differences include the state of the chronically damaged tissue in human disease. After years of disease progression and pathology from other diseases/co-morbidities, individual lifestyle choices, and genetic susceptibilities, human tissues are more likely to have increased pathology; originally healthy muscle tissue becomes replaced by muscle fibres with a lower energy metabolism and muscle can be substituted with fat and connective tissue [104]. However, we still need to utilise pre-clinical animal HLI models to identify potential therapies for clinical use, but these should be scrutinised before human trials to tailor the choice of therapies and favour those with the most potential. MacAskill & colleagues (2018) attempted to overcome one shortcoming of murine HLI by utilising

a diabetic mouse strain to perform their HLI experiments. In fact, they showed very promising results after injection of what they termed hESC derived- EC products into the ischaemic limb. The term product referred to cells that were produced from a clinical-grade cell line with good manufacturing practice (GMP) adhering protocols to enable the approval of these cells for use in humans at a later stage. Their data showed that these cells improved capillary density and blood perfusion in the ischaemic muscle [85]. Never-the-less, although promising, there are still pitfalls with murine HLI models, and it will be interesting to see how this cell product fairs in human CLI patients in the future.

Many clinical trials using cell therapies have been tested in attempts to improve angiogenesis and muscle regeneration in PAD, ranging from endothelial progenitors, hESCs, induced pluripotent SCs, macrophages, to MSCs [105] [106, 107] with mostly underwhelming results. Placental derived adherent stromal cells (PLX-PAD) have been shown to increase capillary density and therefore blood flow after injection in murine hindlimb ischaemia, however, the first use of these cells in humans is still ongoing: The PACE trial is one of the latest ongoing phase III clinical trials which aims to show the long-term effects of this therapy in patients with CLI, by collecting data within 3 years and publishing in 2022 [108]. Pan *et al* (2019) were able to identify that; age, blood fibrinogen levels, arterial occlusion level, transcutaneous oxygen pressure, and the total number of transplanted CD34+ haematopoietic SCs were factors which could be used to identify patients who are likely to respond to SC based therapy [109], presenting an interesting perspective on why these cell therapies have been less successful than expected. They termed responders as those patients who at 6 months post treatment were still alive and had remission of their CLI.

1.5 Therapeutic treatments for myocardial infarction

CAD which can eventually lead to an MI is often asymptomatic. Smoking, being overweight, stress, depression, poor diet, high alcohol consumption, low physical activity levels, family history of disease, and co-morbidities such as diabetes and hypertension are risk factors contributing to CAD and MI risk [110]. Management of patients at a high risk of CAD and MI and for patients diagnosed with stable CAD includes lifestyle modifications to reduce risk and the prescription of established

antianginal medications such as β-blockers and angiotensin-converting enzyme-inhibitors (ACE) to correct hypertension [111, 112]. Statins have been amongst medications used for the management of CAD since the late 1980's and have been shown to be beneficial, particularly for high risk patients and those diagnosed with stable CAD [110]. The function of statins is to aid in lowering circulating levels of LDL in the blood, they work by inhibiting the activity of the enzyme 3-hydroxy-3-methylglutaryl-CoA reductase in the liver which is part of the cholesterol synthesis pathway. Statins also upregulate LDL receptors which increases their clearance from the body [113].

Treatments for patients with an MI commonly involve surgical measures to reinstate circulation including transluminal angioplasty, thrombolysis via a catheter, thrombectomy/endarterectomy, or a coronary artery bypass to either re-open the affected artery or bypass it entirely [104]. Many clinical trials have investigated the potential for various cellular and molecular therapies to aid MI recovery. Most have focused on attempting to induce angiogenesis for the treatment and prevention of ischaemia and to re-establish vital blood flow to the heart muscle. Providing adequate blood flow to the damaged myocardium as early as possible is important as the more muscle damaged, the larger the infarct size which is definitive of patient prognosis being that a larger infarct puts greater restraints on the hearts ability to function properly [114]. As VEGF is one of the most well characterised pro-angiogenic molecules, many clinical trials have attempted to increase its levels in patients through various methods including viral vectors, DNA plasmids, and recombinant human VEGF (rhVEGF) protein, in order to increase angiogenesis and re-establish microvascular circulation. Interestingly, Kranz & colleagues (2000) previously showed that serum VEGF-A levels were already elevated in patients 7- and 10-days post MI. They speculated that the source of endogenous VEGF-A may be the increased number of circulating platelets, produced as a mechanism to induce angiogenesis [115]. Similarly, Hojo & colleagues (2000) reported a peak in patient serum VEGF-A at 14-days post MI but concluded, via *in vitro* research, that peripheral blood mononuclear cells were responsible for this increase. They also suggested that greater myocardial damage correlated with higher VEGF-A serum levels, supporting the hypothesis for endogenous mechanisms of repair which induce angiogenic potential via VEGF upregulation [116].

Attempting to induce angiogenesis via exogenous VEGF comes with challenges such as achieving targeted local delivery in contrast to systemic delivery, overcoming the short half-life of VEGF in circulation [117], and avoiding the unwanted side effects with higher doses (increased vessel permeability and oedema due to disordered barrier function [43]) used to overcome its short half-life [117]. Pre-clinical data provided by several animal MI models have shown positive results: a classic example is that performed by Su & colleagues (2004) who injected an adeno-associated viral construct containing the cardiac specific promoter, myosin light chain 2-v, multiple copies of the HRE sequence, and the VEGF sequence directly into mouse infarcted hearts and found that this not only increased the number of capillaries but decreased infarct size and resulted in improved cardiac function compared with controls [118]. In a rat MI model where intervention with a plasmid encoding VEGF was injected into the heart 7-days post MI, Hao & colleagues (2004) found that capillary density in the heart was increased 3 weeks later [119]. Finally, pigs are another commonly used animal model to study MI as their heart is of a similar size to humans, as well as having a greater similarity in metabolism and blood components to humans, and in contrast to rodents have been found to develop atherosclerosis naturally with age [120]. Tao & colleagues (2010) used a similar approach to the above-mentioned mouse experiments. They utilised an adeno-associated viral construct containing the same cardiac specific promoter and hypoxia inducible VEGF sequence injected into multiple sites of the heart at the time of infarction, in conjunction with another viral vector containing the pro-angiogenic Ang-1 sequence, and reported an increase in vessel density in the infarcted heart and preserved cardiac function at 8 weeks post MI, with the added benefits of less cell death and increased cardiomyocyte proliferation [121]. Despite these and many other positive results in animal models, clinical trials with VEGF have been unable to overcome clinical challenges and ultimately fail. For example, in 2003 the vascular endothelial growth factor in ischaemia for vascular angiogenesis trial (VIVA trial) reported no improvements in myocardial perfusion in MI patients who underwent intracoronary and intravenous infusions of rhVEGF despite patients reporting improved angina at 60 and 120 days after treatment [122], likely due to insufficient uptake. Mendiz & colleagues (2011) administered 3.8 mg of VEGF containing plasmid to the damaged heart via intramyocardial injection and reported improvements in symptoms and ejection fraction (EF) at a 6 month follow up, however, EF results were not retained at 24 months [123]. Relevantly, Kukula & colleagues (2019) recently published a 10 year

follow up of patients from the VIF-CAD trial which administered patients with coronary artery disease an intramyocardial injection of a plasmid containing both VEGFA and basic FGF, but reported no differences in cardiovascular mortality, MI, stroke, or readmission rates of patients in the experimental versus placebo groups [124], further adding to the mixed results already present in the field. Failure of VEGF therapies to result in the expected positive outcomes in patients is likely down to many factors; interestingly, VEGF has more recently been found to have non-angiogenic pleiotropic effects on cell such as neurons, skeletal muscle, and cardiac cells [125], which could contribute to adverse effects in patients, further complicating this molecules use as a pro-angiogenic therapy. Relevantly, as well as angiogenesis having a role in post MI recovery and the prevention of further heart damage by revascularizing the ischaemic tissue, angiogenesis is also a vital part of the disease pathology of atherosclerosis prior to an ischaemic event, as atherosclerotic plaques containing capillaries were found to be at a higher risk of rupturing [126]. Angiogenesis in this instance, is driven by reactive oxygen species (ROS), inflammation, and hypoxia in the plaque [127]. Of note, clinical observation has found that prescribing angiogenesis inhibiting drugs has had a negative effect on patient outcome, by increasing thrombotic events [127].

An interesting approach to tackle increased vessel permeability and oedema caused by prolonged VEGF exposure was that taken by Zangi & colleagues (2013). They showed that intramyocardial injection of synthetic modified RNA (modRNA) (where some nucleotides were substituted for more stable modified nucleotides) of human VEGF in a murine model of MI was superior to plasmid DNA in improving heart function and survival, although both methods successfully reduced infarct size and capillary density. Interestingly the authors concluded the positive outcomes of this approach were due to the VEGF stimulated migration and differentiation of epicardial derived progenitor cells into the myocardium [128]. Although this methodology has yet to progress to clinical trials in human MI patients, the first use of VEGF modRNA was recently carried out by Gan & colleagues (2019) who administered intradermal injections of VEGF modRNA to the forearms of type II diabetic patients. Their analysis revealed elevated VEGF levels in the skin at 24 hours after injection and importantly, increased basal blood flow in the skin 7 days later [129], demonstrating the efficacy and safety of this intervention. Clinical trials in patients with CLI and MI may hopefully be approved in the near future. The 2013 reduction of infarct expansion and ventricular remodelling with erythropoietin after large myocardial infarction trial (REVEAL trial) looked at the effects of the pro-angiogenic molecule erythropoietin

when administered to STEMI patients. However, they did not detect any alteration in infarct size 6 months post MI, and in contrast to previous studies, reported an increase in adverse events such as, but not limited to, another MI, stroke, thrombus, and death [130].

Many groups have attempted to modulate angiogenesis and cardiac function post MI via the use of cell therapies. The 2010 randomised clinical trial by Piepoli & collegeaues (2010) administered STEMI patients with autologous, heterogeneous, bone marrow cell therapy. One year post cell percutaneous coronary injection, left ventricle function was improved, specifically left ventricular ejection fraction (LVEF) and stroke volume [131]. The PROMETHEUS trial in 2014 administered 6 patients with an intracardiac injection of autologous mesenchymal stem cells (MSCs) to damaged areas of myocardium at the time of coronary artery bypass surgery. At an 18 month follow up, patients had improved LVEF and a smaller infarct compared to their baseline measurements [132]. In contrast, the 2016 REGENERATIE-AMI trial studied 100 patients with acute MI who received intracoronary injection of autologous bone marrow derived cells but saw no significant differences in LVEF compared to placebo patients [133]. Bolli & colleagues (2018) have taken an interesting approach of combining autologous MSCs and the 'controversial' c-kit+ cardiac progenitor cells (from endocardial biopsies) in the CONCERT-HF trial in patients with heart failure caused by MI or underlying coronary artery disease. Their aims are to evaluate the efficacy of administering each cell type alone versus and the combination of both cell types on improvements to cardiac function. However, recently c-kit + cardiac stem cells have been highly disregarded and many publications utilising these cells have been retracted with doubts regarding the regenerative capabilities of c-kit + cardiac 'stem cells' due to inconsistent results in the literature [134]. One of the largest currently ongoing studies is the DREAM-HF phase III clinical trial which was started in 2014 with 566 heart failure patients with reduced EF enrolled. This trial administered allogenic mesenchymal precursor cells and is measuring several parameters such as time to major adverse cardiac event, time to cardiac death, time to all cause death, left ventricular remodelling comparison by echocardiography, quality of life assessments, and many more. As their last patient has now received treatment their results are expected to be published soon with great anticipation regarding the positive benefits of this cell therapy in such a large cohort [135].

As cell therapies have so far yielded somewhat disappointing results, researchers have moved onto finding other potential therapies such as the combination of human pluripotent stem cell derived cells and biological scaffolds to aid in recovery post MI. Menasché & colleagues (2015) utilised a human ESC line which they induced differentiation to a cardiac specific lineage and isolated cells expressing the cardiac lineage marker ISL-1. They embedded these cells into a fibrin scaffold which was inserted into the infarcted area of a 68-year-old patients' heart. After 3 months the patients previously very poor EF had improved, indicating contractile function in the area the scaffold was implanted, which was previously non-contractile infarcted tissue [136]. This aspect of regenerative medicine has progressed to the recent first human clinical trial inserting porcine derived, decellularized, ECM hydrogels into post MI patients. This ground-breaking study used trans-endocardial catheter injection to insert the gel into the damaged myocardium. Patients were split into those treated between 60 days – 1 year, or between 1-3 years post MI and results showed improvements to left ventricular remodelling, particularly in the patients treated earlier post MI, and improvements in the 6-minute walk test distance. However, larger more robust trials and preclinical research are being further pursued to investigate the full potential of ECM hydrogels in treating MI [137]. Rodness & colleagues (2016) used a combined targeted approach whereby VEGF was released from biological hydrogel micro-patches placed on rat hearts post MI (to prevent off target effects of VEGF). These patches continued to release VEGF for 5 days and resulted in a higher capillary density in the infarct area and border region, which is thought to improve cardiovascular outcome post MI by improving blood flow to the damaged myocardium and reducing infarct size [138].

Some research is focussing on the transient and dynamic repair environment present after MI and attempting to target and exploit pathways involved at this stage of regeneration [139]. Recent clinical trials targeting cardiac injury and repair after acute MI include Gullestad & colleagues (2013), who carried out an immunomodulation clinical trial administering intravenous immunoglobin G in STEMI patients. However, they did not find any reduction in infarct size or alteration in LVEF [140]. Collectively perhaps these methods are not providing the expected results because we are yet to fully understand the innate mechanisms driving endogenous repair which therapeutic treatments ultimately aim to enhance.

1.6 Non-coding RNA

1.6.1 Short non-coding RNA

Non-coding RNAs (ncRNAs) are sub-grouped based on size into long non-coding RNAs (lncRNAs) and short non-coding RNAs. The short non-coding RNA category includes microRNA (miR), piwi-interacting RNA, transfer RNA (tRNA), ribosomal RNA (rRNA), small nuclear (snRNA), and small nucleolar RNA (snoRNA) [51-53] shown in Figure 1.3. Ranging between 19 - 24 bases in length, miRs are one of the most studied and understood ncRNAs from their bioprocessing through DROSHER and DICER, to their post-translational gene silencing via interference at the mRNA level of gene expression [141]. The first short ncRNA miR, lin-4, was identified in 1993 in *Caenorhabditis elegans* and contains sequences complementary to the 3' untranslated region of the lin-14 and lin-28 mRNAs, which encode developmentally important temporal control proteins [142] [143]. Interestingly, mutations in miRs themselves or the components contributing to their processing have been previously documented in human diseases, ranging from cancers to cardiovascular diseases and neurological disorders [144] [145] [141] [146].

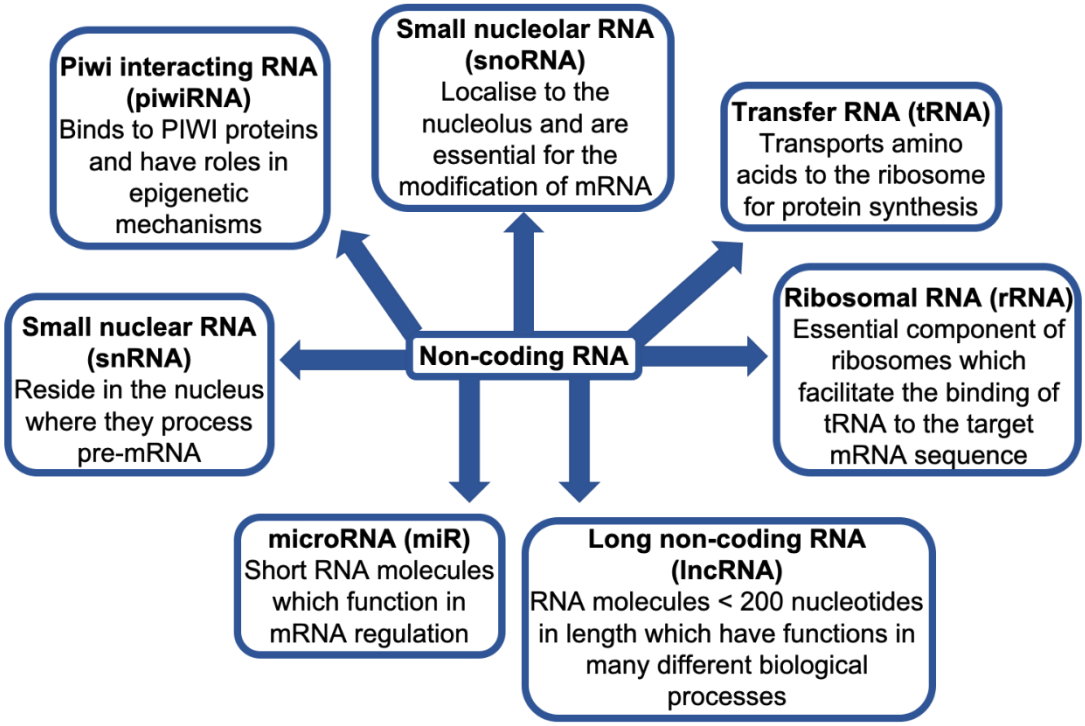

Figure 1.3 Non-coding RNAs.

Non-coding RNAs (ncRNAs) are sub-grouped based on size into long non-coding RNAs (lncRNAs) and short non-coding RNAs. The short non-coding RNA category includes microRNA (miR), piwi-interacting RNA, transfer RNA (tRNA), ribosomal RNA (rRNA), small nuclear (snRNA), and small nucleolar RNA (snoRNA).

1.6.2 Long non-coding RNA

Approximately 98% of the human genome is non-protein coding, however, it is actively transcribed into RNA [147]. Initially thought to be 'noise' caused by transcriptional processing of protein coding genes nearby and therefore non-functional, lncRNAs remained un-investigated for years. Today we know that lncRNAs make up the majority of the ncRNA class yet are the most poorly understood despite the current estimation that the human genome possesses ~ 270,000 lncRNAs and the fact that there are many more lncRNAs than miRs in both human and mouse genomes [148]. LncRNAs are greater than 200 nucleotides, commonly lack conservation across species, and have diverse characteristics from their length to their structure, cellular localisation, expression patterns, and cellular function [149]. Previously, there has been difficulty in correctly annotating them within the genome, contributing to the fact that lncRNAs remained ignored for so long [150]. With the advances in RNA-sequencing (RNA-seq) technology and the increasing number of studies employing this technique to assess the transcriptional differences between healthy and pathological states, the abundance of lncRNA expression in datasets was highlighted, leading the way for further investigations [151].

Two lncRNAs with unique functions have long been known to exist, the X- inactive specific transcript (Xist), and telomeric repeat-containing RNAs. Xist is responsible for X-inactivation in mammalian female cells and binds to polycomb repressive complex 2 (PRC2) recruiting it to chromatin which then functions in a complex with histone methyltransferase activity to inhibit transcription from the now inactivated chromosome [152]. Long non-coding telomeric repeat-containing RNAs (TERRA) are scaffold lncRNAs transcribed from telomeres with repeating bases at the end of chromosomes, and along with their binding partners including RNA molecules and proteins, create telomere heterochromatin under tightly regulated expression in association with different stages of the cell cycle [153]. This is particularly interesting as transcription of telomeres into lncRNA is a function conserved throughout the eukaryote domain [153].

The field of lncRNA knowledge is growing quickly as some lncRNA have been implicated in cancer, developmental biology, neurological disorders, epigenetics and imprinting, cell lineage commitment and pluripotency, post-transcriptional and post-translational modifications, as well as many other functions [54] [64]. Most

interestingly, lncRNAs can have a spatiotemporal and usually cell type specific pattern of expression, which may likely give clues as to their functions [154, 155]. LncRNA were often reported to accumulate in the nucleus indicating roles in gene expression and chromatin organisation [156]. However, this is not the case for all lncRNAs as many have been found to reside in the cytoplasm and contribute to mRNA turn over, stability and translation, protein stability, and sponging of cytosolic molecules [157] [158]. Although they exhibit low sequence conservation, there is evidence for conserved secondary structure, splicing patterns, and subcellular localisation amongst lncRNAs. Many lncRNAs have been found in plants which regulate growth and development, root development, gamete development and fertility, photosensitivity, nutrient uptake, and pathogenic responses to name a few [159, 160]. LncRNAs are even estimated to make up a quarter of the yeast genome [161] indicating their prevalence across species, however, the amount of non-coding DNA in the genome increases with complexity of the organism, particularly after primate evolution [162, 163]. Theoretically, there is less evolutionary pressure on RNA transcripts, as they are non-protein coding there is no need to conserve an amino acid sequence which allows for greater sequence divergence. Not surprisingly then, lncRNAs have been shown to evolve at a greater rate than their coding mRNA relatives [164], therefore, highly conserved lncRNAs have a greater probability of having unidentified protein-coding function after all [165]. Alternatively they may be truly non-coding with an important conserved cellular function. Even among lncRNA across species with low levels of conservation, we must remember to consider that their secondary structure may remain very similar dispite changes to their primary RNA sequences, which would allow for a similar function and binding partners [166]. For example, despite a lack of genomic conservation, lncMyoD regulates skeletal muscle differentiation in human and mouse by controlling myoblast cell cycle exit during myogenesis and is located to the MYOD1 gene in both species [167].

1.6.3 Long non-coding RNA structure and function

LncRNA transcripts carry out many necessary cell functions, for example, through the transcript functioning itself, or through the increased level of transcription activity at their loci which can enhance expression of genes also at that locus (in *cis*) or genes located further away (in trans) via regulation of chromatin states [168]. LncRNAs can also act as the parent strand giving rise to miRs; miRs and lncRNA can compete for target messenger RNA; lncRNAs can act as decoys for miRs resulting in de-

repression of miR targets; and miRs can either stabilise or de-stabilise lncRNA, influencing their degradation [169]. Ultimately, the possibilities for the interactions between miRs, lncRNA, target mRNAs, and other binding partners leads to a complex hierarchical level of finely tuned regulation within cells. Genomic locations of lncRNA are also interestingly diverse, for example, they can be found in-between neighbouring protein-coding genes and are termed long intergenic non-coding RNA (lincRNA), within a known protein-coding gene (intronic), over-lapping with another gene (sense-overlapping), antisense to a gene they are likely to regulate (present on the opposite DNA strand but sequence overlapping), or bi-directional to a gene they likely regulate (present on the opposite DNA strand but sequences not over-lapping) (Figure 1.4A) [170].

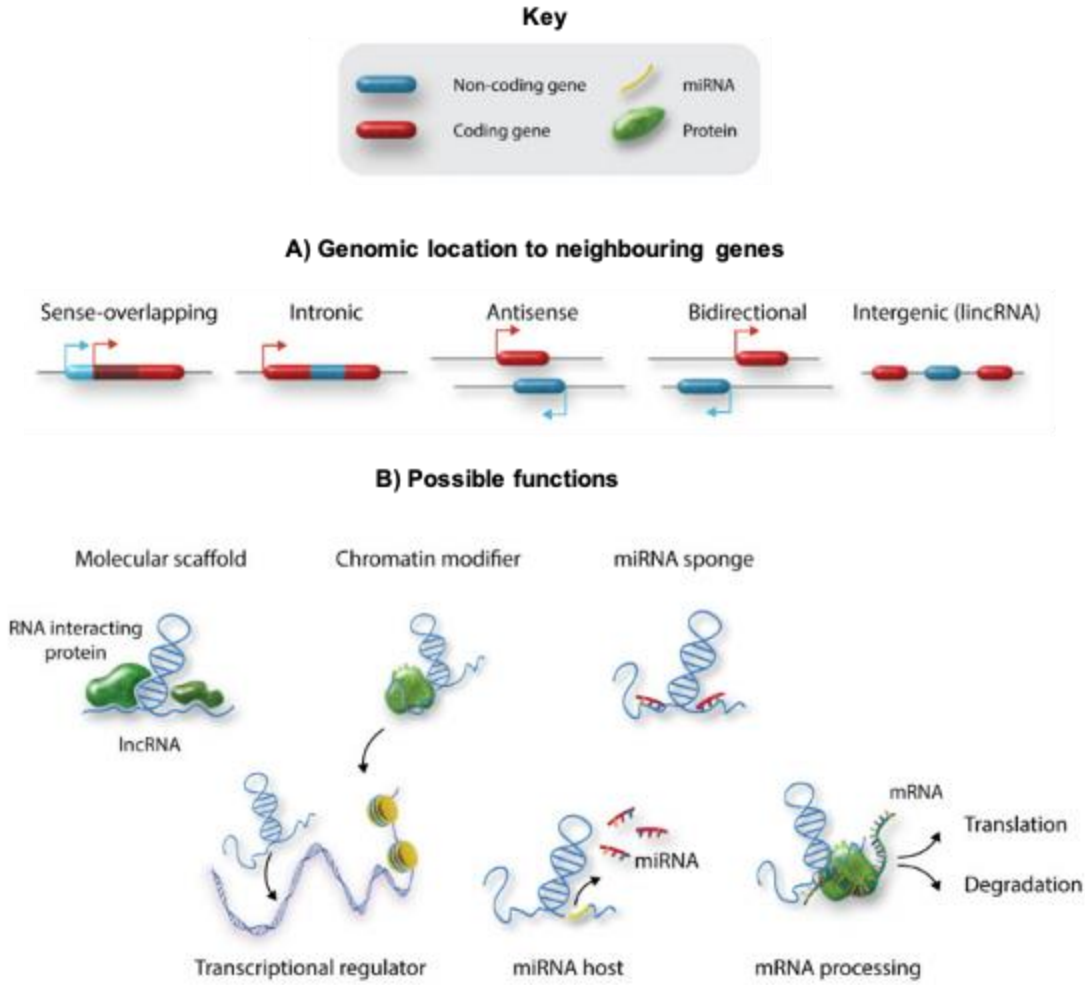

Figure 1.4 Long non-coding RNAs have diverse genomic structures and cellular functions.

A) Long non-coding RNAs (lncRNAs) are found in diverse locations within the genome in relation to their protein-coding neighbours. They can overlap with a gene, be located within a gene itself, or be found spaced between genes on the same strand of DNA. They can also be found antisense to genes (on the opposing DNA strand, with their sequence overlapping with a gene or not. B) LncRNAs also have a diverse range of binding partners such as microRNAs (miRs), proteins, DNA, and other RNA molecules. Their cellular functions include acting as a scaffold to support RNA and protein interactions, acting as a decoy by binding a protein and making it unavailable, modifying chromatin, regulating transcription, acting as miR hosts, sponging miRs, and regulating mRNA processing. Image adapted from Monteiro & colleagues (2019) [170].

Once transcribed lncRNAs have been reported to function in several different ways, for example, the nuclear lncRNA MANTIS acts as a scaffold for the switch/sucrose nonfermentable chromatin-remodelling complex and is necessary for the ATPase activity of the BRG1 subunit, which subsequently leads to the expression of endothelial specific gene expression [171]. Another nuclear lncRNA termed nuclear enriched abundant transcript 1 (NEAT1) localises to and is essential for the formation of paraspeckles (mysterious ribonucleoproteins present in the interchromatin space within the nucleus whose functions are mostly unknown, however, are suspected to be important in regulating transcription), binds chromatin [172, 173], has been implicated as a transcriptional regulator, particularly in some cancers, and is known to sponge (bind to and prevent further interactions with) miR-193a in colorectal cancer thus contributing to cancer progression [174]. Not only do many lncRNAs physically interact with miRs but some act as a host gene housing multiple miRs such as the cardiac mesoderm enhancer-associated non-coding RNA (CARMN) which houses the well-studied miR-143 and miR-145, however, the lncRNA itself functions independently of the miRs by contributing to cardiac lineage specification and maintenance of a cardiomyocyte (CM) phenotype [175]. Meanwhile miR-143 and miR-145 have been extensively studied and found to promote SMC differentiation and are involved in vascular disease arterial remodelling [176]. The cytoplasmic lncRNA termed non-coding RNA activated by DNA damage (NORAD) plays an important role in genome stability via acting as a decoy when upregulated by DNA damage. NORAD sequesters pumilio proteins (a family of proteins defined by their conserved RNA binding domain) and relieves their inhibition on DNA repair and mitotic pathways [177]. Recently, NORAD has also been implicated in colon cancer progression via its sponging of miR-202 [178], highlighting critical roles for lncRNA in maintaining proper cellular functions.

1.6.4 Micro-peptides in long non-coding RNA transcripts

As lncRNA research has expanded, so too has the discovery of micropeptides which are housed by some lncRNA transcripts. Typically, research regarding protein detection has utilised a cut off which excludes proteins less than 100 amino acids as the longer an open reading frame (ORF) is, the more likely it is to be protein coding [179]. However, much smaller proteins have been recognised to exist and have been termed micropeptide's. ORFs in lncRNAs can be remnants from a past evolutionary active gene such as is the case for Xist [152], or appear by chance. Other examples

of lncRNA encoded micropeptides include CIP2A-BP, encoded by LINC00665, which reduces breast cancer metastasis [180], and the mitochondrial located BRAWNIN, encoded by a transcript annotated as 12orf73, that is conserved between zebrafish and humans and is essential for assembly of the respiratory complex III subunits [112]. Skeletal muscle in particular appears to be enriched with micropeptides. The myomixer micropeptide is hosted by an as yet uncharacterised lncRNA termed LOC101929726 and partly controls myofiber formation [181]. Makarewich & colleagues (2018) discovered the micropeptide DWARF which promotes the activity of sarcoplasmic reticulum ATPases and recently showed that its overexpression can rescue pathological cardiac remodelling in a mouse model of dilated cardiomyopathy [182] [183]. The micropeptide LEMP, encoded by MyolncR4, has a role in promoting muscle formation and regeneration in mouse and zebrafish and is conserved in humans [184]. Lastly, the mouse annotated lncRNA 1810058I24Rik encodes a micropeptide termed mitochondrial micropeptide 47 which activates inflammasomes and also has a human orthologue [185]. Interestingly, the PNUTS locus has been termed a bi-functional locus as alternate splicing can switch between the ubiquitously expressed protein which regulates protein phosphatase 1, to transcription of the tightly regulated PNUTS lncRNA which has been shown to sponge miR-205 influencing epithelial- mesenchymal transition promoting tumour progression [186]. The list of known micropeptides continues to grow as we are likely just beginning to understand the extent of micropeptides and lncRNAs in genomes across species.

1.7 Long noncoding RNAs in cardiovascular biology and disease

To date, many lncRNAs have been identified with roles in cardiovascular biology and their functions vary widely including embryological heart development, cardiovascular cell commitment, cell migration, phenotype switching of SMCs, vascular EC commitment and EC angiogenesis [84, 187-191, 229]. The previously mentioned H19 is upregulated in human cardiac hypertrophy and heart failure and has been identified as a negative regulator of cardiac hypertrophy through *in vitro* assays [192, 193]. Micheletti & colleagues (2017) identified the LncRNA Wisper as enriched in cardiac fibroblasts and upregulated in the infarcted mouse heart and in aortic stenosis patient samples. The authors implicated this lncRNA as a regulator of cardiac fibroblast proliferation, migration, and survival [194]. The mitochondrial lncRNA LIPCAR has

been shown to be elevated in patients' plasma post MI. Clinically, it is a predictor of survival in patients suffering heart failure post MI and is a novel biomarker of cardiac remodelling [195]. In contrast, novlnc6 is downregulated in the plasma of coronary artery disease patients [196]. Lastly, the primate specific lncRNA CHROME is upregulated in the plasma and atherosclerotic plaques of CAD patients and was found to contribute to cholesterol homeostasis in humans [197].

During cardiovascular development the lncRNA BRAVEHEART is present in embryonic mesoderm and is required to specify cardiac lineage [198]. Similarly, FENDRR is expressed by lateral plate mesoderm and is also required for heart development [199]. Experiments in zebrafish identified that TERMINATOR expression in undifferentiated pluripotent SCs is vital for cardiovascular development as knock down (KD) resulted in 50% offspring lethality and the presence of cardiovascular defects. The same study also identified ALIEN in zebrafish cardiac progenitors and its depletion resulted in abnormal vascular patterning [189]. Liu & colleagues (2017) identified heart break lncRNA1, which they termed HBL1, as an inhibitor of CM differentiation in ESC and induced pluripotent SC differentiation experiments [200]. In contrast, the previously mentioned lncRNA CARMEN has been found to promote the differentiation and specification of cardiac progenitor cells into SMCs and CMs [175].

Vascular ECs specifically express many known lncRNAs such as TIE1-AS which regulates expression of its host gene, the well-known angiogenic TIE1, in early zebrafish vessel development; dysregulation of this axis causes defects in EC junctions and interestingly, altered TIE1-AS expression has been reported in patients with vascular malformations [201]. Another lncRNA related to an already well characterised gene in heart development is GATA6-AS; it is upregulated in ECs in response to hypoxia where it promotes EndoMT [202]. The lncRNA PUNISHER is conserved between zebrafish and humans and is expressed in mature ECs. Inhibition of PUNISHER results in severe blood vessel defects and altered EC gene expression [189]. Interestingly, the annotated LINC00493 is enriched in EC cytoplasm, however, its function is as yet unknown highlighting the need to further investigate the functions of already identified lncRNAs in cardiovascular diseases as well as uncover those yet to be identified and annotated. Other lncRNAs which show EC enrichment include metastasis associated lung adenocarcinoma transcript 1 (MALAT1), taurine upregulated gene 1 (TUG1), maternally expressed 3 (MEG3), LINC00657, and

myocardial infarction associated transcript (MIAT) [188, 201, 203]. The lncRNA smooth muscle and EC enriched migration/differentiation associated lncRNA (SENCR) positively regulates angiogenesis. Recently, the Baker group discovered its involvement in EC differentiation as *in vitro* overexpression in human umbilical vein ECs (HUVECs) enhanced proliferation and migration as well as angiogenesis [84]. As mentioned previously, MANTIS is necessary for BRG1 activity during chromatin remodelling. Interestingly it was found to be downregulated in patients with idiopathic pulmonary hypertension and upregulated in macaques on an atherosclerotic regression diet and in human glioblastoma ECs. Additionally, MANTIS KD in ECs inhibited sprouting angiogenesis and the cells ability to align when exposed to shear stress [171] making it a potentially interesting target for therapeutic intervention in several aspects of cardiovascular biology.

Several lncRNAs have been identified as enriched in CMs such as HOTAIR which regulates cardiac hypertrophy and represses calcification genes [204, 205]. Similarly, the lncRNAs ROR and CHRF are reported to promote cardiac hypertrophy [191, 206]. The lncRNA cardiac apoptosis related, termed CARL, regulates mitochondrial fission and apoptosis in CMs [207]. Recently, a lncRNA identified as KCNQ1OT1 was upregulated in a mouse model of heart failure, where it promoted CM apoptosis [208]; this is of particular interest as it has previously been suggested as a good biomarker to identify patients with CAD [209] [208]. Finally, the lncRNA BDNF-AS is upregulated in murine CMs during hypoxia, whereas its downregulation improved CM survival [210].

A lncRNA termed smooth muscle–induced lncRNA enhances replication (SMILR) promotes vascular SMC proliferation by regulating part of the cell cycle. Relevant to clinical pathologies, SMILR has been shown to be upregulated in a vein graft pathological model and atherosclerotic plaques [187, 211]. The angiotensin II regulated lncRNA Ang362 has been shown to promote vascular SMC proliferation [212] and more recently has been suggested to promote pulmonary arterial hypertension via the regulation of miR-221 and miR-222, which are housed within the Ang362 locus [213]. Chen & colleagues (2020) also recently reported that Ang362 can promote cardiac fibrosis post MI, through inhibition of SMAD7 [214], highlighting this lncRNA as a potential therapeutic target in several aspects of cardiovascular disease. LincRNA-p21 is also of clinical interest as it is found in macrophages as well as vascular SMCs where it promotes apoptosis and reduces proliferation and

participates in a feedback loop with the oncogenic p53. Furthermore, Wu & colleagues (2014) revealed LincRNA-p21 to be downregulated in patients with coronary artery disease, which correlates with their *in vitro* work that showed its downregulation contributed to neointima formation in a mouse model of coronary artery injury [215]. Interestingly, the well-known hypoxia related gene HIF1A has a lncRNA laying anti-sense to its locus termed HIF1A-AS1, which was found to be upregulated in the serum of patients with an abdominal aortic aneurysm. In this study, the authors suggested that HIF1A-AS1 influenced aneurysm pathogenesis by regulating vascular SMC apoptosis [216].

The roles of immune cells in cardiovascular pathophysiology including atherosclerotic plaque biology and MI resolution and recovery have long been investigated. Atherosclerosis is classed as an inflammatory disease as immune cells form part of the core of the atherosclerotic plaque and influence the progression and outcome of disease. The inflammatory process post MI can be both beneficial for example, by aiding in the clearing of dead CMs, or detrimental, by contributing to hypertrophy and cardiac fibrosis [217] [218]. LncRNAs have been found in various immune cells that influence cardiovascular disease for example, HEAT2 is upregulated in the peripheral blood mononuclear cells of patients with heart failure and contributes to immune cell adhesion to the endothelium and subsequent transmigration [219]. Macrophages are one of the bodies first line of defence and have been shown to be one of the most highly upregulated cell types in the peripheral blood of patients post MI. Interestingly, they have been shown to express several lncRNAs such as THRIL, Linc-Cox2, Linc-AK170409, and Linc-IL7R [218]. The previously mentioned MIAT contains single nucleotide polymorphisms which have been associated with an increased risk of MI and is found not only in peripheral blood cells but also neurons, SMCs, and ECs [203, 220]. The lncRNA NEAT1 mentioned previously is enriched in monocytes and is downregulated in patients who have suffered an MI [221]. More recently, the Baker group identified the lncRNA plaque enriched lncRNA in atherosclerotic and inflammatory bowel macrophage regulation (PELATON) as being enriched in unstable human atherosclerotic plaques, specifically in monocytes and macrophages where it plays a role in plaque progression [222].

1.7.1 Noncoding RNAs in peripheral arterial disease

There is already a long list of miRs attributed to vascular biology such as miR-1, miR-133, and miR-208a involved in arrhythmia, miR-1, miR-133, and miR-208a in hypertrophy, miR-21 and miR-29 in fibrosis, miR-1 and miR-133 in proliferation, and miR-1, miR-21, miR-320, and miR-199a in apoptosis to name a few examples [223]. MiR involvement in vascular biology logically led to the speculation that lncRNAs may also play vital roles in human disease. Stather & colleagues (2013) carried out the first human miR transcriptome-wide profiling research in PAD, which they referred to as a miRNome [13]. Analysing patients' peripheral blood, they concluded that a PAD-specific signature exists which includes downregulation of miRs let-7e, miR-15b, -16, -20b, -25, -26b, -27b, -28-5p, -126, -195, -335, and -363. They also found an inverse correlation of these miRs with several predicted and validated miR target genes, all of which are involved in signalling pathways associated with vascular pathology [13]. In fact, miR-126 (identified above) was confirmed to have a role in a translatable, but small, rabbit HLI model study where increased miR-126 correlated with improved muscle repair post injury, in conjunction with the previously identified positive role of miR-125 in angiogenesis [224]. In addition, Cheng & colleagues (2018) more recently identified upregulated miR-323b-5p in the serum of diabetic CLI patients, thus claiming it could be useful as a biomarker in diabetic PAD patients as a predictive marker for progression to CLI [225]. These data give an indication of the complex regulation of miRs in PAD pathophysiology. This leads to speculation that other RNAs such as lncRNAs may also play a role in the pathophysiology of PAD, and other cardiovascular diseases, or may likely be indicative of disease progression and therefore could be used as diagnostic biomarkers. To the best of our knowledge, no such lncRNA profiles have yet been identified in PAD or CLI, however, SENCR levels were found to be significantly decreased in CLI samples, as well as in premature coronary artery disease samples [84]. Further research is required to fully understand SENCR's role in PAD/CLI, although a limitation which has hindered this research is the fact that SENCR does not have a mouse homologue, complicating *in vivo* investigations.

Several lncRNAs have been identified in the pre-clinical murine HLI model as having pro-angiogenic effects which may be translatable to human PAD/CLI patients [226]. The hypothesis remains that if endogenous angiogenesis can be stimulated in these patients and perfusion improved, then symptoms would likely decrease and

amputation be prevented. Recently, the lncRNA GAPLINC was found to promote angiogenesis in HUVECs during hypoxia [11]. Other previous studied lncRNAs with roles in angiogenesis which may be relevant to human PAD/CLI include MALAT-1 and MEG3. Michalik & colleagues (2014) showed that MALAT-1 inhibition in murine HLI was detrimental to muscle neovascularisation and perfusion and mechanistically switched ECs from a proliferative to a migratory phenotype by altering expression of cell cycle regulatory genes [188]. Likewise, inhibition of the endothelial enriched MEG3 has been shown to promote angiogenesis and perfusion in murine HLI. This is of particular interest as the authors showed that MEG3 expression increased with age in senescent ECs [227].

1.7.2 Cardiovascular long non-coding RNAs without human orthologues

In vivo models of cardiovascular diseases have produced candidate lncRNAs which do not appear to have human orthologues for example, Liang & colleagues (2018) identified pro-fibrotic lncRNA (PFL) as upregulated in the mouse heart post MI where it promoted proliferation and myofibroblast formation, whereas PFL KD significantly alleviated myocardial fibrosis and improved cardiac function post MI, although the authors could not identify a human orthologue [228]. The murine lncRNA Myheart was found to be cardioprotective as it binds to and sequesters the chromatin regulator BRG1, thus preventing activation of a pathological cardiac hypertrophic gene expression profile, however, no human orthologue has been identified to date [229, 230]. Similarly, the lncRNA cardiac-hypertrophy-associated epigenetic regulator (Chaer) also facilitates cardiac hypertrophy via interaction with another chromatin modulator, this time PRC2; by interfering with its ability to methylate H3K27 and activate gene expression; it too does not have an identified human orthologue [231]. As previously mentioned, sequence conservation is not always present across species in lncRNAs with conserved functions. Therefore, with further investigations into the human and mouse loci for genes neighbouring these murine lncRNAs orthologues may be identified in future.

1.8 Long non-coding RNA LINC00961

Understanding EC homeostasis and the endogenous pathways behind their specific behaviours such as barrier function, adherence, and angiogenic potential is of importance for understanding how these pathways become dysfunctional and contribute to cardiovascular disease. This thesis was a project born from the hypothesis that RNA-seq analysis on hESC-derived ECs could identify novel lncRNA transcripts important for endothelial differentiation, specification, and maintaining proper EC functions in terminally differentiated cells. Comparison of lncRNA expression in immature hESCs was therefore compared with HSVECs as a positive control for terminally differentiated ECs. When I started this PhD project, these experiments had been carried out by the Baker group and a list of lncRNAs of interest expressed in differentiated and control ECs had been compiled. The lncRNA LINC00961 was identified as being of particular interest due to the locus being conserved in mice and that it contained an ORF. It was at this point that I joined the Baker group and focussed on dissecting the role of LINC00961 in ECs, specifically with an interest in the mouse LINC00961.

LINC00961 is a lincRNA located at p13.3 on human chromosome 9 (Figure 1.5). There are 4 predicted transcripts with 1 predicted to undergo non-sense mediated decay according to data available on the online database Ensembl (http://www.ensembl.org/Homo_sapiens/Gene/Summarydb=core;g=ENSG00000235387;r=9:35909483-35937153). Isoform 1 is reported as 1612 base pairs (bp), contains 2 exons, of which exon 2 encodes the 75 amino acid micropeptide previously termed small regulatory polypeptide of amino acid response (SPAAR) by Matsumoto & colleagues (2017) who identified 2 potential transcription start sites [232]. The mouse homologue (previously identified as 5430416O09Rik) is located on chromosome 4 with 65.3% conservation of amino acid sequence. To date, orthologues have been identified in 191 species including mammals, invertebrates, and ray-finned fishes, however, no orthologue has been identified in zebrafish (Ensembl, July 2020). Although a higher sequence similarity is observed between humans and primates, the mouse and human locus is conserved in synteny with many of the same neighbouring protein coding genes (Figure 1.5). This level of conservation suggests an importance for this locus in evolutionary conserved mechanisms.

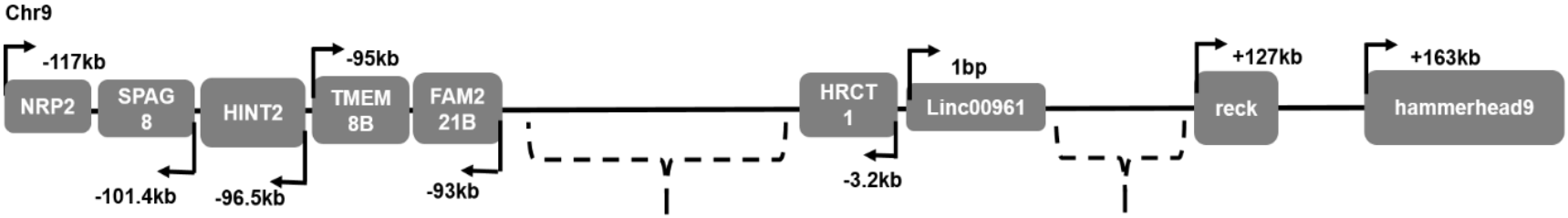

Human locus

Olfactory gene cluster 2
-34.7 > -50.7kb
NDUFA5P4
OR13J1
OR13E1P
LINC00950

Olfactory gene cluster 1
+33.7 > + 112.2kb
PGAM1P2
OR2S2
YBX1P10
OR13C6P
OR13C7
OR2AM1P

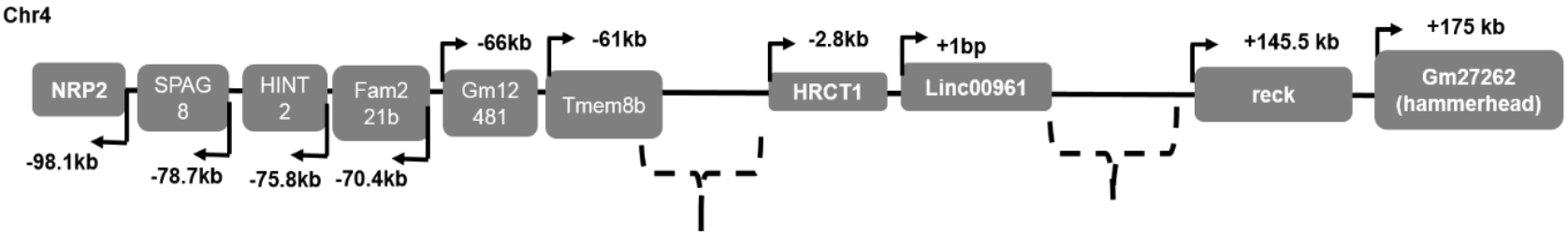

Mouse locus

Olfactory gene cluster 2
-24.4kb > -37.3kb
Olfr71
Olfr70
Gm23257

Olfactory gene cluster 1
+37.4 > + 121.5kb
Olfr269
Olfr159
Olfr29
Gm12392
Olfr156
Olfr157
Olfr155

Figure 1.5 The LINC00961 locus and neighbouring genes are conserved in synteny across the mouse and human genomes.

Top panel is a representation of part of human chromosome 9 showing LINC00961 and its surrounding genes. Bottom panel is a representation of part of mouse chromosome 4 showing conservation of the LINC00961 locus and its surrounding genes. Arrows represent direction of transcription on forward strand (right side arrow), or reverse strand (left side arrow). Large clusters comprising mainly of olfactory related genes have been grouped and labelled olfactory clusters 1 and 2 for simplicity. These loci representations were assembled with reference to ENSEMBL human genome GRch38p7 and mouse genome GRcm38.p6.

At the start of this project there was only 1 publication on LINC00961 by Zheng & colleagues (2016) who utilised RNA-seq and reported LINC00961 to be upregulated 2.5- fold in cisplatin resistant ovarian cancer, however, they did not explore its role further [233]. Shortly after, Matsumoto & colleagues (2017) published their work focussing on the function of the SPAAR micropeptide and not LINC00961 itself; they reported that SPAAR regulates skeletal muscle regeneration via negative regulation of amino acid stimulation of the mammalian target of rapamycin complex 1 (mTORC1), and that downregulation and deletion of SPAAR promoted muscle regeneration and maturation post cardiotoxin injury through de-repression of mTORC1. They also show a 158.8- fold increase in LINC00961 locus expression in murine skeletal muscle compared to bone marrow and a 15.3- fold increase in the heart. LINC00961 was also highly expressed in other vascular enriched tissues such as the kidney (3- fold increase, human and mouse), lungs (35- fold increase, human), and placenta (88- fold increase, human) [232].

At present, literature regarding LINC00961 mostly focuses on its expression in various cancers. Figure 1.6 summarises the pathways which LINC00961 has been implicated in based on all current publications, described in detail in the following paragraphs. Interestingly, several studies have implicated LINC00961 in non-small cell lung carcinoma (NSCLC). Yu and colleagues (2015) reported that LINC00961 was downregulated 1.62- fold in NSCLC; similarly, Huang & colleagues (2018) also reported significant downregulation of LINC00961 in NSCLC tissues [234]. Jiang & colleagues (2018) associated downregulated LINC00961 expression in NSCLC with a later cancer stage and shorter patient survival time [235] [236]. In the same study, the authors concluded that LINC00961 may act as a tumour suppressor in the context of NSCLC and found that the epigenetic regulator lysine demethylase 1A (LSD1) physically binds to the promoter of LINC00961 causing its repression in epithelial lung cells [236]. Collectively, these studies established that LINC00961 inhibits migration, invasion, metastasis [236], proliferation, and induces apoptosis [234] in NSCLC cells. Additionally, LINC00961 has been associated with lung squamous cell carcinoma in the recent paper from Liu & colleagues (2020) who identified LINC00961 in a panel of 11 lncRNAs associated with patient prognosis and identified it as a ‘high-risk’ gene [237].

Downregulation of LINC00961 appears to be an emerging pattern in other cancers, as its downregulation has been correlated with poor prognosis in hepatocellular

carcinoma (HCC) patients and is also downregulated in HCC cell lines. The authors identified a novel mechanistic pathway whereby LINC00961 sponges miR-5581-3p, subsequently de-repressing human cardiolipin synthase 1 (CRLS1), which is reported to repress HCC cell growth; however, with reduced LINC00961, miR-5591-3p levels rise, inhibiting CRLS1 [238]. Chen & colleagues (2018) discovered that LINC00961 was significantly downregulated in renal cell carcinoma (RCC) cell lines compared to healthy cell lines, as well as being downregulated in RCC patients [239]. In this instance the authors began investigating the modulation of the proteins slug and N-cadherin and reported their upregulation upon LINC00961 KD *in vitro,* suggesting a role for LINC00961 in the shift of gene expression towards an epithelial to mesenchymal transition phenotype, however, the evidence to support this was inadequate to come to a firm conclusion and therefore requires further investigation [239]. Other recent studies include the work by Amini & colleagues (2020) who reported that LINC00961 was downregulated in later stage gastric cancer and suggested its use as a novel biomarker for gastric cancer [240]. Interestingly, Mu & colleagues (2019) identified miR-26a, miR-107, miR-367, and miR-5581 as likely downstream targets of LINC00961 based on the potential presence of LINC00961 binding sites, identified using the miRDB database [241]. In the same study, further investigation in melanoma cell lines identified miR-367 expression to be significantly conversely correlated with LINC00961 expression, supporting the hypothesis for its regulation by LINC00961. The authors further reported that the LINC00961 – miR-367 axis regulated the phosphate and tension homologue protein (PTEN) [241], which acts as a tumour suppressor in melanoma [242]. Recently, Layeghi & colleagues (2020) concluded that LINC00961 was downregulated in luminal breast cancer and 2 breast cancer cell lines, compared to adjacent non-cancerous tissues and a normal breast cell line [243]. Lastly, Wu & colleagues (2020) identified LINC00961 as downregulated in colon cancer and through *in vitro* assays identified that it supresses the migration and invasion of colon cancer cells through sponging miR-233-3p which de-represses SOX11 expression [244].

More relevant to this project is the work of Di Salvo and colleagues (2015) who showed a log2fold change of -1.4 in the right ventricle of patients with heart failure compared to healthy unused donor control hearts [245], highlighting that this lncRNA may be of clinical relevance in cardiovascular diseases as well as in certain cancers. Furthermore, LINC00961 has been identified in multiple pathways pertaining to cardiovascular disease; Wu and colleagues (2019) reported that LINC00961 was

downregulated in patients with coronary artery disease and in ApoE$^{-/-}$ mice (a model of atherosclerosis), and that it sponges the previously mentioned miR-367 in SMCs in these patients [246]. This is the same miR that was identified to be potentially regulated by LINC00961 in the work of Mu & colleagues (2019) above, further validating the LINC00961- miR-367 pathway alongside Wu & colleagues (2019) positive luciferase assay experiments [241] [246]. Liu and colleagues (2019) described a potential pathway for LINC00961 in CM hypoxic injury. They show that 24 h of hypoxia increased LINC00961 expression in the H9C2 rat cardiomyoblast cell line and caused an increase of the transcription factor signal transducer and activator of transcription 1 (STAT1), which they showed physically interacted with the promoter of LINC00961 to induce its expression. Downstream phosphorylation of phosphoinositide 3-kinase (PI3K), AKT, and glycogen synthase kinase-3β (GSK3β) were also inhibited [247]; this is of interest as activation of this pathway has been implicated in negating the pathological remodelling in the heart post hypoxia/ reperfusion injury [248].

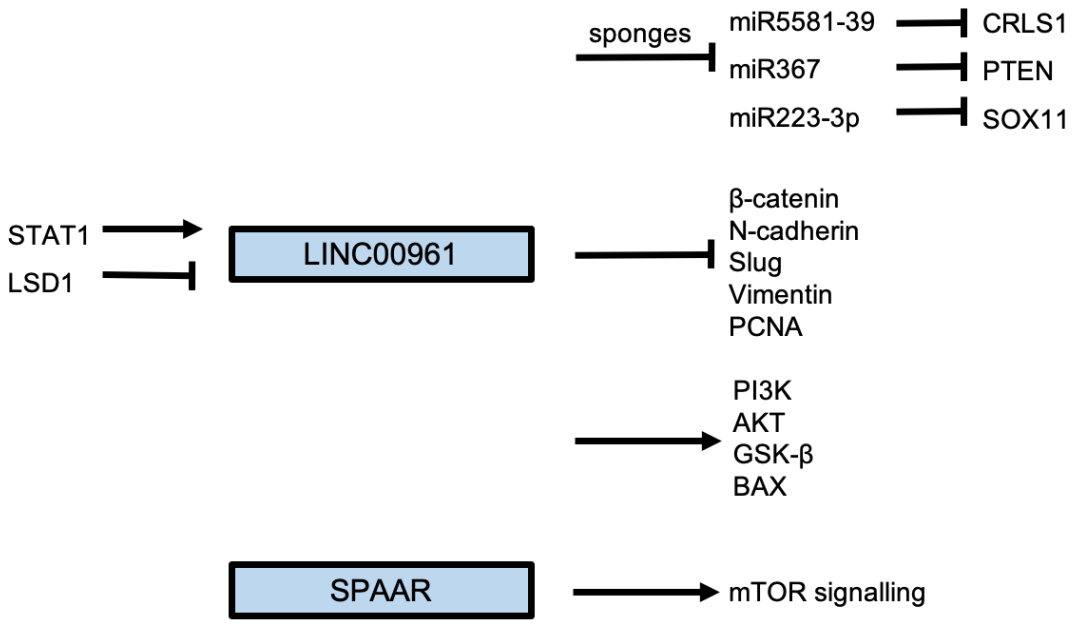

Figure 1.6 Summary of published data regarding LINC00961 and SPAAR interactions.

This figure illustrates pathways the LINC0961 locus has been implicated in. This data was gathered from research in non-small cell lung cancer, tongue squamous cell carcinoma, hepatic cell carcinoma, renal cell carcinoma, glioma, melanoma, colon cancer, gastric cancer, cardiomyocytes following MI, and in skeletal muscle regeneration. Arrows indicate induction or promotion whilst flat ends indicate inhibition [247] [236] [238] [241] [246] [240] [249] [239] [250] [234] [232].

1.9 Hypotheses and aims

Hypotheses:

1) The human LINC00961 locus is essential to EC function.
2) The human LINC00961 RNA transcript is responsible for the contribution of this locus to EC function.
3) The murine LINC00961 locus function is conserved in mice.

Aims:

To investigate the above hypotheses, the aims of this thesis are:

1) To evaluate the phenotype in human ECs following knock down (KD) of LINC00961 locus expression by focusing on EC functional assays, with particular focus on angiogenesis.
2) To identify the mechanism(s) through which LINC00961 elicits its effects; this involves determining if LINC00961 works solely through its encoded micro-peptide, the lncRNA itself, or through a combination of LINC00961 and SPAAR.
3) To identify the role LINC00961 plays *in vivo* by utilising a knockout (KO) mouse line. To test the above hypothesis this thesis will utilise the murine HLI model of angiogenesis to assess the regenerative function of the endothelium in LINC00961$^{-/-}$ mice.

Chapter 2 Methods and Materials

2.1 Ethical approval

All donated human tissues utilised in this project conformed to the principles outlined in the Declaration of Helsinki (Ethics 15/ES/0094). The human saphenous vein endothelial cells (HSVECs) used for RNA-seq analysis were collected by enzymatic collagenase digestion of human saphenous vein samples (Ethics 15/ES/0094).

2.2 Cell culture

2.2.1 Human umbilical vein endothelial cells

Human umbilical vein endothelial cells (HUVEC) (Lonza, Basel Switzerland) were cultured in the EC growth medium EGM2 (Lonza, Basel Switzerland) supplemented with 10 % foetal bovine serum (FBS) (Life Technologies, Paisley UK) and grown at 37 ^{o}C with 5 % CO_2. Growth factors in the EGM2 were hydrocortisone 0.2 ml, human fibroblast growth factor B2 (FGF-B2) 2 ml, VEGF 0.5 ml, Insulin-like growth factor (with long arginine) 0.5 ml, ascorbic acid 0.5 ml, human erythroid growth factor (hEGF) 0.5 ml, Gentamicin sulfate-Amphotericin-1000 0.5 ml, and heparin 0.5 ml. Cells were used for experiments between passages 2 - 5.

2.2.2 Mouse endothelial-like cell lines

Three murine endothelial like cell lines were cultured in Dulbecco's Modified Eagle Medium (DMEM) (Life Technologies, USA) with 10 % FBS and 1% penicillin and streptomycin at 37 ^{o}C with 5 % CO_2: murine brain microvascular endothelial cell line (bEND3), SVEC4-10, and IP1B. The murine cardiac endothelial cell line (MCEC) was cultured in DMEM supplemented with 5 % FBS, 1 % penicillin and streptomycin, and 10 mmol/L HEPES buffer at 37 ^{o}C with 5 % CO_2. Flasks for MCEC use were pre-coated with 0.2 % gelatin (Sigma-Aldrich, USA) and excess gelatin removed before seeding cells.

2.2.3 Human embryonic stem cell differentiation

Previously the Baker lab published a human embryonic stem cell (hESC) to EC differentiation protocol which uses the commercially available H9 hESCs [84]. This protocol was performed by Dr Boulberdaa and colleagues prior to my arrival in the lab, and the resultant ECs were used for RNA-sequencing (RNA-seq). The protocol is as follows: H9 cells were dissociated into single cells using 1×10^4 Tryple Select (Life Technologies, UK) then seeded onto 5 % Pluronic F-127 (Sigma-Aldrich, UK)

coated 96 well round bottom microplates to generate embryoid bodies (EBs). Plates were centrifuged at 300 X g for 3 min and Stemline II Hematopoietic expansion culture medium supplemented with 5 ng/mL Activin A (Peprotech, USA), 10 µmol/L Y-27632 (Millipore, Temecula, USA, 10 ng/mL vascular endothelial growth factor (Peprotech, USA), and 10 ng/mL bone morphogenetic protein 4 (BMP4) (R and D Systems, Minneapolis). Cells were incubated for 48 h with Stemline II Hematopoietic expansion medium, this time containing 10 ng/mL VEGF, 70 ng/mL Wnt3A, 140 ng/mL BMP4 and 35 ng/mL Activin A. After 3 days of culture EBs were transferred to 0.1 % gelatine coated 6 well culture dishes and resuspended in EGM- 2 supplemented with 50 ng/ml of VEGF and the accompanying bullet kit, without its VEGF and FBS, and grown until day 7. For the flow cytometry analysis of the differentiating populations, cells were dissociated by enzymatic digestion, harvested, washed in phosphate buffered saline (PBS), and incubated with specific antibodies. Fluorescently activated cell sorting (FACS) was then performed using anti-human CD326, anti-human CD56, anti-human CD31, and anti-human CD144 by FACS Aria I or Aria III cell sorters (BD Biosciences, San Diego, USA) and RNA isolated from the resultant sorted populations.

2.3 RNA Analysis

2.3.1 RNA Isolation and quantification

RNA was isolated using the QIAzol lysis reagent miRNeasy mini kit (Qiagen, Hilden, Germany) and the manufacturer's protocol. Digestion of genomic DNA was incorporated into the protocol by adding a 5 min DNase 1 incubation. Final RNA concentration and quality was determined using the NanoDrop ND-1000 Spectrophotometer (Nano-Drop Technologies, DE). RNA was immediately stored at -80 ^{o}C.

2.3.2 RNA sequencing

Illumina RNA-seq was performed (45 million paired-end reads per sample) on ribosomal RNA depleted libraries from several replicates of the different cell populations from the differentiation of ECs from the hESC-EC. This protocol was carried out and analysed similarly to the methods previously published by the Baker lab [187] with the RNA-seq data deposited at the Gene expression Omnibus as reference GSE118106. Samples for each population were N=4 hESCs, N=4 mesodermal and non-mesodermal at 3 days, N=2 endothelial and non-endothelial at 7 days, and N=4 HSVEC controls. Publicly available expression data from the

ENCODE Consortium for multiple EC and SMC lines were also accessed for comparison. Dr Julie Rodor carried out the bioinformatic analysis throughout this project.

2.3.3 RNA fractionation

RNA fractionation was performed as previously described [84] and as per manufacturer's instructions (Paris Kit, Life Technologies, UK). Briefly, HUVECs were dissociated and homogenized in 500 μl ice-cold Fractionation Buffer and incubated for 10 min on ice. Nuclei were separated from the cytoplasmic fraction by centrifugation at 500 X g for 5 min. The cytoplasmic supernatant was collected and stored on ice, meanwhile 500 μl of fractionation buffer were added to the pellet and centrifugation repeated and supernatant discarded. Next, 500 μl of disruption buffer was added and sample vortexed, followed by 500 μl of 2 X lysis buffer at room temperature. Cytoplasmic and nuclear fraction samples were then mixed with 500 μl absolute ethanol, before applying sample to a filter cartridge and centrifuged at 500 X g for 1 min. Cartridges were washed with 350 μl of wash solution 1 at room temperature followed by premade DNase I mix (10 μl DNase: 70 μl RDD buffer per sample) incubation for 10-15 min at room temperature; a further 350μl wash solution 1 was added and brief centrifugation were then carried out. Next, samples were washed twice with 500 μl wash solution 2/3 and centrifuged. The membrane was dried with a final 2 min centrifugation and lastly, RNA was eluted with 50 μl of elution buffer, pre-heated to 95 ^{o}C, and then samples used to make cDNA. Remaining samples were stored at -80 ^{o}C.

2.3.4 cDNA Synthesis

Standard cDNA synthesis utilised 300 ng RNA in a 40 μl reaction using the MultiScribe™ Reverse Transcriptase kit (Life Technologies, Paisley, UK). Thermocycler cycles were as follows; 10 min at 25°C, 30 min at 48°C, 5 min at 95°C and finally samples were stored at 4°C for immediate use, or stored longer term at -20°C.

2.4 Quantitative real time PCR

2.4.1 SYBR Green qRT-PCR

LINC00961 gene expression was assessed using SYBR Green based qRT-PCR analysis. This used Power SYBR Green PCR Master Mix (Thermo Fisher, Paisley, UK) and custom PCR primers (Eurofins MWG, Ebensburg, Germany) designed to

target LINC00961. The expression of housekeeping genes human and mouse Ubiquitin protein C (UBC) and murine Glyceraldehyde 3-phosphate dehydrogenase (GAPDH) were used as endogenous controls to normalise changes in target gene expression. Several other genes were also analysed using SYBR Green; all primer sequences are in Table 2.1. All reactions were carried out in triplicate using a QuantStudio 7 Flex Real-Time PCR System real time PCR system (Thermo Fisher, Paisley, UK).

2.4.2 Taqman© qRT-PCR

Some gene expression experiments were performed using the TaqMan® Universal Master Mix II and TaqMan® Gene Expression probes following the manufacturer's protocol (Thermo Fisher, Paisley, UK). All reactions were carried out in triplicate using a QuantStudio 7 Flex Real-Time PCR System real time PCR system (Thermo Fisher, Paisley, UK). Taqman© probes and order codes are in Table 2.2.

2.4.3 qRT-PCR cycle protocol

Both SYBR Green and Taqman© based assays underwent the following cycling qRT-PCR cycling conditions; 1 cycle of 95^{o}C for 10 min, followed by 40 cycles of 15 seconds at 95^{o}C and 60^{o}C for 60 seconds using the QuantStudio 7 Flex Real-Time PCR System (Thermo Fisher, Paisley, UK).

2.4.4 Analysis of qRT-PCR

The 2-ΔΔCt method first described by Livak & Schmittgen [251] was utilised to calculate the fold change in gene expression between experimental and control conditions. Fold change is presented as relative quantification (RQ) on graphs. Raw data was exported into Microsoft Excel for analysis and graphed using GraphPad Prism. For identifying LINC00961 in murine endothelial-like cell lines, data are presented using the 1/ΔCt calculation.

	Transcript	Forward sequence 5'-3'	Reverse sequence 3' -5'
Human	GAPDH	ACAGTCCATGCCATCACTGCC	GCCTGCTTCACCACCTTCTTG
	UBC	TTGCCTTGACATTCTCGATG	ATCGCTGTGATCGTCACTTG
	LINC00961	ACCAGGGAATCTGTGCTCACG	GAAGATGCTGCTCTGAGTCCC
	ERG	GGAGTGGGCGGTGAAAGA	AAGGATGTCGGCGTTGTAGC
Mouse	GAPDH	TGTGAACGGATTTGGCCGTA	ACTGTGCCGTTGAATTTGCC
	LINC00961	GTCACCAGCTCCAGATACAGT	ATGTTGCTAAGACGGAAGCCA
	NEAT1	AGCAGCTTGTCAACTCTCTGG	CCTGCAGTGCCATTATCCCAT
	MALAT1	GCAGTGTGCCAATGTTTCGT	GCTGTTTCCTGCTCCGAGAT

Table 2.1 List of human and murine SYBR Green qRT-PCR primers.

	Taqman Probe Name	Code
Human	GAPDH	Hs02786624_g1
	UBC	Hs05002522_g1
	HRCT1	Hs02742472_s1
	EGFL7	Hs01552509_m1
	SHEP1 (SH2D3C)	Hs01552509_m1
	NPDC1	Hs00209870_m1
	VEGFA	Hs00900055_m1
	VEGFC	Hs01099203_m1
	TMSB4X	Hs03407480_gH
	MSI2	Hs01592569_m1
Mouse	UBC	Mm02525934_g1
	HRCT1	Mm01353653_s1
	EGFL7	Mm00618004_m1
	SHEP1/SH2D3C	Mm01330274_m1
	NPDC1	Mm00476483_m
	VEGFA	Mm00437306_m1
	VEGFC	Mm00437310_m
	MSI2	Mm01304232_m1
	TMSB4X	Mm01129684_g1
	WT1	Mm01337048_m1
	SMARCA 4	Mm01151944_m1
	PAX7	Mm01354484_m1
	MYOG	Mm00446194_m1
	RASIP1	Mm00510273_m1

Table 2.2 List of human and mouse Taqman© probes used for qRT-PCR. Probe/gene name shown with its order code.

2.5 Lentiviral production and infection

Lentiviral vectors were developed and titrated by Dr Helen Spencer using HEK293T cells triple transfected with; a plasmid encoding the envelope of vesicular stomatitis virus (VSVg) (pMDG) (Plasmid Factory, Bielefeld, 130 Germany), a packaging plasmid (pCMV∆8.74) and pLNT/SFFV plasmid employing polyethyleneimine (PEI; Sigma-Aldrich, USA). Quantification was carried out using qRT-PCR with the primers: forward, 5'-TGTGTGCCCGTCTGTTGTGT-3'; reverse, 5'-GAGTCCTGCGTCGAGAGAGC-3'; probe, 5'- (FAM)-CAGTGGCGCCCGAACAGGGA- (TAMRA)-3. The sequences to overexpress LINC00961 full-length, ΔΔATG961 and SPAAR were generated by GeneART Gene synthesis (Life 136 Technologies, UK), and were cloned into pLNT/SFFV-MCS using the *Kpn*I and 137 *Xho*I sites. For all experiments a negative control lentivirus was also used. Multiplicity of infection (MOI) refers to the ratio of viral particles compared to the number of target cells; for all experiments a MOI of 10 was used using, calculated with the formula:

$$\frac{Cell\ no. \times\ MOI}{Viral\ Titre} = \mu\text{L of virus / well}$$

2.6 *In vitro* assays and protocols

2.6.1 Transfection protocol

To knock down LINC00961 expression several dicer-substrate short interfering RNA (siRNA) sequences were designed and purchased from IDT (Leuven, Belgium). Some protein coding gene expression was also knocked down utilising siRNA; see Table 2.3 for all siRNA sequences. Transfections were performed with siRNA using Lipofectamine RNA iMAX (Life Technologies, Paisley, UK)) according to manufacturer's instructions. Briefly, 3 µl of Lipofectamine per well of a 6 well plate were used, in 1 ml per well of optiMEM media (Life Technologies, USA) and the required dose of siRNA in 1 ml per well of optiMEM, prepared separately and incubated for 5 min before being combined. Mixtures were combined and incubated for a further 5 min before adding to cells. Cells were then incubated at 37 ^{o}C for 4 - 6 hr then supplemented with 1 ml of their normal growth medium. Media was removed from cells after 24 and 48 hr, and cells utilised for either RNA extraction or tubule formation assays. Negative control siRNA (IDT, Leuven, Belgium) which lacked target

specificity, was used in all experiments, as well as untransfected cells and a mock condition where Lipofectamine only was transfected.

	Name	Sense strand sequence 5'-3'	Antisense strand sequence 3'- 5'
	Negative Control (NC1)	rCrGrUrUrArArUrCrGrCrGrUrArUrArArUrArCrGrCrGrUAT	rArUrArCrGrCrGrUrArUrUrArUrArCrGrCrGrArUrUrArArCrGrArC
Human	HRCT si1	rGrCrArCrArGrUrCrArArUrUrCrArUrCrGrGrUrGrCrCrUTA	GrArCrGrUrGrUrCrArGrUrUrArArGrUrArGrCrCrArCrGrGrArArU
	HRCT si2	rGrArCrUrUrUrGrCrArUrGrGrCrArUrGrCrCrCrCrArGrUGT	GrArCrGrUrArArArCrGrUrArCrCrGrUrArCrGrGrGrGrUrCrArCrA
	ERG	rCrArGrArUrCrCrUrArCrGrCrUrArUrGrGrArGrUrArCrAGA	rUrCrUrGrUrArCrUrCrCrArUrArGrCrGrUrArGrGrArUrCrUrGrCrU
Mouse	Si1 LINC00961	rGrUrCrArUrCrArCrCrArUrGrGrCrCrArUrUrArCrCrUrGrCrA	rArArCrArGrUrArGrUrGrGrUrArCrCrGrGrUrArArUrGrGrArCrGrU
	Si2 LINC00961	rCrGrUrCrArCrUrUrArGrGrArArUrGrArUrArGrArArArAAT	rArCrGrCrArGrUrGrArArUrCrCrUrUrArCrUrArUrCrUrUrUrUrUrA

Table 2.3 List of human and murine siRNA sequences.
Human ERG siRNA sequence obtained from Dufton & colleagues (2017) [252].

2.6.2 Tubule formation assay

Tubule formation assays were performed using Matrigel© (Corning, USA). Matrigel© was defrosted overnight on ice at 4 ^{o}C in preparation for use the next day. To prepare the wells of a 96 well plate, 70 µl Matrigel© were added on ice and allowed to set for 30 min at 37 ^{o}C. Cells were then plated at a seeding density of 1 x 10^4 for HUVECs and 2 X 10^4 for bEND3 cells in EGM-2 medium (LONZA, UK) and incubated for 5 hr at 37 °C with 5 % CO_2. For experiments where cell viability was confirmed with Calcein AM (Invitrogen, USA), media was aspirated and replaced with Calcein AM diluted 1/500 in the cells' normal medium without FBS. Cells were returned to the incubator

for 30 min then imaged using a fluorescent Nikon ECLIPSE Ti2/ Brightfield images of the tubule networks were taken on a Nikon TS100-R. Assays were performed in triplicate and total branch length was determined using the Angiogenesis Analyser plug in for Image J (FIJI) software and data averaged across the 3 wells per condition.

2.6.3 Endothelial barrier integrity assay

Electric Cell-substrate Impedance Sensing (ECIS) assays were carried out with 8-well arrays (8W1E) on an ECIS® Z-Theta station (Applied Biophysics), as per the manufacturer's instructions. The 8-well arrays were prepared by washing with 10 mM L-cysteine (Sigma-Aldrich, UK) and coated with type I rat tail collagen (Sigma-Aldrich, UK). Previously transfected HUVECs were seeded at a density of 4 X 10^4 per well and left in the incubator overnight to form a monolayer. The next day impedance was then measured over a 10 hr period and analysed using ECIS mathematical software (Applied Biophysics) to calculate cell barrier resistance, expressed as Rb [Ohm x cm^2]. Data were exported to Microsoft Excel for further analysis and graphed using GraphPad.

2.6.4 Hypoxia chamber

Cells were plated in 6 well pates and left overnight in the incubator to adhere. The following day media was replaced, and cells were placed into a 14500 Coy Cabinet - hypoxia chamber (Coy Laboratory Products, USA) set to 1% O_2 (5% CO_2 and 94% N_2) for 24 or 48 hr before removal and immediate treatment with quizol for RNA extraction.

2.6.5 Proliferation assay

The nuclear incorporation of 5-Ethynyl-2´-deoxyuridine (EdU) was used to quantify cell proliferation using the Click-it EdU 488 Proliferation assay (Life Technologies, UK) as per manufactures instructions. Briefly, HUVECs were seeded at a density of 1 x 10^4 per well of a 96 well plate and left to adhere. After 24 hr cells were put into serum starvation conditions for a further 24 hr, consisting of DMEM medium supplemented with 2% heat-inactivated FBS, 50 µg/mL penicillin, 50 µg/mL streptomycin, 2 mmol/L L-Glutamate and 1 mmol/L sodium pyruvate. Following serum starvation, proliferation was induced by culturing cells in complete EGM-2 with 10 % FBS and 10 µM EdU for 24 hr. The percentage of EdU positive cells was analysed by flow cytometry and an anti-EdU 488 antibody following cellular dissociation and fixing in cold 70 % ethanol.

2.6.6 Migration assay

Cell migration assays were performed by Dr Helen Spender using an ECIS machine (Applied BioPhysics) as per Manufacturer's instructions. Briefly, 6 x 10^4 HUVECs were plated in each well of an ECIS wound healing array. The conditions were set to: electroporate 2500 µA; wound: 30 sec; frequency 40000. The rate of migration was calculated after 24 hr using the formula; velocity=r/t, where the radius was 125 µm.

2.6.7 Immunocytochemistry

Cells were fixed for 30 min at room temp with 4 % paraformaldehyde and washed with phosphate buffered saline (PBS) containing 1 % glacial acetic acid (Sigma-Aldrich, UK). Next, cells were permeabilised with 0.1 % Triton-X-100 (Thermo Fisher, UK) in PBS for 5 min at room temperature. A further PBS wash was carried out and cell were blocked for 30 min at room temperature with 5 % goat serum in PBS. The thymosin beta 4-x antibody (Abcam 14335) was diluted 1/200 in 5 % goat serum and incubated on cells for 1 hr at 37 ^{o}C. The primary antibody solution was washed off using PBS and cells incubated with a secondary antibody (goat anti rabbit Alexa-Fluor-488, Abcam 150077) diluted 1/400 in 5 % goat serum for 45 min at 37 ^{o}C, protected from light. Finally, cells were washed with PBS and then mounted with ProLong Gold containing DAPI (Thermo Fisher, UK). Images were taken on a Zeiss LSM 780 confocal microscope.

2.6.8 RNA fluorescent *in situ* hybridisation

All RNA fluorescent *in situ* hybridisation (FISH) experiments were carried out by Dr Helen Spencer using 20 tiled digest oligo probes targeting exons 1 and 2 of human LINC00961, which were custom generated, and RNA- FISH performed following the manufacturer's instructions (QuantiGene ViewRNA cell ISH cell assay, Life Technologies, UK). Probes targeting SNORD3 and UBC were used nuclear and cytoplasmic controls, respectively (Life Technologies, UK). HUVECs were seeded at 1 x 10^4 on 0.2 % gelatin coated 16 mm coverslips and allowed to grow up 80 % confluency. Cells were then fixed in 4 % formaldehyde supplemented with 1 % glacial acetic acid. Detergent QS permeabilise the cells and following a 1:6000 protease digest, cells were then incubated with the probes, with unstained cells as a negative control. After probe hybridisation, cells were incubated with pre- amplifier for 1 hr and, then amplifier for 30 minutes. Cells were incubated with secondary fluorescent probes, and mounted with medium containing DAPI (Vectorshield, UK). Imaging was

carried out using an Andor Revolution XDi spinning disk confocal microscope, and generated Z-stacked files, with the assistance of University of Edinburgh's Confocal and Advanced Light Microscopy Facility.

2.6.9 Western blotting

Cells were washed with PBS and resuspended in 200 µl of RIPA buffer (Life Technologies, UK) supplement with cOmplete Mini, EDTA-free Protease Inhibitor Cocktail tablets (Roche, UK). Lysates were incubated on ice for 30 min then were centrifuged at 15000 X g for 10 min at 4 °C to remove cell debris. Total protein concentration was determined using a Pierce™ BCA Protein Assay Kit (Thermo Fisher, UK) and a Perkin Elmer Victor 2 Microplate Reader. Western blots were then conducted on the Life Technologies Bolt System as per manufacturer's instructions (Life Technologies, UK) and as follows: 30 µg of proteins were diluted in 4 X reducing bolt loading buffer (Life Technologies, UK) and boiled for 5 min at 95°C to denature proteins, and then vortexed. Samples were loaded into a 10 % bolt acrylamide pre-cast gel (Life Technologies, UK) and electrophoresis separation was set up at 200 volts (V) for 1 hr 15 min. Next, proteins were transferred onto a nitrocellulose membrane and transferred at 10V for 1 hour. Membranes were blocked in 5 % milk for 1 hr. The SPAAR antibody (Cell Signalling, USA) and β-Actin antibody (Abcam) were incubated on a roller at 1:1000 overnight at 4 °C. Secondary antibodies were used at 1:5000 (Li-Cor, UK). Finally, the membrane was washed 3 X in TBS-T for 10 min each and band detection performed using (Li-Cor, UK).

2.7 Protein pull-down

All protein pull-down experiments were performed by Dr Helen Spencer. For LINC00961 protein pulldowns: The T7 RiboMAX Express Large-Scale RNA Production System (Promega, UK) was used to generate biotinylated LINC00961 (50 pMol). This RNA was then incubated with streptavidin magnetic beads and 20 µg of HUVECs protein lysate, and the Pierce Mag RNA Protein Pull-down kit (Thermo Scientific) protocol followed.

For SPAAR protein pull-down experiments, HUVECs were infected with our lentiviral constructs; LV-Null, LV-SPAAR untagged, or LV-SPAAR-HA with contained a HA-tag. Anti-HA antibody immunoprecipitation, with an anti-IgG antibody control was then

carried out. These samples for mass spectrometry were sent to the IGMM Mass Spectrometry facility, University of Edinburgh, who generated the data.

2.8 *In vivo* work

2.8.1 Animal ethical approval

All animal experiments were performed in accordance with the Animals (Scientific Procedures) Act (UK) 1986 and under the auspices of UK Home Office Project and Personal Licenses held within The University of Edinburgh facilities. Prior to experiments approval was granted by the University of Edinburgh veterinary staff.
Project license holders:
Dr Patrick Hadoke 60/4523 - colony maintenance and HLI experiments.
Dr Gillian Gray 70-8933 - MI experiments.

Personal license numbers:
Rachel Sanders I85C48607.
Dr. Marco Meloni ID59EF5FC.
Dr. Ana-Mishel Spiroski I8D6B6351.

2.8.2 Generation of LINC00961$^{-/-}$ line

A global LINC00961 locus knock out (KO) mouse line was generated by Taconic Biosciences (USA), using CRISPR/Cas9 technology on a C57BL/6nTAC genetic background. Utilising two guide RNA (gRNA) strands targeted against regions flanking the locus, the Cas9 enzyme induced double stranded DNA breaks leading to deletion of the entire locus (Figure 4.2A). Heterozygous breeding trios were used to establish and maintain the colony, and to generate wild type (WT) and KO littermates for *in vivo* experiments and tissue collection.

Guide strand	Sequence
gRNA 1 (proximal)	ATACACTCCTCGCTCAATGT
gRNA 2 (distal)	CGAGGCTACGCTGTCAGTACT

Table 2.4 Sequences of gRNA used in generation of CRISPR/Cas9 mediated LINC00961 KO mouse.

2.8.3 Colony generation

Six mice were received from Taconic© that had undergone CRISPR/Cas9 deletion of the LINC00961 locus and were therefore mosaic founders. These founders were bred with WT C57BL/6 mice to produce LINC00961 heterozygous mice which served as the first breeders to establish this colony. Ear clip samples from all pups were outsourced to Transnetyx© for genotyping. A number of KO and WT mice were then re-genotyped in house, using RNA extracted from their kidney and used to make cDNA for qPCR analysis, confirming their LINC00961 status from Transnetyx© (Figure 4.2 B, primer sequences in Table 2.1). A subset of offspring were weighed weekly post-weaning to check their health and culled at 9 weeks of age for tissue harvesting and characterisation, with male and female data analysed separately throughout.

2.8.4 Genotyping and maintenance of the LINC00961$^{-/-}$ line

Pups were ear clipped for identification purposes and this tissue used to genotype animals by outsourcing to Transnetyx©. Heterozygous animals were used for breeding to generate animals of all possible genotypes (WT, KO and heterozygotes) for further experiments and to maintain the colony.

2.8.5 Euthanasia

Animals were euthanised with Pentoject/Euthatal (160 mg/kg) administered by intraperitoneal injection. Tissues were then perfusion fixed by snipping the right atria, and intracardiac puncture and infusing with PBS at 6 ml/min using a micro pump; followed by perfusion with 4% paraformaldehyde (PFA) at 6 ml/min. Perfusion fixation of tissues was carried out by Rachel Sanders, Dr Marco Meloni, and Dr Ana-Mishel Spiroski. If perfusion fixation was not required e.g., for collection of samples for freezing / RNA / protein collection), animals were culled *via* cervical dislocation and confirmation of cessation of circulation.

2.8.6 Murine hind limb ischemia

Mice were anesthetised with inhalation isoflurane 4 % with oxygen for induction of unconsciousness, and 1% - 2% isoflurane with oxygen for maintenance of anaesthesia for all surgical procedures and Laser Doppler acquisition. Surgical ligation and cauterisation of the left femoral artery was performed by Dr. Marco Meloni (femoral vein and nerve were left untouched) on male LINC00961$^{-/-}$ and WT littermates at 11 weeks of age. Laser Doppler imaging and analyses were performed by Rachel Sanders. To carefully control the conditions under which LDPI was performed, each mouse was warmed on a heating pad for 5 minutes prior to imaging to stimulate vessel dilation and imaging was performed blind to genotypes. The feet were used to calculate the perfusion ratio between the ischemic and control limbs by carefully drawing around the feet in the moorLDI imaging software using the ankle joint of the foot to maintain consistency. Mice were monitored after surgery and kept warm in a hot box heated to 37 ^{o}C whilst recovering. peri-operative analgesic cover (subcutaneous injection of buprenorphine at 0.05 mg/kg. Mice utilised for histological purposes were injected with 5-ethynyl-2'-deoxyuridine (EdU) at day 0 (time of surgery), and days 2, 4, 6, 9, and 12 post-surgery, to label actively dividing cells. Mice were given 100 µl of EdU solution containing 417 µg EdU diluted in sterile H_2O via intraperitoneal injection (administered by Rachel Sanders or animal unit technicians). Animals were sacrificed at 7 and 21 days post-surgery, and the adductor muscles

used for downstream analysis. Tissues required for RNA extraction were snap frozen in liquid N_2 and stored at -80 ^{o}C.

2.8.7 Cardiac ultrasound echocardiography

Baseline cardiac function on 8 week old male and female mice, and on females 7 and 14 days post-MI data was collected by ultrasound echocardiography with Doppler flow under isoflurane anaesthesia (4% induction, ~1.25% maintenance) by Mr Adrian Thomson (Edinburgh Imaging) using the Vevo 770 and Vevo 3100 preclinical imaging systems with Vevo Lab V3.0 and V3.2.6 software. Briefly, formats collected include: Two-dimensional brightness mode (B-mode) with Doppler flow, and motion mode (M-mode). Left ventricle parasternal long and short axes, and ECG-gated Kilohertz Visualisation. Data were analysed by Dr. Ana-Mishel Spiroski in JMP 12 software where data were assessed for normality.

2.8.8 Murine myocardial infarction

For chronic myocardial infarction (MI) studies which lasted 2 weeks, mice were anesthetised with a mix of 100 mg/kg ketamine and 10 mg/kg xylazine. For acute (30 min) MI studies, mice were anaesthetised with 70 mg/kg of pentobarbitone. Surgeries were performed by Dr Ana-Mishel Spiroski, as previously described elsewhere [253]. Briefly, following induction of anaesthesia, animals were endotracheally intubated and put onto a ventilator set at 100 breaths per min, and a tidal volume of 150 µl. The heart was exposed via. Thoracotomy and delicately puncturing the epicardium to reveal the left descending coronary artery (LAD) which was permanently ligated with a 7-0 prolene suture. Animals were closed and monitored throughout the day whilst recovering from the procedure. For chronic MI studies, Isolectin b4 was injected 15 min prior to euthanasia via tail vein injections performed by Mr. William Mungall (Edinburgh University, animal unit surgical technician) (100 µl of 2 mg/ ml, Sigma-Aldrich, UK).

2.9 Tissue analysis

2.9.1 Histology processing

Dissected tissues (adductor muscle or heart) were placed into 4% PFA overnight at 4^{o}C, and then PFA replaced with PBS for 24 hr before transferring to 70% ethanol and embedding in paraffin by the SuRF histology service at Edinburgh University. Tissues were cut into 5 µm thick sections on a microtome (Thermo Fisher) and baked onto slides overnight at 50 ^{o}C. Haematoxylin and Eosin staining on the adductor muscle sections was carried out by staff at the SurF histology service at Edinburgh University. For heart sections anatomical landmarks such as the papillary muscles and the appearance of the right ventricle were used to guide section cutting from the apex upwards.

2.9.2 Immunohistochemistry

Tissue sections were deparaffinised and rehydrated through incubations in xylene (2 X 5 min), 100% ethanol (2 X 5 min) 95% ethanol (3 mins, 70% ethanol (3 min), 50% ethanol (3 min), and 30% ethanol (3 min). Next, sections were rinse in distilled H_2O and antigen retrieval performed using 10 mM sodium citrate buffer at pH6 and microwaving sections for 3 X 4 min, then ran under cold water for a further 15 min. Sections were then incubated in 1 X PBS with 0.1% tween20 (Sigma-Aldrich, UK) for 3 min, followed by blocking with 10% goat serum in PBS for 1 hr in a humidified chamber. Sections were incubated over night at 4^{o}C with antibodies diluted in 10% goat serum/PBS (Biotinylated isolectin B4 diluted 1/100, αSMA-Cy3 direct conjugate diluted 1/400). The next day sections were washed in 1 X PBS 0.1% tween20, 2 X 3 min, then incubated with the secondary antibody streptavidin-Alexa 488 diluted 1/100 in 10% goat serum/PBS for 1 hr in a dark humidified chamber. Sectioned were washed in PBS 2 X 3 min. Finally, sections were mounted with Vectashield containing DAPI (Vector Laboratories, UK) and glass coverslips. Tissues were imaged either on a Zeiss LSM 780 confocal microscope (Z-stacked images were generated and compressed for analysis) or on the Zeiss Axio scan. Z1, at 40 X objective. For HLI and MI tissue analysis, the adductor muscle and heart were investigated, respectively. To investigate capillary density and mature vessel density, 5 regions of interest (0.42 µm^2) were imaged, on 3 tissue sections, at least 50 µm apart, per sample. Mature vessel counts were carried out by eye using Image J (FIJI). Capillary counts were either carried out either by eye or underwent batch analysis utilising the following

Macro (designed by Dr Amy Cochrane) which counted positive particles in the green (isolectin B4) channel only:

```
run("Subtract Background...", "rolling=50");
setOption("BlackBackground", false);
run("Make Binary");
run("Watershed");
run("Analyze Particles...", "size=0.03-Infinity show=Ellipses exclude include summarize
in_situ");
```

(Images were analysed with a size limit of particles set to 0.02 or 0.03).

Antibody	Species	Code/Company	Use
Isolectin GD-IB4 biotin-XX conjugate (IB4)	*Griffonia simplicifolia*	I21414 Thermo Fisher	Immunohistochemistry (IHC)
Alpha smooth muscle actin (α-SMA)- Cy3 conjugate	Mouse hybridoma	Sigma C6198	IHC
Thymosin beta 4-x (Tβ4)	Rabbit	Abcam 14335	IHC
Streptavidin, Alexa Fluor 488 Conjugate	*Streptomyces avidinii*	S32354 Thermo Fisher	IHC
Alexa-Fluor 488 secondary	Goat (anti-rabbit)	A32731 Invitrogen/ Thermo Fisher	IHC
SPAAR	Rabbit monoclonal	25823 Cell Signalling	Western blot
LICOR 488 anti rabbit	Goat (anti-rabbit)	LICOR	Western blot

Table 2.5 List of antibodies used for immunohistochemistry and immunocytochemistry.

2.9.3 Masson's trichrome staining

Deparaffinise and rehydrate sections through incubations in xylene (2 X 5 mins), 100% ethanol (2 X 5 mins) 95% ethanol (3 mins), 70% ethanol (3 mins), 50% ethanol (3 mins), and 30% ethanol (3 mins). Rinse slides in distilled H_2O and incubate in pre heated Buin's fluid at 60^{O}C for 1 hr, followed by cooling at room temperature for 10 min. Rinse slides in tap water until water runs clear then rinse in distilled H_2O. Incubate slides in Weigert's haematoxylin for 5 min and rinse for 2 min in tap water. Next, incubator slides in Biebrich Scarlet /Acid Fuchsin Solution to slide for 15 min then rinse in distilled H_2O. Rinse slides in distilled water. The slides then need incubating in phosphomolybdic/phosphotungstic acid solution for 10 min, and then submerging directly into aniline blue solution for 8 min and finally rinsing in distilled H_20. Slides are placed into acetic acid (1%) to fix the staining for 4 min. Lastly, slides are dehydrated with quick rinses in 2 X 90% ethanol, 2 X 100% ethanol and then cleared in xylene before mounting and left to dry overnight in a fume cupboard. Tissues were imaged on an Axio scan.Z1. Images were viewed and % infarct calculated using ImageJ (Fiji).

2.9.4 Evans Blue staining

Evan's Blue staining on MI hearts was carried out and quantified by Dr. Ana-Mishel Spiroski. Evans blue (Sigma-Aldrich, UK)**.** Evans blue dye was used to stain the infarcted area of the heart after acute (30 min) induction of myocardial infarction. Briefly, 1% Evans blue was infused into the heart slowly via cannulation of the aorta and the heart then dissected, wrapped in cling film and frozen at -20 °C for at least 1 hr. Next, the hearts were cut into 1mm sections (above the suture) and transferred to a tube containing 2% 2,3,5-triphenyltetrazolium chloride (TTC) incubated for 24 hrs at 37°C. Image J was used to calculate infarct size and at-risk area.

2.10 Statistical analyses

2.10.1 In vitro

Data are expressed as the mean ± the standard error of the mean (SEM) on 3 biological replicates unless otherwise indicated in the figure legend. SEM was calculated and chosen for plotting as calculating the mean involves utilising the standard deviation (the spread of the data values), as well as the sample size to calculate how closely your sample mean recapitulates the true population mean**.** (https://www.graphpad.com/guides/prism/latest/statistics/stat_semandsdnotsame.htm). qRT-PCR data is presented graphically as RQ of the expression of the transcript of interest, relative to a housekeeping gene. The statistics for these data are carried out on the calculated dCt value. For a *p* value to be considered statistically significant, it had to be less than or equal to 0.05. All graphs were generated utilising GraphPad PRISM versions 7 and 9, and all statistics are described in each figure legends. The student's t-test (two-tailed, unpaired) was used to compare data between 2 experimental groups throughout. Where 3 replicates are present in 3 or more experimental conditions, a one-way ANOVA with multiple comparisons was carried out. Any other statistical tests utilised in publications is stated in the publication methods.

2.10.2 In vivo

Data are expressed as the mean ± the standard error of the mean (SEM) on the number of mice indicated in each figure legend. The student's t-test (two-tailed, unpaired) was used to directly compare data between 2 groups i.e., wild type and LINC00961$^{-/-}$. Comparisons between more than 2 groups with more than 1 parameter used a 2-way ANOVA with Sidak's multiple comparisons test.

Chapter 3 The LINC00961 transcript and its encoded micropeptide, small regulatory polypeptide of amino acid response, regulate endothelial cell function

3.1 Introduction

The aim of the research in this Chapter was to show the importance of LINC00961 in health and disease and, more specifically, to highlight the identification of LINC00961 enrichment in the endothelium. Here, we demonstrate that the LINC00961 locus has roles in multiple endothelial functions *in vitro*, which translate to roles *in vivo*. We were able to separate the independent roles of LINC00961 and SPAAR, at least in regard to angiogenesis, providing crucial evidence for the role of LncRNAs as non-coding transcripts, despite the presence of functional micropeptides within their locus. As well as peer reviewed published data, this Chapter contains additional data which further investigates the role of the LINC00961 locus in regulating gene expression by analysing potential LINC00961 downstream targets and the analysis of LINC00961 modulation in endothelial and non-ECs from the adductor muscle of WT mice having undergone HLI. Finally, a panel of 11 genes of interest in the adductor muscle of KO animals in their control and ischaemic muscles 7 days post-surgery were analysed to observe any alterations in expression caused by deletion of the LINC00961 locus.

Having determined that LINC00961 and SPAAR have independent effects on angiogenesis [254], next, we wanted to determine if the SPAAR micropeptide is present in unstimulated and therefore non-angiogenic ECs.

This Chapter then investigates the upstream regulation of this locus. Given that LINC00961 is endothelial enriched, we hypothesised that an established endothelial transcription factor may directly regulate LINC00961 locus expression. As shown in our publication below, the endothelial markers CDH5 (VE-Cad), PECAM-1, and the erythroblast transformation-specific (ETS) related gene (ERG) were all upregulated along with LINC00961 in our day 7 differentiated ECs [254]. We collaborated with Professor Anna Randi and her group at Imperial College London who have expertise in the endothelial transcription factor ERG [255, 256]. ERG is a known oncogene and a master regulator of transcription which induces an endothelial specific gene profile essential to mantaining several endothelial functions such as endothelial

homeostasis, angiongenesis, cell adhesion, and ECM contribution [257, 258]. Recently, ERG was shown to regulate super-enhancers, which are clusters of enhancers in the promoter region of a gene, in ECs [259]. Examples of ERG regulated genes include CDH5, DLL4, CLDN5, vWF, ANG1, NOTCH4, Delta-like ligand 4, ICAM2, FLK1, EGFL7, endothelin-1, ZO-1, and MMP1 [256, 260-262]. Relevantly, ERG has even been shown to regulates lncRNAs, such as PCAT5, in the context of prostate cancer [263, 264]. ERG has also been implicated in the inhibition of inflammation and endoMT which also contribute to maintaining an endothelial phenotype in healthy vessels [256, 265].

In the following publication I contributed to writing and editing the original manuscript as joint first author. I also led the additional studies and writing associated with the response to reviewer documents, which involved experiments over 2 revisions based on reviewer comments, alongside contributions and feedback from co-authors. My contributions to Figures are listed below:

- Figure 3 – I performed RNA extractions, the qRT-PCR analysis in panel A, and carried out the siRNA KD of LINC00961 followed by endothelial barrier integrity assessment in panel E.
- Figure 4 – HLI surgery and perfusion fixing of tissues for histology was conducted by Dr Marco Meloni. I carried out the Laser Doppler imaging immediately after femoral artery ligation and at other time points for the duration of the HLI experiments. The SuRF department at The University of Edinburgh paraffin embedded the adductor muscle tissue, and I was responsible for cutting the tissue sections, performing immunohistochemistry (IHC) staining and analysis, thus generating figure data.
- Figure 5 – I performed the experiments required to generate the endothelial barrier integrity assay data in panel F.
- Supplementary Figure 3 – I generated the endothelial barrier integrity assay data in panel B, which relates to the previously mentioned data in Figure 3E.
- Supplementary Figure 5 – I performed all experiments required to generate the data for this Figure.
- Supplementary Figure 6 - I performed all experiments required to generate the data for this Figure.

- Supplementary Figure 7 – I generated this endothelial barrier integrity assay data which relates to the previously mentioned data in Figure 5F.
- Supplementary Figure 9 – I repeated siRNA mediated KD experiments to ensure data were robust and that we had the biological replicates required for analysis, from siRNA transfections through to qRT-PCR and analysis shown in panels A-C.
- Supplementary Figure 10 – I performed the IHC for Tβ4 in HUVECs in panel B.
- I created the graphical abstract with feedback from co-authors.

3.2 Aims

The aims of this Chapter were:

- To identify LINC00961 as endothelial enriched and that its expression is vital for proper endothelial functions *in vitro*.
- To validate that this locus' role in angiogenesis *in vitro* translates to functions *in vivo*.
- To provide additional non-published data which supports a role for LINC00961 in regeneration after injury.
- To provide additional non-published data which explores the alterations in gene expression in LINC00961$^{-/-}$ mice at baseline and after ischaemic injury.
- Determine the level of SPAAR micropeptide expression in human unstimulated endothelial cells (HUVECs).
- Determine whether expression of the LINC00961 locus is regulated by the endothelial transcription factor ERG.

3.3 Publication

ESC European Society of Cardiology

Cardiovascular Research (2020) **116**, 1981–1994
doi:10.1093/cvr/cvaa008

The LINC00961 transcript and its encoded micropeptide, small regulatory polypeptide of amino acid response, regulate endothelial cell function

Helen L. Spencer[1†], Rachel Sanders[1†], Mounia Boulberdaa[1], Marco Meloni[1], Amy Cochrane[1], Ana-Mishel Spiroski[1], Joanne Mountford[2], Costanza Emanueli[3], Andrea Caporali[1], Mairi Brittan[1], Julie Rodor[1], and Andrew H. Baker[1,2*]

[1]University/BHF Centre for Cardiovascular Science, Queens Medical Research Institute, University of Edinburgh, 47 Little France Crescent, Edinburgh EH16 4TJ, UK; [2]Institute of Cardiovascular and Medical Sciences, University of Glasgow, 126 University Pl, Glasgow G12 8TA, UK; and [3]National Heart and Lung Institute, Vascular Sciences and Cardiac Function, Imperial Centre for Translational and Experimental Medicine, Imperial College London, London W12 0NN, UK

Received 30 March 2019; revised 10 September 2019; editorial decision 10 January 2020; accepted 11 February 2020; online publish-ahead-of-print 28 January 2020

Time for primary review: 22 days

This manuscript was handled by Consulting Editor Professor Jeremy Pearson.

Aims Long non-coding RNAs (lncRNAs) play functional roles in physiology and disease, yet understanding of their contribution to endothelial cell (EC) function is incomplete. We identified lncRNAs regulated during EC differentiation and investigated the role of *LINC00961* and its encoded micropeptide, small regulatory polypeptide of amino acid response (SPAAR), in EC function.

Methods and results Deep sequencing of human embryonic stem cell differentiation to ECs was combined with Encyclopedia of DNA Elements (ENCODE) RNA-seq data from vascular cells, identifying 278 endothelial enriched genes, including 6 lncRNAs. Expression of LINC00961, first annotated as an lncRNA but reassigned as a protein-coding gene for the SPAAR micropeptide, was increased during the differentiation and was EC enriched. *LINC00961* transcript depletion significantly reduced EC adhesion, tube formation, migration, proliferation, and barrier integrity in primary ECs. Overexpression of the SPAAR open reading frame increased tubule formation; however, overexpression of the full-length transcript did not, despite production of SPAAR. Furthermore, overexpression of an ATG mutant of the full-length transcript reduced network formation, suggesting a bona fide non-coding RNA function of the transcript with opposing effects to SPAAR. As the LINC00961 locus is conserved in mouse, we generated an LINC00961 locus knockout (KO) mouse that underwent hind limb ischaemia (HLI) to investigate the angiogenic role of this locus *in vivo*. In agreement with *in vitro* data, KO animals had a reduced capillary density in the ischaemic adductor muscle after 7 days. Finally, to characterize *LINC00961* and SPAAR independent functions in ECs, we performed pull-downs of both molecules and identified protein-binding partners. *LINC00961* RNA binds the G-actin sequestering protein thymosin beta-4x (Tβ4) and Tβ4 depletion phenocopied the overexpression of the ATG mutant. SPAAR binding partners included the actin-binding protein, SYNE1.

Conclusion The LINC00961 locus regulates EC function *in vitro* and *in vivo*. The gene produces two molecules with opposing effects on angiogenesis: SPAAR and *LINC00961*.

* Corresponding author. Tel: +44 0131 24 26728, E-mail: andy.baker@ed.ac.uk

† These authors have contributed equally to this work.

Graphical Abstract

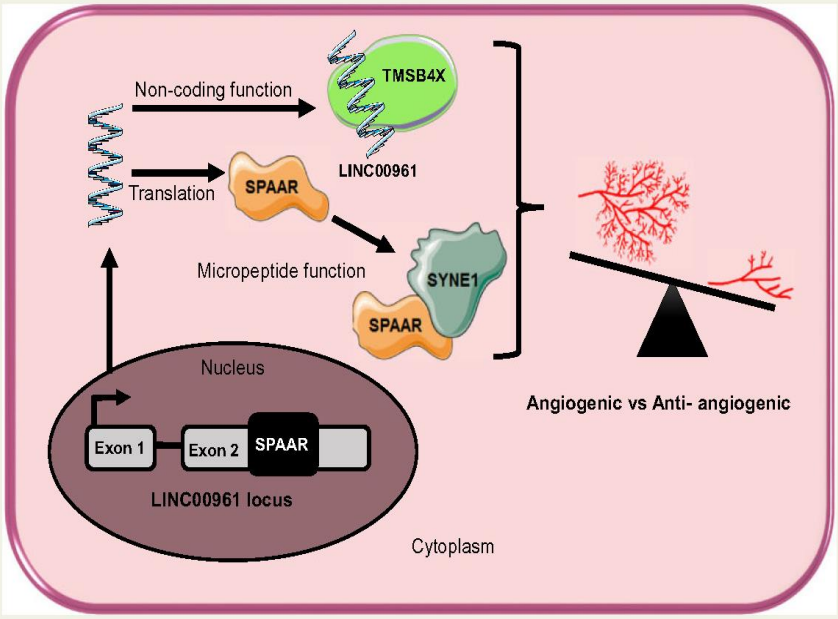

Keywords Angiogenesis • LncRNA • Endothelial cell • Micropeptide • Hind limb ischaemia

1. Introduction

The endothelium is a heterogeneous organ system that regulates homeostasis of the vasculature and represents a permeable monolayer barrier between the vessel wall and the blood. Endothelial cells regulate and adapt to shear stress, leucocyte extravasation, blood clotting, inflammation, vascular tone, extracellular matrix deposition, vasoconstriction/vasodilation, and angiogenesis. During angiogenesis, ECs become activated and undergo sprouting, proliferation, migration along a gradient of pro-angiogenic factors [e.g. vascular endothelial growth factor (VEGF), fibroblast growth factor (FGF), and platelet-derived growth factor (PDGF)], and anastomose to form new capillaries before returning to their quiescent state.[1] Aberrant activation however, leads to EC dysfunction that can cause systemic vascular pathology.[1,2] This uncontrolled activation is a significant factor contributing to coronary artery disease, diabetes, hypertension patients, hypercholesterolaemia, lupus, and has been reported as increased in smokers.[3,4]

Several groups have demonstrated the ability to differentiate ECs from human embryonic stem cells (hESC).[5–7] This protocol yields ECs that are relatively immature and express genes that are somewhat distinct from those of mature ECs from various vascular beds,[8] highlighting the importance of understanding the molecular mechanisms controlling both general and specialized EC differentiation, specification, and function. These derived ECs have been extensively proven to be functional both *in vitro*, by the ability to form capillary-like networks on Matrigel[7] and *in vivo*, by their ability to improve vascular density and perfusion in a murine model of hind limb ischaemia (HLI).[9] These data provide evidence of the benefits to hESC-derived EC for therapeutics and as a model to characterize early vascular development.

Data from the human Encyclopedia of DNA Elements (ENCODE) project indicate that approximately 93% of the genome is transcribed, with less than 2% encoding protein sequences.[10] Currently, these non-coding RNAs (ncRNAs) are classified based on size, into long non-coding RNAs (lncRNAs) >200 bp and small ncRNAs <200 bp. LncRNAs correspond to a heterogeneous class of genes, with subtypes classified based on neighbouring protein-coding genes. In particular, lincRNAs are intergenic lncRNAs with no overlap with protein-coding genes. While some lincRNAs regulate in *cis* their protein-coding neighbours expression, a large range of *trans*-functions have been reported including chromatin remodelling, transcriptional and post-transcriptional regulation, translation control, and regulation of protein activity.[11] LncRNAs show spatio-temporal expression, and are poorly conserved between species[12]; however, to date only a few of the lncRNAs known to exist have been functionally characterized. Recent literature highlights the important functions of lncRNAs as regulators of the cardiovascular system.[13,14] In the vascular endothelium, TIE1-AS1 was the first described endothelial-specific lncRNA, involved in modulating TIE-1 expression and regulating endothelial vessel formation.[15] A comprehensive transcriptome analysis of early cardiovascular development revealed the regulation of several lncRNAs and led to the characterization of ALIEN and

PUNISHER.[16] Recently, the hypoxia-induced lncRNA, GATA6-AS, was shown to epigenetically regulate angiogenesis through its interaction with the epigenetic regulator LOXL2.[17,18]

The 'non-coding' property of some lncRNAs has been disputed by the discovery of small open reading frames (ORFs) in some lncRNA transcripts, able to generate functional micropeptides.[19,20] For example, LINC00948 has been reclassified as a protein-coding gene, as it encodes myoregulin, which inhibits the calcium ATPase SERCA in muscle.[21] Similarly, the micropeptide DWORF encoded by lncRNA NONMMUG026737 activates the SERCA pump.[22] Noteworthy to this study, a conserved micropeptide termed small regulatory polypeptide of amino acid response (SPAAR) was recently shown to be encoded by the *LINC00961* locus.[23] SPAAR attenuates lysosomal v-ATPases interaction with mTORC1 under amino acid stimulation and modulates skeletal muscle regeneration following cardiotoxin injury.[23] These studies focused on the function of the derived micropeptide; however, some micropeptides have been shown to be expressed from lncRNAs with previously characterized non-coding functions,[24] suggesting the possibility of bi-functional loci.

We identified the *LINC00961*/SPAAR locus as EC enriched and sought to identify the role of this micropeptide-encoding gene. This led to dissection of the contribution of the *LINC00961* RNA transcript itself and the SPAAR micropeptide on endothelial function. *LINC00961* RNA was found to act as a bona fide lncRNA that inhibited angiogenesis and bound to the known angiogenic and actin-binding protein thymosin beta 4-x (Tβ4). Whereas SPAAR was found to be pro-angiogenic and bound to another actin-binding protein, SYNE1.

2. Methods

2.1 EC isolation and cell culture

All donated tissues have been obtained under proper informed consent and the investigation conforms with principles in the Declaration of Helsinki. Human saphenous vein endothelial cells (HSVECs) were obtained by enzymatic collagenase digestion of human saphenous veins (Ethics 15/ES/0094). Human umbilical vein endothelial cells (HUVEC) were obtained from Lonza (Basel Switzerland).

2.2 RNA-Seq of hESC differentiation to ECs

A previously published protocol was employed to generate ECs from H9 hESCs.[7] RNA-Seq analysis was performed as previously described[25] with minor modifications. Ensembl GRCh38 was used for transcriptome annotation. Read counts for each gene were obtained using HTSeq.[26] The differential expression was analysed using DESeq2.[27] RNA-seq data are deposited at the Gene expression Omnibus as GSE118106.

Expression data from several human endothelial and smooth muscle cell (SMC) lines were obtained from the ENCODE Consortium. The list of analysed data and their abbreviated name can be found in Supplementary material online, *Table S1*. Candidate filtering was done as follow: (i) Genes enriched in day 7 EC vs. hESC and non-EC day sample based on a LogFC $\geq$ 1, Padj < 0.01, FPKM $\geq$ 2; (ii) Genes up-regulated in HSVEC vs. hESC (LogFC $\geq$ 1, Padj < 0.01, FPKM $\geq$ 2); (iii) Genes expressed in ENCODE ECs (min of 2 FPKM in 10 samples); (iv) Enriched expressed in ENCODE ECs vs. ENCODE SMCs (two-fold enrichment between the average expression in ECs and SMCs).

2.3 HUVEC transfection and phenotype analysis

All phenotypes were assessed in HUVECs at 24 h after transfection with dicer substrate siRNA (dsiRNA) or infection with lentiviral constructs (details of reagents and protocols in Supplementary material online, *Methods*). *In vitro* tubule network formation was assessed using Matrigel (Corning, USA) according to the manufacturer's protocol. Proliferation was assessed using the Click-it EdU 488 Proliferation assay (Life Technologies, UK). Migration and endothelial barrier function assays were performed using an Electric Cell-substrate Impedance Sensing (ECIS) machine (Applied BioPhysics, USA) and cell viability assessed with a FITC Annexin V Detection Kit with PI (BioLegend).

2.4 Hind limb ischaemia

All animal experiments were performed in accordance with the Animals (Scientific Procedures) Act (UK) 1986 and under the auspices of UK Home Office Project and Personal Licenses held within The University of Edinburgh facilities. LINC00961$^{-/-}$mouse line was obtained from Taconic©. Validation of genotype was two-fold. Ear clip samples from pups were sent to Transnetyx© for genotyping, and in-house validation was also carried out using qRT-PCR on mRNA extracted from the kidney. Surgical procedures were performed under inhaled general anaesthesia (isoflurane at 5% for induction and 1–2% for maintenance) and with appropriate peri-operative analgesic cover (subcutaneous injection of buprenorphine at 0.05 mg/kg). Unilateral HLI was surgically induced by left femoral artery ligation at two points and cauterization of this segment of artery, leaving the femoral vein and nerve untouched. Mice were maintained for 7 days after surgery. Male LINC00961$^{-/-}$and wild type (WT) littermates on the C57Bl/b6NTAC were studied at 11 weeks of age. Animals were euthanized with pentobarbital (160 mg/kg) given by intraperitoneal injection. Tissues were perfusion fixed with PBS at 6 mL/min with a micropump and then with 4% paraformaldehyde at 6 mL/min.

2.5 Pull-down

LINC00961 RNA pull-down was carried out with 50 pmol biotinylated lncRNA, obtained using the T7 RiboMAX Express Large Scale RNA Production System (Promega, UK). The biotinylated lncRNA was incubated with streptavidin magnetic beads and 20 µg of HUVECs protein lysate, using the Pierce Mag RNA Protein Pull-down kit (Thermo Scientific). For the SPAAR pull-down HUVECs expressing either LV-Null, LV-SPAAR untagged, or LV-SPAAR-HA tagged were cultured in EGM-2 media. Immunoprecipitation with either anti-IgG or anti-HA antibody was performed in two replicates. SPAAR binding partners were defined as proteins detected in the two pull-down replicates and with a two-fold enrichment compared with the IgG pull-down controls or pull-down in cells not overexpressing HA-tagged SPAAR. Keratin contaminants and unknown proteins were removed from the final candidate list.

2.6 Statistical analysis

Statistical analysis was performed as described in the figure legends using GraphPad Prism version 5.0. Data are expressed as mean ± SEM. Comparisons between two groups were analysed using two-tailed unpaired Student's *t*-tests. Comparisons between more than two groups were analysed using one-way ANOVA. For qRT-PCR analysis, graphs display the expression relative to the housekeeping gene based on the double dCt analysis while the statistical analyses were done on dCt

values. For data represented as fold change, the statistical analysis was done on the Log2 fold change using an one sample *t*-test.

3. Results

3.1 Identification of EC-enriched genes

To identify genes specifically induced during endothelial fate specification and differentiation, we utilized an embryoid body-based protocol to generate ECs from hESCs (*Figure 1A*).[7] This protocol was previously shown to generate functional hESC-EC, expressing CD144 and CD31 and able to form tube-like structures on Matrigel.[7] RNA-seq was performed (45 million paired-end reads per sample) on ribosomal RNA depleted libraries from several replicates of the different cell populations (*Figure 1A*). Principal component analysis (PCA) demonstrated tight clustering of replicates and segregation of populations (*Figure 1B*). The purified EC samples obtained at day 7 (d7 EC) were closer to the human saphenous vein EC (HSVEC) samples in the PCA plot, but clearly clustered separately suggesting the immaturity of this EC population (*Figure 1B*). As expected, hESC pluripotency markers showed a down-regulation after day 3 of differentiation while mesoderm markers are up-regulated. We confirmed the expression of several endothelial markers in the d7 EC population but also showed the expression of arterial, venous, and lymphatic phenotype markers, suggesting endothelial heterogeneity (Supplementary material online, *Figure S1A*). As expected, we observed a high overlap between the genes up-regulated in d7 EC vs. hESC and the genes up-regulated in HSVEC vs. hESC (Supplementary material online, *Figure S1B*), validating their endothelial identity.

To identify genes important for endothelial identity and function, we focused on candidates showing high expression in immature and mature ECs. We specifically selected 409 genes enriched in the day7 EC population but also expressed in our HSVEC samples. Then, we took advantage of RNA-seq data from the ENCODE consortium to assess their expression in several EC lines from different origins but also in SMCs. We retrieved a list of 278 genes with high expression in ECs and lower expression in SMCs (Supplementary material online, *Table S2*). This list contains known markers of ECs including PECAM1, CDH5, and ERG, and the Gene Ontology (GO) analysis revealed the enrichment of terms related to vessel development and angiogenesis (Supplementary material online, *Figure S1C*).

3.2 LINC00961 is enriched in immature and mature ECs

Among the 278 genes enriched in immature and mature ECs, we found 6 lncRNAs: 3 antisense lncRNAs and 3 intergenic lncRNAs (*Figure 2A, B*). While antisense RNAs often regulate the expression of their sense genes,[24] intergenic lncRNAs have function generally unrelated to their neighbouring protein-coding genes. From the three intergenic lincRNA, LINC00961 is the only one conserved in mouse (*Figure 2C*). LINC00961 is located on chromosome 9 and while *LINC00961* transcript expression was detected in the d7 EC population and HSVECs with a read profile confirming a two-exon gene structure, neighbouring *HRCT1* expression was restricted to HSVECs (*Figure 2C*). Although LINC00961 was initially annotated as a lncRNA, the locus encodes a small ORF in the second exon and has been re-annotated as a protein-coding gene. Interestingly, the peptide was independently identified based on a proteomic strategy and termed SPAAR for small regulatory polypeptide of amino acid response.[23] To validate the RNA-seq, *LINC00961* gene expression was evaluated by qRT-PCR in the same sample set used for RNA-seq, which demonstrated the same profile of expression (Supplementary material online, *Figure S2*).

3.3 LINC00961/SPAAR gene silencing affects endothelial function

To assess the impact of silencing *LINC00961* transcript on endothelial function, we depleted *LINC00961* levels in HUVECs by 70%, utilizing dsiRNAs (*Figure 3A*). In an *in vitro* 2D Matrigel tubule network formation assay, *LINC00961* silencing resulted in attenuated branch formation (*Figure 3B, C*). Calcein AM was used to confirm that the lack of branch formation following *LINC00961* depletion was not a consequence of apoptosis (*Figure 3C*). We confirmed that *LINC00961* silencing did not affect cell viability using Annexin V and PI staining (Supplementary material online, *Figure S3A*). We then replicated the network formation phenotype via a GapmeR depletion strategy (Supplementary material online, *Figure S4*). Moreover, silencing *LINC00961* led to a significant reduction in cell adhesion (*Figure 3D*) and endothelial membrane barrier integrity (*Figure 3E* and Supplementary material online, *Figure S3B*). We also observed a trend towards a reduction in cell proliferation (Supplementary material online, *Figure S3C*) and migration (Supplementary material online, *Figure S3D*). To investigate whether *LINC00961* played a *cis*-regulatory role in the expression of the closely located gene HRCT1, we tested *HRCT1* transcript levels in siRNA *LINC00961* depleted cells. qRT-PCR analysis showed that *HRCT1* expression was unaltered by *LINC00961* modulation (Supplementary material online, *Figure S5A, B*). Similarly, siRNA silencing of *HRCT1* did not affect *LINC00961* levels (Supplementary material online, *Figure S5C, D*).

3.4 Murine LINC00961/SPAAR locus knock out reduces adductor muscle capillary density following HLI

To assess the role of the LINC00961 locus *in vivo*, we established a knockout (KO) mouse where the entire locus was deleted (*Figure 4A*). We first confirmed the absence of the LINC00961 mouse transcript by qRT-PCR (Supplementary material online, *Figure S6A*). We then tested the efficacy of injury-induced angiogenesis compared with wild type (WT) littermate controls at two time points. After 7 days, the capillary density between KO and WT animals was not significantly altered in the non-ischaemic leg ($P = 0.2471$). However, at 7 days after HLI LINC00961$^{-/-}$ mice had a lower capillary density in the ischaemic adductor muscle compared with controls (*Figure 4B*). This was, therefore, comparable with the *in vitro* tubule formation data in *LINC00961* depleted HUVECs. Interestingly, KO animals had a significant decrease in the number of α-smooth muscle actin (αSMA) positive vessels at baseline compared with WT animals but this difference was not evident after injury (*Figure 4C*). We also analysed Laser Doppler ratio, capillary density, and αSMA positive vessels at 21 days. No significant differences at this later time point were observed (Supplementary material online, *Figure S6*).

3.5 The LINC00961 locus encodes a biologically functional RNA

We next investigated the angiogenic effect of overexpressing either the full-length *LINC00961* transcript or the SPAAR ORF sequence in HUVECs, using lentiviral vectors (LV) (*Figure 5A*). We also generated a LV-ΔΔATG961 construct (*Figure 5A*), corresponding to the full-length transcript with mutations in the ORF initiation codons to block translation. qRT-PCR (*Figure 5B*) and western blotting (*Figure 5C*) confirmed

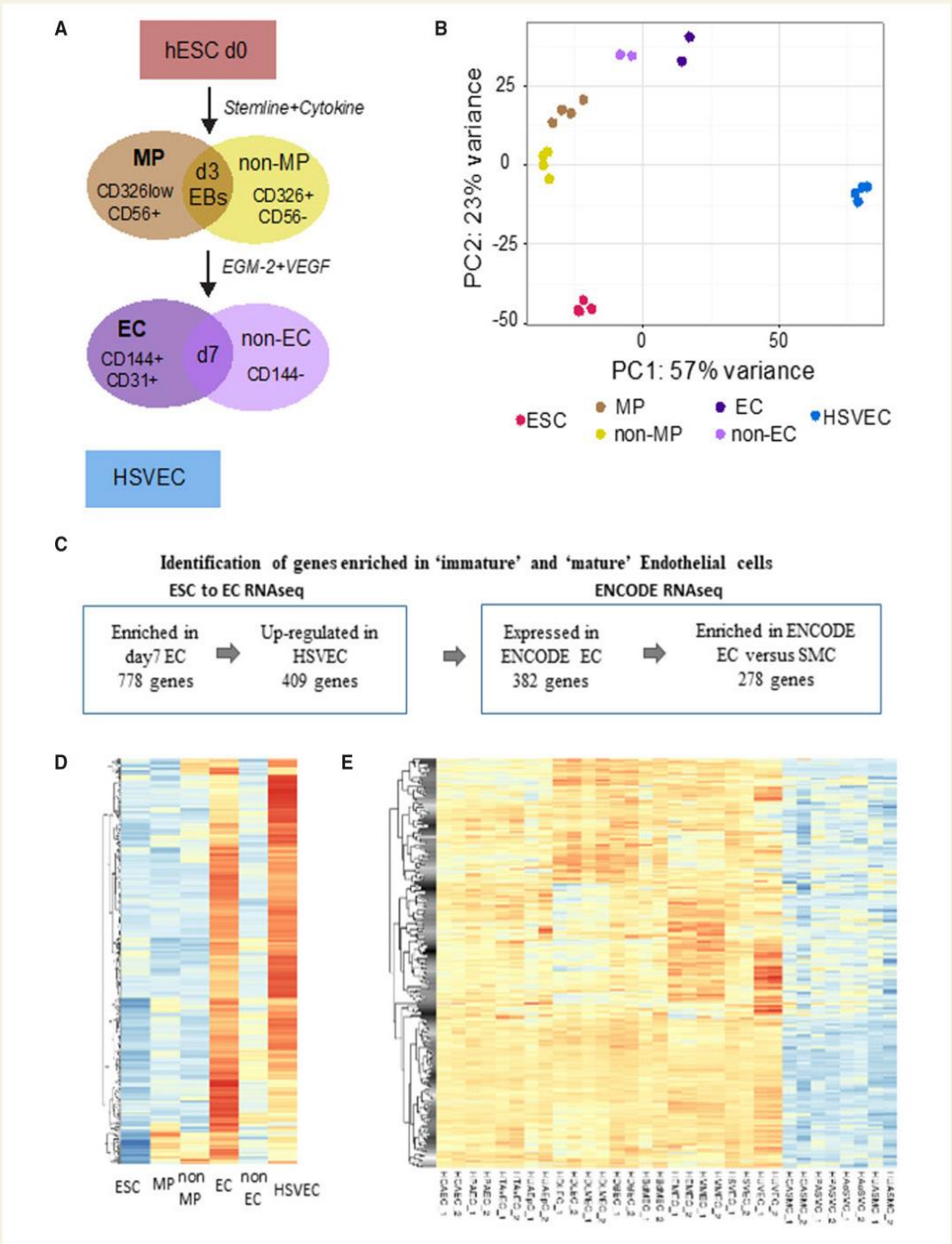

Figure 1 Identification of endothelial cell enriched genes. (*A*) Schematic representation of the RNA-seq samples: day 0 H9 hESC (ESC); Day 3 mesodermal population $CD326^{low}CD56^{+}$ (MP); Day 3 remaining population (non-MP); Day 7 EC $CD144^{+}CD31^{+}$(EC); Day 7 remaining population (non-EC); HSVEC. (*B*) PCA of the RNA-seq samples. The plot was generated on the regularized log-transformed data using DESEq2. (*C*) Summary of the selection of candidates to identify genes enriched in 'immature' and 'mature' ECs. (*D*) Heatmap showing the expression data [as row z-score of the Log2(FPKM + 1)] during differentiation of the 278 EC-enriched genes. (*E*) Heatmap showing the expression data [as row z-score of the Log2 (FPKM + 1)] of the 278 EC-enriched genes in ENCODE RNA-seq samples.

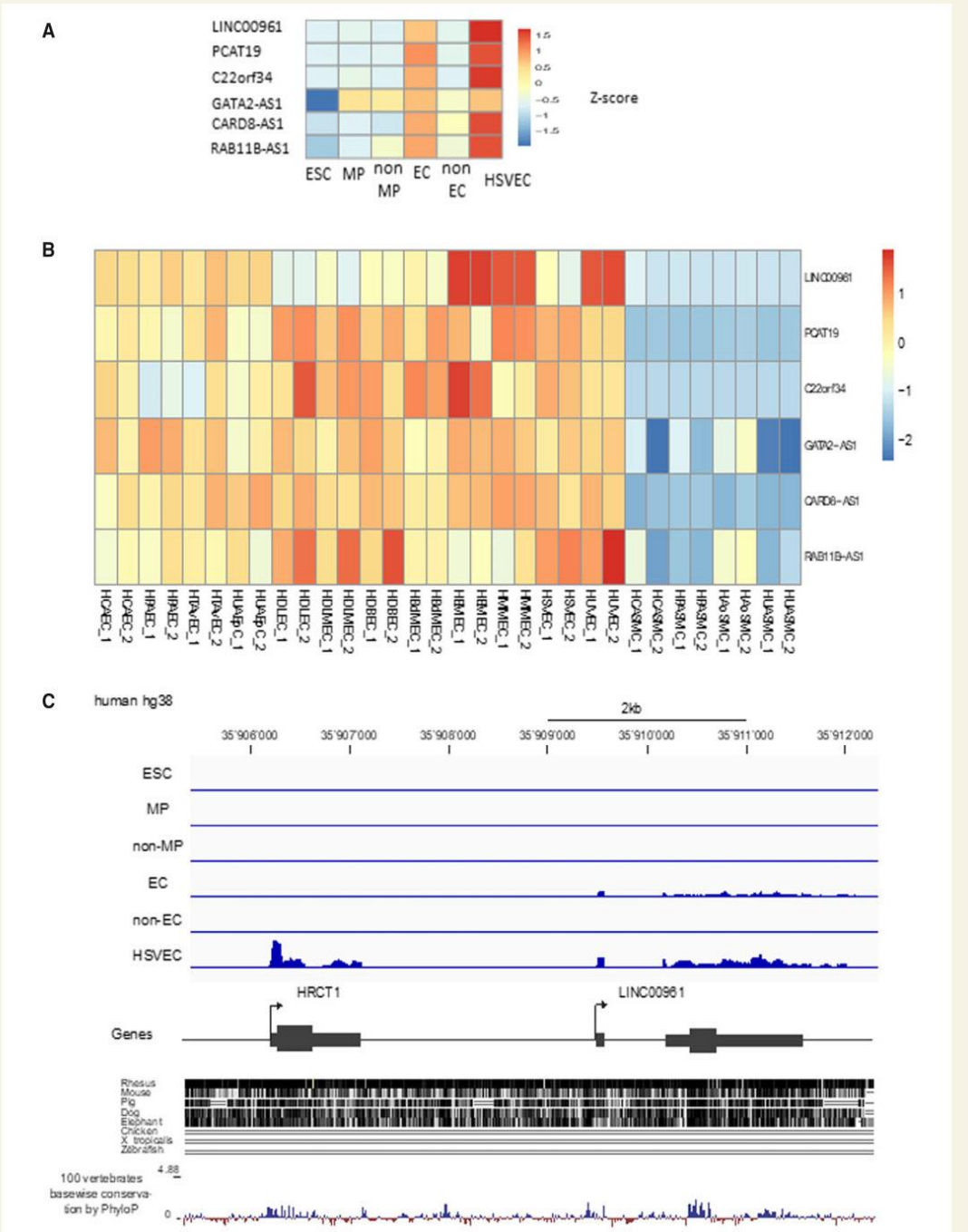

Figure 2 LINC00961 is enriched in immature and mature ECs. (*A*) Heatmap of the six lncRNAs identified in our EC differentiation protocol in each of the isolated cell populations. (*B*) Heatmap of these six lncRNAs in ENCODE RNA-seq samples including various types of EC lineages such as, venous, arterial, and lymphatic ECs. (*C*) Genomic organization of the LINC00961 gene, read profile from the ESC to EC RNA-seq, and conservation track based on UCSC alignment and PhyloP score.

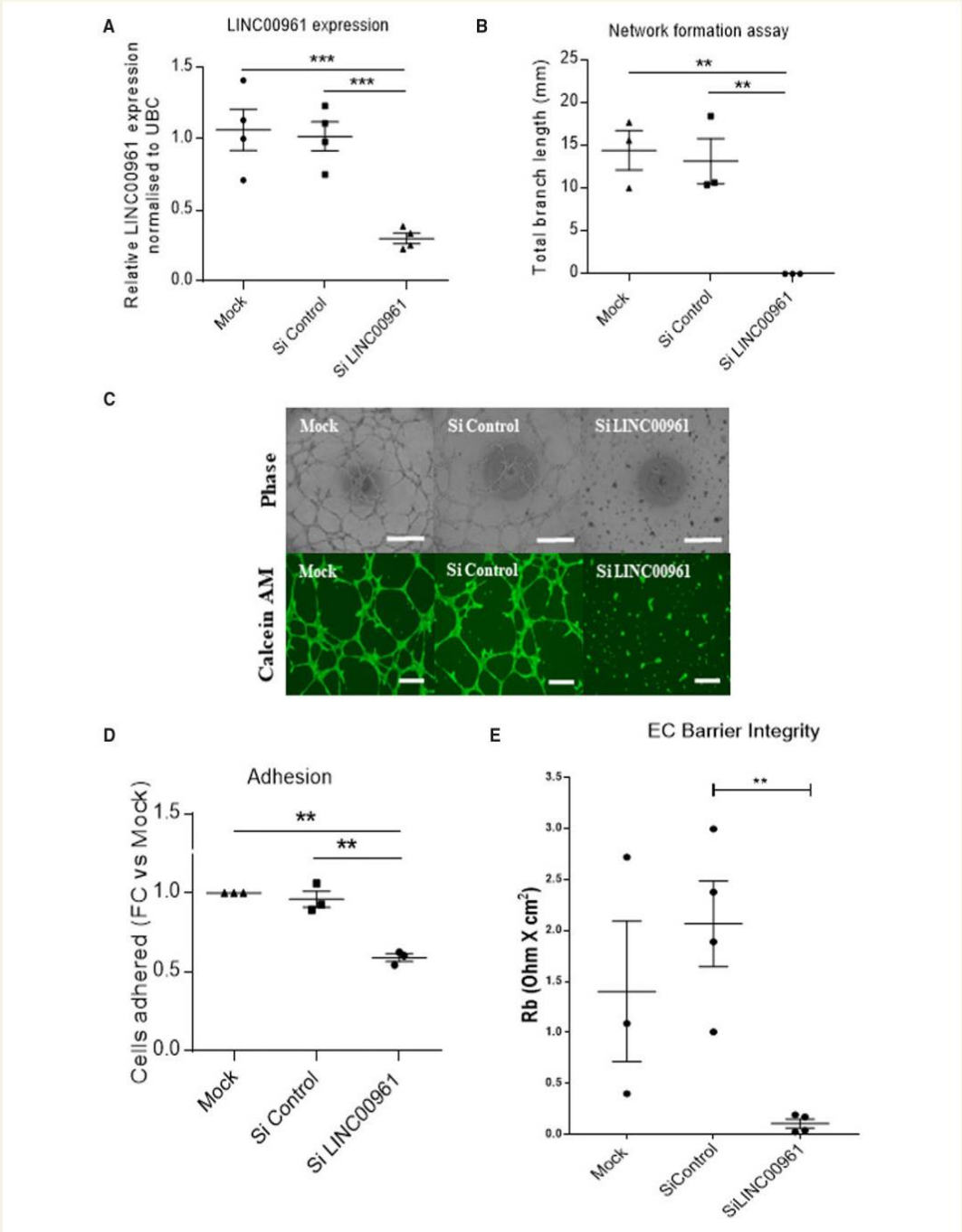

Figure 3 Functional impact of LINC00961/SPAAR depletion in ECs. (*A*) Confirmation of the dsiRNA-mediated depletion of *LINC00961* transcript in HUVECs by qRT-PCR ($n = 4$, unpaired *t*-test). (*B*) Network formation assay in *LINC00961* depleted HUVECs. Branch length assessed by Image J Angiogenesis plugin ($n = 3$, unpaired *t*-test). (*C*) Representative phase contrast and Calcein AM staining of network formation assay of *LINC00961* depleted and control HUVECs. Phase Scale bar = 0.5 mm. Calcein AM Scale bar = 0.1 mm. (*D*) Impact of *LINC00961* depletion on HUVEC adhesion ($n = 3$). (*E*) Analysis of average barrier resistance, expressed as Rb [Ohm × cm^2], across a 10 h time course ($n = 4$ except for mock $n = 3$, one-way ANOVA). For data represented as fold change, the statistical analysis was done on the Log2 fold change using an one sample *t*-test. On the graphs, $^*P < 0.05$ $^{**}P < 0.01$ $^{***}P < 0.001$.

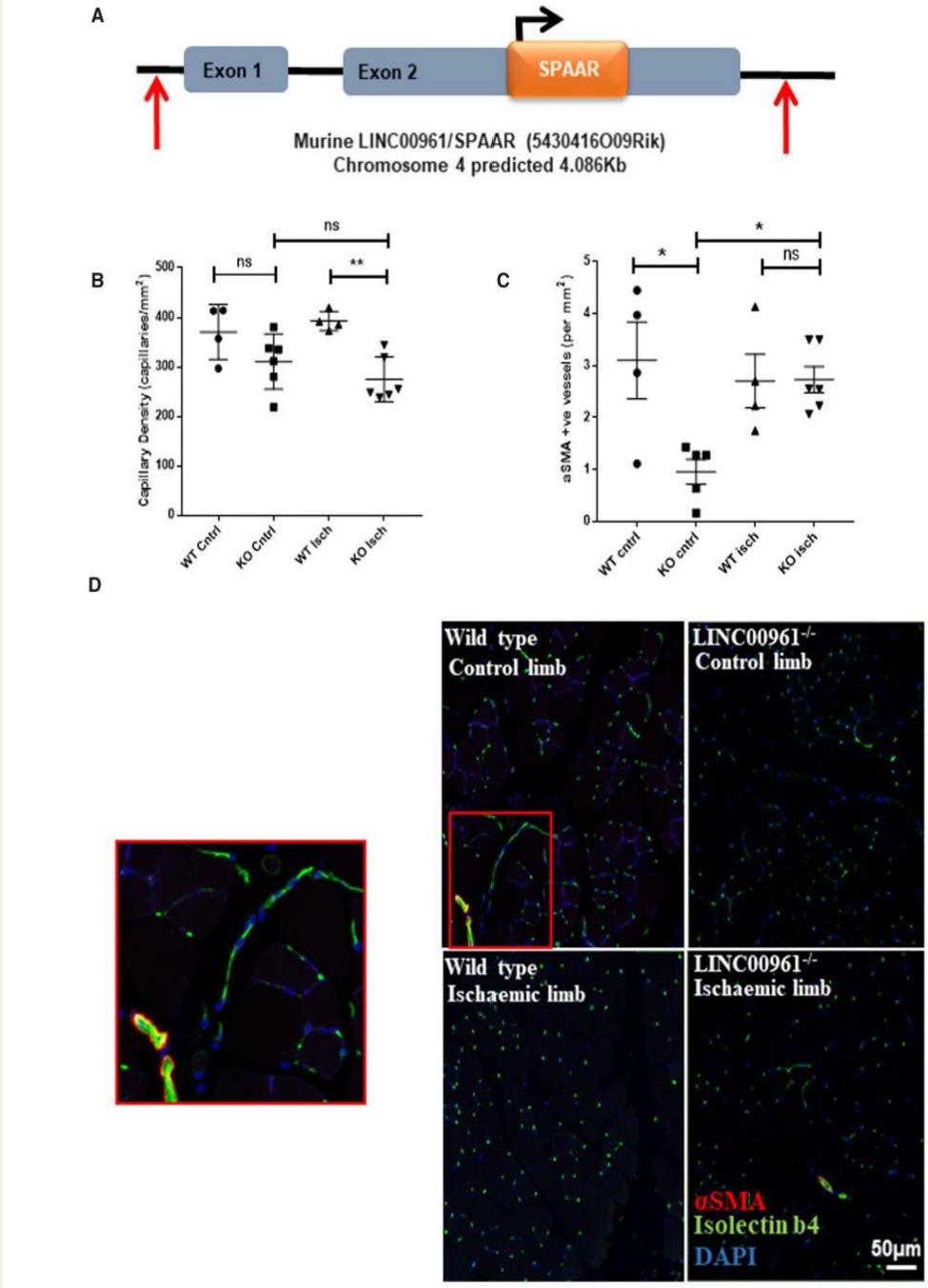

Figure 4 LINC00961/SPAAR KO mice have a reduced adductor muscle capillary density following HLI at 7 days. (*A*) Schematic representation of the deleted region of the LINC00961 mouse locus using CRISPR/Cas9 technology by Taconic©. Red arrows indicate the position of the guide RNA strands utilized to delete the whole locus. (*B*) Capillary density per sample. Five random regions of interest from three sections per sample were counted ($n = 4$ WT mice/6 KO mice, one-way ANOVA, ** $P < 0.01$, ns, not significant). (*C*) αSMA positive vessel density per sample. (*D*) Representative adductor muscle immunofluorescent images: Isolectin b4 (IB4) capillary/endothelium, αSMA, and nuclear DAPI, scale bar 50 μm. Zoomed panel on left corresponds to red box on area of WT control limb image.

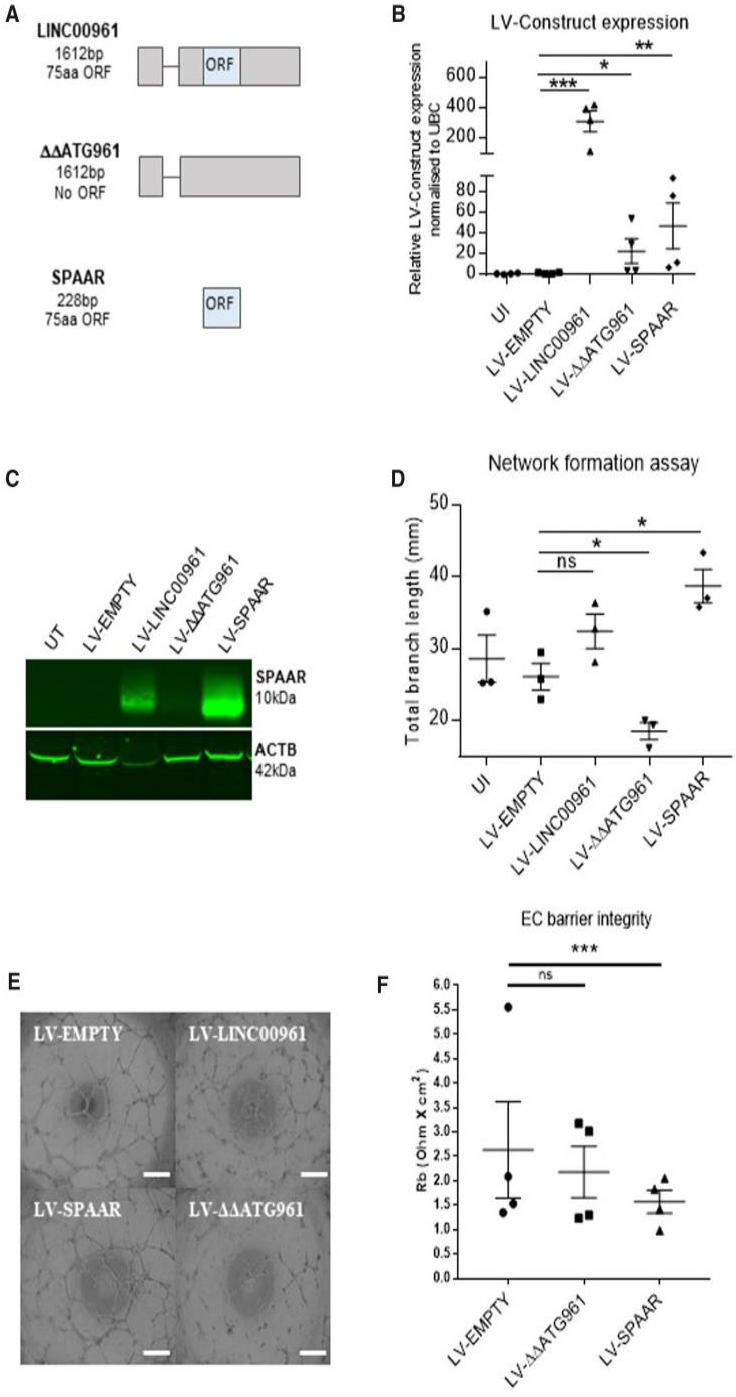

Figure 5 Impact of *LINC00961* transcript and SPAAR micropeptide overexpression in *in vitro* angiogenic assays. (*A*) Schematic representation of *LINC00961* LV constructs with transcript length in base pairs (bp) and encoded peptide length in amino acids (aa). (*B*) qRT-PCR validation of the LV constructs overexpression in HUVECs using primers targeting the ORF sequence. Unpaired *t*-test, comparison test vs. LV-EMPTY ($n = 4$). (*C*) Representative western blot of SPAAR micropeptide and β-actin in HUVECs infected with the LV constructs. (*D*) Network formation assay comparing HUVECs transfected with LV constructs. Branch length assessed by Image J Angiogenesis plugin. Unpaired *t*-test vs. LV-EMPTY ($n = 3$). (*E*) Representative Phase contrast of network formation assay of HUVECs transfected with LV constructs. (*F*) Analysis of average barrier resistance, expressed as Rb [Ohm × cm^2], across a 10 h time course ($n = 4$, one-way ANOVA). Scale bar = 0.5 mm. On the graphs, $^*P < 0.05$, $^{**}P < 0.01$, $^{***}P < 0.001$.

overexpression. Overexpression of the LV-SPAAR construct significantly enhanced endothelial network formation, whereas LV-ΔΔATG961 produced opposite results, significantly inhibiting angiogenesis (*Figure 5D, E*). These data showed that the production of SPAAR induces network formation, whereas the *LINC00961* RNA alone possesses an inhibitory effect, independent of SPAAR micropeptide production, thus unveiling a bona fide lncRNA function for the *LINC00961* RNA. Furthermore, we observed that LV-mediated overexpression of SPAAR, but not the LINC00961 transcript, reduced endothelial barrier integrity (*Figure 5F*, and Supplementary material online, *Figure S7*). As cellular localization of lncRNA transcripts is informative with regards to their associated mechanisms, we determined the subcellular localization of *LINC00961* using RNA-fluorescent *in situ* hybridization (FISH) (Supplementary material online, *Figure S8A, B*) and cell fractionation (Supplementary material online, *Figure S8C*) and showed the presence of *LINC00961* in both the nucleus and the cytoplasm.

3.6 Identification of binding partners for *LINC00961* RNA and SPAAR micropeptide

As both *LINC00961* and SPAAR are functionally relevant for ECs, we used RNA and protein pull-downs combined with mass spectrometry to identify the protein-binding partners of the lncRNA and SPAAR micropeptide in HUVECs (*Figure 6*). One hundred and forty-seven proteins were found in the *LINC00961* pull-down samples, which were not in the pull-down with the beads alone or the control GFP RNA (*Figure 6B* and Supplementary material online, *Tables S3* and *S4*). GO term analysis showed enrichment of terms related to cell–cell adhesion and cortical actin arrangement (*Figure 6D*). The top candidate was the G-actin sequestering molecule, thymosin beta 4-x (Tβ4) which is associated with reorganization of the actin cytoskeleton[28] and is also involved in angiogenesis.[29,30] Tβ4 functions within an actin organization pathway with other actin-associated molecules including Cofilin-1 and Profilin-1.[31] Both Profilin-1 and Cofilin-1 were enriched in the *LINC00961* immunoprecipitation (Supplementary material online, *Table S3*); suggesting *LINC00961* may play a role in actin cytoskeleton remodelling. To confirm the interaction between *LINC00961* and Tβ4, we carried out immunoprecipitation of endogenous Tβ4 protein in HUVECs. qRT-PCR confirmed the detection of *LINC00961* in Tβ4 immunoprecipitation samples, thus independently validating an interaction of *LINC00961* with Tβ4 (Supplementary material online, *Figure S10A*). Immunofluorescence of Tβ4 in HUVECs confirmed the presence of Tβ4 in the cytoplasm in accordance with a plausible interaction with *LINC00961* (Supplementary material online, *Figure S10B*).

We next identified protein-binding partners for SPAAR. We found 40 proteins enriched in the HA-SPAAR pull-down compared with the IgG pull-down controls and compared with the pull-downs in control cells not expressing the fusion protein (Supplementary material online, *Tables S5* and *S6*). GO analysis of SPAAR targets showed enrichment of terms related to immunity (*Figure 6E*). SPAAR has been previously shown to bind the v-ATPase complex in HEK293.[23] However, these proteins were not found in the SPAAR pull-down in HUVECs, suggesting a different function for SPAAR in ECs. The top hit for SPAAR interactors was SYNE1, also known as NESPRIN-1, a regulator of EC shape and migration.[32]

3.7 Thymosin beta 4-x depletion phenocopies LV-ΔΔATG961 overexpression

To characterize the function of *LINC00961* and Tβ4 interaction, we assessed whether they co-regulated each other's expression. siRNA silencing of *TMSB4X* (Supplementary material online, *Figure S9A*) did not alter *LINC00961* transcript levels (Supplementary material online, *Figure S9B*). Similarly, silencing *LINC00961* or overexpressing LV-ΔΔATG961 did not change *TMSB4X* transcript levels (Supplementary material online, *Figure S9C, D*). The known pro-angiogenic effect of Tβ4[29,30] was confirmed in our system, with a 49% ± 16% reduction in network formation following *TMSB4X* depletion (*Figure 7A, B*). This reduction is similar to the overexpression of *LINC00961* transcript without the production of SPAAR micropeptide (LV-ΔΔATG961), suggesting that *LINC00961* lncRNA might negatively regulate Tβ4-mediated angiogenesis.

4. Discussion

Using RNA-seq, we identified *LINC00961* as an endothelial enriched transcript. The strong impact on the endothelial phenotype following *LINC00961* level manipulations confirmed the relevance of our candidate selection using the combination of our hESC to EC RNA-seq with ENCODE RNA-seq datasets. This further highlights the need to investigate the role of lncRNA transcripts in endothelial biology.

In this study, we provide *in vitro* and *in vivo* evidence that the LINC00961 locus has a function in ECs. Whilst siRNA knock down (KD) *in vitro* affects many aspects of EC biology (angiogenesis, adhesion, proliferation, migration, and membrane integrity), we assessed the angiogenic role in a murine KO model. LINC00961$^{-/-}$ mice had fewer αSMA positive vessels at day 7 baseline, suggesting a defect in the development, maturity, and or stability of larger vessels. After injury, KO mice have fewer capillaries at day 7, indicating a reduced capacity of the endothelium to undergo angiogenesis after injury. However, the effect of the KO was not observed by day 21 post-HLI. This suggests the KO animals may have a slower recovery rate after injury (due to an impairment in EC function), or activate compensatory mechanisms to maintain vessel numbers after injury. As we have a global KO, we cannot exclude the contribution of LINC00961 deletion in other cell types to this phenotype. To further investigate the role of this locus in EC behaviour, it would be worthwhile to switch to an EC-specific and conditional LINC00961 KO mouse model. In addition, it would be interesting to assess the effect of LINC00961 deletion in early development of vessel establishment and further characterize the dynamics of vessel recovery early in the HLI model.

Previous studies have outlined the role of the micropeptide SPAAR, encoded from the LINC00961 locus, during muscle regeneration.[23] In our study, we showed opposing roles of *LINC00961* RNA and SPAAR micropeptide in angiogenesis, one being anti- and the other pro-angiogenic, respectively. The reduction in endothelial barrier integrity with SPAAR overexpression further validates our hypothesis that SPAAR is pro-angiogenic. Indeed, plastic junctions are required for sprouting angiogenesis.[33] Therefore, It would be interesting to test the permeability of new SPAAR-induced vessels in an animal system using a plasma tracer.

To our knowledge, this is the first reported bi-functional locus in a cardiovascular setting. In other biological contexts, loci producing protein or functional ncRNAs through alternative splicing have been described.[34–36] The novelty of the *LINC00961* locus is that the SPAAR micropeptide is produced from the functional *LINC00961* RNA instead of an alternative splicing transcript without an ORF. This configuration implies the requirement of a regulatory mechanism to control the levels of *LINC00961* RNA and SPAAR micropeptide independently of each other. The switch between *LINC00961* and SPAAR could be controlled

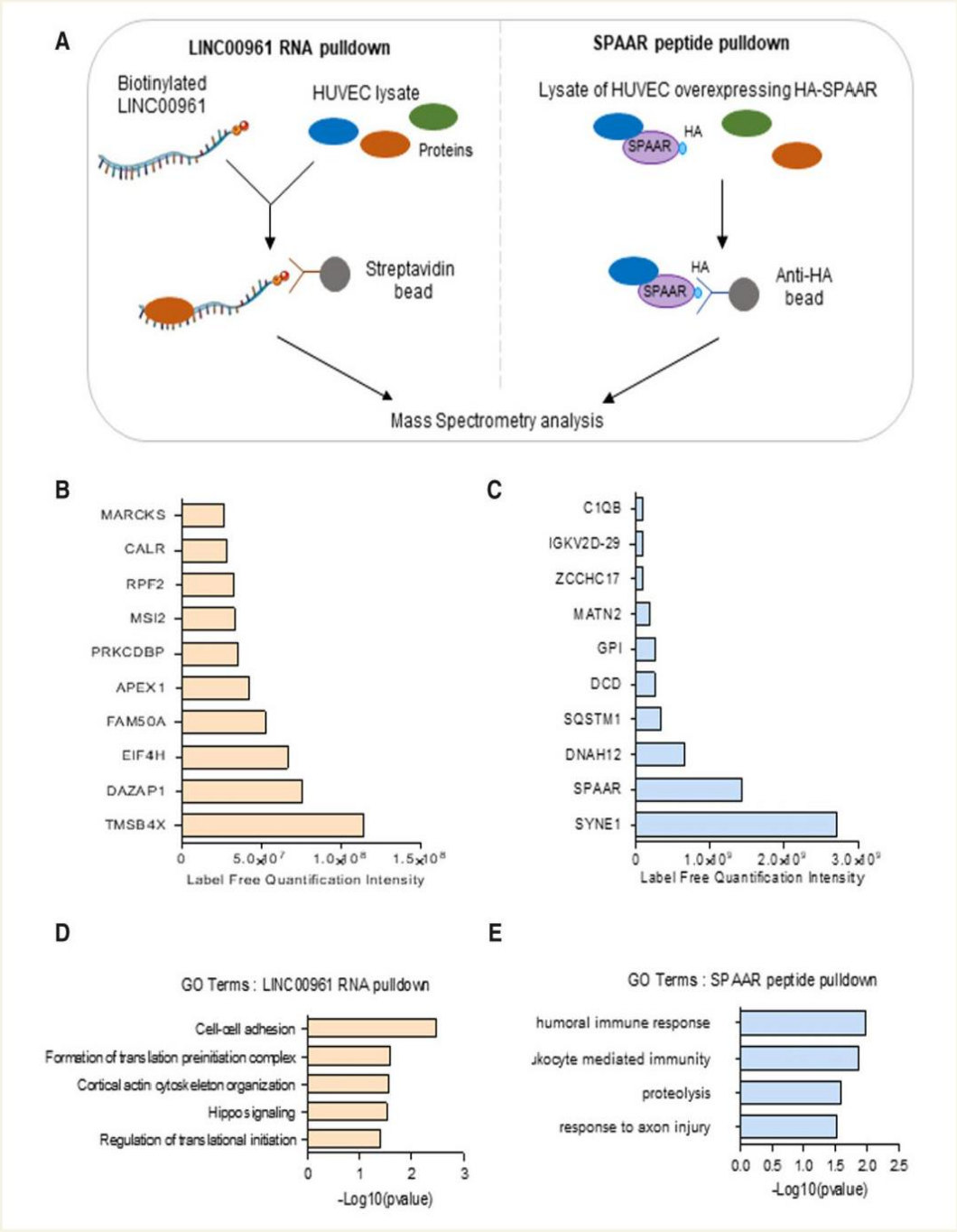

Figure 6 *LINC00961* and SPAAR both bind to actin-binding proteins. (*A*) Schematic of the *LINC00961* RNA and SPAAR peptide pull-down experiments in HUVECs. (*B*) List of the top 10 proteins identified in *LINC00961* RNA pull-down (ranked on label-free quantification value). (*C*) List of the top 10 proteins identified in HA-SPAAR peptide pull-down (ranked on label-free quantification value). (*D*) GO analysis on enriched proteins from *LINC00961* immunoprecipitation. (*E*) GO analysis on enriched proteins from *SPAAR* immunoprecipitation.

at the translation level, similarly to the STORM micropeptide whose translation initiation is regulated by eIF4E phosphorylation.[37] However, the functional activity of the lncRNA encoding the STORM micropeptide has never been demonstrated. Expression of the *LINC00961* transcript is high in basal HUVECs and detectable by qRT-PCR, in contrast, we are only able to see the presence of SPAAR micropeptide in LV-SPAAR conditions. This limitation is likely due to either very low protein levels in basal HUVECs or the detection limit of the antibody. The precise

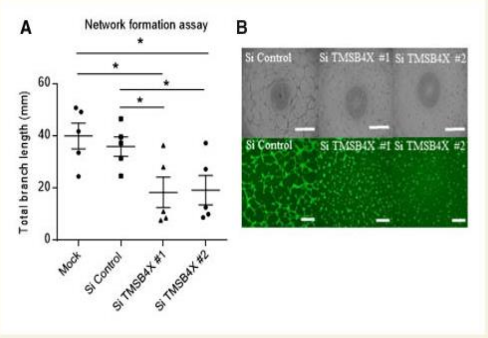

Figure 7 Thymosin beta 4-x KD in HUVECS has a similar phenotype to LV-ΔΔATG961 overexpression on tubule formation. (*A*) Network formation assay in dsiRNA-mediated *TMSB4X* depleted HUVECs. Branch length assessed by Image J Angiogenesis plugin, $n = 5$, unpaired *t*-test. (*B*) Representative phase contrast and Calcein AM staining of network formation assay of depleted HUVECs. Phase contrast Scale bar = 0.5 mm. Calcein AM Scale bar = 0.1 mm. On the graphs, $*P < 0.05$, $**P < 0.01$, $***P < 0.001$.

molecular control of *LINC00961* transcript and SPAAR levels needs further dissection in light of these findings.

We show that *LINC00961* RNA binds Tβ4, a well-established actin-binding protein with many additional functions including anti-inflammatory and anti-apoptotic properties, and a role in cell migration and angiogenesis.[28] As *TMSB4X* transcript levels were not affected by *LINC00961* depletion, we propose that *LINC00961* regulates Tβ4 protein function. The enrichment of Profilin-1 and Cofilin-1, actin monomer-binding proteins, in the *LINC00961* immunoprecipitation suggests a potential role for *LINC00961* in actin recycling. Like Tβ4, Profilin-1 sequesters G-actin maintaining a large pool of monomeric actin. Unlike Tβ4 however, the high affinity of Profilin-1 for ATP allows it to act as a catalyst for the conversion of G-actin.ADP to G-actin.ATP, hence aiding the polymerization of G-actin to F-actin filaments.[38] In fact, Profilin-1, Tβ4, and actin have been shown to produce a complex.[39] This, alongside the fact that Cofilin-1 and Tβ4 have been shown to co-localize in multiple cells types, further validates the nature of their finely balanced roles in cytoskeletal dynamics.[40,41] It would be of interest to dissect the interactions of these three proteins with *LINC00961* in future.

We show that SPAAR binds to SYNE1, another actin-binding protein, which suggests that the pro-angiogenic effects of SPAAR could be mediated through SYNE1 and the actin cytoskeleton. This is in contrast to our proposed mechanism of action of *LINC00961*, which may negatively affect actin cytoskeleton rearrangement through interaction with Tβ4. SYNE1 is involved in the cellular organization of organelles via connecting them to the actin cytoskeleton. SYNE1 is especially important as a member of the linker of nucleoskeleton and cytoskeleton complex which tethers the nuclear lamina to the actin cytoskeleton during nuclear positioning and cell polarization.[42] Interestingly, SYNE1 is highly expressed in skeletal and cardiac muscle cells as it is essential in maintaining the characteristic peripherally located nuclei.[43] Matsumoto and colleagues (2017) describe rapid muscle regeneration in mice lacking SPAAR; it would be interesting to ascertain if this phenomenon is in part mediated by an interaction, or lack thereof, between SPAAR and SYNE1. Furthermore, SYNE1 siRNA KD in HUVECs has been shown to reduce tubule formation in a Matrigel assay and decreased migration[34,44] similar to our results with KD of the LINC00961/SPAAR locus.

Cytoskeletal remodelling is a dynamic process which is constantly being influenced by internal and external signals, with many actin-binding proteins having been identified.[45] Here, we show that *LINC00961 and* SPAAR have independent actin-binding protein partners that could influence downstream cytoskeletal architecture. It will be of interest to investigate if, and how, lncRNA and micropeptide levels can change cellular behaviour through cytoskeletal changes.

In conclusion, our study provides important evidence for the expression and function of *LINC00961* in ECs. Our work shows a role for the *LINC00961* RNA, independent of the micropeptide SPAAR. This highlights the importance of a detailed bioinformatic and experimental approach to reveal the contribution of putative lncRNAs and their encoded proteins in cell behaviours.

Supplementary material

Supplementary material is available at *Cardiovascular Research* online.

Authors' contributions

A.H.B. conceived the study. A.H.B., H.L.S., R.S., M.B., and J.R. designed experiments and interpreted data. H.L.S., R.S, M.B., M.B., M.M., and C.R.P. performed experiments. J.R. performed the bioinformatics analysis, A.C., M.B., J.M., J.R., and A.H.B. supervised the research. A.H.B., H.L.S., R.S., and J.R. wrote the manuscript. All the authors discussed the data and edited the manuscript.

Acknowledgements

Flow cytometry data were generated with support from the QMRI Flow Cytometry and cell-sorting facility, University of Edinburgh. Mass spectrometry data were generated with support from the IGMM Mass Spectrometry facility, University of Edinburgh. Animal experiments were supported by the BVS facility, University of Edinburgh. We thank G. Aitchison, Y. Harcus, K. Newton, O. Kelepouri, and L. Rose for technical assistance.

Conflict of interest: none declared.

Funding

The British Heart Foundation supported this work (programme grants: RG/14/3/30706 to A.H.B., RG/15/5/31446 to C.E., and RG/17/4/32662 to A.M.R. and project grant and FS/17/27/32698 to A.H.B.). Professor Baker is supported by EU CARDIOREGENIX, The British Heart Foundation Chair of Translational Cardiovascular Sciences (CH/ 11/2/28733), European Research Council (EC 338991 VASCMIR) and BIRAX Project 16BX17ABIU. A.H.B., M.B., A.M.R., and C.E. are all supported by the British Heart Foundation Regenerative Medicine Centre (RM/13/2/30158). M.B. is supported by the British Heart Foundation (FS/16/4/31831). M.B. is further supported by the British Heart Foundation Centre for Vascular Regeneration (RM/17/3/33381).

References

1. Toborek M, Kaiser S. Endothelial cell functions. Relationship to atherogenesis. *Basic Res Cardiol* 1999;**94**:295–314.
2. De Vries MR, Simons KH, Jukema JW, Braun J, Quax PH. Vein graft failure: from pathophysiology to clinical outcomes. *Nat Rev Cardiol* 2016;**13**:451–470.
3. Pearson J. Normal endothelial cell function. *Lupus* 2000;**9**:183–188.

4. Su JB. Vascular endothelial dysfunction and pharmacological treatment. *World J Cardiol* 2015;**7**:719.
5. Zhao H, Zhao Y, Li Z, Ouyang Q, Sun Y, Zhou D, Xie P, Zeng S, Dong L, Wen H. FLI1 and PKC co-activation promote highly efficient differentiation of human embryonic stem cells into endothelial-like cells. *Cell Death Dis* 2018;**9**:131.
6. Rufaihah AJ, Huang NF, Jamé S, Lee JC, Nguyen HN, Byers B, De A, Okogbaa J, Rollins M, Reijo-Pera R, Gambhir SS, Cooke JP. Endothelial cells derived from human iPSCS increase capillary density and improve perfusion in a mouse model of peripheral arterial disease. *Arterioscler Thromb Vasc Biol* 2011;**31**:e72–e79.
7. Boulberdaa M, Scott E, Ballantyne M, Garcia R, Descamps B, Angelini GD, Brittan M, Hunter A, McBride M, McClure J, Miano JM, Emanueli C, Mills NL, Mountford JC, Baker AH. A role for the long noncoding RNA SENCR in commitment and function of endothelial cells. *Mol Ther* 2016;**24**:978–990.
8. McCracken IR, Taylor RS, Kok FO, de la Cuesta F, Dobie R, Henderson BEP, Mountford JC, Caudrillier A, Henderson NC, Ponting CP, Baker AH. Transcriptional dynamics of pluripotent stem cell-derived endothelial cell differentiation revealed by single-cell RNA sequencing. *Eur Heart J* 2019; doi: 10.1093/eurheartj/ehz351.
9. MacAskill MG, Saif J, Condie A, Jansen MA, MacGillivray TJ, Tavares AAS, Fleisinger L, Spencer HL, Besnier M, Martin E, Biglino G, Newby DE, Hadoke PWF, Mountford JC, Emanueli C, Baker AH. Robust revascularization in models of limb ischemia using a clinically translatable human stem cell-derived endothelial cell product. *Mol Ther* 2018;**26**:1669–1684.
10. Birney E, Stamatoyannopoulos JA, Dutta A, Guigo R, Gingeras TR, Margulies EH, Weng ZP, Snyder M, Dermitzakis ET, Stamatoyannopoulos JA, Thurman RE, Kuehn MS, Taylor CM, Neph S, Koch CM, Asthana S, Malhotra A, Adzhubei I, Greenbaum JA, Andrews RM, Flicek P, Boyle PJ, Cao H, Carter NP, Clelland GK, Davis S, Day N, Dhami P, Dillon SC, Dorschner MO, Fiegler H, Giresi PG, Goldy J, Hawrylycz M, Haydock A, Humbert R, James KD, Johnson BE, Johnson EM, Frum TT, Rosenzweig ER, Karnani N, Lee K, Lefebvre GC, Navas PA, Neri F, Parker SCJ, Sabo PJ, Sandstrom R, Shafer A, Vetrie D, Weaver M, Wilcox S, Yu M, Collins FS, Dekker J, Lieb JD, Tullius TD, Crawford GE, Sunyaev S, Noble WS, Dunham I, Dutta A, Guigo R, Denoeud F, Reymond A, Kapranov P, Rozowsky J, Zheng DY, Castelo R, Frankish A, Harrow J, Ghosh S, Sandelin A, Hofacker IL, Baertsch R, Keefe D, Flicek P, Dike S, Cheng J, Hirsch HA, Sekinger EA, Lagarde J, Abril JF, Shahab A, Flamm C, Fried C, Hackermuller J, Hertel J, Lindemeyer M, Missal K, Tanzer A, Washietl S, Korbel J, Emanuelsson O, Pedersen JS, Holroyd N, Taylor R, Swarbreck D, Matthews N, Dickson MC, Thomas DJ, Weirauch MT, Gilbert J, Drenkow J, Bell I, Zhao X, Srinivasan KG, Sung WK, Ooi HS, Chiu KP, Foissac S, Alioto T, Brent M, Pachter L, Tress ML, Valencia A, Choo SW, Choo CY, Ucla C, Manzano C, Wyss C, Cheung E, Clark TG, Brown JB, Ganesh M, Patel S, Tammana H, Chrast J, Henrichsen CN, Kai C, Kawai J, Nagalakshmi U, Wu JQ, Lian Z, Lian J, Newburger P, Zhang XQ, Bickel P, Mattick JS, Carninci P, Hayashizaki Y, Weissman S, Dermitzakis ET, Margulies EH, Hubbard T, Myers RM, Rogers J, Stadler PF, Lowe TM, Wei CL, Ruan YJ, Snyder M, Birney E, Struhl K, Gerstein M, Antonarakis SE, Gingeras TR, Brown JB, Flicek P, Fu YT, Keefe D, Birney E, Denoeud F, Gerstein M, Green ED, Kapranov P, Karaoz U, Myers RM, Noble WS, Reymond A, Rozowsky J, Struhl K, Siepel A, Stamatoyannopoulos JA, Taylor CM, Taylor J, Thurman RE, Tullius TD, Washietl S, Zheng DY, Liefer LA, Wetterstrand KA, Good PJ, Feingold EA, Guyer MS, Collins FS, Margulies EH, Cooper GM, Asimenos G, Thomas DJ, Dewey CN, Siepel A, Birney E, Keefe D, Hou MM, Taylor J, Nikolaev S, Montoya-Burgos JI, Loytynoja A, Whelan S, Pardi F, Massingham T, Brown JB, Huang HY, Zhang NR, Bickel P, Holmes I, Mullikin JC, Ureta-Vidal A, Paten B, Seringhaus M, Church D, Rosenbloom K, Kent WJ, Stone EA, Gerstein M, Antonarakis SE, Batzoglou S, Goldman N, Hardison RC, Haussler D, Miller W, Pachter L, Green ED, Sidow A, Weng ZP, Trinklein ND, Fu YT, Zhang ZDD, Karaoz U, Barrera L, Stuart R, Zheng DY, Ghosh S, Flicek P, King DC, Taylor J, Ameur A, Enroth S, Bieda MC, Koch CM, Hirsch HA, Wei CL, Cheng J, Kim J, Bhinge AA, Giresi PG, Jiang N, Liu J, Yao F, Sung WK, Chiu KP, Vega VB, Lee CWH, Ng P, Shahab A, Sekinger EA, Yang A, Moqtaderi Z, Zhu Z, Xu XQ, Squazzo S, Oberley MJ, Inman D, Singer MA, Richmond TA, Munn KJ, Rada-Iglesias A, Wallerman O, Komorowski J, Clelland GK, Wilcox S, Dillon SC, Andrews RM, Fowler JC, Couttet P, James KD, Lefebvre GC, Bruce AW, Dovey OM, Ellis PD, Dhami P, Langford CF, Carter NP, Vetrie D, Kapranov P, Nix DA, Bell I, Patel S, Rozowsky J, Euskirchen G, Hartman S, Lian J, Wu JQ, Urban AE, Kraus P, Van Calcar S, Heintzman N, Kim TH, Wang K, Qu CX, Hon G, Luna R, Glass CK, Rosenfeld MG, Aldred SF, Cooper SJ, Halees A, Lin JM, Shulha HP, Zhang XL, Xu MS, Haidar JNS, Yu Y, Birney E, Weissman S, Ruan YJ, Lieb JD, Iyer VR, Green RD, Gingeras TR, Wadelius C, Dunham I, Struhl K, Hardison RC, Gerstein M, Farnham PJ, Myers RM, Ren B, Snyder M, Thomas DJ, Rosenbloom K, Harte RA, Hinrichs AS, Trumbower H, Clawson H, Hillman-Jackson J, Zweig AS, Smith K, Thakkapallayil A, Barber G, Kuhn RM, Karolchik D, Haussler D, Kent WJ, Dermitzakis ET, Armengol L, Bird CP, Clark TG, Cooper GM, de Bakker PIW, Kern AD, Lopez-Bigas N, Martin JD, Stranger BE, Thomas DJ, Woodroffe A, Batzoglou S, Davydov E, Dimas A, Eyras E, Hallgrimsdottir IB, Hardison RC, Huppert J, Sidow A, Taylor J, Trumbower H, Zody MC, Guigo R, Mullikin JC, Abecasis GR, Estivill X, Birney E, Bouffard GG, Guan XB, Hansen NF, Idol JR, Maduro VVB, Maskeri B, McDowell JC, Park M, Thomas PJ, Young AC, Blakesley RW, Muzny DM, Sodergren E, Wheeler DA, Worley KC, Jiang HY, Weinstock GM, Gibbs RA, Graves T, Fulton R, Mardis ER, Wilson RK, Clamp M, Cuff J, Gnerre S, Jaffe DB, Chang JL, Lindblad-Toh K, Lander ES, Koriabine M, Nefedov M, Osoegawa K, Yoshinaga Y, Zhu BL, de Jong PJ; ENCODE Project Consortium. Identification and analysis of functional elements in 1% of the human genome by the ENCODE pilot project. *Nature* 2007;**447**:799–816.
11. Ransohoff JD, Wei Y, Khavari PA. The functions and unique features of long intergenic non-coding RNA. *Nat Rev Mol Cell Biol* 2018;**19**:143–157.
12. Ulitsky I. Evolution to the rescue: using comparative genomics to understand long non-coding RNAs. *Nat Rev Genet* 2016;**17**:601–614.
13. Deng L, Bradshaw AC, Baker AH. Role of noncoding RNA in vascular remodelling. *Curr Opin Lipidol* 2016;**27**:439–448.
14. Uchida S, Dimmeler S. Long noncoding RNAs in cardiovascular diseases. *Circ Res* 2015;**116**:737–750.
15. Maisonpierre PC, Suri C, Jones PF, Bartunkova S, Wiegand SJ, Radziejewski C, Compton D, McClain J, Aldrich TH, Papadopoulos N, Daly TJ, Davis S, Sato TN, Yancopoulos GD. Angiopoietin-2, a natural antagonist for Tie2 that disrupts in vivo angiogenesis. *Science* 1997;**277**:55–60.
16. Kurian L, Aguirre A, Sancho-Martinez I, Benner C, Hishida T, Nguyen TB, Reddy P, Nivet E, Krause MN, Nelles DA, Esteban CR, Campistol JM, Yeo GW, Belmonte J. Identification of novel long noncoding RNAs underlying vertebrate cardiovascular development. *Circulation* 2015;**131**:1278–1290.
17. Neumann P, Jae N, Knau A, Glaser SF, Fouani Y, Rossbach O, Kruger M, John D, Bindereif A, Grote P, Boon RA, Dimmeler S. The lncRNA GATA6-AS epigenetically regulates endothelial gene expression via interaction with LOXL2. *Nat Commun* 2018;**9**:237.
18. Monteiro JP, Bennett M, Rodor J, Caudrillier A, Ulitsky I, Baker AH. Endothelial function and dysfunction in the cardiovascular system: the long non-coding road. *Cardiovasc Res* 2019;**115**:1692–1704.
19. Andrews SJ, Rothnagel JA. Emerging evidence for functional peptides encoded by short open reading frames. *Nat Rev Genet* 2014;**15**:193–204.
20. Makarewich CA, Olson EN. Mining for micropeptides. *Trends Cell Biol* 2017;**27**:685–696.
21. Anderson DM, Anderson KM, Chang CL, Makarewich CA, Nelson BR, McAnally JR, Kasaragod P, Shelton JM, Liou J, Bassel-Duby R, Olson EN. A micropeptide encoded by a putative long noncoding RNA regulates muscle performance. *Cell* 2015;**160**:595–606.
22. Nelson BR, Makarewich CA, Anderson DM, Winders BR, Troupes CD, Wu F, Reese AL, McAnally JR, Chen X, Kavalali ET, Cannon SC, Houser SR, Bassel-Duby R, Olson EN. A peptide encoded by a transcript annotated as long noncoding RNA enhances SERCA activity in muscle. *Science* 2016;**351**:271–275.
23. Matsumoto A, Pasut A, Matsumoto M, Yamashita R, Fung J, Monteleone E, Saghatelian A, Nakayama KI, Clohessy JG, Pandolfi PP. mTORC1 and muscle regeneration are regulated by the LINC00961-encoded SPAR polypeptide. *Nature* 2017;**541**:228–232.
24. van Heesch S, Witte F, Schneider-Lunitz V, Schulz JF, Adami E, Faber AB, Kirchner M, Maatz H, Blachut S, Sandmann C-L, Kanda M, Worth CL, Schafer S, Calviello L, Merriott R, Patone G, Hummel O, Wyler E, Obermayer B, Mücke MB, Lindberg EL, Trnka F, Memczak S, Schilling M, Felkin LE, Barton PJR, Quaife NM, Vanezis K, Diecke S, Mukai M, Mah N, Oh S-J, Kurtz A, Schramm C, Schwinge D, Sebode M, Harakalova M, Asselbergs FW, Vink A, de Weger RA, Viswanathan S, Widjaja AA, Gärtner-Rommel A, Milting H, dos Remedios C, Knosalla C, Mertins P, Landthaler M, Vingron M, Linke WA, Seidman JG, Seidman CE, Rajewsky N, Ohler U, Cook SA, Hubner N. The translational landscape of the human heart. *Cell* 2019;**178**:242–260.e29.
25. Ballantyne MD, Pinel K, Dakin R, Vesey AT, Diver L, Mackenzie R, Garcia R, Welsh P, Sattar N, Hamilton G, Joshi N, Dweck MR, Miano JM, McBride MW, Newby DE, McDonald RA, Baker AH. Smooth Muscle Enriched Long Noncoding RNA (SMILR) regulates cell proliferation. *Circulation* 2016;**133**:2050–2065.
26. Anders S, Pyl PT, Huber W. HTSeq—a Python framework to work with high-throughput sequencing data. *Bioinformatics* 2015;**31**:166–169.
27. Love MI, Huber W, Anders S. Moderated estimation of fold change and dispersion for RNA-seq data with DESeq2. *Genome Biol* 2014;**15**:550.
28. Kuzan A. Thymosin beta as an actin-binding protein with a variety of functions. *Adv Clin Exp Med* 2016;**25**:1331–1336.
29. Smart N, Risebro CA, Melville AA, Moses K, Schwartz RJ, Chien KR, Riley PR. Thymosin beta4 induces adult epicardial progenitor mobilization and neovascularization. *Nature* 2007;**445**:177–182.
30. Smart N, Rossdeutsch A, Riley PR. Thymosin beta4 and angiogenesis: modes of action and therapeutic potential. *Angiogenesis* 2007;**10**:229–241.
31. Skruber K, Read TA, Vitriol EA. Reconsidering an active role for G-actin in cytoskeletal regulation. *J Cell Sci* 2018;**131**:jcs203760.
32. Chancellor T, Lee J, Thodeti CK, Lele T. Actomyosin tension exerted on the nucleus through nesprin-1 connections influences endothelial cell adhesion, migration, and cyclic strain-induced reorientation. *Biophys J* 2010;**99**:115–123.
33. Gordon EJ, Fukuhara D, Westrom S, Padhan N, Sjostrom EO, van Meeteren L, He L, Orsenigo F, Dejana E, Bentley K, Spurkland A, Claesson-Welsh L. The endothelial adaptor molecule TSAd is required for VEGF-induced angiogenic sprouting through junctional c-Src activation. *Sci Signal* 2016;**9**:ra72.
34. Caretti G, Schiltz RL, Dilworth FJ, Di Padova M, Zhao P, Ogryzko V, Fuller-Pace FV, Hoffman EP, Tapscott SJ, Sartorelli V. The RNA helicases p68/p72 and the noncoding RNA SRA are coregulators of MyoD and skeletal muscle differentiation. *Dev Cell* 2006;**11**:547–560.

35. Hube F, Velasco G, Rollin J, Furling D, Francastel C. Steroid receptor RNA activator protein binds to and counteracts SRA RNA-mediated activation of MyoD and muscle differentiation. *Nucleic Acids Res* 2011;**39**:513–525.
36. Grelet S, Link LA, Howley B, Obellianne C, Palanisamy V, Gangaraju VK, Diehl JA, Howe PH. A regulated PNUTS mRNA to lncRNA splice switch mediates EMT and tumour progression. *Nat Cell Biol* 2017;**19**:1105–1115.
37. Min KW, Davila S, Zealy RW, Lloyd LT, Lee IY, Lee R, Roh KH, Jung A, Jemielity J, Choi EJ, Chang JH, Yoon JH. eIF4E phosphorylation by MST1 reduces translation of a subset of mRNAs, but increases lncRNA translation. *Biochim Biophys Acta* 2017;**1860**:761–772.
38. Xue B, Leyrat C, Grimes JM, Robinson RC. Structural basis of thymosin-β4/profilin exchange leading to actin filament polymerization. *Proc Natl Acad Sci USA* 2014;**111**:E4596–E4605.
39. Yarmola EG, Parikh S, Bubb MR. Formation and implications of a ternary complex of profilin, thymosin β4, and actin. *J Biol Chem* 2001;**276**:45555–45563.
40. Al Haj A, Mazur AJ, Buchmeier S, App C, Theiss C, Silvan U, Schoenenberger C-A, Jockusch BM, Hannappel E, Weeds AG, Mannherz HG. Thymosin beta4 inhibits ADF/cofilin stimulated F-actin cycling and hela cell migration: reversal by active Arp2/3 complex. *Cytoskeleton* 2014;**71**:95–107.
41. Mannherz HG, Hannappel E. The β-thymosins: intracellular and extracellular activities of a versatile actin binding protein family. *Cell Motil Cytoskeleton* 2009;**66**:839–851.
42. Mellad JA, Warren DT, Shanahan CM. Nesprins LINC the nucleus and cytoskeleton. *Curr Opin Cell Biol* 2011;**23**:47–54.
43. Zhou C, Rao L, Shanahan CM, Zhang Q. Nesprin-1/2: roles in nuclear envelope organisation, myogenesis and muscle disease. *Biochem Soc Trans* 2018;**46**:311–320.
44. King SJ, Nowak K, Suryavanshi N, Holt I, Shanahan CM, Ridley AJ. Nesprin-1 and nesprin-2 regulate endothelial cell shape and migration. *Cytoskeleton* 2014;**71**:423–434.
45. Revenu C, Athman R, Robine S, Louvard D. The co-workers of actin filaments: from cell structures to signals. *Nat Rev Mol Cell Biol* 2004;**5**:635–646.

Translational perspective

Treatment of ischaemic conditions remains a major cardiovascular health burden. Identification of genes and non-coding RNAs that regulate the function of the vascular endothelium is important to understand and evolve potential new strategies that might enhance vascular regeneration. Here, we describe and dissect the functional importance of a micropeptide-encoding RNA transcript in the vascular endothelium, and demonstrate that both the RNA and the peptide regulate endothelial biology. Modulation of this axis may be a novel approach to regulate angiogenesis.

Corrigendum

doi:10.1093/cvr/cvaa157
Online publish-ahead-of-print 17 June 2020

Corrigendum to: The ACE2 expression in human heart indicates new potential mechanism of heart injury among patients infected with SARS-CoV-2 [*Cardiovasc Res* 2020;116:1097–1100].

In the Methods section, the sentence 'Transcriptome analysis was based on an in-house RNA sequencing dataset containing 15 donor hearts and 40 failing explanted hearts, which were obtained from the heart transplantation centre of Fuwai Hospital.' has been corrected to 'Transcriptome analysis was based on an in-house RNA sequencing dataset containing 15 donor hearts and 40 failing explanted hearts, which were obtained from previous studies (GSE135055 and GSE120064).' in the online version of the article.

SUPLEMENTAL MATERIAL

DETAILED METHODS

Directed endothelial differentiation from human embryonic stem cells

A previously published protocol was employed to generate endothelial cells (ECs) from H9 human embryonic stem cells (hESCs) [1]. Briefly, hESCs, were dissociated into single cells using Tryple Select (Life Technologies, UK). 1×10^4 cells were seeded into a 5% Pluronic F-127 (Sigma-Aldrich, UK) coated 96- well round bottom microplates to generate embryoid bodies (EBs). The plates were centrifuged at 300 g for 3 minutes. Cells were cultured in Stemline II Hematopoietic expansion medium with the addition of 5 ng/mL Activin A (Peprotech, USA), 10 μmol/L Y-27632 (Millipore, Temecula, USA, 10 ng/mL vascular endothelial growth factor (VEGF) (Peprotech, USA), and 10 ng/mL bone morphogenetic protein 4 (BMP4) (R and D Systems, Minneapolis). After 2 days, the EBs were supplemented with Stemline II Hematopoietic expansion medium containing 10 ng/mL VEGF, 70 ng/mL Wnt3A, 140 ng/mL BMP4 and 35 ng/mL Activin A. On day 3, EBs were transferred to 0.1% gelatine-coated 6 well culture dishes (Sigma-Aldrich, UK) and resuspended in endothelial growth medium-2 (EGM-2) (Lonza, UK). The media was supplemented with 50 ng/ml of VEGF and the accompanying bullet kit, minus the VEGF and FBS supplement. Cells were maintained until day 7. Flow cytometry was performed as previously described [1]. Briefly, cell populations were dissociated by enzymatic digestion. Harvested cells were washed in PBS and incubated with specific antibodies (BD Bioscience, USA). FACS sorting was performed using anti-human CD326, anti human-CD56, anti human-CD31, and anti-human-CD144 by FACS Aria I or Aria III cell sorter (BD Biosciences, San Diego, USA. RNA was then extracted from these sorted populations.

Cell culture

Human saphenous vein endothelial cells (HSVECs) were obtained by enzymatic collagenase digestion of human saphenous veins (Ethics 15/ES/0094) and maintained in EC growth medium (EGM-2 BulletKit™) (Lonza, Basel, Switzerland) supplemented with foetal bovine serum (10%, Life Technologies, Paisley, UK) and Penicillin-Streptomycin (100U/ml) (Gibco, Paisley, UK). Human umbilical vein endothelial cells (HUVEC) (Lonza, Basel Switzerland) were cultured in the EC growth medium EGM2 (Lonza, Basel Switzerland) supplemented with 10% foetal bovine serum (FBS) (Life Technologies, Paisley UK) at 37°C and 5% CO_2. All cells lines were used between passages 3 and 6, and kept at 37°C in a humidified atmosphere containing 5% CO_2.

dsiRNA and GapmeR transfections

GapmeRs were obtained from Exiqon (Denmark) and double stranded dicer-substrate short interfering RNA (dsiRNA) obtained from IDT (Leuven, Belgium) or Qiagen (UK). Sequences or product references are listed in Supplementary table 7. Transfection were performed using RNA iMAX (Life Technologies, USA).

RNA-Sequencing

RNA was obtained using the miRNeasy kit (Qiagen, U.K) from hESCs (4 replicates), the mesodermal and non-mesodermal population (4 replicates), the endothelial and non-endothelial population (2 replicates) and HSVECs (4 replicates). Ribosomal-depleted stranded libraries were prepared by Beckman Coulter Genomics and sequenced with an Illumina HiSeq at an average of 90 million reads per sample (paired end 2 x 100bp). Mapping was performed on the human genome reference sequence GRCh38, using Tophat version 2.0.10 [2] in conjunction with Bowtie version 1.0.0 based on a GRCh38 Ensembl transcriptome annotation. HTSeq was used to obtain a read count [3]. The differential expression was assessed using DESeq2 [4] and we considered a threshold of absolute Fold Change > 2 and adjusted p value < 0.01 to identify significant changes between two conditions. Sample clustering was evaluated using the Principal component analysis (PCA) tool available in DESeq2 on the regularized log

transformed data. The gene expression value, given as Fragments Per Kilobase of transcript per Million map read (FPKM) was obtained using Cufflinks [5]. Enriched genes in the day 7 endothelial population were obtained by selecting the significant changes versus the embryonic stem cell samples as well as the non-endothelial cell population. Genes with an expression above 2 FPKM were retained. The gene ontology analysis was carried out using topGO) on enriched genes over a background of expressed genes (FPKM>2 in at least one condition) (https://bioconductor.org/packages/release/bioc/html/topGO.html). Fisher's exact test was used to calculate p-values. GO terms were subsequently filtered to remove redundant terms using GO Trimming [6] with a soft threshold of 0.4. Heatmap of the z-score was generated thanks to the package 'pheatmap' (https://cran.r-project.org/web/packages/pheatmap/index.html). The z-score represents the deviation from the mean by standard deviation units of the Log2(FPKM+1) for each gene.

Transcript expression analysis

Total RNA was isolated using the miRNeasy kit (Qiagen, U.K). RNA was reverse transcribed using random primers, following manufacturer's instructions. Quantitative PCR (qPCR) was carried with TaqMan (Life Technologies, UK) or Power SYBR technologies (Life Technologies, UK). Ubiquitin C (UBC) was used as a reference gene. qPCR reactions were performed in technical duplicates with the QuantStudio 5 Real-time PCR system (Life Technologies, Paisley, UK). Relative quantification (RQ) was calculated using the 2-(ΔΔCT) method. The sequences of primers or TaqMan probes are provided in Supplementary Table 5.

Network formation assay

Network formation assay was performed using Matrigel (Corning, USA) according to the manufacturer's protocol. Briefly, 70 µl of Matrigel was used per well of a 96 well plate and allowed to set at 37 °C and 5 % CO_2 for 30 minutes. After which, 1 x 10^4 dissociated HUVECs were plated upon the Matrigel layer and incubated in EGM-2 (LONZA, UK) for 5.5 hours at 37 °C and 5 % CO_2. Calcein AM (Invitrogen) was used to determine cell viability. Tubule-like networks were visualised with a light microscope and phase images were taken at 4x magnification. Matrigel assays were performed in triplicate and total branch length was determined using angiogenesis analyser for Image J.

Proliferation assay

Proliferation was assessed using the Click-it EdU (5-Ethynyl-2´-deoxyuridine) 488 Proliferation assay (Life Technologies, UK) as per manufactures instructions. Briefly, HUVECs were seeded at a density of 1 x 10^5 per well of a 96 well plate 24 hrs prior to serum starvation conditions consisting of DMEM supplemented with 2% heat-inactivated FBS, 50 µg/mL penicillin, 50 µg/mL streptomycin, 2 mmol/L L-Glutamate and 1 mmol/L sodium pyruvate. After which, cells were induced to proliferate for 24 hrs by culturing in complete EGM-2 media in 10 % serum with 10 µM EdU. Cells were then dissociated and fixed in ice-cold 70 % ethanol for EdU flow cytometry analysis. EdU incorporation was confirmed using anti-EdU 488 antibody.

Migration assays

Migration assays were performed using an Electric Cell-substrate Impedance Sensing (ECIS) machine (Applied BioPhysics) as per Manufacturer's instructions. Briefly, 6 x 10^4 HUVECs were seeded into each well of an ECIS wound healing slide. The following conditions were used: electroporate 2500µA; wound: 30 second; frequency 40000. Migration ability was calculated after 24h by: velocity=r/t, where the radius is 125µm.

Cell viability assay

Cell viability assay (BioLegend) was performed using FITC Annexin V Detection Kit with PI (BioLegend) according to the manufacturer's protocol. In brief, cells were resuspended in 100 µl of binding buffer. 5 µl of Annexin V was added to the cell solution for 15 minutes before the addition of a further 400 µl of binding buffer. Prior to flow cytometry analysis 1:1000 of ToPro 3 (Life Technologies, UK), was added to the samples. Unstained and single stained samples were used to calibrate the setting on the flow cytometer. Samples were analysed on a BD LSR Fortessa Cell Analyzer (BD Biosciences, USA). The resulting data was analysed with FlowJo software (FlowJo LCC, USA).

Endothelial barrier integrity assay

An ECIS machine was used as per Manufacturer's instructions to measure resistance between cells in previously transfected cells. Briefly, 4 x 10^4 HUVECs were seeded into each well of an ECIS chamber side. Cells were allowed to adhere and then resistance was measured over 10 hours. Barrier resistance is expressed as Rb [Ohm x cm^2].

Lentiviral mediated production and induction

To generate lentiviral vectors, HEK293T cells were triple transfected with; a plasmid encoding the envelope of vesicular stomatitis virus (VSVg) (pMDG) (Plasmid Factory, Bielefeld, Germany), a packaging plasmid (pCMVΔ8.74) and pLNT/SFFV plasmid employing polyethylenimine (PEI; Sigma-Aldrich, USA) as previously described [1, 7]. Titres were determined by TaqMan qPCR. The following primers were used for the quantification: forward, 5'-TGTGTGCCCGTCTGTTGTGT-3'; reverse, 5'-GAGTCCTGCGTCGAGAGAGC-3'; probe, 5'- (FAM)- CAGTGGCGCCCGAACAGGGA- (TAMRA)-3. LINC00961 full-length, ΔΔATG961 and SPAAR sequences were generated by GeneART Gene synthesis (Life Technologies, UK). The sequences were cloned into pLNT/SFFV-MCS using the Kpn1 and XhoI sites (kind gift from Adrian J. Thrasher, London, UK).

Western blotting

HUVECs were washed with PBS and resuspended in 200 µl of RIPA buffer (Life Technologies, UK) supplement with cOmplete Mini, EDTA-free Protease Inhibitor Cocktail tablets (Roche, UK). Lysates were incubated on ice for 30 mins to allow complete lysis then were centrifuged at 15000 g for 10 mins at 4 °C to remove cell debris. Total protein concentration was determined using a Pierce™ BCA Protein Assay Kit (Thermo Fisher, UK) and a Perkin Elmer Victor 2 Microplate Reader. Western blots were conducted on the Life Technologies Bolt System as per manufacturer's instructions (Life Technologies, UK). 30 µg of protein with reducing Bolt loading buffer (Life Technologies, UK) was boiled for 5 minutes at 95°C. Samples were loaded into a 10 % bolt acrylamide gel (Life Technologies, UK). The proteins were transferred onto a nitrocellulose membrane and transferred at 10V for 1 hour. Membranes were blocked in 5% milk for 1 hour. SPAAR antibody (Cell Signalling) and β-Actin antibody (Abcam) were used at 1:1000 overnight for 4 °C. Secondary antibodies were used at 1:5000 (Li-Cor, UK). Detection was performed using the Li-Cor Odyssey Blot System (Li-Cor, UK). Protein loading levels were determined using the REVERT total protein stain normalisation protocol as per manufacturer's instructions (Li-Cor, UK).

RNA fractionation

RNA fractionation was performed as previously described [1] and as per manufacturer's instructions (Paris Kit, Life Technologies, UK). Briefly, HUVECs were dissociated and homogenized in ice-cold Fractionation Buffer and incubated for 5 minutes at 4° C. Nuclei were separated from the cytoplasmic fraction by centrifugation. Intact nuclei were then lysed using the Cell Disruption Buffer. The lysed cellular components were mixed in equal volumes with Lysis/Binding solution and applied to a filter containing cartridge. The RNA was then washed three times before eluting in nuclease free water. For cDNA synthesis, equal volumes of nuclear and cytoplasmic RNA were used. *NEAT1* RNA expression in the fractions was used to confirm effective nuclear-cytoplasmic separation.

RNA fluorescence in situ hybridization (FISH)

20 tiled digest oligo probes targeting both exons of LINC00961 were custom generated. RNA-FISH was performed following the manufacturer's instructions (QuantiGene ViewRNA cell ISH cell assay, Life Technologies, UK). For spatial localisation of LINC00961, SNORD3 and UBC were used as controls (Life Technologies, UK). 1 x 10^4 HUVECs were seeded on 0.2 % gelatin coated 16-mm coverslips until 80 % confluency. After which the cells were washed and fixed in 4 % formaldehyde supplemented with 1 % glacial acetic acid. Detergent QS was used to permeabilise the cells and following a 1:6000 protease digest, cells were incubated with a combination of LINC00961 probe and UBC or SNORD3. Unstained cells, incubated with only the probe set buffer served as a negative control. The presence of SNORD3 indicated the permeabilisation of the nucleus. After probe hybridisation, cells were incubated with pre-amplifier for 1 hr and, then amplifier for 30 minutes. Following incubation with fluorescent probes, samples were counterstained with DAPI mounting medium (Vectorshield, UK). Staining was visualised by Andor Revolution XDi spinning disk confocal microscope. Z-stacking confirmed staining within the nucleus. Confocal images were generated with the assistance of University of Edinburgh's Confocal and Advanced Light Microscopy Facility.

Biotinylated LINC00961 RNA pull-down

Biotinylated RNA was *in vitro* transcribed using the T7 RiboMAX Express Large Scale RNA Production System (Promega, UK) as per manufacturer's instructions. Briefly, 1 µg of the cDNA template was used as a template for T7 RNA polymerase *in vitro* transcription and incubated at 37 °C for 30 minutes. The primers used are detailed in Supplementary Table 7. The generated RNA was extracted using the miRNeasy kit (Qiagen, UK) following manufacturer's instructions. The resulting RNA had pCp–Desthiobiotin (Jena Biosciences, UK) attached to the 3'end of the RNA strand via T4 RNA ligase and Pierce RNA 3' End Desthiobiotinylation kit (ThermoScientific, UK). Biotinylated lncRNA was incubated with streptavidin magnetic beads and 20 µg of HUVECs protein lysate. This was performed following the manufacturer's instructions using the Pierce Mag RNA Protein Pulldown kit (Thermo Scientific). Non-specific interactions were removed by stringent washes and the leftover lncRNA-binding proteins were eluted off the beads. The elution buffer was non-denaturing. Samples were analysed by liquid chromatography mass spectrometry (LC-MS).

Mass spectrometry

Eluting peptides were ionised at +2kV before data-dependent analysis on a Thermo Q-Exactive Plus. MS1 was acquired with mz range 300-1650 and resolution 70,000, and top 12 ions were selected for fragmentation with normalised collision energy of 26, and an exclusion window of 30 seconds. MS2 were collected with resolution 17,500. The AGC targets for MS1 and MS2 were 3e6 and 5e4 respectively, and all spectra were acquired with 1 microscan and without lockmass. Finally, the data were analysed using MaxQuant (ver. 1.5.2.8) in conjunction with Uniprot Fasta database, with match between runs (MS/MS not required), LFQ with 1 peptide required, and statistical analyses performed in R. Subtractive proteomics was performed to identify proteins in the LINC00961 pull-downs compared to the GFP control and/or beads only pull-downs (n=2). Identified peptides were considered only if they have over 2 unique peptides and were chosen based on LFQ. These candidates were taken forward for targeted immunoprecipitation.

Thymosin beta 4-x immunoprecipitation

Tβ4 immunoprecipitation was performed as previously described [8]. Briefly, five 10cm^2 dishes of HUVECs were crosslinked with 0.4% formaldehyde for 10 minutes and then neutralised with 1 M glycine. Cells were harvested by scraping and lysing with Triton X-100-supplemented hypotonic buffer [10 mM Tris-HCL pH 7.5, 10 mM NaCl, 10 mM EDTA, 0.5% Triton X-100, and cOmplete Mini, EDTA-free Protease Inhibitor Cocktail tablets (Roche, UK)]. The supernatant was then centrifuged and NaCl adjusted to 150mM. 10 % of the total supernatant was removed for downstream RNA extraction. Supernatants were pre-cleared with 20 µl of

Dynalbeads G (Life Technologies, UK) at 4°C for 1 hr using an orbital rotator. Beads were then removed using a DynaMag and the supernatant was transferred to a fresh tube. 20 µl of Dynalbeads G and 4 µg Anti-TMSB4X antibody (Santa Cruz Biotechnology, UK) was introduced into the supernatant, which was further supplemented with RNase inhibitors. Samples were incubated at 4°C for 2 hrs on an orbital rotator. Using the DynalMag magnet, the bead bound complexes were washed 5 times with NET-2 buffer (NET-2 buffer [50 mM Trsi-HCl pH 7.4, 200 mM NaCl, 0.05 % NP40, and cOmplete Mini, EDTA-free Protease Inhibitor Cocktail tablets, RNase inhibitors). After the final wash was removed, the bound complexes were de-crosslinked by incubation at 70 °C for 1 hour before RNA extraction.

Immunofluorescent staining

Adductor muscle was paraffin embedded and 5µm sections were taken. Tissues were stained with isolectin-B4 to show capillaries (endothelium) (Thermo Fisher) and α-smooth muscle actin (α-SMA) (Sigma) to show smooth muscle and pericyte cells (arteries/arterioles). Tissue was imaged using either a Zeiss LSM 780 or Slide scanner Axio Scan.Z1, Zeiss. Five regions of interest (0.42 μm^2) were taken from 3 sections of each adductor muscle. Capillary density and αSMA positive vessels were quantified utilising Image J software and created a macro to detect positive (capillaries) which we used on the green channel only of each image:

```
run("Subtract Background...", "rolling=50");
setOption("BlackBackground", false);
run("Make Binary");
run("Watershed");
run("Analyze Particles...", "size=0.03-Infinity show=Ellipses exclude include summarize in_situ");
```

Images were analysed with a size limit of particles set to 0.02 or 0.03.

Cells were fixed for 30 min at room temp with 4% paraformaldehyde and washed with phosphate buffered saline (PBS). Next, cells were permeabilised with 0.1% Triton-X-100 in PBS for 5 min at room temperature. A furtherPBS wash was carried out and cell were then blocked for 30 min at room temperature with 5% goat serum in PBS. Tβ4 antibody (Abcam 14335) was prepared in 5% goat serum (1/200) and cells incubated for 1 hour at 37ºC. The primary antibody solution was washed off using PBS before cells were incubated with a secondary antibody (goat anti rabbit Alexa-Fluor-488, Abcam 150077) diluted 1/400 in 5% goat serum for 45 min at 37ºC, protected from light. Finally, cells were washed with PBS and then mounted with ProLong Gold containing DAPI (Thermo Fisher). Images were taken on a Zeiss LSM 780 confocal microscope.

SUPPLEMENTAL REFERENCES

1. Boulberdaa M, Scott E, Ballantyne M, Garcia R, Descamps B, Angelini GD, Brittan M, Hunter A, McBride M, McClure J, Miano JM, Emanueli C, Mills NL, Mountford JC, Baker AH. A Role for the Long Noncoding RNA SENCR in Commitment and Function of Endothelial Cells. *Mol Ther* 2016;**24**:978-990.
2. Kim D, Pertea G, Trapnell C, Pimentel H, Kelley R, Salzberg SL. TopHat2: accurate alignment of transcriptomes in the presence of insertions, deletions and gene fusions. *Genome Biol* 2013;**14**:R36.
3. Anders S, Pyl PT, Huber W. HTSeq--a Python framework to work with high-throughput sequencing data. *Bioinformatics* 2015;**31**:166-169.
4. Love MI, Huber W, Anders S. Moderated estimation of fold change and dispersion for RNA-seq data with DESeq2. *Genome Biol* 2014;**15**:550.
5. Trapnell C, Roberts A, Goff L, Pertea G, Kim D, Kelley DR, Pimentel H, Salzberg SL, Rinn JL, Pachter L. Differential gene and transcript expression analysis of RNA-seq experiments with TopHat and Cufflinks. *Nat Protoc* 2012;**7**:562-578.
6. Jantzen SG, Sutherland BJ, Minkley DR, Koop BF. GO Trimming: Systematically reducing redundancy in large Gene Ontology datasets. *BMC Res Notes* 2011;**4**:267.
7. Ballantyne MD, Pinel K, Dakin R, Vesey AT, Diver L, Mackenzie R, Garcia R, Welsh P, Sattar N, Hamilton G, Joshi N, Dweck MR, Miano JM, McBride MW, Newby DE, McDonald RA, Baker AH. Smooth Muscle Enriched Long Noncoding RNA (SMILR) Regulates Cell Proliferation. *Circulation* 2016;**133**:2050-2065.
8. Elbarbary RA, Li W, Tian B, Maquat LE. STAU1 binding 3' UTR IRAlus complements nuclear retention to protect cells from PKR-mediated translational shutdown. *Genes Dev* 2013;**27**:1495-1510.

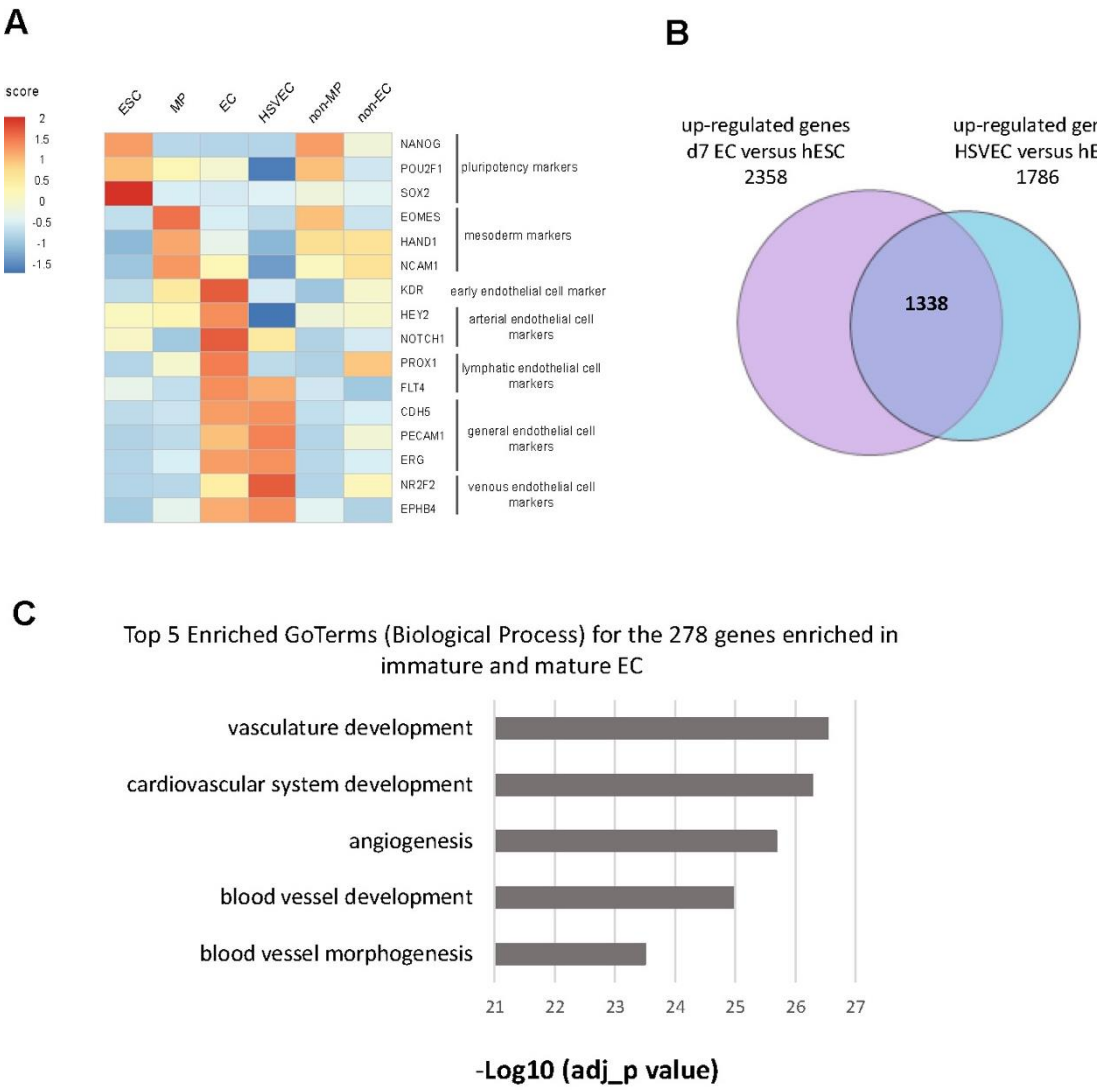

Supplementary Figure 1: Validation and characterization of the endothelial cell identity of the day7 EC population.(A) Heatmap (as z-score of Log2(FPKM+1)) showing the down-regulation of pluripotency associated genes and the up-regulation of mesoderm and endothelial specific transcripts. The rows are displayed based on a hierarchical clustering. The different conditions are day 0 H9 hESC (ESC); Day 3 mesodermal population $CD326^{low}CD56^{+}$ (MP); Day 3 remaining population (non-MP); Day 7 EC $CD144^{+}CD31^{+}$(EC); Day 7 Remaining population (non-EC); Human Saphenous vein endothelial cell (HSVEC). (B) Venn diagram showing the overlap of up-regulated genes between d7 EC *versus* hESCs, and HSVECs *versus* hESCs. (C) GO analysis on the genes enriched in the d7 EC population. The graph shows the top 10 biological GO terms ranked by p-value.

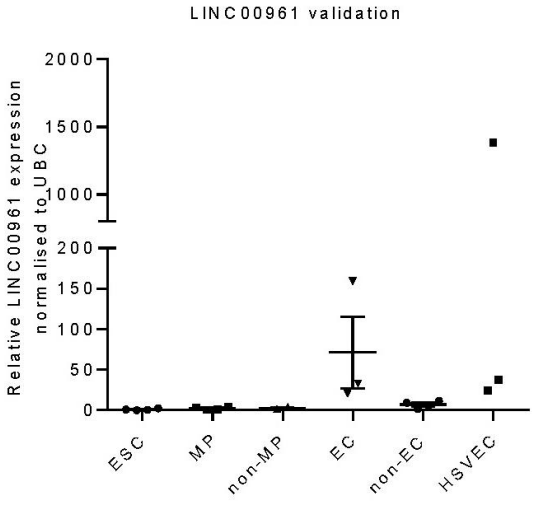

Supplementary Figure 2: Validation of LINC00961 expression in day7 population. qRT-PCR showed that day7 EC and HSVEC positive control samples were both enriched for *LINC00961* transcript expression.

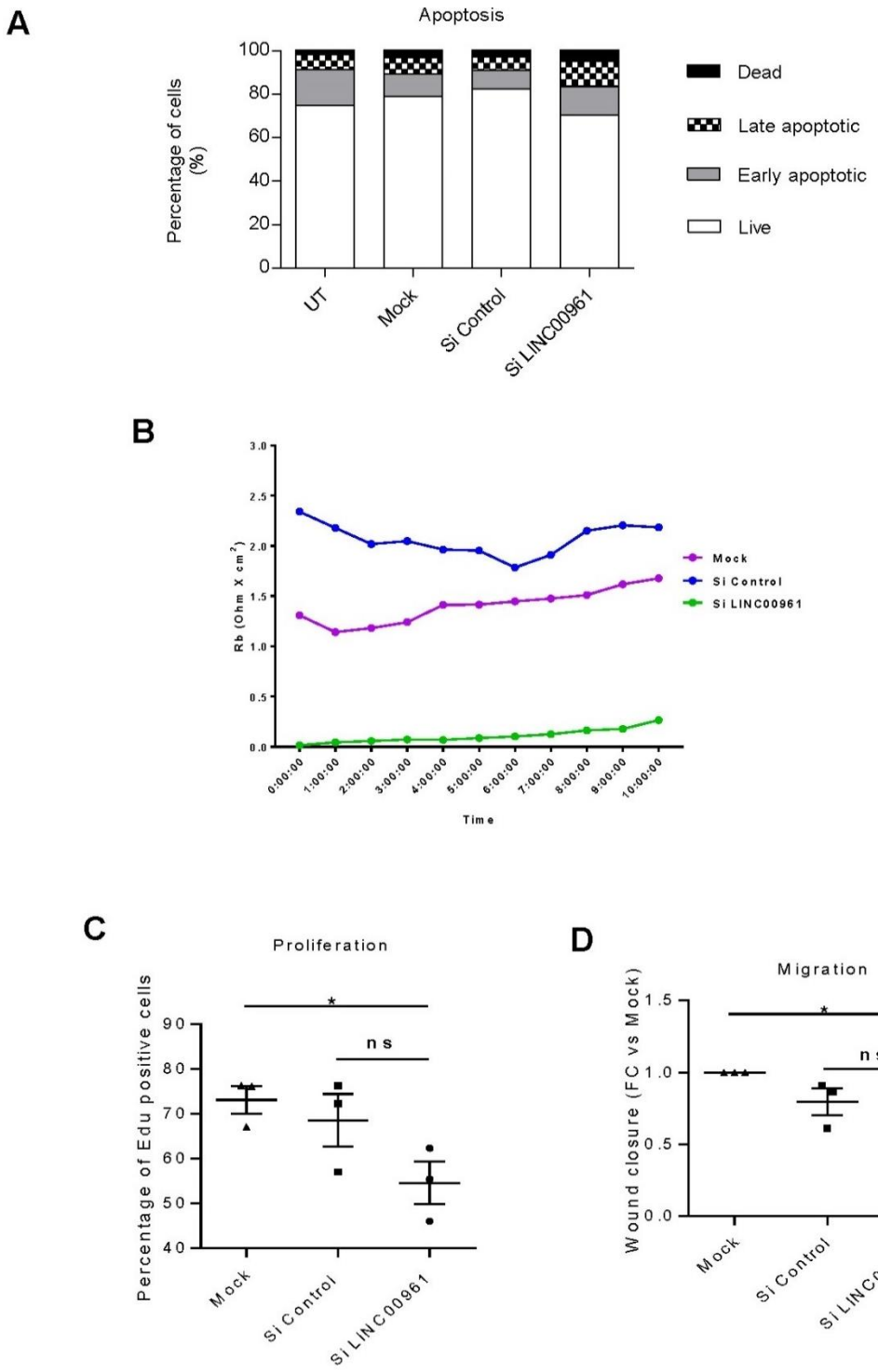

Supplementary Figure 3: Effect of LINC00961/SPAAR depletion on apoptosis and endothelial membrane integrity. (A) Impact of dsiRNA-mediated LINC00961/SPAAR depletion on cell death as assessed by Annexin V and PI staining compared to controls. (B) Trace of average barrier resistance between cells, in ohm x cm² (Rb), over a 10 hour period, n=4 except for mock n=3. (C) Impact of *LINC00961* depletion on proliferation based on EdU incorporation, n=3. (D) Impact of *LINC00961* depletion on migration, n=3. On the graphs, * $p<0.05$, unpaired t-tests.

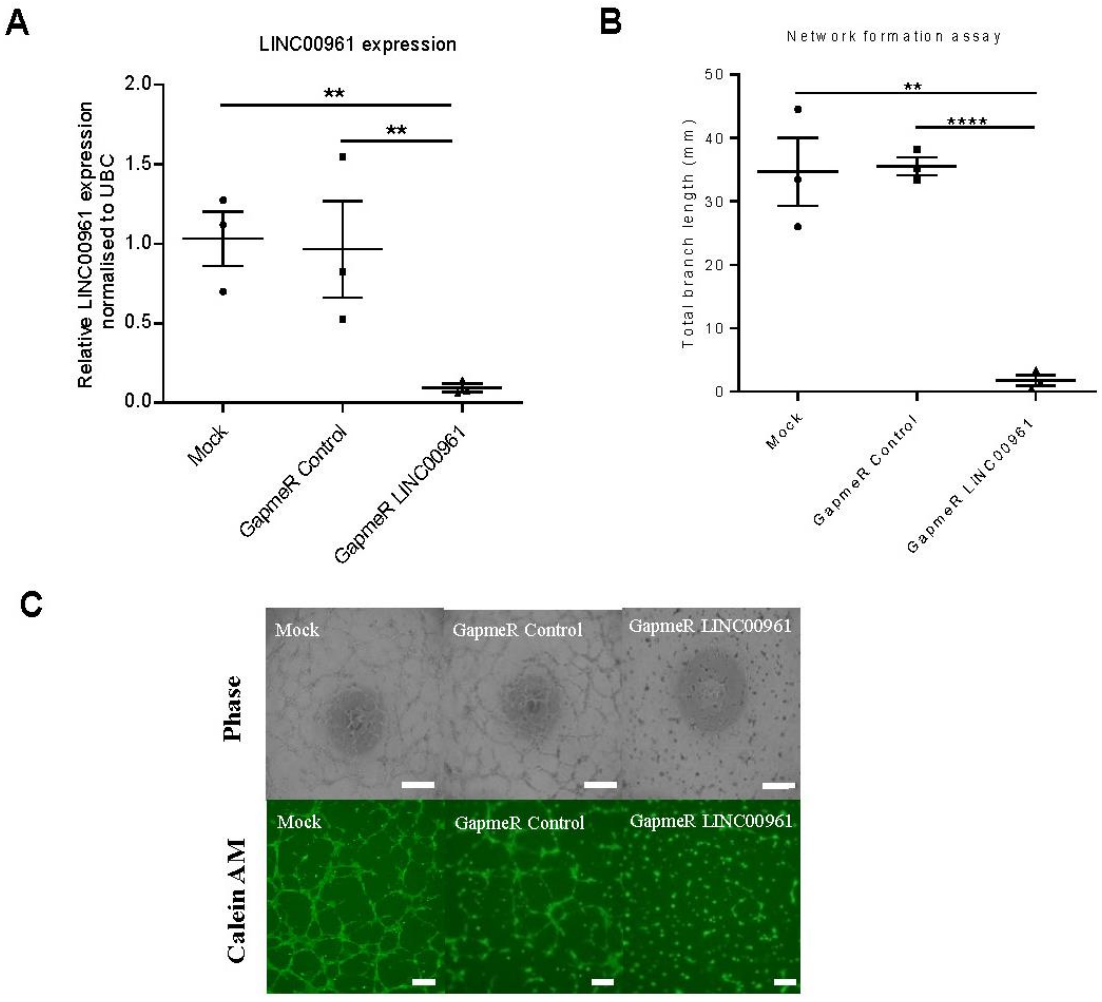

Supplementary Figure 4: Confirmation of the network formation phenotype of LINC00961/SPAAR knock down using GapmeR mediated depletion. (A) qRT-PCR of *LINC00961* in GapmeR depleted HUVECs (compared to GapmeR control and mock transfected cells), n=3.(B) Network formation assay in *LINC00961* depleted HUVECs. Branch length assessed by Image J Angiogenesis plugin., n=3. (C) Representative phase contrast and Calcein AM staining of network formation assay of *LINC00961* depleted HUVECs compared to controls. Phase Scale bar =0.5mm. Calcein AM Scale bar =0.1mm. On the graphs, **p<0.01 ****p<0.0001, unpaired t-tests.

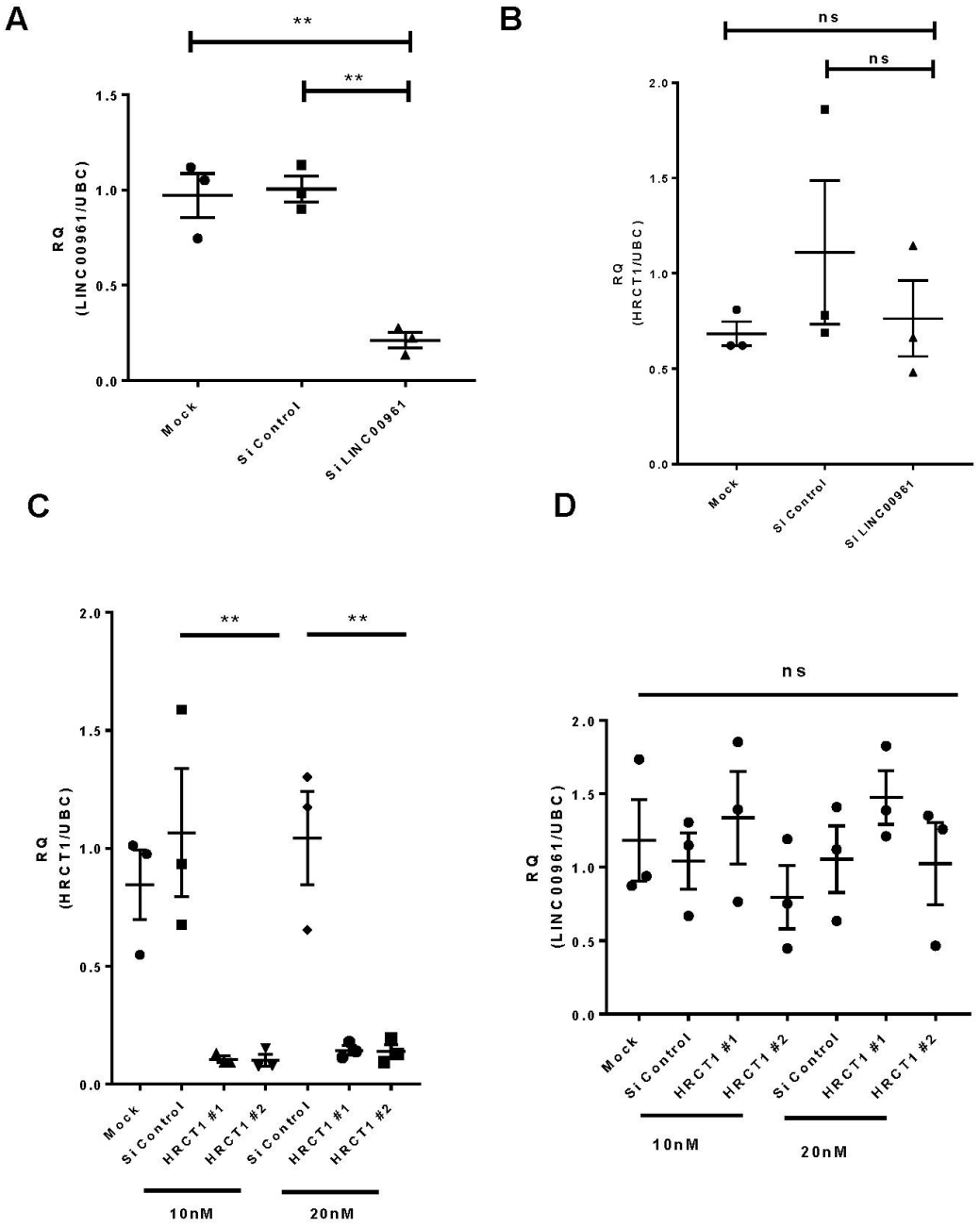

Supplementary Figure 5: *LINC00961* transcript does not regulate *HRCT1* transcript level and *vice versa*. **(A)** Confirmation of *LINC00961* KD by qRT-PCR on dsiRNA treated HUVECs (compared to dsiRNA control and mock transfected cells), n=3. (B) Impact of *LINC00961* dsiRNA on *HRCT1* transcript expression as assessed by qRT-PCR n=3. (C) Confirmation of *HRCT1* KD by qRT-PCR, n=3. (D) Impact of *HRCT1* dsiRNA on *LINC00961* transcript expression as assessed by qRT-PCR, n=4. On the graphs, ns = not significant. **p<0.001, unpaired t-tests.

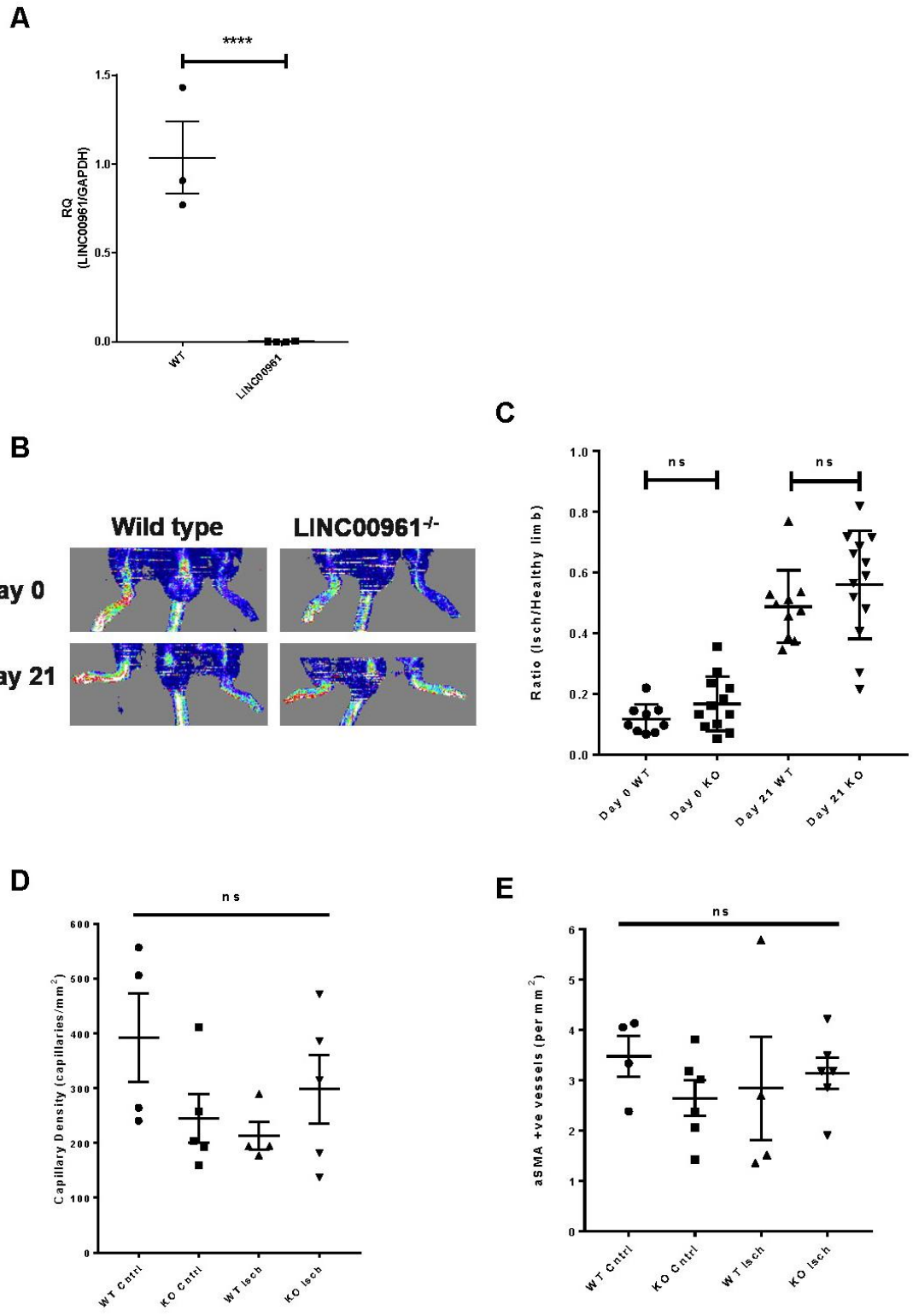
A
****
RQ (LINC00961/GAPDH)
1.5
1.0
0.5
0.0
WT
LINC00961
B
Wild type
LINC00961-/-
Day 0
Day 21
C
ns
ns
Ratio (Isch/Healthy limb)
1.0
0.8
0.6
0.4
0.2
0.0
Day 0 WT
Day 0 KO
Day 21 WT
Day 21 KO
D
ns
Capillary Density (capillaries/mm2)
600
500
400
300
200
100
0
WT Cntrl
KO Cntrl
WT Isch
KO Isch
E
ns
aSMA +ve vessels (per mm2)
6
5
4
3
2
1
0
WT Cntrl
KO Cntrl
WT Isch
KO Isch

F

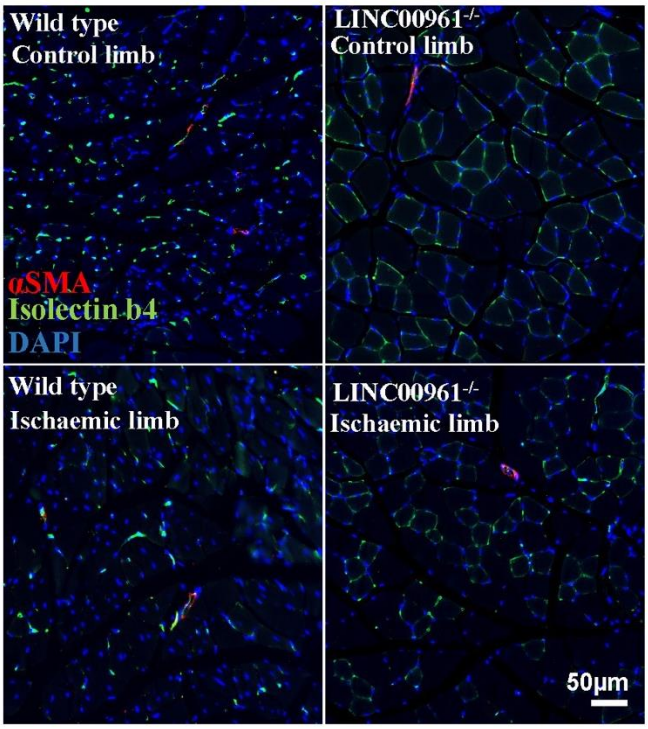

Supplementary Figure 6: *LINC00961*$^{-/-}$ animals show no differences in vessel densities after 21 days hind limb ischemia. (A) Confirmation of *LINC00961* deletion in knock out animals. *LINC00961* transcript expression as assessed by qRT-PCR in whole kidney tissue, n= 3 WT/ 4 KO **** $p<0.0001$, unpaired t-test. (B) Representative Laser Doppler images of WT and KO animals immediately after ischemia induction and after 21 days. (C) Graph shows the ratio of blood flow to the ischemic paw compared to the control paw of WT and KO animals after surgery and after 21 days (D) Capillary density per sample. Five random regions of interest from 3 sections per sample were counted (n= 4 WT /5 KO, one-way ANOVA, ns = not significant). (E) αSMA positive vessel density per sample (F) Representative adductor muscle immunofluorescent images: Isolectin b4 (IB4) capillary/endothelium, αSMA, and nuclear DAPI, scale bar 50μm.

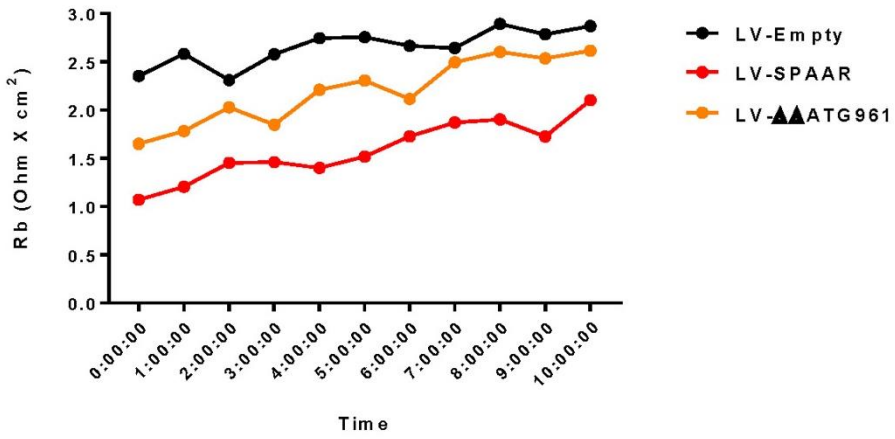

Supplementary Figure 7: : SPAAR micropeptide overexpression but not LINC00961 transcript expression affects endothelial barrier integrity. Impact of *LINC00961* (without SPAAR) and SPAAR only lentiviral construct overexpression in HUVEC endothelial barrier integrity over a 10 hour period, n= 4.

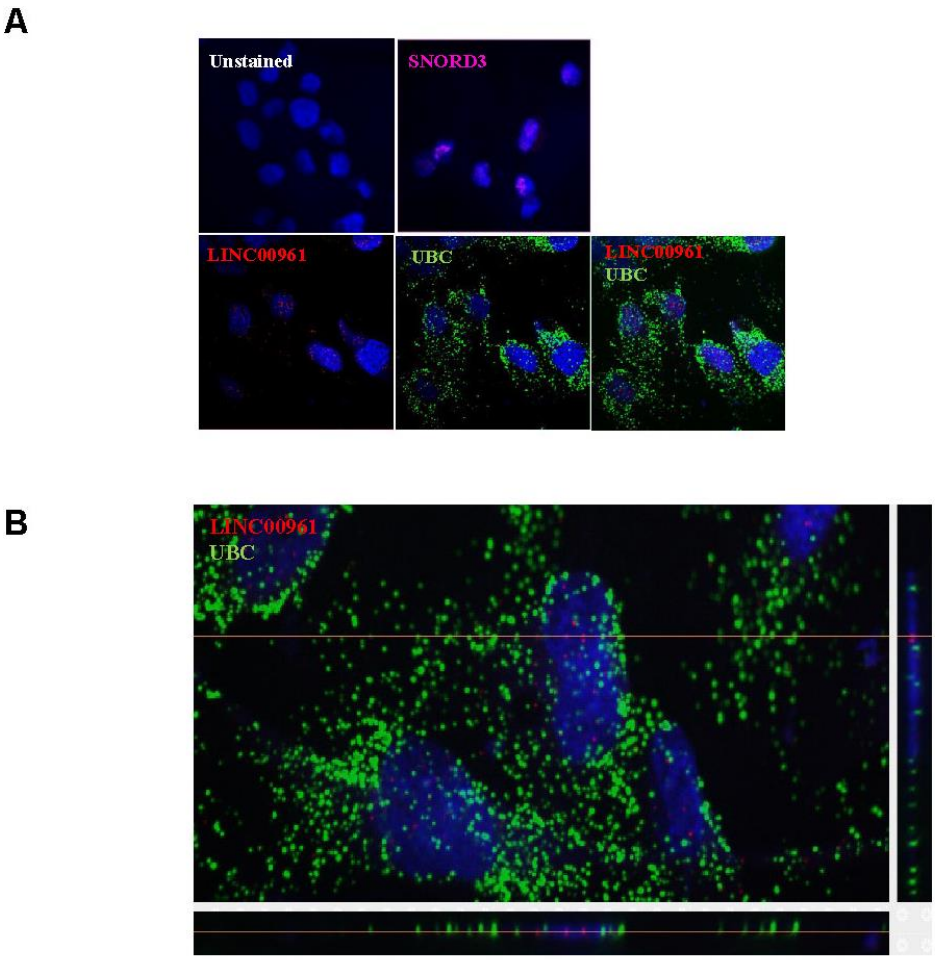

Supplementary Figure 8: Endogenous localisation of the *LINC00961* transcript. (A) RNA-FISH of *LINC00961* in HUVECS. *UBC* mRNA confirmed cytoplasmic localisation, whilst *SNORD3* expression is restricted to the nuclear compartment. Magnification X63 for all panels. (B) RNA-FISH of *LINC00961* in HUVECs (X63) Z-stacking slice to assess *LINC00961* localisation within the nucleus. (C) *LINC00961* qRT-PCR on cytoplasmic and nuclear fractions in HUVECs (n=8). *NEAT1* was used as a nuclear fraction control.

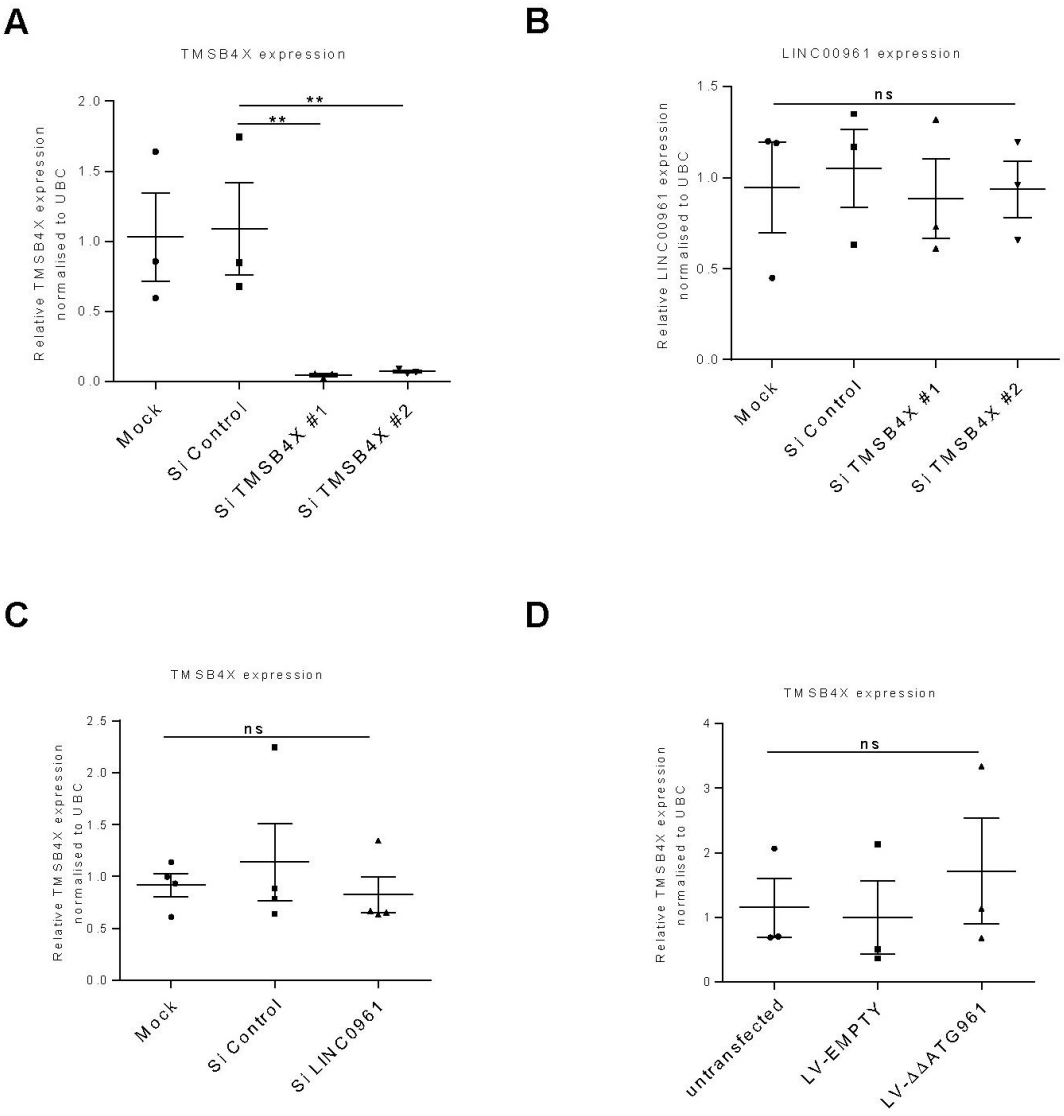

Supplementary Figure 9: ***LINC00961*** **does not regulate** ***TMSB4X*** **transcript level and** ***vice versa.*** (A) Confirmation of *TMSB4X* knockdown by qRT-PCR on dsiRNA treated HUVECs (compared to dsiRNA control and mock transfected cells) (n=3). (B) Impact of *TMSB4X* dsiRNA on *LINC00961* transcript expression as assessed by qRT-PCR (n=3). (C) Impact of *LINC00961* dsiRNA on *TMSB4X* transcript expression as assessed by qRT-PCR (n=4). (D) Impact of LV-ΔΔATG961 on *TMSB4X* transcript expression as assessed by qRT-PCR (n=3). Statistical analysis was done using unpaired t-tests. On the graphs, ** indicates $p<0.01$ and ns = not significant.

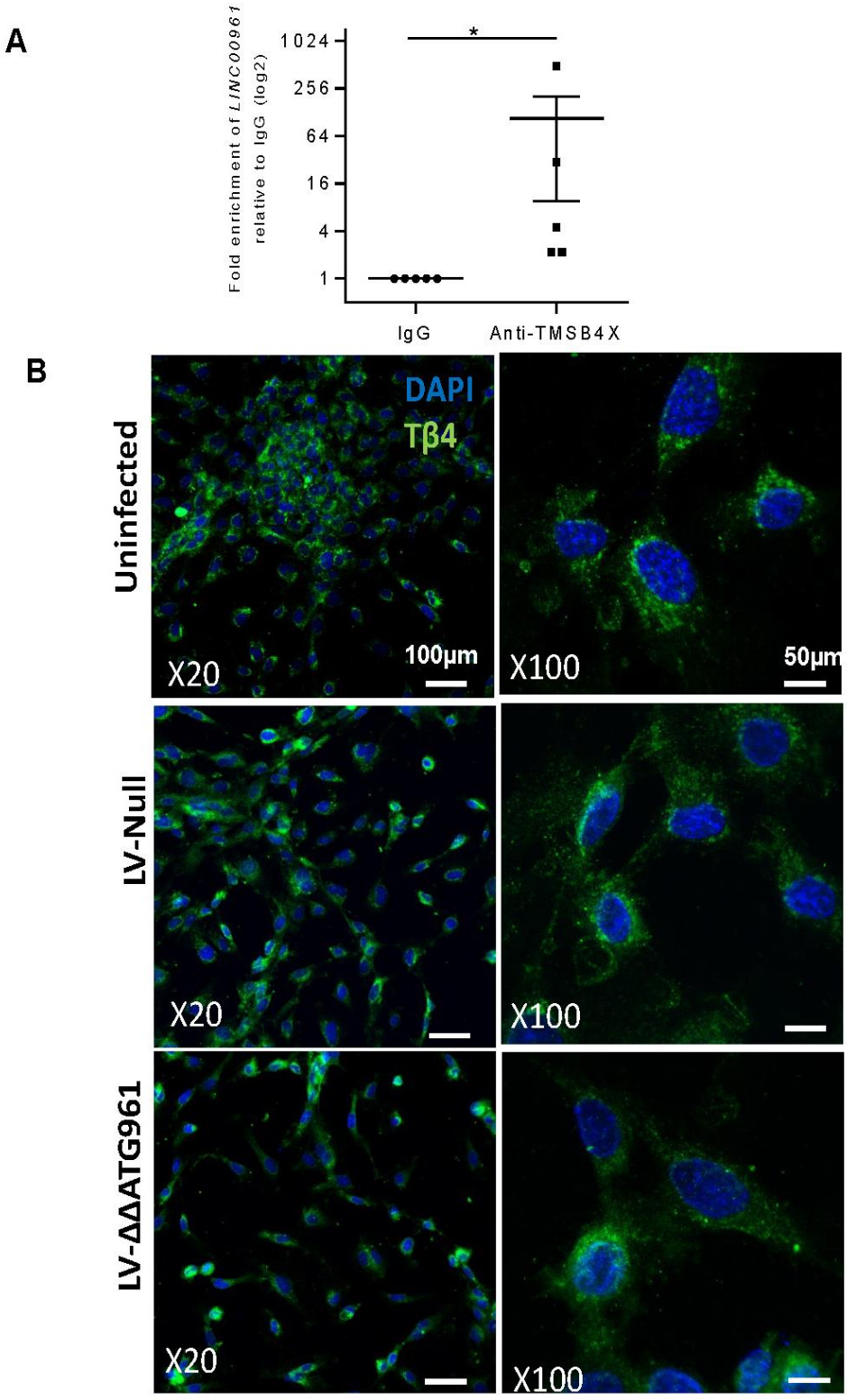

Supplementary Figure 10: Validation of thymosin beta 4-x and *LINC00961* interaction, and localisation of thymosin beta 4-x in HUVECs. (A) qRT-PCR analysis of *LINC00961* levels after pull-down with anti-Tβ4 antibody, student's t-test, * $p<0.05$, n=5. (B) Immunofluorescent staining of Tβ4 protein in HUVECs in uninfected, LV-null, and LV-ΔΔATG961 conditions. Tβ4 is green with nuclear DAPI in blue. Left hand panes show X20 magnification, scale bar 100µm, right hand panes show X100 magnification, scale bar 50µm.

3.4 Additional results

3.4.1 LINC00961 *trans*-regulation of target genes

To identify potential downstream targets of LINC00961, the hESC-EC differentiation RNA-seq dataset was used to search for genes which followed a similar pattern of expression to LINC00961. i.e., present only in the day 7 EC population and the positive controls. Dr. Helen Spencer, Dr. Julie Rodor, and Dr. Mounia Boulberdaa carried out this search and identified 3 genes: SH2 domain-containing Eph receptor-binding protein 1 (SHEP1, also known as SH2D3C), Neural proliferation, differentiation, and control 1 protein (NPDC1), and epidermal growth factor like domain multiple 7 (EGFL7), (explained in more detail in section 3.5.1) clustered on human chromosome 9. Following 24 h siRNA KD of LINC00961 in HUVECs, the expression qRT-PCR analysis revealed that SH2D3C and NPDC1, but not EGFL7, were in fact downregulated with LINC00961 (Figure 3.1). Unfortunately, we do not have any protein level expression data for these genes at this time, and it should be noted that this gene expression analysis pre-dated the experimental data published above.

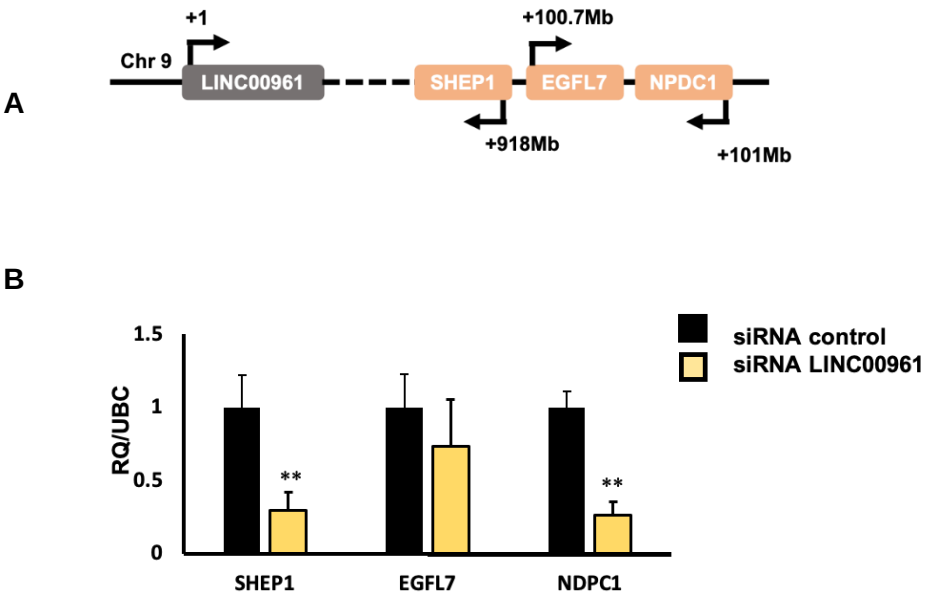

Figure 3.1 Knockdown of LINC00961 in HUVECs effects the expression of downstream target genes.

A) Schematic representation of target genes on chromosome 9 in relation to LINC00961. B) The expression of potential downstream LINC00961 targets was analysed after siRNA knockdown of LINC00961. SHEP1 and NPDC1, but not EGFL7 were significantly downregulated after 24 h. N=3, On the graphs, ** $p < 0.01$, student's t-test. Data in B provided by Dr. Helen Spencer.

3.4.2 LINC00961 expression is modulated in a cell specific manner during hind limb ischaemia

RNA samples extracted from the adductor muscles of WT mice having undergone HLI at 3, 7, and 15 days post-surgery were kindly donated by Dr. Andrea Caporali. The ECs had been isolated from the adductor muscles using CD31+ magnetic activated cell sorting beads (Miltenyi Biotech, USA) [266]. They showed that the remaining fractions had adequate cells/RNA present to analyse the non-EC fraction. Theoretically, this fraction should include skeletal muscle cells, fibroblasts, immune cells, and SMCs, and is hereafter referred to as the 'muscle cell fraction'. Analysis by qRT-PCR showed that LINC00961 expression was significantly down regulated in the ECs at all 3 time points compared to the WT EC fractions (Figure 3.2A). The corresponding muscle cell fractions from these mice did not follow this pattern of expression. At 3 days post-surgery, LINC00961 was significantly upregulated, whilst data at 7- and 15-days post-surgery expression was unchanged (Figure 3.2B).

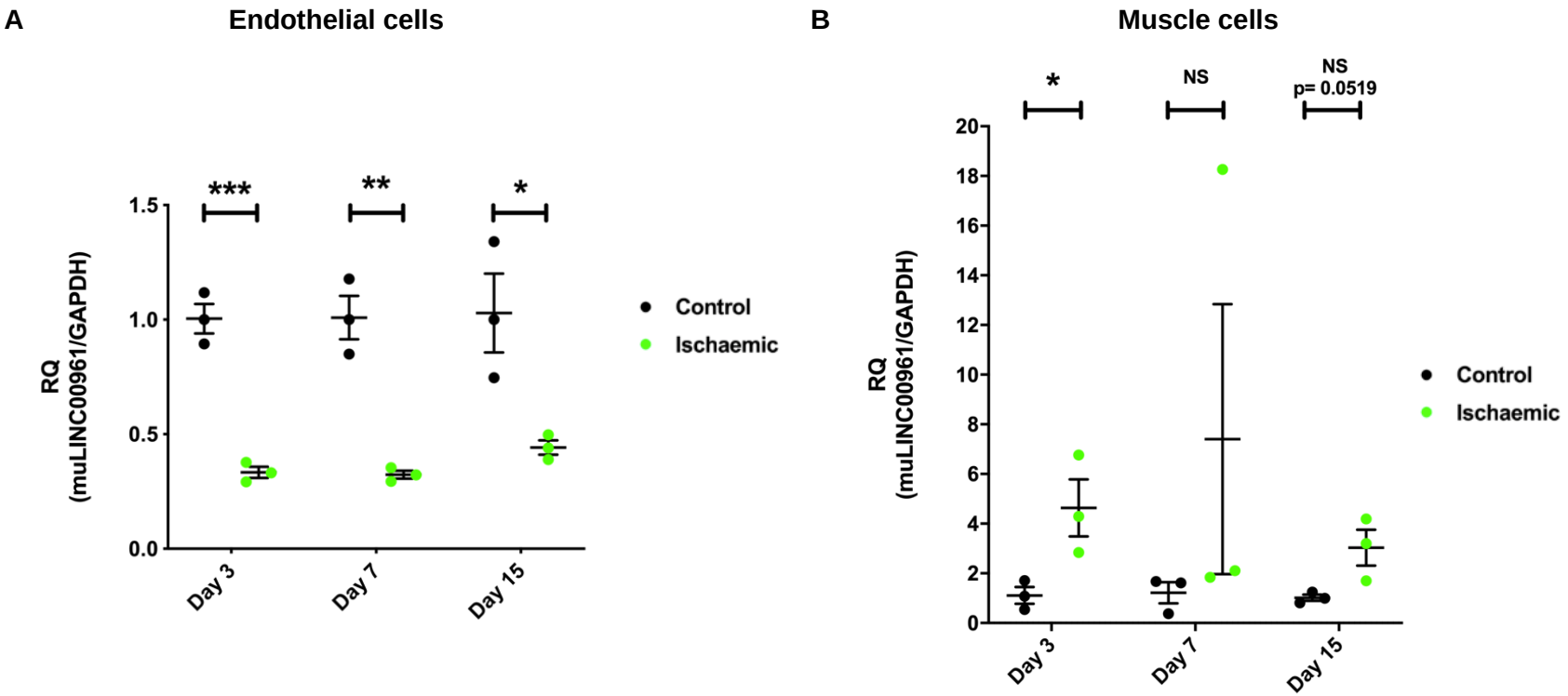

Figure 3.2 LINC00961 is modulated in a cell specific manor during hind limb ischaemia.

A) LINC00961 was significantly downregulated in endothelial cells isolated from the adductor muscle of wild type mice having undergone hindlimb ischaemia at all time points tested. B) In contrast, LINC00961 was upregulated in the corresponding day 3 muscle fraction (from the same mice). This upregulation was not found to be maintained at 7 and 15 days post-surgery, N=3 for all conditions, student's t-tests carried out. On the graphs, NS not significant, * p< 0.05, ** p< 0.001, error bars are mean +/- SEM.

3.4.3 Altered perfusion recovery trajectory in LINC00961$^{-/-}$ mice

To confirm the induction of limb ischaemia at the time of femoral artery ligation, Laser Doppler analysis was carried out immediately after surgical site closure whilst the animals remained under aesthesia. At 3, 7, 15, and 21 days after surgery Laser Doppler analysis was repeated in order to track blood flow recovery to the limb and the ratio of blood flow/perfusion between the control and ischaemic foot was obtained (Figure 3.3). As expected, both genotypes show an improvement in limb perfusion over the course of the experiment as the mice recovered, which is reflected in the 2-way ANOVA statistical test where the effect of time was significant ($p < 0.0001$). The data also revealed that KO mice had increased limb perfusion at 7 days post-surgery ($p < 0.01$), but this was not evident at the later time points measured. Some of the mice used to collect this data were also used for histological analysis of the adductor muscle at 21 days which is shown in Supplementary Figures 6C, D, E & F in the published work above, the remainder of the mice were used to snap freeze tissues.

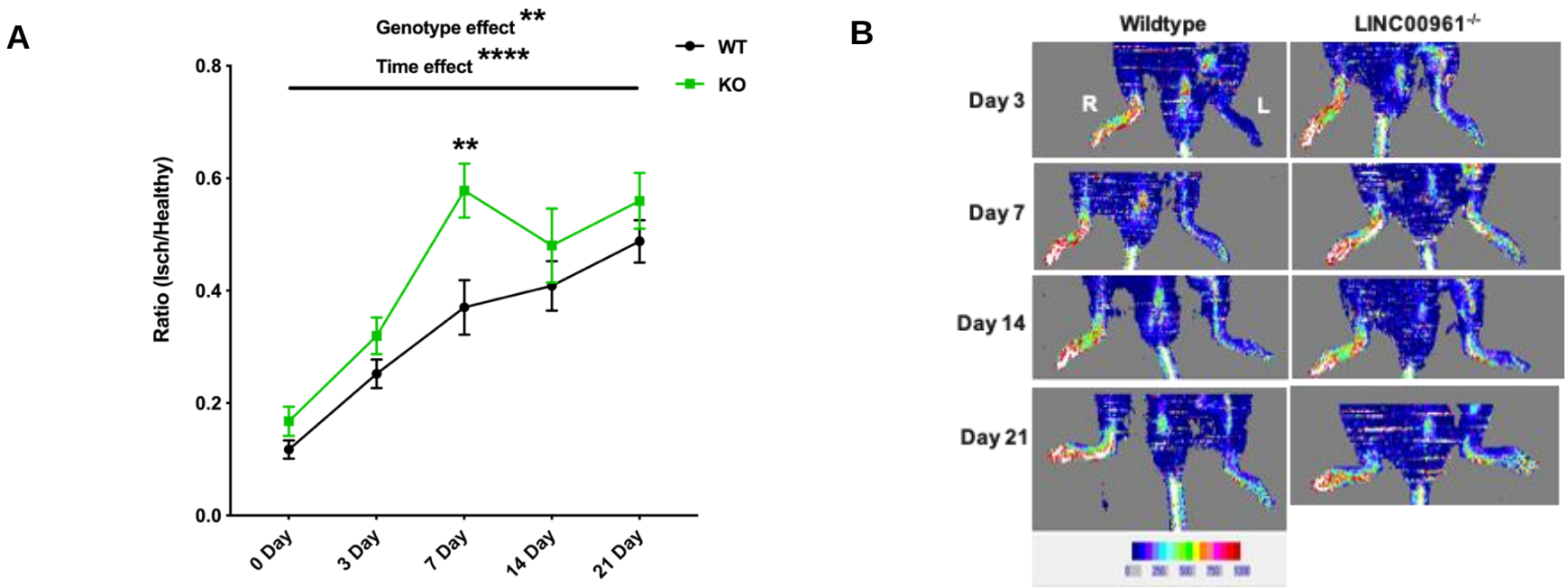

Figure 3.3 Altered perfusion recovery trajectory in LINC00961$^{-/-}$ as measured by Laser Doppler.

A) Laser Doppler analysis over the course of 21 days represented as the perfusion ratio between the ischaemic and healthy foot. Data demonstrates perfusion recovery across the length of the experiment in both genotypes (time effect) and a genotype effect concluding that the pattern of perfusion recovery was altered in LINC00961$^{-/-}$ mice, specifically on day 7. B) Representative images of Laser Doppler used to calculate the ratio of perfusion between the ischaemic and non-ischaemic foot, using the ankle joint as a boundary for analysis. R= control right limb, L= ischemic left limb. On the graph, ** p <0.01 and **** p <0.0001. Statistical analysis is a 2 Way ANOVA with Sidak's multiple comparisons test. Error bars are mean +/- SEM. N=13WT/ 13KO.

3.4.4 Altered gene expression profiles in LINC00961$^{-/-}$ adductor muscle

A panel of 11 genes were chosen for expression analysis between WT and LINC00961$^{-/-}$ mice at 7 days post ischaemia induction. This time point was chosen to try and understand what might be going on at this stage of the recovery process, and to correspond to the published capillary density immunohistochemistry data, also taken at 7 days (Figures 4B, C & D in published data). The non-ischaemic adductor muscle served as a baseline measurement of gene expression, whereas the ischemic muscle served as a snapshot of expression alteration in response to injury between genotypes. The genes of interest chosen were; SH2D3C, NPDC1, and EGFL7, (i.e. as previously mentioned, 3 candidates for LINC00961 downstream targets); HRCT1, the closest protein coding gene to LINC00961, VEGF-A and VEGF-C which are relevant to angiogenesis [38] and lymphangiogenesis [43] , respectively; TMSB4X, MSI2 and SMARCA4 which were identified through the RNA-protein pull down experiments (Figure 6 in published data) as binding to LINC00961; and finally, Pax7 and Myogenin (MYOG) which are markers of satellite cells (muscle SCs) [232].

3.4.4.1 Healthy adductor muscle

Of the 11 genes analysed, only SMARCA4 (also known as BRG1) showed a statistically significant alteration in expression in healthy adductor muscle which was upregulated in LINC00961$^{-/-}$ mice (Figure 3.4A).

3.4.4.2 Ischaemic adductor muscle

In the ischaemic muscle SMARCA4/BRG1 upregulation was no longer significant but appeared to show a shift towards upregulation in the LINC00961$^{-/-}$ mice. In contrast, MSI2 was significantly upregulated in LINC00961$^{-/-}$ mice. SHEP1, and NPDC1, both showed a trend towards an increase in expression in the LINC00961$^{-/-}$ ischaemia adductor, although this was not statistically significant as there is a wide variation in the WT and LINC00961$^{-/-}$ samples. The most altered expression was a statistically significant downregulation of MYOG in LINC00961$^{-/-}$ mice.

A **Healthy Adductor Muscle**

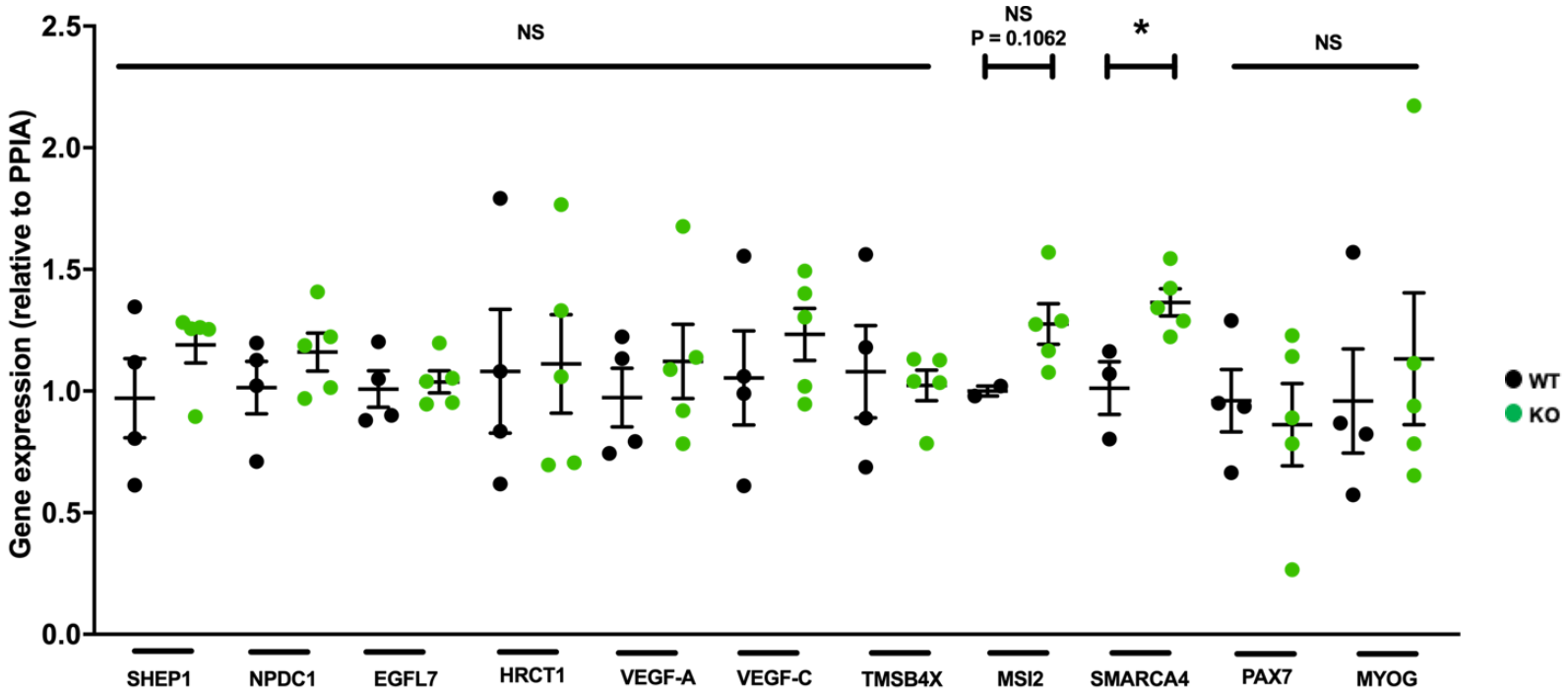

B **Ischaemic Adductor Muscle**

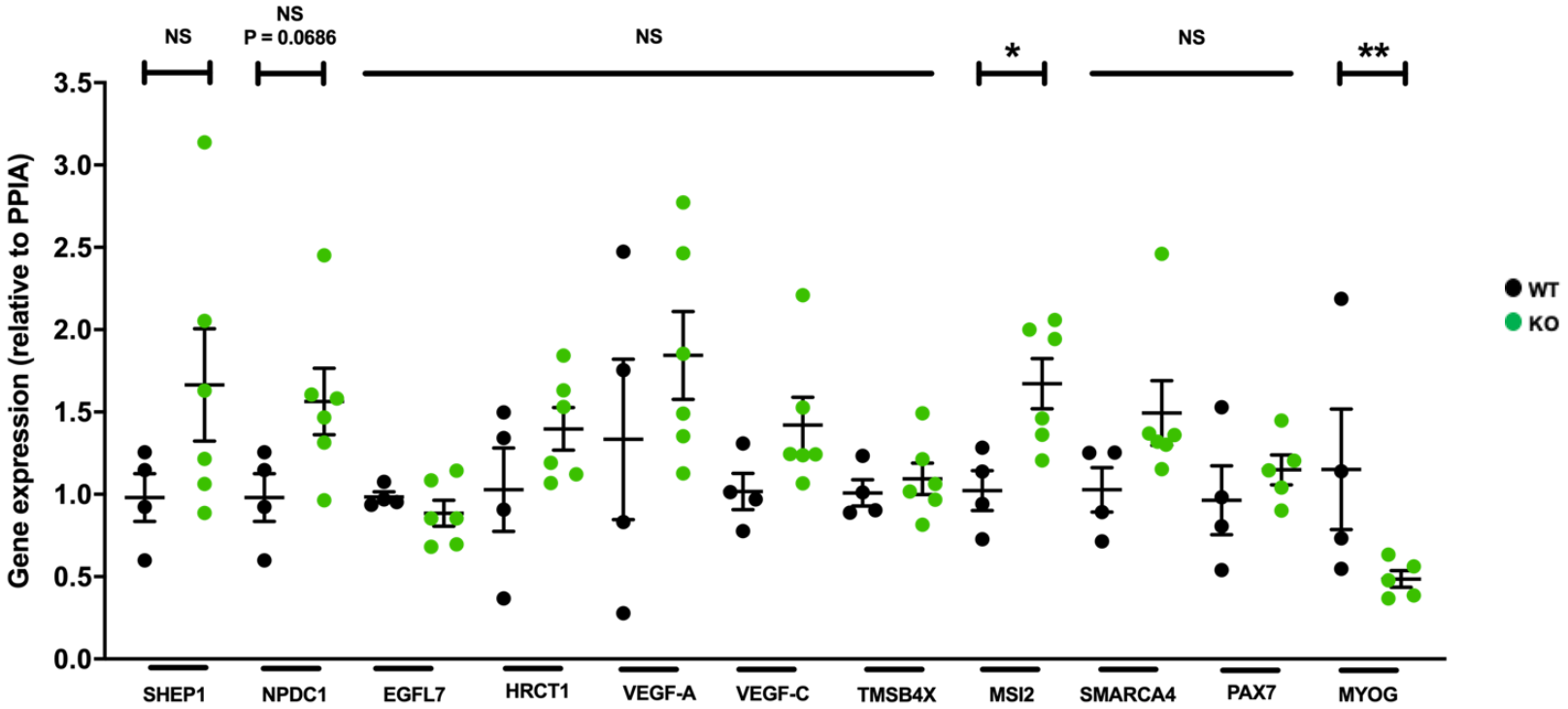

Figure 3.4 Differential gene expression between genotypes in healthy and ischaemic adductor muscle.

Tissues were taken at 7 days post unilateral limb ischemia induction. A) healthy ischaemic tissue from right limb. B) ischemic tissues from left limb having undergone femoral artery ligation. On the graphs NS= not significant, student's t-test used where * $p < 0.05$, and ** $p < 0.01$. Error bars are mean +/- SEM. N= 2-4 WT, N= 5-6 KO.

3.4.5 Pro-angiogenic SPAAR is not detected in unstimulated HUVECs

Mass spectrometry analysis was carried by the staff at the IGMM Spectrometry facility at the University of Edinburgh. Unstimulated HUVEC lysate was analysed alongside two positive controls for SPAAR expression: HELA lysate, shown to have high LINC00961 by Matsumoto & colleagues [232], and LV-SPAAR infected HUVECs we previously validated as overexpressing SPAAR [254]. A HUVEC LV-null condition was also included as a control, and all conditions are N=1. The mass spectrometry analysis was carried out using a targeted approach to search for SPAAR cleaved peptides, based on the data previously generated by the facility when they carried out the SPAAR overexpression pull down mass spectrometry [254]. This approach looked for the amino acid sequence: AQDPQGGPGR, which was present in the positive controls, however, was not identified in the unstimulated HUVECs or LV-null HUVECs (Figure 3.5).

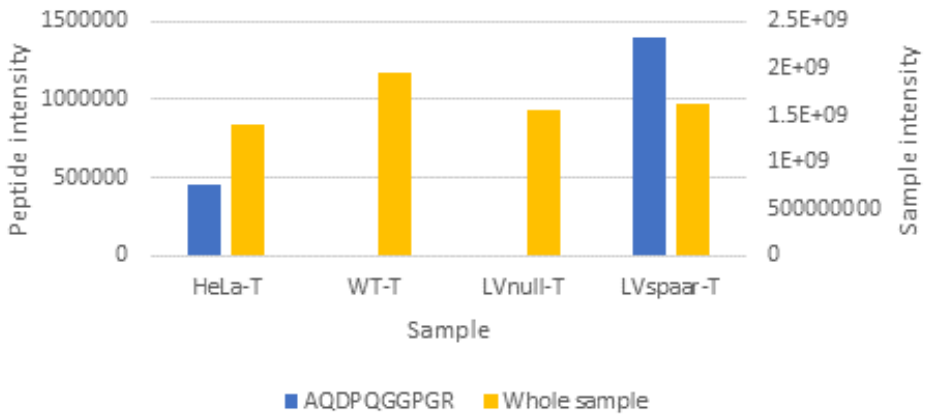

Figure 3.5 SPAAR is not present in unstimulated HUVECs.

Results of mass spectrometry analysis show that the SPAAR peptide is present only in the positive controls (HeLa cells and LV-SPAAR infected HUVECs) (blue bars) and not in unstimulated HUVECs or LV-null HUVECs. Data analysed and provided by the IGMM Spectrometry facility at the University of Edinburgh, N=1 for each condition.

3.4.6 ERG binds to multiple regions of the human LINC00961 promoter

Our collaborators at Imperial College London, Professor Anna Randi and her group, had previously performed ChIP-seq analysis where they fixed chromatin interactions in HUVECs, pulled down ERG and sequenced the bound DNA sequences. Mapping the reads to the human genome, they were able to identify 2 sites approximately 1 Kb apart within the promoter region of LINC00961. They were also able to show reduced ERG occupation of those sites when ERG was depleted by siRNA (Figure 3.7A). Figure 3.6B shows a schematic representation of the locus including the ERG binding sites within the promoter (not to scale). Dr Julie Rodor utilised the programme JaspeR to identify areas in the promoter region that are likely the sites for ERG binding identified by the ChIP-seq Figure 3.6C.

A

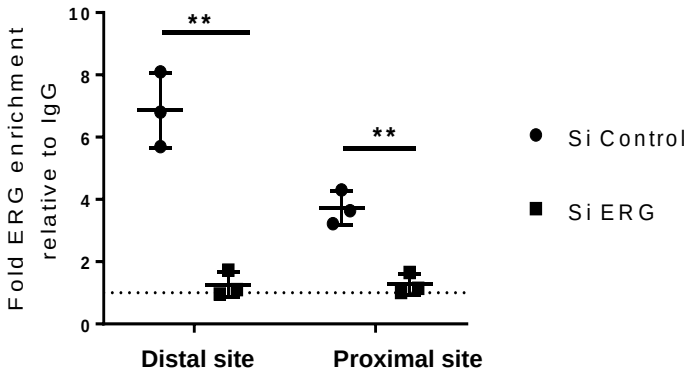

B

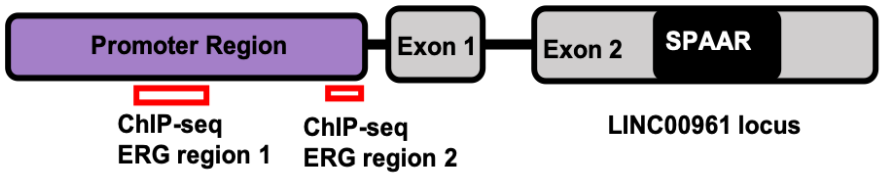

C

```
GGGTTTCTTCTCCAAGCCTTGCGTTTTCAGCCATCCTGCCCCAGCTGGTGCCTGTGTGTGGTGGGAGGGCTGGGAGGCAGCGAGTGGAGTTCTTTAAAGT      100
GGAGGCTGTGGTGCTGGGGTGCAGGGTGTTGGATGGCCTTGGGAGAATGCTGGGGTCTCACTTTCCTCTTCTCTGCAATGGGGTGGATAACAGAGATGCC      200
CACGTGCCGAAGCCTGGAGGCTCGTTGGAATATGCTCTGTGAACAGCTAGTGGGATCCACAGCGAGGAAGGAAGCCTGGCTCTGAGGCCTTCAGCCTGTG      300
CCTGTGAGCTGAGGTGGGAATTGGGGGAAGACAAGGACTGGGGGCCAGGAGAGGCAGTGGGGAGGGGCTGGAGAGCAGGCCAGAGACTCAGGGACCTGGT      400
GACTCACTGGAATAGAATGTCCTCTTTCCTTTCTATTTCCCAGTGGATTCTCTGTGAGGGCTGCAGGAGGAGGGAGTGAGAGAGAGAGGGAGGCAAATTC      500
ACACTGATTTCTCCCACCTGAGGTTTCTGGGTTGGGAAAGTTGACCCTAGGCTGCCGTGCAGTGTCGATTTTCTCTGCAGTGTCCTTCAAATCCACCCCC      600
TTCTCCATTCCCATGCCCTGCCTAGCCCAGCCCCCTCCATCCCCCTCCTGGATTCCTGCCAGCCTGCTCCCTGCAGCCCTGCCCCTTTCCCAGGCATCTC      700
CAGGCTGATTTCACAGATGAATCAAAGATGGGGAGGAGGTTCCCCGAAAGCAGGAAACGGAAAAGGAAGCCTATGCAGGGCAGGAGAGAACCCGCTGAGC      800
AATTGCCCTTTATTCCAGTTCAAAAATGCGGAACCACTCAGACAATCTGCAGGCGGCCTATGGCTGCGTGTACACAGGAAGAATAGGCGATGAGAAATCA      900
AAGGAACAAATGTTAAAGCTTGAGGCATAGTCTCCTGGTGCCCTCTATCACCCCAGTTAAGGAGGTGATGTTGGTAACTCAACCTGAAACCACAGGCCCT     1000
GCAGATCAGCCCGTCGTCTCCTTCCTCCTGGTCATCCCAGTTAATACAAACAATCCAAGGAATTGGCTTCCTGTCATGGCCCACAGCCTGCTCCATGTGG     1100
AGGAGGAGCCCAGGGCCCAGATGGTCTCATCATCTCAGAAAAGGGACAGATTGAGAATATGACAGGCTATCGTTTGCTCTGAAAAGTTGCTCTCCCATTC     1200
TGTGCAAAGTGCCAGTTTCCTAATGCTGATACTAAAGAAAGTTCCCTTGGGCCTTGGAGAAACTGAAAAGGACCCAGGCTATGTGAACTTGGGCCAGCCC     1300
TCTGCCCTTTCTGGCACTTTGCACCCAGATCATTAAAACCGCAGAATCAGATGGTCGCTCTGTGGTCCCATGGTAACTGGAAAGTGCACTGAGCTAGGAG     1400
TGGAGGGAGGGCGGTCCCTCCTCGGCCATTGCTCGTGCCTGTTAACATGGCTAATTCAGAATGGGGGGCAGGTCATTTAACTTCTATGACCATAGGATCT     1500
TTTTCTATAAAATGGAGGCTATATCGCTATGCAGGGTTGCTGGGGAGGTTATATGAGATCATGTCTGGTGAGGTCCCATGCCTGGAGTTATTGTTCTCAC     1600
TACTCTGTTTCCCAGAATATGGACAAAGTGGGGCTAATAGCCCAGTCTCCTTTCTGGAAGTGGTGGGGGTCTCAGGAGGTGCTGGGTGTGAAAGGGCTCT     1700
CACCTGGCAGACTAACTCAGTTGCCTGGGCCTAGCTTATTCCCCTGACCTCCTGGCAGGGAGGAGGGTGGAAAAGGCCTGGGGTGCGCATGGCGGGACGG     1800
GATAACTGCTGAGCGGGGGTTGGAGGGCTGCAGTGTGGGTCCTGGGCCCTCGCTCACAATTGGAGGAAAGAATTCAGGAAGTGCTCACAGCTGCTCAGAC     1900
ATCTCGGAGCCAAGTTCCAACCAGGACAGAGGCTGCAGCACCCAGGGAGGAACGCCGTGGTCCCTGGGACGGCCACCAGGCCAGGAGGCTGCAGCACCAG     2000
GTACAGCCAGGGCTGGCCTTTGGGGAGCCCAGGGTAAATCTTAATAGTTCAAGAATGTGAGCAAC                                  2065
```

Figure 3.6 ERG binds to two regions of the human LINC00961 promoter.

A) ERG ChIP-seq identified that ERG bound 2 separate regions of the LINC00961 promoter, approximately 1Kb apart. Knock down of ERG by siRNA depleted the amount of ERG localising to both sites. N=3 for each condition. Student's t-test used, ** P<0.01. Data in A was generated by Professor Randi's group. B) Schematic representation of the LINC00961 locus including a 2Kb promoter region, red boxes indicate approximate location of the identified ERG binding sites (not to scale). C) DNA sequence of the 2Kb region upstream of LINC00961 showing the location of predicted ERG binding sites within the LINC0961 promoter using JaspeR (red boxes). The green box highlights exon 1 of the LINC00961 transcript and the yellow boxes indicate other 'GGAA' ERG binding sequences within the sequence.

3.4.7 Depletion of ERG does not alter LINC00961 expression in HUVECs

To further investigate whether LINC00961 expression is regulated by ERG, siRNA against ERG (20nM) was used to deplete HUVEC ERG levels. At 24, 48 and 72 h after KD qRT-PCR analysis revealed that ERG expression was successfully depleted (Figure 3.7A, C, and E), however, LINC00961 levels remained unchanged compared to mock and control siRNA conditions at all time points (Figure 3.7B, D, & F).

24 hour ERG knockdown

A ERG expression

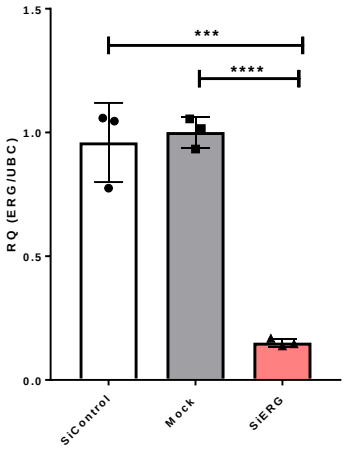

B LINC00961 expression

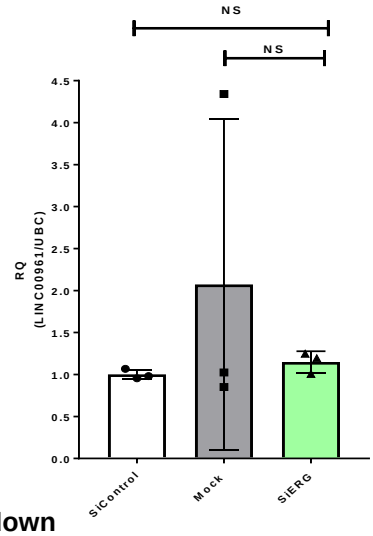

48 hour ERG knockdown

C ERG expression

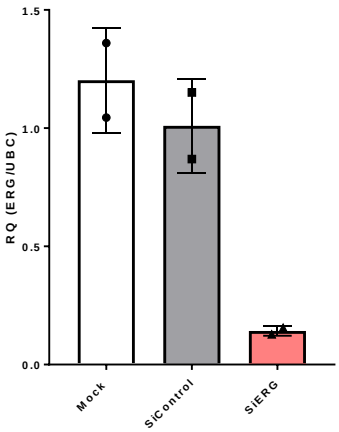

D LINC00961 expression

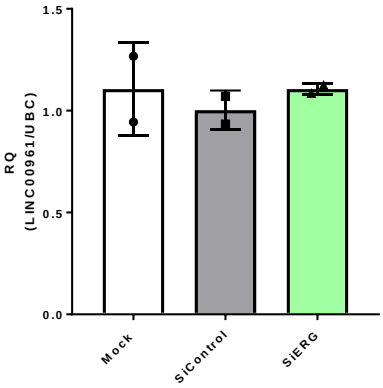

72 hour ERG knockdown

E

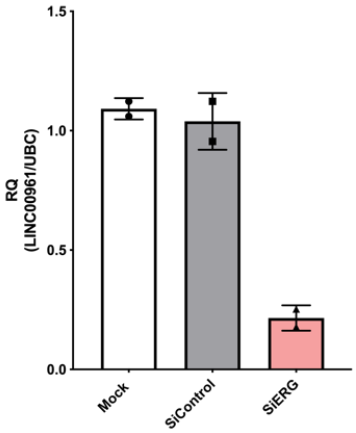

F

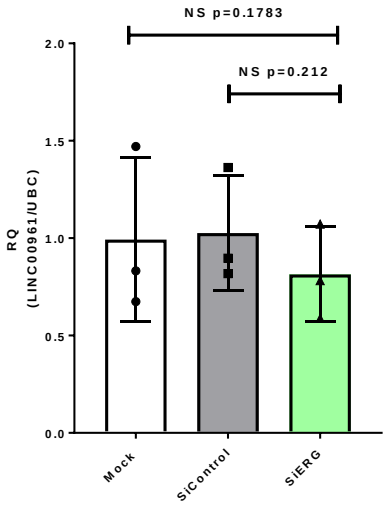

Figure 3.7 Investigation of LINC00961 expression in response to ERG knockdown.

ERG expression was substantially depleted at all time points tested (24, 48, and 72 h, A, C, & E respectively), however, LINC00961 expression was unchanged at all time points tested (B, D & F). ERG siRNA was used at 20nM. N=2-3 replicates per condition, where there are 2 replicates, one data point was removed due to wide variation in the triplicates in the PCR for that sample. Where 3 replicates are present a one-way ANOVA with multiple comparisons was carried out. On the graphs, NS = not significant.

3.5 Conclusions of the further experimental work in this Chapter

- KD of LINC00961 in HUVECs downregulates the expression of SHEP1 and NPDC1.
- LINC00961 expression is independently regulated in different cell types during HLI. i.e., LINC00961 is downregulated in EC and upregulated in muscle cells.
- LINC00961$^{-/-}$ animals have increased vessel perfusion at day 7 but not at other time points measured.
- Differential gene expression between genotypes in healthy and ischaemic adductor muscle.
- SPAAR is not expressed in unstimulated HUVECs
- ERG binds to the promotoer region of LINC0061
- ERG alone does not regulate LINC00961 expression

3.6 Discussion

This Chapter summarises data demonstrating *in vitro* and *in vivo* evidence of the LINC00961 locus' role in the endothelium which was our original hypothesis. We also summarise our initial experiments in investigating what upstream factors may regulate this locus. This Chapter includes peer reviewed published data and additional data relevant to those results. We initially discovered LINC00961 in a hESC-EC differentiation assay with RNA-seq analysis in the search for endothelial enriched LncRNAs. Therefore, the initial experiments in this Chapter and publication focused on assessing this locus' role in EC functions, specifically angiogenesis. To the best of our knowledge, LINC00961 is only the 3rd lncRNA whose modulation *in vivo* has been shown to affect re-vascularisation in HLI experiments in mouse [226]. Similar to the LINC00961 locus KO, MALAT-1 KD also inhibited muscle revascularisation in HLI recovery [188] [267] and in contrast, MEG3 KD improved revascularisation [227]. These are excellent candidates to investigate in human PAD/CLI, however, there are likely many more lncRNA candidates with roles in angiogenesis and revascularisation after injury yet to be discovered.

As this model is a global KO, we cannot rule out the possibility of the phenotype underlying the vessel differences at baseline and in response to injury is solely due to endothelial insufficiencies. However, by using a global KO model, we have incidentally uncovered that the LINC00961 locus may have a role in muscle regeneration, besides that previously reported specifically for SPAAR [232]. In support of this, this Chapter provides evidence of cell type specific differential regulation of the LINC00961 locus in a WT mouse during HLI recovery and evidence that LINC00961 deletion causes altered gene expression in the adductor muscle of mice at baseline and during HLI recovery.

The main finding to highlight from this Chapter and publication is that the LINC00961 locus is required for vessel maturation. This is shown by the lack of mature αSMA supported vessels in the control adductor muscle which had not undergone any surgical intervention. The finding of this basal vascular phenotype in our LINC00961 KO animals is extremely interesting as we were initially focused on the effects of this locus in ECs. We are therefore curious as to the mechanism behind this reduction in αSMA expressing mural cell supported vessels and whether this is a consequence of

maladapted ECs and a failure in their signalling to communicate with such cells, or by another mechanism altogether.

3.6.1 LINC00961 *trans* regulation of target genes

To identify potential downstream targets of LINC00961, it was logical to dissect the original RNA-seq dataset which identified LINC00961 in the endothelium. Dr. Helen Spender and Dr. Mounia Boulberdaa identified SH2D3C, NPDC1, and EGFL7 as having a similar expression pattern as LINC00961. These 3 genes are located on human chromosome 9 but on the opposite arm to LINC00961. SH2D3C, also reported as SHEP1, is a cytoplasmic signalling molecule with roles in cell adhesion and migration and is widely expressed in human tissues, although there are some differences in tissue expression patterns between human and mouse. Interestingly it has been reported as expressed in the blood vessels of breast tumours in mice. In the same study the authors suggested a potential upregulation of SH2D3C expression by the pro-angiogenic VEGF [268], highlighting that this gene may contribute to angiogenesis.

NPDC1 has previously been reported as a developmentally regulated gene expressed only in differentiating neurons, and is present in vesicles [269, 270]. To our knowledge, there is no current literature regarding a role for NPDC1 in the endothelium. SH2D3C and NPDC1 were shown to be downregulated with siRNA against LINC00961 in HUVECs (Figure 3.1) suggesting their transcriptional and/or post-transcriptional regulation by LINC00961 in trans. However, whether this is direct or indirect is not clear. Considering LINC00961's almost equal split between the nucleus and cytoplasm it is logical to expect that LINC00961 may also have functions which influence gene expression or epigenetics, similar to other lncRNAs with nuclear localisation [156], such as those described in section 1.6.3.

The most interesting of these candidates is EGFL7, which is secreted from ECs and binds to fibronectin in the ECM [271]. Relevantly, EGFL7 was recently reported to inhibit NOTCH signalling [272] in HUVECs which is interesting as NOTCH signalling is involved in establishing tip and stalk cells in sprouting angiogenesis [273]. Conversely, EGFL7 has also been reported to inhibit angiogenic sprouting; Usuba & colleagues (2019) showed that KD of EGFL7 supressed VEGF induced angiogenesis and EC collagen deposition, impaired endothelial barrier integrity, and increased

vessel permeability in an *in vitro* human micro vessel model [274]. EGFL7 is also a host for miR-126 which has been shown to be vital for angiogenesis [275]. Both EGFL7 and miR-126 have also been shown to be regulated by the lncRNA lncEGFL7Os located next to the EGFL7 gene locus and regulates expression of its neighbours EGFL7 and mirR-126 [276] [277]. However, in this study EGFL7 expression was not affected by LINC00961 KD. It is possible that EGFL7 may be regulated by LINC00961 in other contexts, for example in hypoxic conditions, and additional stimuli specific co-factors may be required for LINC00961 to affect EGFL7. EGFL7 was not found to bind to LINC00961 in the RNA-protein pull down experiments, ruling out a physical interaction with the protein. It would have been interesting to analyse any changes in expression of these genes in the EC and muscle cell fractions during HLI in WT animals, however, these samples were gifted and only had a small amount of cDNA available which was sufficient to analyse LINC00961 expression.

3.6.2 Cell type specific expression patterns of LINC00961

Cells isolated from the adductor muscle of WT mice having undergone HLI were able to provide insight into LINC00961 regulation under ischaemic conditions. RNA samples provided by Dr. Caporali were taken from ECs isolated from WT adductors at 3, 7, and 15 days post HLI induction. The remaining non-ECs were also provided which allowed for cell specific gene expression analysis. To our surprise we found the first evidence for cell-type specific regulation of the LINC00961 locus. LINC00961 was consistently downregulated in ECs at each time point tested during HLI recovery. Whereas LINC00961 was significantly upregulated in the muscle cell fractions from the same mice at day 3, but not at the other timepoints, however, the small N numbers and natural variation amongst the mice, particularly seen with the large SEM at day 15, may be masking an upregulation and in order to accurately determine LINC00961 levels, more samples are required. When we consider the anti-angiogenic role of the LINC00961 transcript which we identified during lenti-viral (LV) over-expression experiments this downregulation makes sense as the ECs are hypoxic after injury and therefore in a pro-angiogenic state, upregulating a pro-angiogenic gene profile and down regulating anti-angiogenic genes (such as the LINC00961 transcript) to allow for sprouting angiogenesis to occur. What we do not know in these cells is the status of SPAAR translation as we have been unable to detect SPAAR protein levels by western blot utilising the only commercially available antibody, which is specified as

anti-human LINC00961 not mouse LINC00961. To investigate SPAAR expression levels in future, we could perform mass spectrometry analysis on cell lysates, however to the best of our knowledge mouse SPAAR, which differs in sequence to human SPAAR by 35%, has never been investigated by mass spectrometry analysis.

It is interesting to hypothesise that as LINC00961 is anti-angiogenic and SPAAR is pro-angiogenic (based on the published LV overexpression data), that when LINC00961 is downregulated such as in this instance, that SPAAR could be upregulated to support angiogenesis. The possibility of an inverse regulation between LINC00961 and SPAAR in muscle would make sense when we look at the upregulation of the LINC00961 locus in the muscle fraction of cells from WT mice. Matsumoto & colleagues (2017) demonstrated that SPAAR inhibits muscle regeneration via negatively regulating amino acid stimulation of the mTORC1, an effect that was abolished in SPAAR$^{-/-}$ mice which showed increased skeletal muscle regeneration [232]. As SPAAR negatively impacts muscle regeneration it makes sense that it would be downregulated in the regenerating adductor muscle cells during recovery. As LINC00961 transcript levels are upregulated, it could be that SPAAR protein may be downregulated. At present, we do not know the mechanisms of regulation between LINC00961 and SPAAR in human or mouse, especially as most research on this locus has focussed only on the LINC00961 RNA.

3.6.3 Altered perfusion recovery trajectory in LINC00961$^{-/-}$ measured by Laser Doppler

Classically, Laser Doppler perfusion imaging (LDPI) is a technique used extensively in HLI research to provide an indication of blood flow recovery. Its advantages are that it is non-invasive and can penetrate to the level of small vessels close to the surface of the skin. To our surprise, the Laser Doppler data over 21 days suggested that limb perfusion in the LINC00961$^{-/-}$ mice was increased at 7 days post-surgery which was the opposite to what we expected according to our hypothesis. Interestingly, day 7 was the only time point where the data significantly differed between the genotypes. From this data we initially hypothesised that loss of LINC00961 could be causing a transient effect in recovery, be that via affecting angiogenesis or muscle regeneration. To explore this further, tissues from the HLI experiments were taken at 7 days as well as the initial 21 days post-surgery in order to observe histologically what was happening. It is important to consider the Doppler

data together with the IHC staining and analyses which showed that LINC00961$^{-/-}$ mice had no difference in capillary density in their adductor muscles at baseline (control limb) in comparison with controls, however, they did have a significantly reduced number of mature αSMA positive larger vessels. Interestingly, and relevant to the Doppler data, after 7 days of injury LINC00961$^{-/-}$ had significantly fewer capillaries in their ischaemic muscles compared with controls, which resolved by day 21. This indicates a delayed response in angiogenesis in LINC00961$^{-/-}$ mice. This may be due to endothelial impairment, which is supported by our *in vitro* data following KD of LINC00961 in HUVEC's, which affected multiple endothelial functions. At 21 days post-surgery, LINC00961$^{-/-}$ mice had an increased number of αSMA positive vessels which was similar to those of the WT mice, suggesting that their mural cell supported vessels had responded to the hypoxic injury and undergone arteriogenesis to recover blood flow to the limb.

Considering the capillary and mural cell supported vessel density quantifications, possible explanations for the alteration of perceived perfusion include fluid retention and inflammation in the limb, especially if the vessels in the KO mice have increased permeability allowing for oedema to occur. To investigate this odd result further vessel permeability, vessel reactivity, and tissue inflammation would need to be assessed by blood vessel myography (explained in Chapter 4) and immune cell infiltration via IHC staining.

3.6.4 LINC00961$^{-/-}$ mice have altered adductor muscle gene expression

To establish differences in the adductor muscles of LINC00961$^{-/-}$ and WT mice at baseline and during recovery from ischaemic injury, a panel of target genes was chosen to investigate any differential regulation. Any differences would then give us insight into the downstream pathways regulated by LINC00961.

The Musashi RNA binding protein 2 (MSI2) was identified among the top 10 interactors in the LINC00961 RNA- protein pull down. It is a pluripotency marker [278] from the highly conserved Musashi family [279] which has been shown to be ubiquitously expressed [280], in contrast to MSI1 with whom it shares some overlapping functions and 90% sequence homology, which is neural cell specific [281]. MSI2 is highly expressed in haematopoietic cells, regulating haematopoiesis and is involved in malignancies and tumorigenesis such as in leukaemia's [280, 282].

MSI2 is a transcription factor expressed in many tissue types, is involved in development, and has a role in regulating the cell cycle [283]. Never-the-less, this has important implications as MSI2 is known to repress NOTCH1 signalling, hence supressing VEGFR2 [284], which is an important pathway in sprouting angiogenesis [273]. Musashi repression of Notch signalling has been extensively studied in neural SCs and in cancer [280], however, to the best of our knowledge there is no literature regarding MSI2's role (relating to notch or otherwise) in the endothelium. Of interest, 3 other lncRNAs have been shown to interact in a pathway with MSI2; the LINC01296 - miR143-3p – MSI2 pathway regulates thyroid cancer [285]; lncRNA DANCR is upregulated in bladder cancer where it sponges miR-149, reliving its inhibition of MSI2 [286]; and the recently identified lncRNA SOX2OT positively regulates SOX2, resulting in a downregulation of MSI2, also in bladder cancer [287]. Curiously, MSI2 is also involved in NSCLC, a disease where LINC00961 is highly researched and has continuously be shown to be downregulated correlating with poorer outcomes. High expression of MSI2 in NSCLC increases invasiveness promoting cancer progression [288]. It would therefore be of interest not only in angiogenesis and ischaemic injury but also in NSCLC and other cancers to explore further the possible link between LINC00961 and MSI2.

The SWI/SNF Related, Matrix Associated, Actin Dependent Regulator of Chromatin (SMARCA4), also known as BRG1, was identified as binding to LINC00961 from the RNA-protein pulldown and is an ATPase with a role in chromatin remodelling [289]. Interestingly, SMARCA4/BRG1 binds to TMSB4X (shown to bind to LINC00961 in our publication) and helps translocate it to the nucleus where it upregulates Wilm's tumour 1 (WT1), a gene involved in cardiac development [290] and angiogenesis [291, 292] by activating transcription of VEGF under hypoxic stimuli [293].

Looking at the gene expression changes in the ischaemic muscles, SHEP1 and NPDC1 showed non-significant trends towards upregulation with a wide variation amongst individual KO mice. Of the 3 genes (SHEP1, NPDC1, and EGFL7) identified as potential downstream candidates of LINC00961, however neither SHEP1 and NPDC1 have been associated with angiogenesis or muscle regeneration to the best of our knowledge. It would be interesting to investigate this possible pathway of LINC00961 action as previously mentioned by measuring their protein expression levels when LINC00961 is modulated. Pax7 and MYOG are muscle satellite cell/SC markers and transcription factors essential in myogenesis in the embryo [294]. Pax7

has been demonstrated several times to be crucial for skeletal muscle regeneration after injury [295] [296], whilst MYOG is a regulator of myogenesis and muscle cell differentiation, and is responsible for inducing myoblast fusion [294, 297] with some evidence that is not necessary for post-natal muscle growth [298]. Matsumoto & colleagues (2017) showed that Pax7 and MYOG were upregulated in SPAAR$^{-/-}$ mice 4 days after cardiotoxin injury [232] at the RNA and protein level. Here, Pax7 RNA expression was unaltered in LINC00961$^{-/-}$ mice even after ischaemic injury. Interestingly, MYOG RNA expression was significantly downregulated in the ischemic limb of LINC00961$^{-/-}$ mice, in complete contrast to the upregulation seen my Matsumoto & colleagues (2017). However, there are some important differences between the two studies, here hypoxic injury was caused to the adductor muscle whereas Matsumoto & colleagues (2017) utilised cardiotoxin to injure the anterior tibialis muscle creating a different type of injury with likely more muscle cell apoptosis and necrosis than is induced during femoral artery ligation. What should also be considered is that Matsumoto & colleagues (2017) deleted SPAAR but maintained LINC00961 expression in their mouse model, here, our LINC00961$^{-/-}$ mouse lacks both SPAAR and LINC00961; we are therefore observing the additive effects of deleting 2 molecules in our study. It would therefore be interesting to repeat the HLI study in the SPAAR$^{-/-}$ mouse to compare capillary densities and gene expression analysis to help determine the precise effects of the 2 molecules in this circumstance. Importantly, here only RNA expression was measured; it would be worthwhile to measure the protein levels of Pax7 and MYOG at this timepoint. It is possible that both Pax7 and MYOG expression may have peaked earlier after injury and that Pax7 RNA levels have since returned to baseline and MYOG may be downregulated at the RNA level but remain upregulated at the protein level. However, to fully determine whether this is the case protein analysis via western blots is required, specifically at earlier time points such as day 3. Nether-the-less, these data are interesting and may point to a role for the LINC00961 locus in muscle regeneration further to that identified for SPAAR in muscle regeneration. Of course, there are other muscle regulatory factors involved in myogenesis and muscle differentiation which may also be analysed to further elucidate the role of the LINC00961 locus in muscle regeneration such as MYOD1, MYF5, MRF4.

Other genes in this panel which showed no changes in gene expression were VEGF-A and VEGF-C, which are crucial factors in the control of angiogenesis and lymph-angiogenesis respectively, and HRCT1, the closest neighbouring protein coding gene

to the LINC00961. In agreement with the published LINC00961 KD data, HRCT1 expression was unaltered, however, demonstrates a wide variation amongst individual mice.

Besides the need to analyse protein levels, there are other limitations of this study to consider. For accurate depiction of RNA expression changes during HLI recovery the number of animals used should be calculated using a power analysis, due to the number of offspring which were available at the time of these experiments and the exclusion of qRT-PCR samples where replicates were not tight enough and therefore unreliable, or outliers were found; the low N numbers for some data points may be masking true expression alterations due to the natural variation with *in vivo* data. One important result this Chapter has highlighted is the opposing cell type specific modulation of LINC00961 in ECs and skeletal muscle cells. To obtain further data for gene and protein expression it would be useful in future to isolate ECs from the hind limbs using the same CD34+ MACS beads used by Dr. Caporali to generate the EC and muscle cell fraction data in Figure 3.4. Pax7 and MYOG for example will not be expressed in ECs, whereas some genes will be expressed in both cell types. However, as the whole muscle was used for gene expression analysis it is impossible to determine EC and skeletal muscle specific alterations between genotypes and it is possible that some genes may be differentially regulated between cells types. Lastly, in light of the cell type specific regulation of LINC00961 transcript levels, to further investigate the full effects of the LINC00961 locus in endothelium as previously mentioned an endothelial conditional KO mouse model would be beneficial. A skeletal muscle specific KO model would also be of interest to further investigate the impact of LINC00961 on muscle regeneration, in comparison to the known role of SPAAR in inhibiting mTORC1 activation during muscle regeneration. Considering the opposing pro-angiogenic and anti-angiogenic roles of SPAAR and LINC00961 in the endothelium, it would be interesting to explore if there is also an opposing role for LINC00961 in muscle regeneration, perhaps in promoting muscle regeneration to balance the effects of SPAAR.

3.6.5 Pro-angiogenic SPAAR is not expressed in unstimulated HUVECs

Despite high levels of LINC00961 transcript being present in unstimulated HUVECs [254] we have been unable to detect SPAAR protein levels by western blot utilising the only commercially available antibody. As this could be due to the limit of detection of the antibody we chose to investigate SPAAR expression via mass spectrometry analysis. Interestingly, SPAAR was detected in our 2 positive controls only (HeLa cell lysate and LV-SPAAR infected HUVEC lysate) and not in unstimulated HUVECs (Figure 3.5). Considering the pro-angiogenic role we identified for SPAAR previously [254] this is a logical finding and to the best of our knowledge, we are the first to identify it's lack of expression in unstimulated ECs. This led to the hypothesis that SPAAR is only expressed in the endothelium following angiogenic stimuli, such as hypoxia or VEGF.

3.6.6 Depletion of ERG does not alter LINC00961 expression in HUVECs despite promoter binding

Identifying the upstream regulators of the LINC00961 expression is important to help understand this locus' function. With the help of our collaborators, we were able to investigate whether the known endothelial enriched transcription factor ERG could regulate LINC00961. Using HUVECs, their ChIP-seq data identified that ERG binds to the promoter region of human LINC00961 at 2 sites, one close to the start of exon 1 and the other approximately 1000kb further upstream (Figure 3.6). Based on this data we hypothesised that ERG is likely to regulate LINC00961 expression. We tested this by depleting ERG and testing whether LINC00961 expression would also be reduced. Time points of 24, 48, and 72 h of siRNA KD were chosen to be sure that transcript depletion would lead to protein depletion as we know for example that ERG-2 protein has a half life of 21 h [299]. Although there is a need to check protein levels of ERG with western blots alongside PCR analysis to further validate this KD qRT-PCR data did show ERG depletion (Figure 3.7). To our surprise, LINC00961 levels were unchanged at each time point. Based on this result we are currently unable to prove that LINC00961 is directly regulated by ERG. It is possible however, that LINC00961 up- or down-regulation by ERG requires the addition of a stimulus or additional co-factors, as other ETS family members are known to bind a number of partners, which influence their downstream target activation. This is known as combinatorial control and involves the binding with other families of transcription

factors such as; PAX, SRF, AP1, bZIP and Runt, as well as others [300]. Although not investigated here, expression of these ERG family members in KD samples could be carried out by qPCR and western blot to decipher any regulation and pin point potential co-factors for this process for further investigation.

This combinational mechanism allows for a synergistic effect of increased transcription of a target gene when multiple transcription factors bind to its promoter or enhancer. This can also serve as a backup if one partner is mutated or deleted and can no longer bind. Binding of a similar pair or a substituted family member may ensure maintained target transcription and avoid cellular pathology [301].

The canonical ERG binding motif is 5'-(C/a/g)(A/C)GGAA(G/A)-3' where GGAA is the core sequence to which all ETS family members bind [302] and the flanking nucleotides affect the binding affinity for different family members which demonstrate a preference for flanking nucleotides of up to 15 bases [256, 259, 303]. Using the transcription factor binding profile database JASPAR (http://jaspar.genereg.net/), Dr. Julie Rodor was able to identify 2 predicted potential ERG binding sites in the LINC00961 promoter which are highlighted in red in Figure 3.6C. This matched closely with the data provided by Professor Randi's group and further supported our original hypothesis that ERG could regulate LINC00961 expression. All instances of the 'GGAA' core sequence for ETS family binding are highlighted in yellow. To further investigate the potential for ERG to regulate LINC00961 expression a luciferase reporter assay could be utilised. Each of the ERG binding sites identified by Professor Randi's group could be tested separately and in combination to show whether they have a synergistic effect.

3.6.7 Could ERG regulate SPAAR?

As ERG plays a role in regulating angiogenesis [255, 256, 304] perhaps it is the pro-angiogenic SPAAR whose expression ERG may regulate and not the anti-angiogenic LINC00961 transcript. Therefore, it could be hypothesised that ERG regulates SPAAR expression, not LINC00961 expression, and that it does so under angiogenic stimuli. To test this hypothesis, HUVECs placed in hypoxia for at least 24 h could be used to look at ERG expression both at the RNA and protein level, and SPAAR expression via mass spectrometry and western blot (with the caveat that depending on the extent of expression it may not be detectable with the current available antibody

in a western blot). In addition to this, ERG overexpression experiments in HUVECs could be used, via LV-infection, to hypothetically induce SPAAR expression which could be analysed by mass spectrometry and western blot.

3.7 Conclusion

In conclusion, this Chapter demonstrates that the *in vitro* effects of endothelial LINC00961 KD translate to functional effects *in vivo,* specifically in regard to angiogenesis and arteriogenesis. Endothelial barrier maintenance, migration, proliferation, and adhesion which were affected by KD *in vitro* may also be affected by LINC00961 locus loss *in vivo*, especially when we consider the underlying vessel issues seen in the decreased number of αSMA supported vessels in the LINC00961$^{-/-}$ mice before injury, however, the extent of endothelial dysfunction *in vivo* requires further investigation. This work, along with that of others, has highlighted that although enriched in the endothelium this locus is very likely to have effects in other cell types which could contribute to other diseases. We were able to separate the independent roles of LINC00961 and SPAAR, at least in regard to angiogenesis, providing crucial further evidence to the field for the role of LncRNAs as genuine non-coding transcripts, despite the presence of functional micropeptides within their locus. The analysis here of potential downstream targets of LINC00961 and the brief investigation of gene expression changes in the LINC00961$^{-/-}$ mice demonstrates that this locus could have further implications in the organism as a whole and further investigations are required into other molecular pathways and morbidities these mice may have, and relevantly, how these may translate to human disease.

Although we are still unsure what pathways regulate LINC00961 locus expression upstream, ERG remains a candidate for positive regulation of this locus which could be investigated further in future. This Chapter provides further evidence that LINC00961 and SPAAR have independent functions, given the lack of SPAAR expression under quiescent conditions.

Chapter 4 The influence of the LINC00961/SPAAR locus loss on murine development, myocardial dynamics, and cardiac response to myocardial infarction

4.1 Introduction

This Chapter addresses whether the inhibition of tubule formation in LINC00961 KD of human ECs is recapitulated in mouse ECs, to establish whether the mouse and human locus function in a similar manner. One of the aims of this Chapter was then to determine whether our CRISPR/Cas9 generated LINC00961$^{-/-}$ mouse line was viable and would be suitable to investigate the role of the locus *in vivo*. Schematic representation of the murine LINC00961 locus and position of proximal and distal gRNA (red arrows) used for deletion of the locus by Taconic© and validation of the LINC00961$^{-/-}$ genotype by qRT-PCR on kidney tissue can be found in Figure 4A and Supplementary Figure 6A respectively, in the publication in Chapter 3. Secondly, we aimed to broadly characterise this mouse line, therefore, this Chapter includes a manuscript recently published in the International Journal of Molecular Sciences, summarising our findings on mouse and organ weight post-weaning, as well as additional and incomplete data from experiments focusing on KO myocardial dynamics and their response to inducedMI. After confirming a role for the LINC00961 locus in angiogenesis and reperfusion after injury in HLI, our hypothesis evolved to question whether loss of this locus would also affect neovascularisation in the heart after an MI. Before we could investigate this surgically we needed to confirm that the animals had no underlying heart functional issues. To do this, we utilised cardiac ultrasound equipment available at Edinburgh University (carried out by Mr. Adrian Thomson). The incomplete data from MI experiments is at the end of this Chapter. Issues which contributed to the inability to complete this work before the end of my PhD studies include the time and labour involved in finding the accurate point for analysis in each heart. Our protocol for analysis of the MI hearts was to find the middle section taken of each heart based on the total number of slides/sections for each individual heart. Unfortunately, H&E and Sirius red staining's revealed that we were

not in the correct position for analysis in many of these samples and would need to re-stain after finding the correct sections.

In the following publication, I contributed to writing and editing the original manuscript as joint first author. My contributions to Figures are listed below:

- Figure 1 - I performed the hypoxia experiments and analysis generating the data in panels C and D.
- Figure 2 – The technical staff at the University of Edinburgh Biomedical and Veterinary Sciences assisted in weighing the mice weekly. I collected, collated, and analysed the growth curve chart data.
- Table 1 – Dr Ana-Mishel Spiroski and I jointly performed perfusion fixation on the mouse tissues, harvested organs, recorded weights and measurements, and collated data.

4.2 Aims

The aims of this chapter were:

- To determine LINC00961$^{-/-}$ offspring viability.
- To monitor LINC00961$^{-/-}$ post natal growth and development.
- To determine basal cardiac function in LINC00961$^{-/-}$ offspring.
- To determine the response of LINC00961$^{-/-}$ to myocardial infarction.

4.3 Publication

International Journal of
Molecular Sciences

MDPI

Communication

The Influence of the LINC00961/SPAAR Locus Loss on Murine Development, Myocardial Dynamics, and Cardiac Response to Myocardial Infarction

Ana-Mishel Spiroski [1,†], Rachel Sanders [1,†], Marco Meloni [1], Ian R. McCracken [1], Adrian Thomson [2], Mairi Brittan [1], Gillian A. Gray [1] and Andrew H. Baker [1,*]

[1] Centre for Cardiovascular Science, Queens Medical Research Institute, University of Edinburgh, Edinburgh EH16 4TJ, UK; am.spiroski@ed.ac.uk (A.-M.S.); rachel.sanders@ed.ac.uk (R.S.); marco.meloni@sanofi.com (M.M.); ian.mccracken@ed.ac.uk (I.R.M.); mbrittan@exseed.ed.ac.uk (M.B.); gillian.gray@ed.ac.uk (G.A.G.)

[2] Edinburgh Preclinical Imaging, Edinburgh Preclinical Imaging, BHF Centre for Cardiovascular Science, University of Edinburgh, Edinburgh EH16 4TJ, UK; adrian.thomson@ed.ac.uk

* Correspondence: Andy.Baker@ed.ac.uk; Tel.: +44-0131-24-26728

† Authors have contributed equally.

Abstract: Long non-coding RNAs (lncRNAs) have structural and functional roles in development and disease. We have previously shown that the LINC00961/SPAAR (small regulatory polypeptide of amino acid response) locus regulates endothelial cell function, and that both the lncRNA and micropeptide counter-regulate angiogenesis. To assess human cardiac cell SPAAR expression, we mined a publicly available scRNSeq dataset and confirmed LINC00961 locus expression and hypoxic response in a murine endothelial cell line. We investigated post-natal growth and development, basal cardiac function, the cardiac functional response, and tissue-specific response to myocardial infarction. To investigate the influence of the LINC00961/SPAAR locus on longitudinal growth, cardiac function, and response to myocardial infarction, we used a novel CRISPR/Cas9 locus knockout mouse line. Data mining suggested that SPAAR is predominantly expressed in human cardiac endothelial cells and fibroblasts, while murine LINC00961 expression is hypoxia-responsive in mouse endothelial cells. LINC00961$^{-/-}$ mice displayed a sex-specific delay in longitudinal growth and development, smaller left ventricular systolic and diastolic areas and volumes, and greater risk area following myocardial infarction compared with wildtype littermates. These data suggest the LINC00961/SPAAR locus contributes to cardiac endothelial cell and fibroblast function and hypoxic response, growth and development, and basal cardiovascular function in adulthood.

Keywords: lncRNA; LINC00961; SPAAR; scRNASeq; CRISPR/Cas9; cardiovascular physiology; fetal growth restriction; myocardial infarction

Citation: Spiroski, A.-M.; Sanders, R.; Meloni, M.; McCracken, I.R.; Thomson, A.; Brittan, M.; Gray, G.A.; Baker, A.H. The Influence of the LINC00961/SPAAR Locus Loss on Murine Development, Myocardial Dynamics, and Cardiac Response to Myocardial Infarction. *Int. J. Mol. Sci.* **2021**, *22*, 969. https://doi.org/10.3390/ijms22020969

Received: 9 December 2020
Accepted: 14 January 2021
Published: 19 January 2021

1. Introduction

Over 17 million deaths worldwide annually are due to cardiovascular diseases (CVD) [1]. With no clinically utilised therapeutics available to reverse the disease process, management focuses on reducing risk factors that exacerbate the "silent symptoms" which contribute to ischaemic diseases of the heart and vasculature. Myocardial infarction (MI), which causes a prolonged lack of blood flow to the heart muscle, ultimately resulting in tissue necrosis and formation of a fibrotic scar, is one such disease. Whilst an MI shortens a patient's life expectancy by >16 years [2,3], greater acute survival rates increases the incidence of subsequent heart failure. In concert with higher worldwide life expectancies and burgeoning increases in CVD risk factors, the economic and social burden of disease is ever-increasing. Investigating the underlying mechanisms which contribute to cardiovascular dysfunction and identifying potential therapeutic targets provides the most impactful opportunity for reducing the compounding costs of CVD.

As approximately 98% of the human genome that is transcribed into RNA does not code for protein [4], non-coding RNAs (ncRNA) provide a possible target to investigate both their physiological relevance and therapeutic capacity as novel interventional approaches. Long non-coding RNAs (lncRNAs) can be within a known protein-coding gene (intronic) and over-lapping with another gene (sense-overlapping), antisense to a gene they are likely to regulate (present on the opposite DNA strand, sequence overlapping), or bi-directional to a gene they likely regulate (present on the opposite DNA strand, sequences not over-lapping). LncRNAs located between neighbouring protein-coding genes are termed long intergenic non-coding RNA (lincRNA). Various lincRNAs have been reported to contribute to cardiovascular biology, with their functions contributing to embryological heart development, cardiovascular cell commitment, cell migration, smooth muscle cell (SMC) phenotype-switching, vascular endothelial cell (EC) commitment, and angiogenesis [5–10].

LINC00961, a lincRNA located on human chromosome 9 at p13.3, has 4 predicted transcripts with 1 predicted to undergo non-sense-mediated decay (ENSG00000235387). The locus is 1557 base pairs (bp) and contains 2 exons, of which exon 2 encodes the 75 amino acid micropeptide previously termed small regulatory polypeptide of amino acid response (SPAAR) by Matsumoto and colleagues, who identified 2 potential transcription start sites [11]. The mouse homologue (previously 5430416O09Rik) maps to chromosome 4 with 65.33% amino acid sequence conservation. Although greater conservation is observed between humans and non-human primates, the mouse and human locus is conserved in synteny with many of the same neighbouring protein-coding genes. Interestingly, Di Salvo and colleagues show a 1.4 log2 (fold change) in the right ventricle of heart failure patients compared to healthy donor controls [12]. Additionally, LINC00961 is expressed in highly vascular tissues such as the kidney, lungs, and placenta, and SPAAR deletion results in a 15.3-fold increase in LINC00961 locus expression in the murine heart [11]. Thus, based on the association of LINC00961 with vascular endowment, the loss of LINC00961 could influence structure and function from prenatal life onward. From reduced vascular enrichment in the placenta and its influence on foetal and postnatal growth and development, to adult disease risk and pathological response, particularly in the cardiovascular and pulmonary systems, LINC00961 loss of function could have clinical implications throughout the lifespan.

LINC00961 has been identified in multiple disease pathways associated with cardiovascular dysfunction. Wu and colleagues recently reported that LINC00961 is downregulated in patients with coronary artery disease (CAD) and in $APOE^{-/-}$ mice [13]. In response to hypoxia, the H9C2 rat cardiomyoblast cell line demonstrates increased signal transducer and activator of transcription 1 (STAT1) interaction with the LINC00961 promoter and subsequent LINC00961 expression [14]. Downstream phosphorylation of phosphoinositide 3-kinase (PI3K), protein kinase B (AKT), and glycogen synthase kinase-3β (GSK3β) were also inhibited. Activation of this pathway has been implicated in abrogating the pathological remodelling of the heart post-hypoxia/reperfusion injury [15], suggesting LINC00961's potential contribution to cardiomyocyte maintenance. Additionally, we have previously demonstrated that the LINC00961 locus directly regulates endothelial cell (EC) function, with SPAAR and LINC00961 counter-regulating angiogenesis in vitro and evidenced in a murine hindlimb ischaemia model of critical limb ischaemia [16]. In our previous work, we showed that LINC00961 binds the actin-binding protein thymosin beta-4x, which is involved in regulating cytoskeletal dynamics, angiogenesis, and cell migration [17], while SPAAR binds the actin-binding protein spectrin repeat-containing nuclear envelope protein 1 (SYNE1/NESPRIN-1), which is highly expressed in cardiomyocytes [18]. These initial data suggest the importance of the LINC00961/SPAAR locus in cellular maintenance and response to environmental insult. However, the cardiac effects of LINC00961 locus knockout (KO) in vivo are still unknown. Therefore, we investigated the expression of SPAAR with single-cell RNA sequencing (scRNAseq) data mining of human cardiac cell populations, the expression of the LINC00961 locus in a mouse endothelial-like cell line,

and the effects of CRISPR/Cas9 LINC00961 locus deletion on murine growth and development, basal cardiac function, risk area following acute cardiac ischaemia, and physiological function following 7 days of chronic cardiac ischaemia in a surgical model of MI.

2. Results

2.1. Human Cardiac SPAAR Expression and the Endothelial Cell LINC00961 Response to Hypoxia

Mining of the Human Cell Atlas global heart dataset revealed SPAAR expression primarily in human cardiac EC (Figure 1A,B). LINC00961 expression is significantly reduced in murine bEnd.3 cells following 24 and 48 h hypoxia (1% O_2) exposure compared with cells cultured in normoxia (5% O_2) (Figure 1C,D).

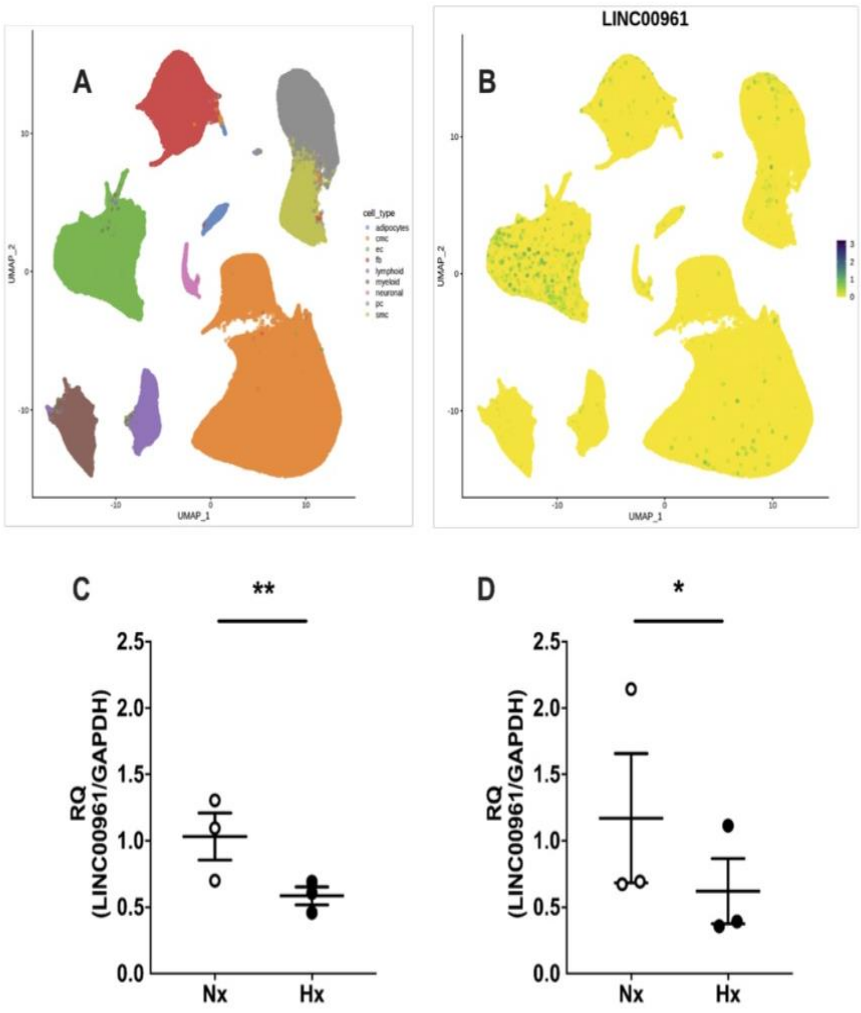

Figure 1. Human cardiac SPAAR (small regulatory polypeptide of amino acid response) expression and LINC00961 response to hypoxia. Uniform manifold approximation and projection for dimension reduction (UMAP) visualisation of (**A**) human cardiac endothelial cells (EC, green), fibroblast (FB, red), pericyte (PC, grey), SMC (olive), cardiomyocyte (CMC, orange), adipocyte (blue), neuronal cell (pink), myeloid (brown), and lymphoid (purple) fraction [19], and (**B**) SPAAR expression in human cardiac cell populations. LINC00961 expression is reduced in bEnd.3 mouse cells following 24 h (**C**, black $n = 3$) and 48 h (**D**, black $n = 3$) exposure to hypoxia (H, 1% O_2) compared with bEnd.3 cells cultured in normoxia (Nx, 5% O_2) collected in parallel (both $n = 3$). Student's *t*-test. Data are mean ± SEM. * $p < 0.05$, ** $p < 0.01$.

2.2. Post-Weaning Growth and Development

Whilst there was no effect of genotype on female weight gain post-weaning (Figure 2A), longitudinal weight gain was delayed in male LINC00961$^{-/-}$ mice (Figure 2B). There was an effect of sex and genotype on adult body weight, and a sex × genotype interaction, with male LINC00961$^{-/-}$ mice attaining a lower adult weight (Table 1). Male LINC00961$^{-/-}$ mice also had a greater brain to body weight ratio in adulthood, with a sex × genotype interaction. LINC00961$^{-/-}$ mice had reduced tibia and head lengths, and absolute liver weight, with no difference in relative liver weight.

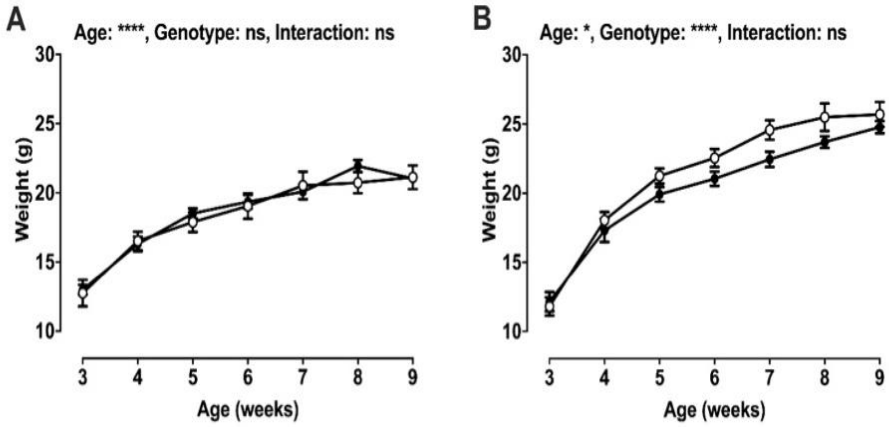

Figure 2. Post-weaning growth by sex. Weight gain from weaning (3 weeks) to 9 weeks of age in females (**A**: WT, white, n = 2–12; KO, black, n = 8–13) and males (**B**: WT, white, n = 6–11; KO, black, n = 2–7); 2-way ANOVA. Mean ± SEM. * $p < 0.05$, **** $p < 0.0001$, ns = not significant.

Table 1. Adult post-mortem organ weights.

	Female		Male		Significance (p)		
	WT $n = 9$	**KO** $n = 9$	**WT** $n = 10$	**KO** $n = 9$	**Sex**	**Genotype**	**Interaction**
Weight (g)	20.8 ± 0.9	20.9 ± 0.5	27.1 ± 0.6	23.7 ± 0.9	0.01	0.03	0.02
Brain (mg)	443.9 ± 8.8	428.4 ± 10.6	450.7 ± 5.3	435.5 ± 12.5	ns	ns	ns
Brain:Body weight (mg/g)	21.5 ± 0.5	20.5 ± 0.5	16.7 ± 0.4	18.5 ± 0.5	0.01	ns	0.009
Heart (mg)	124.2 ± 7.2	125.7 ± 9.6	137.0 ± 6.3	115.2 ± 6.6	ns	ns	ns
Heart:Body weight (mg/g)	6.0 ± 0.4	6.1 ± 0.4	5.0 ± 0.3	4.9 ± 0.3	0.03	ns	ns
Lungs, total (mg)	167.7 ± 16.5	147.1 ± 7.4	148.0 ± 3.6	139.9 ± 4.9	ns	ns	ns
Lungs:Body weight (mg/g)	7.5 ± 0.3	7.1 ± 0.3	5.5 ± 0.2	5.9 ± 0.3	0.01	ns	ns
Liver (mg)	1212 ± 64	1104 ± 34	1111 ± 71	1174 ± 69	ns	0.004	ns
Liver:Body weight (mg/g)	58.4 ± 2.5	53.2 ± 2.5	53.5 ± 2.4	49.6 ± 2.5	ns	ns	ns
Spleen, total (mg)	88.3 ± 5.8	88.0 ± 3.8	84.9 ± 4.3	80.3 ± 8.6	ns	ns	ns
Spleen:Body weight (mg/g)	4.2 ± 0.2	4.2 ± 0.2	3.1 ± 0.2	3.4 ± 0.2	0.009	ns	ns
Soleus, total (mg)	6.4 ± 0.4	6.4 ± 0.6	8.6 ± 0.6	8.1 ± 0.8	ns	ns	ns
Soleus:Body weight (mg/g)	0.31 ± 0.02	0.31 ± 0.03	0.32 ± 0.02	0.34 ± 0.03	ns	ns	ns
	WT $n = 5$	**KO** $n = 8$	**WT** $n = 10$	**KO** $n = 8$	**Sex**	**Genotype**	**Interaction**
Nose to anus (mm)	79.5 ± 1.5	79.7 ± 1.1	82.3 ± 1.1	79.0 ± 0.8	ns	ns	ns
Head length (mm)	25.0 ± 0.6	26.7 ± 0.3	26.4 ± 0.2	26.5 ± 0.6	ns	0.006	ns
Biparietal diameter (mm)	11.6 ± 0.2	11.2 ± 0.2	11.8 ± 0.1	11.7 ± 0.2	ns	ns	ns
Tibia length (mm)	15.4 ± 1.1	18.4 ± 0.7	17.5 ± 0.5	17.0 ± 0.4	ns	0.05	ns

Post-mortem organ weights were collected in female (WT, n = 5–9; KO, n = 8–9), and male (WT, n = 10; KO, n = 8–9) adults (9.7 ± 0.3 and 9.9 ± 0.3 weeks, respectively). Data are mean ± SEM. Statistical differences are indicated: main effect of sex, main effect of genotype, and sex × genotype interaction (two-way ANOVA with Tukey's post-hoc comparison).

2.3. Basal Cardiac Dimensions and Function

Measures of cardiac function with ultrasound echocardiography left ventricular mitral/aortic blood flow, stroke volume (SV), ejection fraction (EF), fractional area change (FAC), and cardiac output (CO) were not different in WT and LINC00961$^{-/-}$ mice (Figure 3A–D) at baseline. Adult LINC00961$^{-/-}$ mice had significantly smaller left ventricular (LV) systolic and diastolic area, and lower end-systolic volume (ESV) and end-diastolic volume (EDV) (Figure 3E–H). Mitral valve function was not different in LINC00961$^{-/-}$ compared with WT.

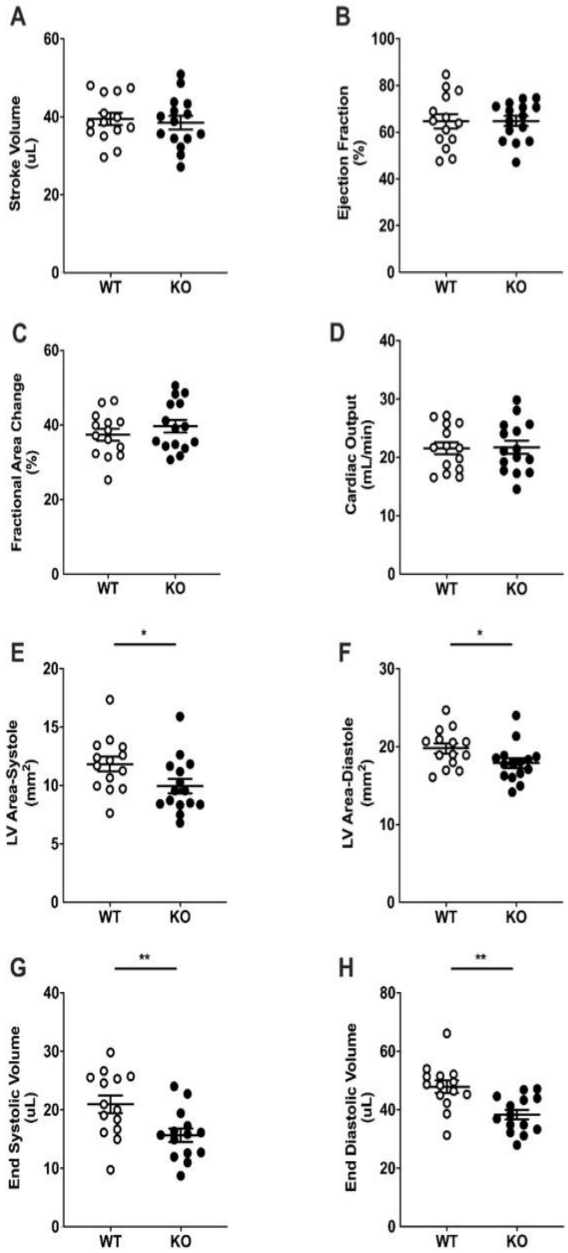

Figure 3. Basal cardiac dimensions and function by ultrasound echocardiography. Stroke volume (SV, **A**), ejection fraction (EF, **B**), fractional area change (FAC, **C**), cardiac output (CO, **D**), left ventricular systolic (**E**) and diastolic (**F**) areas, end systolic volume (ESV, **G**) and end diastolic volume (EDV, **H**) in 8-week-old female WT (white, $n = 14$) and KO (black, $n = 14$) mice. Student's *t*-test. Data are mean ± SEM. * $p < 0.05$, ** $p < 0.01$.

2.4. Acute Myocardial Risk Area

There was a significant increase in risk area 30 min after left anterior descending (LAD) coronary artery ligation (~17%, $p < 0.01$) in adult male LINC00961$^{-/-}$ compared with WT mice (Figure 4A,B).

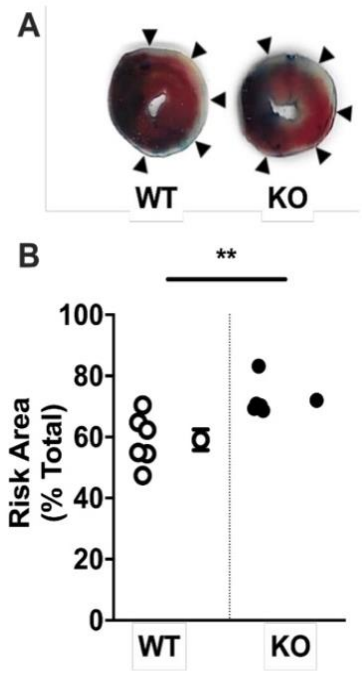

Figure 4. LINC00961 knockdown increases area at risk of myocardial infarction. (**A**) Myocardial infarction risk area (pink and white, indicated by arrows) relative to total heart area (blue, pink, and white) in heart tissue collected 30 min after left anterior descending coronary artery ligation in 9-week-old male mice. (**B**) Individual (left) and mean areas at risk in WT (white) and KO (black) mice (both $n = 6$). Student's *t*-test. Data are mean ± SEM. ** $p < 0.01$.

2.5. Cardiac Function Following Surgically Induced Myocardial Infarction

There was no difference between WT and LINC00961$^{-/-}$ mice in measures of cardiac function by ultrasound echocardiography with Doppler flow (SV, EF, FAC, CO, ESV, or EDV) at 7 days post-MI (Figure 5A–F). Mitral valve function was not different in LINC00961$^{-/-}$ compared with WT mice (data not shown).

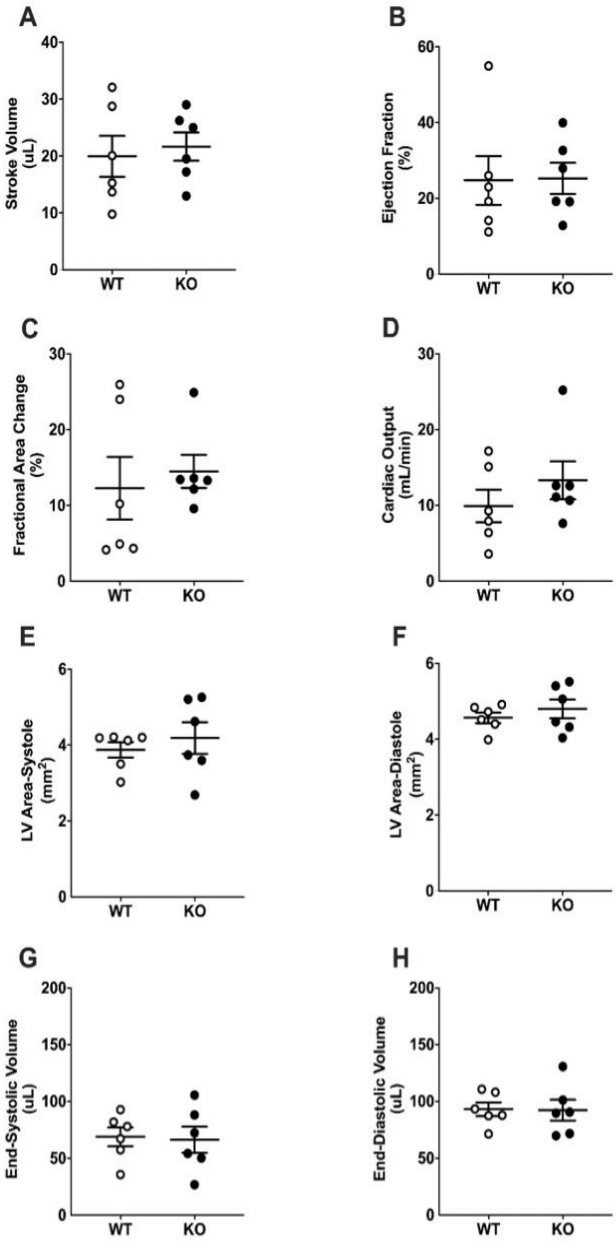

Figure 5. Cardiac dimensions and function following myocardial infarction (MI). SV (**A**), EF (**B**), FAC (**C**), CO (**D**), left ventricular systolic (**E**) and diastolic (**F**) areas, ESV (**G**) and EDV (**H**) in WT (white, $n = 6$) and KO (black, $n = 6$) female mice 7 days and 14 days following chronic LAD ligation. Student's *t*-test. Data are mean ± SEM.

3. Discussion and Conclusions

3.1. Discussion

We have shown that genetic LINC00961$^{-/-}$ reduces adult LV area, ESV, and EDV, suggesting an overall reduction in LV size, and greater risk area following MI. We have previously reported that LINC00961 locus CRISPR/Cas9 KO reduces alpha-smooth muscle

actin (αSMA) cell-density in the mouse hindlimb skeletal muscle without altering capillary density [16]. Global dysfunction in EC endowment resulting in compromised development of the vascular network could limit the capacity for myocardial growth and the maintenance of functional myocardium throughout life [20]. Reduced LV volume independent of adult size in LINC00961$^{-/-}$ mice suggests that the vascular influence on cardiac development requires further investigation. Regardless, an appropriate relative heart size and adequate basal cardiac function suggests that at this relatively young age, the heart is able to adapt to reduced LV volumes and maintain physiological homeostasis.

The novel finding of asymmetric, delayed postnatal growth and a brain-sparing phenotype in male LINC00961$^{-/-}$ offspring indicates that the reduced vascular endowment previously reported in adults likely compromises embryonic implantation, the development of foetal vasculature, and subsequent growth [21,22]. This foetal growth restriction (FGR) phenotype is the result of preferential shunting of blood away from peripheral organs in order to protect brain growth and development in utero. As inadequate endothelial endowment results in chronic foetal ischaemia and foetal oxygenation, the foetal adaptation to an inhospitable in utero environment results in the pathological programming of cardiovascular function [23]. Although females are relatively protected from environmental insults on the developing embryo [21], adult manifestations of hypoxic pregnancy include impaired ventricular relaxation, enhanced myocardial contractility, and cardiac sympathetic dominance, which contribute to maintained cardiac output [23–28]. Overall, these data suggest a role for the LINC00961/SPAAR locus in somatic growth and development, and adult cardiovascular function.

Establishment of an efficient microvascular network in order to supply blood flow matched to metabolic demand is necessary throughout the body; however, nowhere more so than in the continuously active myocardium. We showed that human cardiac endothelial cells and fibroblasts express SPAAR, and that LINC00961 expression in murine endothelial-like cells is hypoxia-responsive. These data suggest the LINC00961/SPAAR locus is expressed in basal conditions, and that regulation of the LINC00961 transcript is evident in response to environmental insults, such as those associated with pro-angiogenic states. We have previously reported that the LINC00961/SPAAR locus contributes to angiogenesis in the peripheral musculature, and here we have shown the potential for its influence on in vivo cardiovascular function and response to localised cardiac ischaemia. As we focused on the acute cardiac remodelling window, progression toward heart failure was outside of the scope of this current study. The apparent "normalisation" of left ventricular volume and area in LINC00961$^{-/-}$ compared with wildtype mice at 7 days post-MI may suggest a relative acceleration in ventricular dilation in KO mice. Although LINC00961$^{-/-}$ structural and functional cardiac deficiencies do not compromise homeostatic regulation at this young age, we hypothesise that disease severity and progression toward heart failure may be more pronounced during pathological remodelling. Future work investigating LINC00961 over-expression, for example using viral vector-based approaches for delivery to the heart, would elucidate the suitability of this lncRNA as a potential therapy.

Microvascular dysfunction is associated with cardiovascular dysfunction, accelerated pathological processes, and increased mortality [29,30]. ECs contribute to the regulation of shear stress, permeable barrier maintenance, leukocyte extravasation, blood clotting, inflammation, vascular tone, extracellular matrix (ECM) deposition, and vasoconstriction and vasodilation [31–34]. By adapting to altered blood flow and composition, EC activation primes the tissue environment for coagulation, inflammation, and vasoconstriction, a necessary cascade for wound healing and repair [31]. Inadequate vascular endowment has the potential not only to influence cardiac function, but also the tissue response to pathological processes. Future work would benefit from assessment of sex-specific assessment of initial cardiac risk area, either directly or by proxy with a troponin assay. This study is limited by the CRISPR approach to global LINC00961 KO, rather than with a conditional approach. Due to the influence of LINC00961 on vascular endowment and subsequent somatic growth

and development, future work would benefit from a conditional KO, either inducible or at the organ-specific level.

3.2. Conclusions

We have shown that the left ventricular risk area following an acute MI is greater in LINC00961$^{-/-}$ mice compared to wildtype littermates. However, at 7 days post-LAD ligation in an MI model, cardiac function in LINC00961$^{-/-}$ was not different from wildtype littermates. These data suggest that the cardiac vascular network may be compromised, but the progression toward heart failure, with a significant ~40% reduction in ejection fraction, is not compounded by LINC00961$^{-/-}$. It has previously been reported that reduced coronary vascularity increases cardiac vulnerability to fibrosis [35–37]. Reduced blood flow to the functional myocardium compromises coronary flow reserve required during increased cardiovascular work and pathological conditions [30,38]. Future investigations on the microvascular network during the acute remodelling window post-MI will help to identify the contribution of LINC00961 and SPAAR to extracellular matrix remodelling and the secretion of matrix metalloproteinases, fibronectin, and proteoglycans during cardiac scar maturation. As SPAAR expression has already been detected in the human heart [39], it will be important to understand the effect of the peptide, specifically on cardiac function, and whether this is counterbalanced by the LINC00961 transcript.

4. Materials and Methods

4.1. Ethical Approval

All animal procedures were performed at a University of Edinburgh Biomedical and Veterinary Sciences facility. This research was conducted in accordance with the Animals (Scientific Procedures) Act 1986 Amendment Regulations 2012, following ethical review by the University of Edinburgh Animal Welfare and Ethical Review Board (AWERB), under project (70/8933) and personal licenses held within the University of Edinburgh and conducted in accordance with ARRIVE (Animal Research: Reporting of In Vivo Experiments) guidelines [40]. To align with the National Centre for the Replacement, Refinement, and Reduction of Animals in Research (NC3Rs) principles, both male and female mice were used for this work.

4.2. Single Cell RNASeq Data Mining

Normalised SPAAR expression uniform manifold approximation and projection for dimension reduction (UMAP) visualisation was extracted from the Heart Cell Atlas global heart dataset (www.heartcellatlas.org), a publicly available database maintained within the scope of the Human Cell Atlas project [19] of scRNASeq cardiac cell data.

4.3. In Vitro Endothelial Cell Response to Hypoxia

Murine brain microvascular endothelial-like cell line bEnd.3 (ATCC) cells were cultured in Dulbecco's Modified Eagle Medium (DMEM; Life Technologies, Glasgow, UK) with 10% FBS, and 1% penicillin and streptomycin at 37 °C and 5% CO_2. Cells were plated in 6-well plates and incubated overnight to allow to adhere. The media was replaced the following day, and cells were incubated in a hypoxic chamber (Coy Laboratory Products, Grass Lake, Michigan, USA) at 1% O_2 (5% CO_2 and 94% N_2) for 24 or 48 h. Three biological replicates were collected for each timepoint and condition. Cells were lysed with QIAzol (QIAGEN, Crawley, UK), RNA was extracted, and qRT-PCR was run, as previously described [6,16].

4.4. Generation of Experimental Groups

The LINC00961 locus knockout (KO) mouse line was generated using CRISPR/Cas9 technology (gRNA, proximal: ATACACTCCTCGCTCAATGT; gRNA, distal: CGAGGCTACGCTGTCAGTACT) on a C57BL/6nTAC genetic background by Taconic Biosciences (USA). KO and wild-type (WT) littermates were produced through heterozygous breeding,

offspring ear clip samples were collected and genotyped by Transnetyx (Cordova, Tennessee, USA), as previously described [16], and experimentation was conducted as follows (Figure 6). A subset of females (WT, n = 2–12; KO, n = 8–13) and males (B: WT, n = 6–11; KO, n = 2–7) were weighed weekly, from 3–9 weeks of age, culled by cervical dislocation, and tissues were harvested at 9 weeks (female: WT and KO, both n = 9; male: WT, n = 10, KO n = 9) to analyse longitudinal growth and adult organ size. Adult female mice were allocated to undergo cardiac ultrasound echocardiography at 8 weeks of age to assess basal cardiac function (WT and KO, both n = 14), and a subset of these underwent surgical coronary artery ligation (CAL) to assess the in vivo physiological response to a heart failure procedure (WT and KO, both n = 6). Adult male mice were allocated to undergo CAL (WT and KO, both n = 6) to assess the in vivo cardiac response to acute cardiac ischaemia. Tissues from these offspring were utilised in other studies.

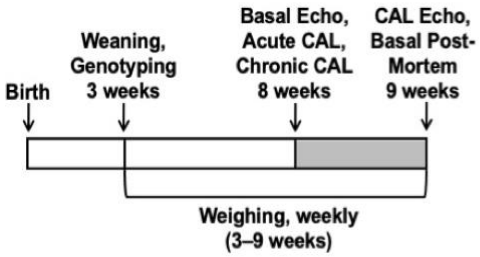

Figure 6. Schematic of age at experimental time points: Weaning and genotyping (3 weeks); basal ultrasound echocardiography (Echo) with Doppler flow, acute coronary artery ligation (CAL), chronic CAL induction (all 8 weeks); CAL Echo, and basal post-mortem (9 weeks); weekly weighing (3–9 weeks).

4.5. Cardiac Ultrasound Echocardiography

Basal cardiac function was acquired by ultrasound echocardiography with Doppler flow under isoflurane anaesthesia (4% induction, ~1.75% maintenance) on the Vevo 770 and Vevo 3100 preclinical imaging systems and analysed in Vevo 770 V3.0 and Vevo lab V3.2.6 image analysis software (FUJIFILM VisualSonics, Inc., Toronto, Canada) following independent in-house confirmation of individual system analytic outcomes (data not shown). Post-CAL cardiac function (7 days) was acquired on a Vevo 3100. Left ventricle (LV) function was assessed with brightness mode (B-mode), Pulse Wave Doppler (PWD), and motion mode (M-mode) in parasternal long axes, short axes and apical 4 chamber view (as appropriate), and EKV, ECG-gated Kilohertz Visualisation. All echocardiography analyses were blinded.

4.6. Acute Coronary Artery Ligation

Male mice at 8 weeks of age were anaesthetised with 70 mg·kg^{-1} intraperitoneal pentobarbital sodium (Euthatal), intubated endotracheally, and ventilated with 3 cm H_2O positive-end expiratory pressure, with ventilation ventilated at 110 breaths per minute (tidal volume dependent on weight, 125–150 µL). Mice were maintained on homeothermic heading pads (Physitemp, Clifton, NJ, USA) and depth of anaesthesia was monitored with corneal and withdrawal reflexes. The CAL was conducted as previously described [41]. Briefly, the heart was exposed via left sternal thoracotomy, the epicardium was punctured to reveal the main branch of the LAD coronary artery, and the LAD occluded by looping a 7-0 prolene suture. Following 30 min ischaemia, the aorta was catheterised, the LAD suture loosened, and the mouse perfused with PBS. Following PBS perfusion, Evans blue dye was perfused, hearts were collected, processed as previously described, and stained with 2% triphenyltetrazolium chloride (TTC) to assess the cardiac risk area and infarct area [42]. Briefly, stained hearts were cut into 1 mm transverse sections to the level above the suture, incubated in 2% TTC for 30 min at 37 °C, blotted dry, and post-fixed in 4%

formalin. Sections were scanned, and risk and infarct area were quantified manually in Fiji by an experienced user (Dr Spiroski).

4.7. Chronic Coronary Artery Ligation

Female mice at 8 weeks of age were anaesthetised with intraperitoneal 100 $mg \cdot kg^{-1}$ ketamine (Velatar, Boehringer Ingelheim, Berkshire, UK) + 10 $mg \cdot kg^{-1}$ xylazine (Rompun. 2%, Bayer, Berkshire, UK), intubated endotracheally, ventilated with 3 cm H2O positive-end expiratory pressure, and ventilated at 110 breaths per minute (tidal volume dependent on weight, 125–150 µL). Eye lubricant (Lacri-Lube Eye Ointment 5g, Allergan, Marlow, UK) and mice were maintained on homeothermic heading pads (Physitemp, Clifton, NJ, USA) and depth of anaesthesia was monitored with corneal and withdrawal reflexes. To induce chronic CAL, the heart was exposed via a left thoracotomy between the second and third ribs performed by blunt dissection, the epicardium was punctured to reveal the main branch of the LAD coronary artery, and the LAD was permanently occluded with a 7-0 prolene suture (Henry Schein, Gillingham, UK). After thoracic and skin closure with 6-0 prolene sutures (Henry Schein, Gillingham, UK), the anaesthetic was reversed with 1.0 $mg \cdot kg^{-1}$ subcutaneous atipamezole (Antisedan, Henry Schein, Gillingham, UK) and 500 uL 0.9% sterile saline. Mice were provided with 0.20 $mg \cdot kg^{-1}$ buprenorphine (Temgesic, Henry Schein, Gillingham, UK) at the time of surgery, 24 and 48 h post-operative, and housed in individually ventilated cages in a heat cabinet for 24 h to help maintain body temperature.

4.8. Statistical Analysis

Data analyses were blinded. Power calculations based on previous datasets were performed to determine the minimum sample size required to achieve statistical significance. For CAL procedures, with a power of 80% and a 5% chance of Type I error, 6 successful animals/group are needed to achieve significant differences in LV function in the chronic MI model. At an 80% survival rate, 8 animals/group are needed. With echocardiography as a clinically relevant endpoint for this study, with a power of 80% and a 5% chance of Type I error, 12 successful animals/group are needed to achieve significant differences in LV function for basal echocardiography procedures.

Data were analysed in JMP 12 (SAS Institute, Inc., Cary, North Carolina, USA). Distribution was verified with the Shapiro–Wilk test and non-parametric data were log-transformed where necessary. Sex comparisons and sex by genotype interactions were analysed by factorial analysis of variance (two-way ANOVA). Tukey's post hoc testing was conducted where appropriate. Data are presented as the mean ± SEM.

Author Contributions: Conceptualization, A.H.B., G.A.G., M.B., A.-M.S., and R.S.; methodology, A.-M.S., M.M., and R.S.; formal analysis, A.-M.S., R.S., I.R.M., and A.T.; investigation, A.-M.S., M.M., and R.S.; resources, A.H.B., G.A.G., and A.-M.S.; data curation, A.-M.S. and R.S.; writing—original draft preparation, A.-M.S. and R.S.; writing—review and editing, A.H.B., G.A.G., M.B., A.T., I.R.M., M.M., A.-M.S., and R.S.; visualization, A.-M.S. and I.R.M.; supervision, A.H.B., G.A.G., M.B., A.-M.S., and M.M.; project administration, A.-M.S., R.S., and M.M.; funding acquisition, A.H.B. All authors have read and agreed to the published version of the manuscript.

Funding: This project has received funding from the European Union's Horizon 2020 Programme for Research and Innovation (825670). The British Heart Foundation supported this work (Program grants: RG/14/3/30706 to A.H.B., and project grant and FS/17/27/32698 to A.H.B.). Professor Baker is supported by The British Heart Foundation Chair of Translational Cardiovascular Sciences (CH/11/2/28733), European Research Council (EC 338991 VASCMIR). A.H.B., M.B., and A.M.S. are supported by the BHF Centre for Vascular Regeneration (RM/17/3/33381), and A.H.B. and M.B. are supported by the BHF Regenerative Medicine Centre (RM/13/2/30158). M.B. is supported by the British Heart Foundation (FS/16/4/31831).

Institutional Review Board Statement: This research was conducted in accordance with the Animals (Scientific Procedures) Act 1986 Amendment Regulations 2012, following ethical review by the

University of Edinburgh Animal Welfare and Ethical Review Board (AWERB), under project (70/8933, approved 29/04/2016).

Informed Consent Statement: Not applicable.

Data Availability Statement: The data presented in this study are available on request from the corresponding author. The data within the Heart Cell Atlas project are publicly available.

Acknowledgments: We are grateful to the staff of the University of Edinburgh Biomedical and Veterinary Sciences for their exemplary technical assistance.

Conflicts of Interest: The authors declare no conflict of interest.

Abbreviations

AKT	Protein kinase B
αSMA	Alpha-smooth muscle actin
bEnd.3	Brain microvascular endothelial-like cell line
CAD	Coronary artery disease
CAL	Coronary artery ligation
CMC	Cardiomyocyte
CO	Cardiac output
CVD	Cardiovascular disease
EC	Endothelial cell
ECM	Extracellular matrix
EDV	End-systolic volume
EF	Ejection fraction
ESV	End-systolic volume
FB	Fibroblast
FAC	Fractional area change
FGR	Foetal growth restriction
GSK3B	Glycogen synthase kinase-3B
LAD	Left anterior descending coronary artery
lincRNA	Long intergenic non-coding RNA
lncRNAs	Long non-coding RNAs
LV	Left ventricle
MI	Myocardial infarction
MTORC1	Mammalian target of rapamycin complex 1
ncRNA	Non-coding RNA
PC	Pericyte
PI3K	Phosphorylation of phosphoinositide 3-kinase
SMC	Smooth muscle cell
SPAAR	Small regulatory polypeptide of amino acid response
STAT1	Signal transducer and activator of transcription 1
SV	Stroke volume
TTC	Triphenyltetrazolium chloride

References

1. WHO. Available online: https://www.who.int/news-room/fact-sheets/detail/cardiovascular-diseases-(cvds) (accessed on 1 June 2020).
2. Benjamin, E.J.; Virani, S.S.; Callaway, C.W.; Chamberlain, A.M.; Chang, A.R.; Cheng, S.; Chiuve, S.E.; Cushman, M.; Delling, F.N.; Deo, R.; et al. Heart Disease and Stroke Statistics-2018 Update: A Report From the American Heart Association. *Circulation* **2018**, *137*, e67–e492. [CrossRef]
3. Matsumura, Y.; Zhu, Y.; Jiang, H.; D'Amore, A.; Luketich, S.K.; Charwat, V.; Yoshizumi, T.; Sato, H.; Yang, B.; Uchibori, T.; et al. Intramyocardial injection of a fully synthetic hydrogel attenuates left ventricular remodeling post myocardial infarction. *Biomaterials* **2019**, *217*, 119289. [CrossRef]
4. Yoon, J.H.; Abdelmohsen, K.; Gorospe, M. Functional interactions among microRNAs and long noncoding RNAs. *Semin. Cell Dev. Biol.* **2014**, *34*, 9–14. [CrossRef]
5. Ballantyne, M.D.; McDonald, R.A.; Baker, A.H. lncRNA/MicroRNA interactions in the vasculature. *Clin. Pharmacol. Ther.* **2016**, *99*, 494–501. [CrossRef]

6. Boulberdaa, M.; Scott, E.; Ballantyne, M.; Garcia, R.; Descamps, B.; Angelini, G.D.; Brittan, M.; Hunter, A.; McBride, M.; McClure, J.; et al. A Role for the Long Noncoding RNA SENCR in Commitment and Function of Endothelial Cells. *Mol. Ther.* **2016**, *24*, 978–990. [CrossRef]
7. Kurian, L.; Aguirre, A.; Sancho-Martinez, I.; Benner, C.; Hishida, T.; Nguyen, T.B.; Reddy, P.; Nivet, E.; Krause, M.N.; Nelles, D.A.; et al. Identification of novel long noncoding RNAs underlying vertebrate cardiovascular development. *Circulation* **2015**, *131*, 1278–1290. [CrossRef]
8. Michalik, K.M.; You, X.; Manavski, Y.; Doddaballapur, A.; Zörnig, M.; Braun, T.; John, D.; Ponomareva, Y.; Chen, W.; Uchida, S.; et al. Long noncoding RNA MALAT1 regulates endothelial cell function and vessel growth. *Circ. Res.* **2014**, *114*, 1389–1397. [CrossRef]
9. Ounzain, S.; Burdet, F.; Ibberson, M.; Pedrazzini, T. Discovery and functional characterization of cardiovascular long noncoding RNAs. *J. Mol. Cell Cardiol.* **2015**, *89*, 17–26. [CrossRef]
10. Wang, K.; Liu, F.; Zhou, L.Y.; Long, B.; Yuan, S.M.; Wang, Y.; Liu, C.Y.; Sun, T.; Zhang, X.J.; Li, P.F. The long noncoding RNA CHRF regulates cardiac hypertrophy by targeting miR-489. *Circ. Res.* **2014**, *114*, 1377–1388. [CrossRef]
11. Matsumoto, A.; Pasut, A.; Matsumoto, M.; Yamashita, R.; Fung, J.; Monteleone, E.; Saghatelian, A.; Nakayama, K.I.; Clohessy, J.G.; Pandolfi, P.P. mTORC1 and muscle regeneration are regulated by the LINC00961-encoded SPAR polypeptide. *Nature* **2017**, *541*, 228–232. [CrossRef]
12. Di Salvo, T.G.; Guo, Y.; Su, Y.R.; Clark, T.; Brittain, E.; Absi, T.; Maltais, S.; Hemnes, A. Right ventricular long noncoding RNA expression in human heart failure. *Pulm. Circ.* **2015**, *5*, 135–161. [CrossRef]
13. Wu, C.T.; Liu, S.; Tang, M. Downregulation of linc00961 contributes to promote proliferation and inhibit apoptosis of vascular smooth muscle cell by sponging miR-367 in patients with coronary heart disease. *Eur. Rev. Med. Pharmacol. Sci.* **2019**, *23*, 8540–8550. [CrossRef]
14. Liu, S.; He, Y.; Shi, J.; Liu, L.; Ma, H.; He, L.; Guo, Y. STAT1-avtiviated LINC00961 regulates myocardial infarction by the PI3K/AKT/GSK3β signaling pathway. *J. Cell Biochem.* **2019**, *120*, 13226–13236. [CrossRef]
15. Arslan, F.; Lai, R.C.; Smeets, M.B.; Akeroyd, L.; Choo, A.; Aguor, E.N.; Timmers, L.; van Rijen, H.V.; Doevendans, P.A.; Pasterkamp, G.; et al. Mesenchymal stem cell-derived exosomes increase ATP levels, decrease oxidative stress and activate PI3K/Akt pathway to enhance myocardial viability and prevent adverse remodeling after myocardial ischemia/reperfusion injury. *Stem Cell Res.* **2013**, *10*, 301–312. [CrossRef]
16. Spencer, H.L.; Sanders, R.; Boulberdaa, M.; Meloni, M.; Cochrane, A.; Spiroski, A.M.; Mountford, J.; Emanueli, C.; Caporali, A.; Brittan, M.; et al. The LINC00961 transcript and its encoded micropeptide SPAAR regulate endothelial cell function. *Cardiovasc. Res.* **2020**, *116*, 1981–1994. [CrossRef] [PubMed]
17. Kuzan, A. Thymosin β as an Actin-binding Protein with a Variety of Functions. *Adv. Clin. Exp. Med.* **2016**, *25*, 1331–1336. [CrossRef]
18. Zhou, C.; Rao, L.; Shanahan, C.M.; Zhang, Q. Nesprin-1/2: Roles in nuclear envelope organisation, myogenesis and muscle disease. *Biochem. Soc. Trans.* **2018**, *46*, 311–320. [CrossRef] [PubMed]
19. Litviňuková, M.; Talavera-López, C.; Maatz, H.; Reichart, D.; Worth, C.L.; Lindberg, E.L.; Kanda, M.; Polanski, K.; Heinig, M.; Lee, M.; et al. Cells of the adult human heart. *Nature* **2020**. [CrossRef]
20. Goodwill, A.G.; Dick, G.M.; Kiel, A.M.; Tune, J.D. Regulation of Coronary Blood Flow. *Compr. Physiol.* **2017**, *7*, 321–382. [CrossRef]
21. Hemberger, M.; Hanna, C.W.; Dean, W. Mechanisms of early placental development in mouse and humans. *Nat. Rev. Genet.* **2020**, *21*, 27–43. [CrossRef]
22. Swanson, A.M.; David, A.L. Animal models of fetal growth restriction: Considerations for translational medicine. *Placenta* **2015**, *36*, 623–630. [CrossRef] [PubMed]
23. Giussani, D.A.; Camm, E.J.; Niu, Y.; Richter, H.G.; Blanco, C.E.; Gottschalk, R.; Blake, E.Z.; Horder, K.A.; Thakor, A.S.; Hansell, J.A.; et al. Developmental programming of cardiovascular dysfunction by prenatal hypoxia and oxidative stress. *PLoS ONE* **2012**, *7*, e31017. [CrossRef] [PubMed]
24. Kumar, P.; Morton, J.S.; Shah, A.; Do, V.; Sergi, C.; Serrano-Lomelin, J.; Davidge, S.T.; Beker, D.; Levasseur, J.; Hornberger, L.K. Intrauterine exposure to chronic hypoxia in the rat leads to progressive diastolic function and increased aortic stiffness from early postnatal developmental stages. *Physiol. Rep.* **2020**, *8*, e14327. [CrossRef] [PubMed]
25. Kane, A.D.; Herrera, E.A.; Camm, E.J.; Giussani, D.A. Vitamin C prevents intrauterine programming of in vivo cardiovascular dysfunction in the rat. *Circ. J.* **2013**, *77*, 2604–2611. [CrossRef]
26. Lindgren, I.; Altimiras, J. Prenatal hypoxia programs changes in β-adrenergic signaling and postnatal cardiac contractile dysfunction. *Am. J. Physiol. Regul. Integr. Comp. Physiol.* **2013**, *305*, R1093–R1101. [CrossRef]
27. Hauton, D.; Ousley, V. Prenatal hypoxia induces increased cardiac contractility on a background of decreased capillary density. *BMC Cardiovasc. Disord.* **2009**, *9*, 1–14. [CrossRef]
28. Niu, Y.; Kane, A.D.; Lusby, C.M.; Allison, B.J.; Chua, Y.Y.; Kaandorp, J.J.; Nevin-Dolan, R.; Ashmore, T.J.; Blackmore, H.L.; Derks, J.B.; et al. Maternal allopurinol prevents cardiac dysfunction in adult male offspring programmed by chronic hypoxia during pregnancy. *Hypertension* **2018**, *72*, 971–978. [CrossRef]
29. Pries, A.R.; Reglin, B. Coronary microcirculatory pathophysiology: Can we afford it to remain a black box? *Eur. Heart J.* **2017**, *38*, 478–488. [CrossRef]

30. Charytan, D.M.; Skali, H.; Shah, N.R.; Veeranna, V.; Cheezum, M.K.; Taqueti, V.R.; Kato, T.; Bibbo, C.R.; Hainer, J.; Dorbala, S.; et al. Coronary flow reserve is predictive of the risk of cardiovascular death regardless of chronic kidney disease stage. *Kidney Int.* **2018**, *93*, 501–509. [CrossRef]
31. Toborek, M.; Kaiser, S. Endothelial cell functions. Relationship to atherogenesis. *Basic Res. Cardiol.* **1999**, *94*, 295–314. [CrossRef]
32. Davignon, J.; Ganz, P. Role of endothelial dysfunction in atherosclerosis. *Circulation* **2004**, *109*, III27–III32. [CrossRef] [PubMed]
33. Hong, Y.K.; Harvey, N.; Noh, Y.H.; Schacht, V.; Hirakawa, S.; Detmar, M.; Oliver, G. Prox1 is a master control gene in the program specifying lymphatic endothelial cell fate. *Dev. Dyn.* **2002**, *225*, 351–357. [CrossRef] [PubMed]
34. Nakashima, Y.; Chen, Y.X.; Kinukawa, N.; Sueishi, K. Distributions of diffuse intimal thickening in human arteries: Preferential expression in atherosclerosis-prone arteries from an early age. *Virchows Arch.* **2002**, *441*, 279–288. [CrossRef] [PubMed]
35. Mohammed, S.F.; Hussain, S.; Mirzoyev, S.A.; Edwards, W.D.; Maleszewski, J.J.; Redfield, M.M. Coronary microvascular rarefaction and myocardial fibrosis in heart failure with preserved ejection fraction. *Circulation* **2015**, *131*, 550–559. [CrossRef] [PubMed]
36. Campbell, D.J. Letter by Campbell Regarding Article, "Coronary Microvascular Rarefaction and Myocardial Fibrosis in Heart Failure with Preserved Ejection Fraction". *Circulation* **2015**, *132*, e205. [CrossRef] [PubMed]
37. Xiao, Y.; Liu, Y.; Liu, J.; Kang, Y.J. The association between myocardial fibrosis and depressed capillary density in rat model of left ventricular hypertrophy. *Cardiovasc. Toxicol.* **2018**, *18*, 304–311. [CrossRef] [PubMed]
38. Kaijser, L.; Grubbström, J.; Berglund, B. Coronary circulation in acute hypoxia. *Clin. Physiol.* **1990**, *10*, 259–263. [CrossRef]
39. van Heesch, S.; Witte, F.; Schneider-Lunitz, V.; Schulz, J.F.; Adami, E.; Faber, A.B.; Kirchner, M.; Maatz, H.; Blachut, S.; Sandmann, C.-L.; et al. The Translational Landscape of the Human Heart. *Cell* **2019**, *178*, 242–260. [CrossRef]
40. Kilkenny, C.; Browne, W.; Cuthill, I.C.; Emerson, M.; Altman, D.G. Animal research: Reporting in vivo experiments: The ARRIVE guidelines. *Br. J. Pharmacol.* **2010**, *160*, 1577–1579. [CrossRef]
41. Pell, V.R.; Spiroski, A.M.; Mulvey, J.; Burger, N.; Costa, A.S.H.; Logan, A.; Gruszczyk, A.V.; Rosa, T.; James, A.M.; Frezza, C.; et al. Ischemic preconditioning protects against cardiac ischemia reperfusion injury without affecting succinate accumulation or oxidation. *J. Mol. Cell Cardiol.* **2018**, *123*, 88–91. [CrossRef]
42. Chouchani, E.T.; Pell, V.R.; Gaude, E.; Aksentijević, D.; Sundier, S.Y.; Robb, E.L.; Logan, A.; Nadtochiy, S.M.; Ord, E.N.J.; Smith, A.C.; et al. Ischaemic accumulation of succinate controls reperfusion injury through mitochondrial ROS. *Nature* **2014**, *515*, 431–435. [CrossRef] [PubMed]

4.4 Additional results

4.4.1 Expression and manipulation of the murine LINC00961 locus

LINC00961 expression was quantified in 4 mouse EC lines by qPCR to find a suitable cell line for further experimentation. The cell lines investigated were:

- bEND3 – murine brain microvascular endothelial-like cells, kindly donated by Dr. Andrea Caporali (University of Edinburgh).
- IP1B – purchased from ATCC (USA) and originally isolated from ascites tumours from axillary lymph node tissue.
- SVEC-4-10 – purchased from ATCC (USA) and originally isolated from ascites tumours from axillary lymph node tissue.
- MCEC – Immortalised murine microvascular cardiac endothelial cells, kindly donated by Dr. Marco Meloni.

The bEND3 ECs were the only cell line found to express LINC00961 at a level suitable for taking forward into cell fractionation and LINC00961 depletion experiments with the highest expression (Ct value of 25). The Ct values of IP1B, SVEC4-10, and MCEC were 32.4, 32.7, and 30.5, respectively. This data in Figure 4.1A is represented as 1/ delta Ct value of LINC00961 compared to the housekeeping gene Glyceraldehyde 3-phosphate dehydrogenase (GAPDH). Fractionation of bEND3 cells determined that the LINC00961 transcript was present, in basal conditions, predominantly in the cytoplasm (62% cytoplasmic compared to 38% nuclear (Figure 4.1B). The lncRNAs NEAT1 and MALAT1 served as nuclear controls [172].

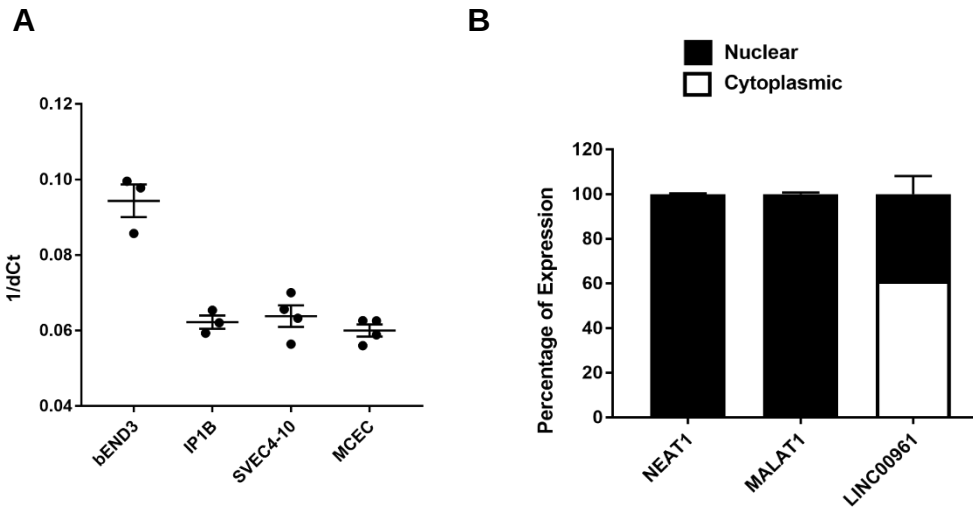

Figure 4.1 LINC00961 expression and transcript location in murine endothelial-like cells.

A) LINC00961 levels in bEND3, IP1B, SVEC4-10, and MCEC murine endothelial-like cell lines, assessed by qRT-PCR. Data represented as 1/dCT of LINC00961 compared to GAPDH. N=3, for bEND3 and IP1B, N=4 for SVEC4-10 and MCEC. B) Nuclear to cytoplasmic split (38% : 62%) of LINC00961 in the bEND3 cells with nuclear controls NEAT1 and MALAT1, N=6.

4.4.2 Depletion of murine LINC00961 in endothelial cells

Dicer substrate mediated degradation of target mRNA is achieved via the use of siRNA that is complementary to and binds to a target transcript, leading to its degradation predominantly in the cytoplasm. Two siRNAs against murine LINC00961 (denoted siRNA1 and siRNA2; siRNA sequences in Table 2.3) were tested at doses of 7.5, 10, and 15 nM. LINC00961 expression was analysed at 24 and 48 h post transfection. At all doses, siRNA2 was effective at depleting LINC00961 expression at both time points, whereas siRNA1 failed to deplete LICN00961 expression to a level which was statistically significant (Figures 4.2A for and 4.3A, respectively). At the highest dose of 15 nM siRNA transfection, tubule formation on Matrigel©, a commonly used assay to determine angiogenic potential [305], was significantly inhibited at 24 h. Lower doses did not result in alterations to tubule formation (Figure 4.2B). Despite the maintenance of LINC00961 depletion at 48 hrs post transfection, there appeared to be no difference in tubule formation, at any dose, at this time point (Figure 4.3B). For each biological replicate, 3 separate wells were quantified and branch length averaged.

A **B**

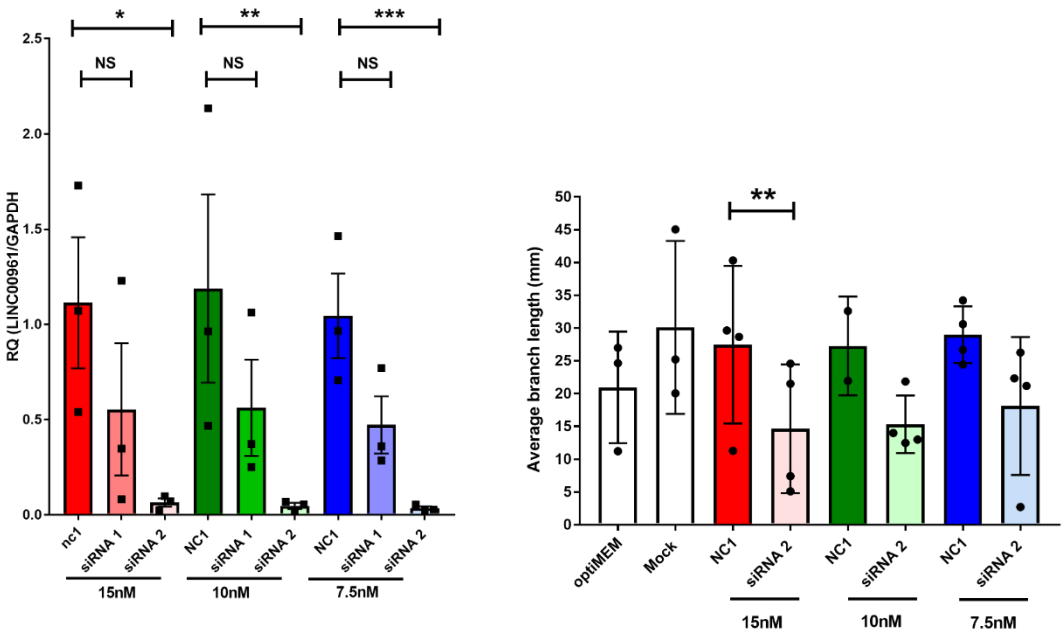

C

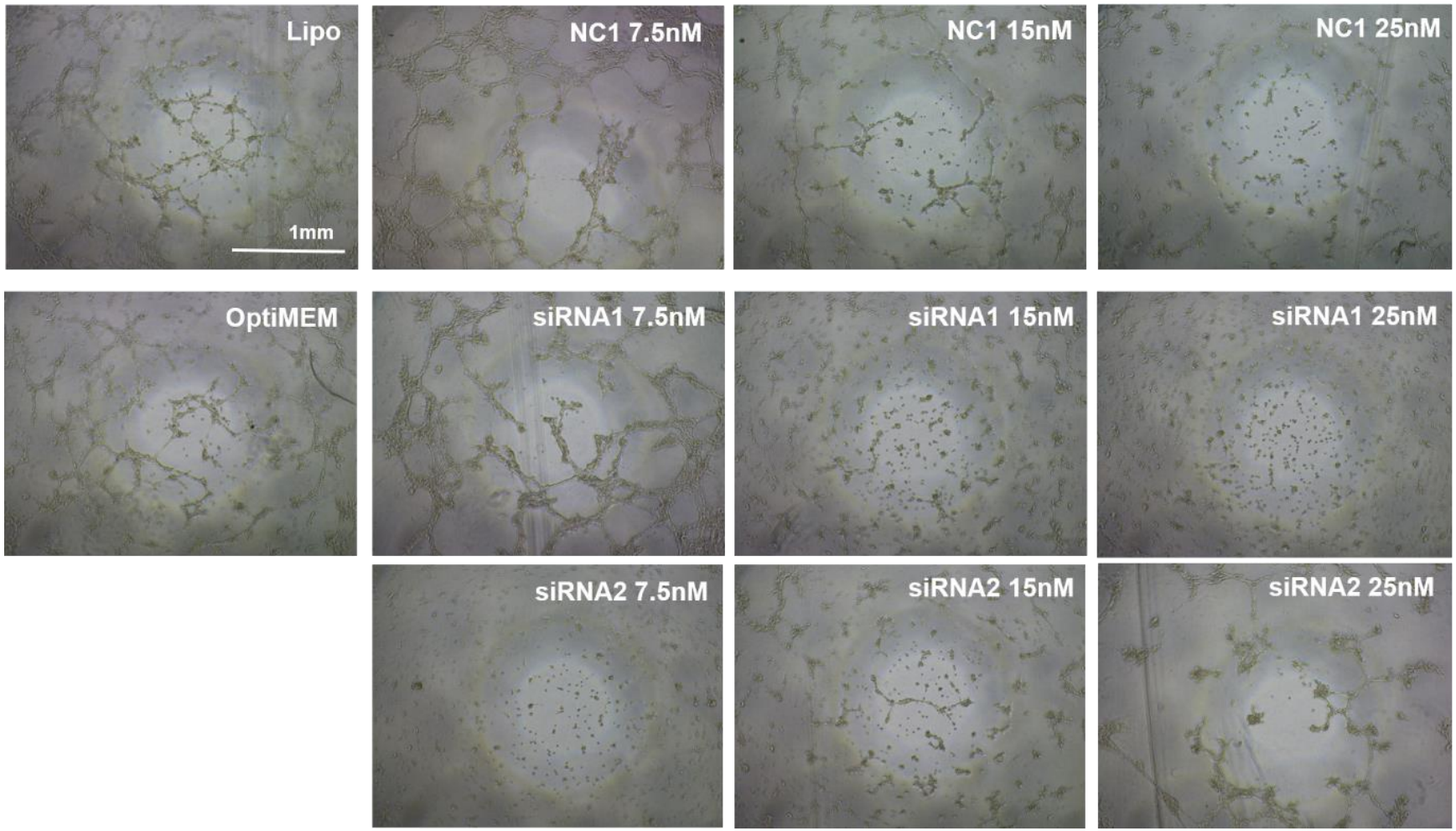
Lipo
1mm
NC1 7.5nM
NC1 15nM
NC1 25nM
OptiMEM
siRNA1 7.5nM
siRNA1 15nM
siRNA1 25nM
siRNA2 7.5nM
siRNA2 15nM
siRNA2 25nM

Figure 4.2 The effect of siRNA mediated depletion of murine LINC00961 after 24 hours on tubule formation.

High (15nM), medium (10nM), and low (7.5nM) doses of 2 siRNA sequences were transfected into bEND3 cells. A) qRT-PCR confirmed significant depletion of LINC00961 with siRNA2 but not siRNA1, at all concentrations tested. N=3 for all conditions, a one-way ANOVA was carried out, on the graphs NS= not significant, * $p<0.05$, ** $p<0.01$, and *** $p<0.001$. B) Total branch length quantification of Matrigel© assay using ImageJ angiogenesis analyser. The high dose of siRNA2 significantly inhibited tubule formation. N=2 – 4, One-way ANOVA was performed between negative control and siRNA for each concentration. C) Representative brightfield images of tubule formation on Matrigel©. Scale bar = 1mm. Lipo = Lipofectamine/mock conditio

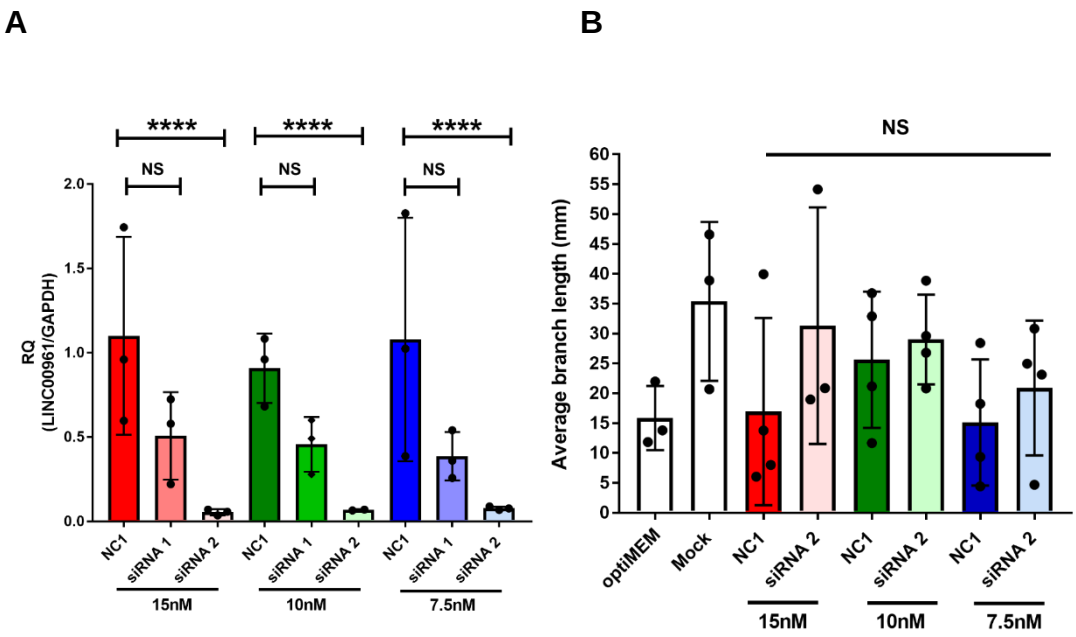
A
B
****
****
****
NS
NS
NS
RQ
(LINC00961/GAPDH)
2.0
1.5
1.0
0.5
0.0
NC1
siRNA 1
siRNA 2
15nM
10nM
7.5nM
NS
Average branch length (mm)
60
55
50
45
40
35
30
25
20
15
10
5
0
optiMEM
Mock
NC1
siRNA 2
NC1
siRNA 2
NC1
siRNA 2
15nM
10nM
7.5nM

C

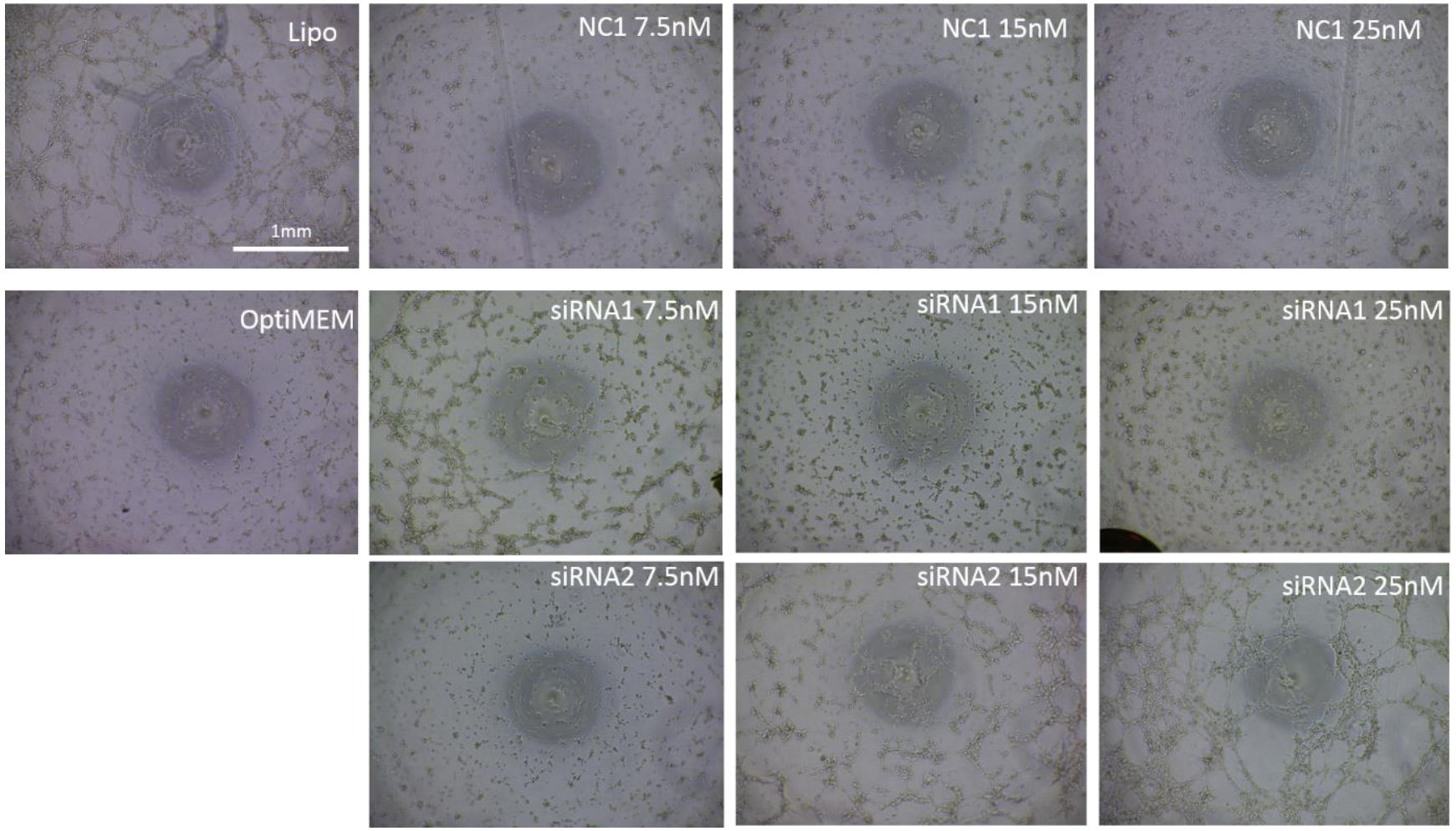
Lipo
1mm
NC1 7.5nM
NC1 15nM
NC1 25nM
OptiMEM
siRNA1 7.5nM
siRNA1 15nM
siRNA1 25nM
siRNA2 7.5nM
siRNA2 15nM
siRNA2 25nM

Figure 4.3 The effect of siRNA mediated depletion of murine LINC00961 after 48 hours on tubule formation.

High (15nM), medium (10nM), and low (7.5nM) doses of 2 siRNA sequences were transfected into bEND3 cells. A) qRT-PCR confirmed significant depletion of LINC00961 with siRNA2 but not siRNA1, at all concentrations tested. N=3 for all conditions, a one-way ANOVA was carried out, on the graphs NS= not significant and **** $p<0.0001$. B) Quantification of total branch length in a Matrigel© assay using ImageJ angiogenesis analyser. No significant differences in branch length were seen for any dose of either siRNA. N=2 – 4, One-way ANOVA was performed between each negative control and siRNA for each concentration. C) Representative brightfield images of tubule formation on Matrigel©. Scale bar = 1mm. Lipo = Lipofectamine/mock condition.

4.4.3 Publicly available expression data for LINC00961

Expression data for LINC00961, previously identified as 5430416O09Rik, in murine tissues is publicly available via Expression Atlas and reports high LINC00961 transcript levels in the heart, lungs, kidneys, testis, muscle and brain. (https://www.ebi.ac.uk/gxa/genes/ensmusg00000028475?bs=%7B%22mus%20musculus%22%3A%5B%22ORGANISM_PART%22%5D%7D&ds=%7B%22kingdom%22%3A%5B%22animals%22%5D%7D#baseline). Moreira & colleagues (2019) investigated the dynamic changes in transcription across several organs in multiple species, including human and mouse, from embryonic development into adulthood and their publicly available data sets show that murine LINC00961 expression can first be seen at embryonic day (E) 12.5 and reaches a constant level of expression shortly after birth (Figure 4.4A) [306]. Although cell type specificity is unknown, expression from an early time point and sustained postnatal whole tissue expression suggests LINC00961 has important functional roles during development and beyond. Matsumoto & colleagues (2017) compared mouse and human expression profiles, which similarly showed high LINC00961 expression in the lung, heart, and skeletal muscle (Figure 4.4 B & C) [232]. Despite this data, the role of this locus within foetal development or adulthood is largely unknown.

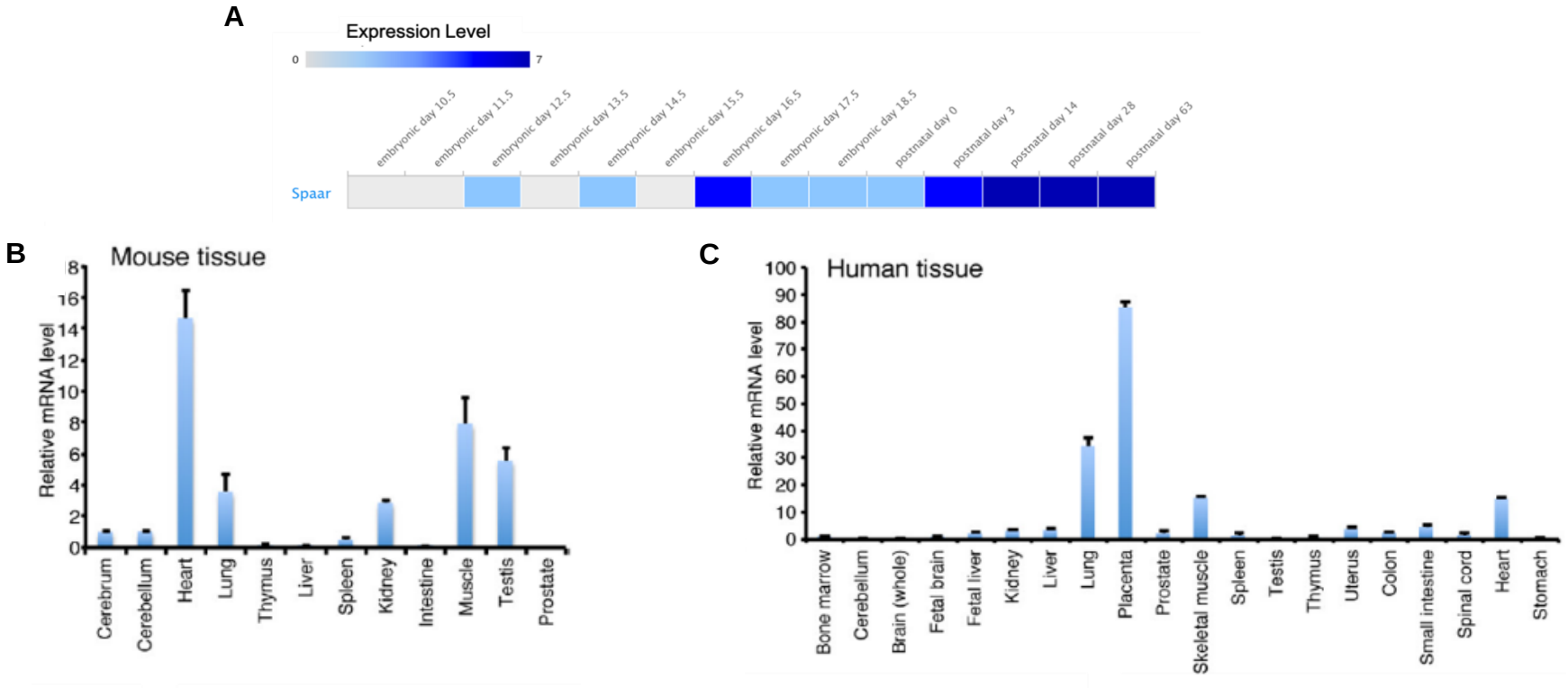

Figure 4.4 LINC00961 expression profile in murine and human tissues.

A) LINC00961 expression levels in embryonic murine tissue (Image adapted from the online expression atlas (ebi.ac.uk) and original data from Moreira *et al* 2019. [306] B) LINC00961 expression levels in adult murine tissue, relative to cerebrum levels. C) Human tissues showing their relative LINC00961 expression, relative to bone marrow levels. B and C Adapted from Matsumoto *et al* (2017) [232].

4.4.4 LINC00961$^{-/-}$ offspring are viable

LINC00961 heterozygous mice produced offspring of all possible genotypes in the expected mendelian ratios of 1:2 heterozygotes, 1:4 WT, and 1:4 KO (284, 167, & 146 respectively), with no gender bias within KO mice (78 males: 68 females), which was determined by Chi squared (X^2) analysis (Tables 4.1 & 4.2, and Figure 4.5).

$$\chi^2 = \sum \frac{(O-E)^2}{E}$$

	Observed (O)	Expected (E)	O-E	$(O-E)^2$	$(O-E)^2/E$
KO	146	149.25	-3.25	10.5625	0.07077
WT	167	149.25	17.75	315.063	2.11097
Het	284	298.5	-14.5	210.25	0.70436
Total	597				**2.8861**

Table 4.1 Chi squared calculation table for distribution of genotypes.

X^2 calculation shown above with tabular results. X^2 Value in bold (2.8861) is less than the critical value of 5.99 for 2 degrees of freedom (number of experimental groups – 1), therefore a null hypothesis is accepted: Distribution of genotypes follows a Mendelian pattern of inheritance. See appendices for X^2 table critical values and P values.

	Observed (O)	Expected (E)	O-E	$(O-E)^2$	$(O-E)^2/E$
Male	78	73	5	25	0.34247
Female	68	73	-5	25	0.34247
Total	146				**0.68493**

Table 4.2 Chi squared calculation table for distribution of gender amongst LINC00961$^{-/-}$ mice.

X^2 Value in bold (0.68493) is less than the critical value of 3.84 for 1 degree of freedom (number of experimental groups – 1), therefore a null hypothesis is accepted: Distribution of gender within KO mice follows a Mendelian pattern of inheritance. See appendices for X^2 table critical values and P values.

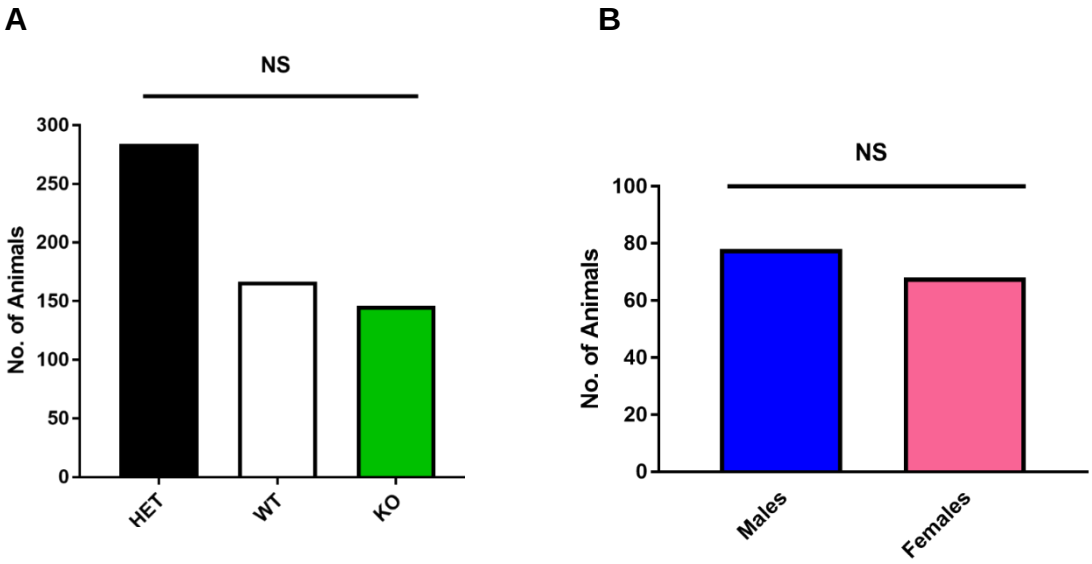

Figure 4.5 Chi squared analysis of genotypes in the LINC00961$^{-/-}$ line.

A) Graphical representation of the analysis of genotype distribution. N= 284 heterozygous, 167 WT, & 146 KO mice. Data from Table 4.1. B) Graphical representation of the analysis of gender distribution. N= 78 male and 68 female KO mice. Data from Table 4.2.

4.4.5 Male LINC00961$^{-/-}$ exhibit signs of foetal growth restriction

Male, but not female, LINC00961$^{-/-}$ mice were identified as significantly lighter during the time frame measured (Figures 4.6A and B respectively). They were also shorter than their WT littermates at 9 weeks of age (82.3 mm +/- 1.1 for KO compared to 79.02 mm +/- 0.8 for WT) with an increased brain weight to body ratio (18.5 +/- 0.5 for KO compared to 16.8 +/- 0.4 for WT) (data in Table 1 in the above manuscript). In contrast to LINC00961$^{-/-}$ mice, Matsumoto & colleagues generated a SPAAR$^{-/-}$ mouse line with deletion of the SPAAR ATG start sites within exon 2 of the LINC00961 transcript in order to maintain the expression of the host lncRNA and abolish SPAAR expression only. They show that at 8 weeks of age, there is no difference in weight between KO and WT mice of either gender (Figure 4.6C).

Additional parameters tested in LINC00961$^{-/-}$ which did not show any significant difference between genotypes included: head length, biparietal diameter, tibia length, and tibia length/weight ratio. Other organs weighed included: pancreas, liver, heart, lungs, soleus muscle, adductor muscle, spleen, kidneys, and thymus (refer to Table 1 in the above manuscript.

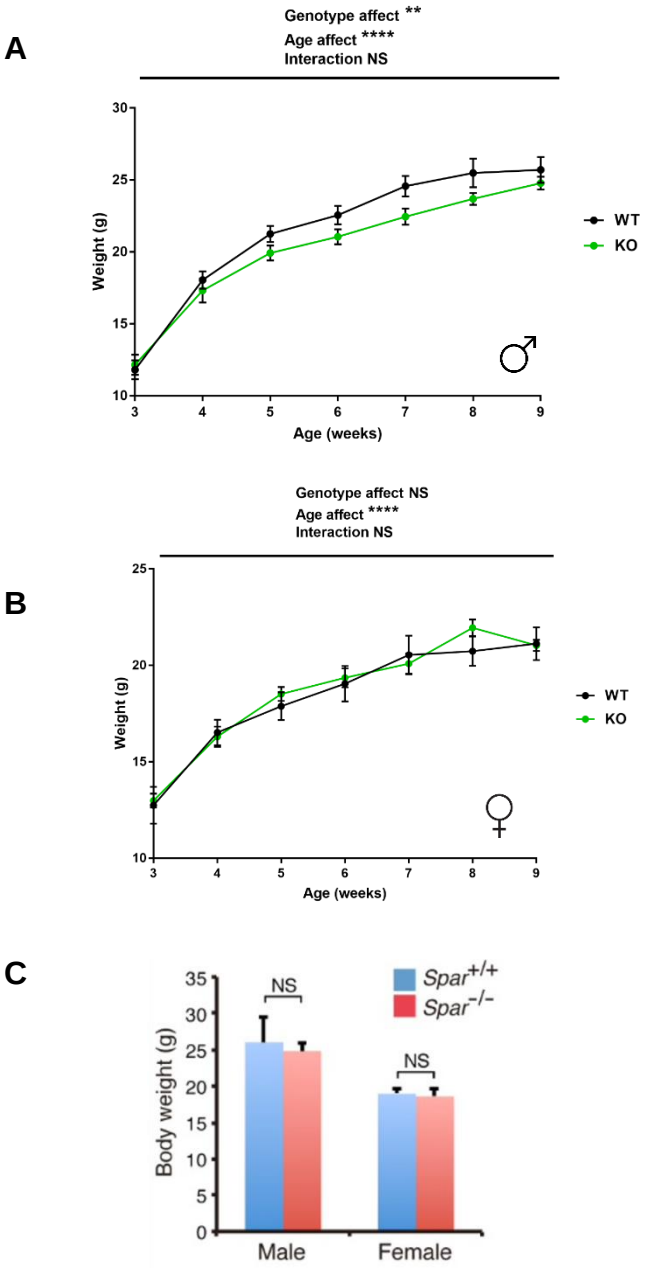

Figure 4.6 Comparison of LINC00961$^{-/-}$, wildtype, and SPAAR$^{-/-}$ growth.

(A) Weekly weights of males from weaning at 3 weeks of age, to 9 weeks of age N= 2-12 WT/ 8-13 KO (B) Weekly weights of females from weaning to 9 weeks of age N= 6-11 WT/ 2-7 KO. Statistical test used was a 2-way ANOVA. Data in A and B is the same as that in Figure 2 of the above manuscript. C) Data from Matsumoto & colleagues (2017) showed no difference in weight at 8 weeks of age between SPAAR$^{-/-}$ and WT controls [232]. On the graphs NS= not significant, ** p<0.01, **** p<0.0001. Error bars are mean +/- SEM.

4.4.6 Female LINC00961$^{-/-}$ mice do not differ in weight at 6 months of age

Female mice at 6 months of age (24 - 26 weeks) were used to investigate any differences in mouse weight and fat depot weight, with no significant differences found in either at this aged time point (Figure 4.7A, P = 0.1521). Fat depots and organs collected include brown adipose tissue (BAT), inguinal white adipose tissue (iWAT), gonadal WAT (gWAT), perirenal WAT (pWAT), mesenteric WAT (mWAT), pericardial fat, thymus, and pancreas (Figure 4.7B).

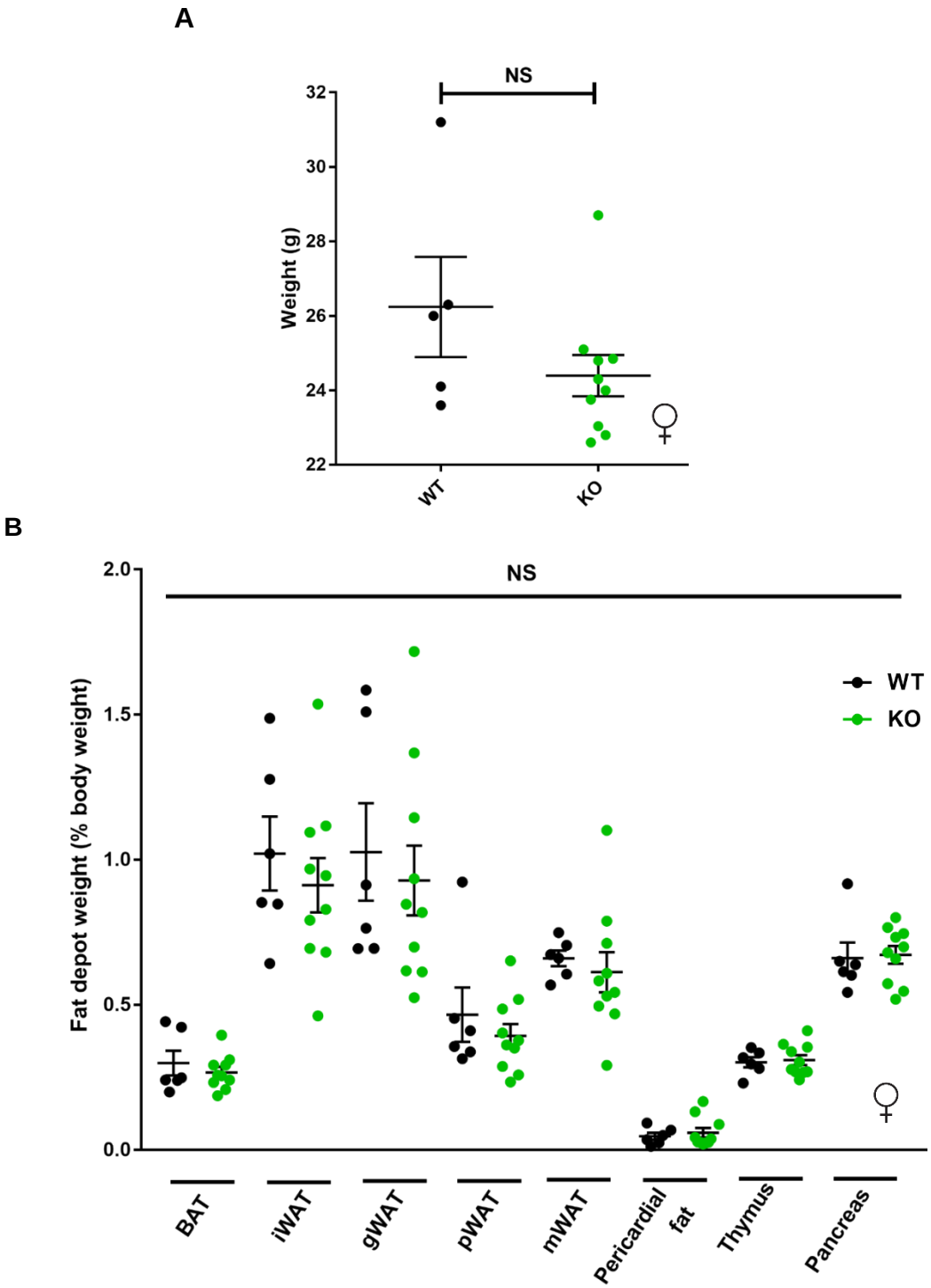

Figure 4.7 Comparison of body weights and fat depots between female wildtype and LINC00961$^{-/-}$ at 6 months of age.

(A) N= 5WT/10KO, mice were 24-26 weeks of age at weighing. Students' t-test, (B) individual fat depots as well as the thymus and pancreas. N=5WT/10KO, Students' t-test was used. On the graph NS= not significant.

4.5 Preliminary data regarding the loss of LINC00961 on the heart following myocardial infarction

We utilised cardiac ultrasound imaging as a non-invasive tool to assess heart function which could be repeated on the same mice at different time points, in this instance; at baseline, 7 days, and 14 days post MI. The baseline heart dynamics/function of 8 week old female WT and LINC00961$^{-/-}$ offspring were assessed and found to not be significantly altered (Figure 3 in the above manuscript) confirming that these animals could be used for MI experiments. These baseline measurements included stroke volume, the amount of blood (μl) ejected from the left ventricle with every beat; ejection fraction, the percentage of blood ejected from the left ventricle compared to the total volume of blood it holds when filled during diastole; fractional shortening, the % size change of the left ventricle from diastole to systole; and cardiac output, the μl of blood pumped through the heart per minute, calculated by multiplying the stroke volume by the heart rate. Also measurable by ultrasound was the area of left ventricle muscle in systole and diastole, and the end systolic and diastolic volumes. Based on these results we concluded that we could go ahead with MI experiments. MI's were carried out on the same animals whose data are reported in the above mentioned Figures at 10 weeks of age, and the same functional measurements were taken by cardiac ultrasound at 7 days post MI. Figure 5 in the above manuscript shows that there was so significant difference in any parameter measured between KO and WT animals, however, in the manuscript we discuss the implications of MI on the heart at later times points as Evan's blue staining on hearts 30 min after MI demonstrated a clear increased in % risk area of the heart in KO animals. Below, we show some data collected on these same animals at 14 days post MI.

4.5.1 Functional dynamics of the heart assessed by cardiac ultrasound

During surgery animals were carefully monitored by Dr. Ana-Mishel Spiroski who performed the procedures. This monitoring included tracking of the animal's temperature, heart rate in beats per minute (BPM), and their respiration rate recorded as beat rhythm per minute (BrPM). This data is summarised in Figure 4.8 and there was no significant difference in these measurements between WT and KO mice. Animals recovered from the procedure and were monitored daily for 14 days. On day 14 animals had a final cardiac ultrasound. Unfortunately, due to issues with anaesthesia, a number of animals died during surgery which accounts for the large

difference in data points in Figure 4.8 (N=18 WT/20 KO) and Figure 4.9 (N=5 WT/6 KO). Figure 4.9 shows that there were no significant differences in stroke volume, ejection fraction, fractional shortening or cardiac output between WT and KO mice at 14 days post MI.

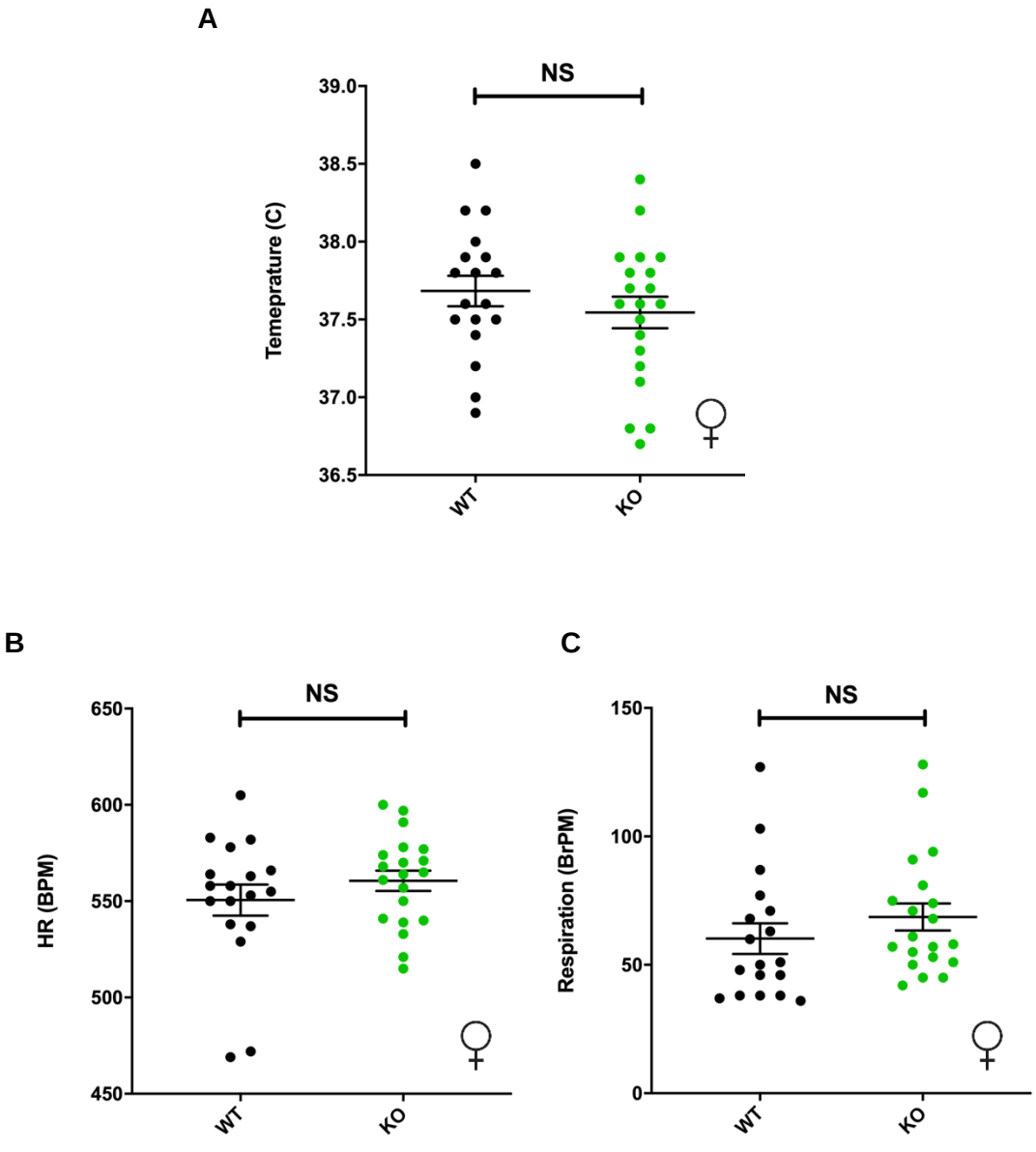

Figure 4.8 LINC00961$^{-/-}$ physical characteristics under anaesthesia at time of baseline ultrasound acquisition.

(A) core temperature (B) heart rate (C) respiration rate in beat rhythm per minute (BrPM). N=18WT/20KO, Students' t-test was used. On the graph NS= not significant.

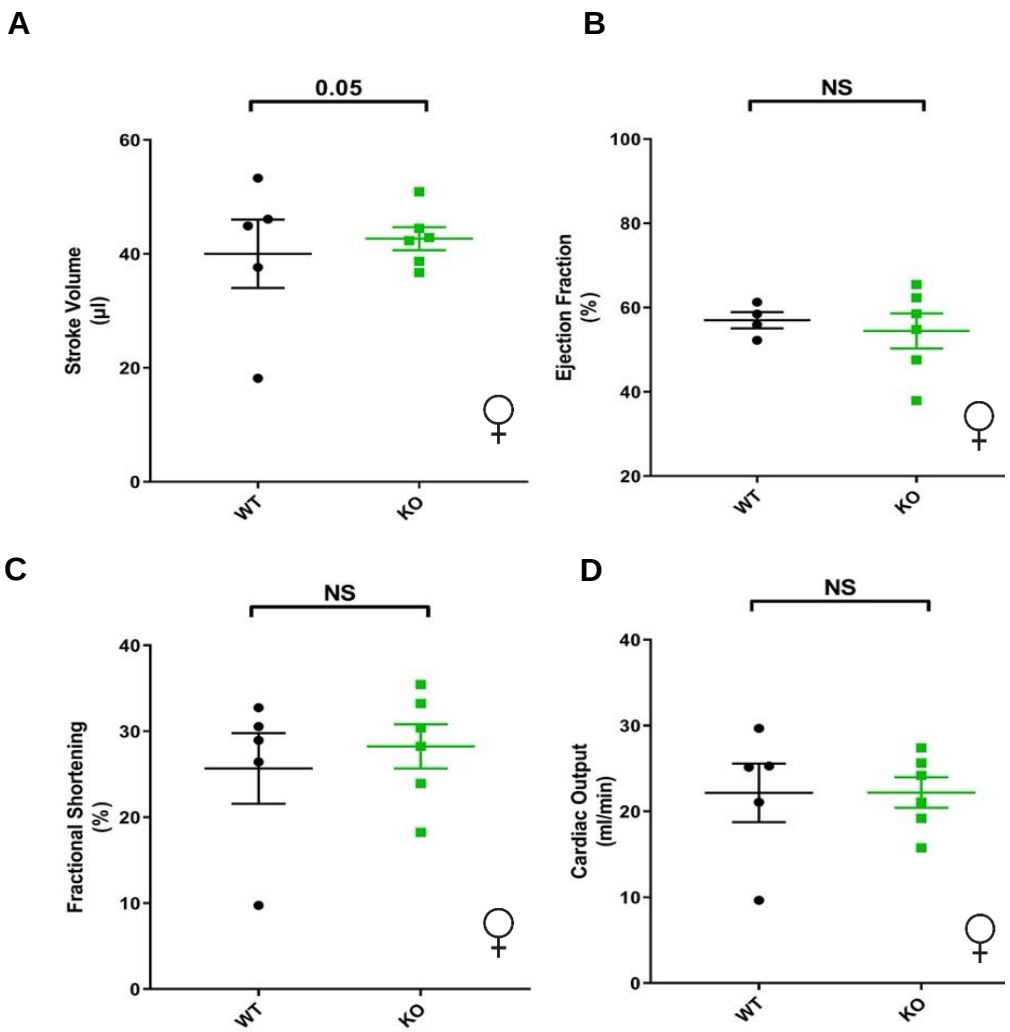

Figure 4.9 Functional output of the LINC00961$^{-/-}$ heart 14 days after myocardial infarction.

Functional output measurements of the heart muscle include stroke volume (A), ejection fraction (B), fractional shortening (C), and cardiac output (D). N=5WT, N=6KO, errors bars are mean +/- SEM, Students' t-test used. On the graph NS = not significant.

4.5.2 Histological analysis of LINC00961$^{-/-}$ hearts following myocardial infarction

Our initial plans to analyse the outcome of the MI experiments were to quantify the size of the infarcts by staining hearts with Masson's Trichrome which is commonly utilised to visualise pathologies such as an infarct as it stains fibrous collagen a blue colour [307]. Below are some representative examples of this incomplete work. Figure 4.10 shows representative images of a WT and KO mid-section of heart with the collagenous fibrotic infarct clearly visible in both as a blue colour with a thin left ventricle wall, particularly visible in the WT heart (Figure 4.10A). Graphical quantification of the infarct size is shown in Figure 4.10C, however, lacks any statistical analysis due to the small N numbers of hearts where we were able to isolate the correct sections for infarct analysis.

Similar to capillary quantification carried out in the HLI experiments in Chapter 3, immunohistochemistry was used to stain isolectin b4 (injected via tail vein prior to cull) and α-SMA. Ideally, we wanted to analyse and compare vessel densities at 3 points of interest: within the infarct, the border region, and the peri-infarct healthy tissue. Figure 4.11A is a representative image of a WT heart section in a 3 colour immunohistochemical stain (isolectin B4 in green, α-SMA in red, and DAPI in blue). For each heart section 2 areas of equal size were taken from the border region of the infarct and 2 from the remote areas of healthy tissue. These areas were used to analyse the number of capillaries present which is quantified in Figure 4.11B and C for the border and remote regions, respectively.

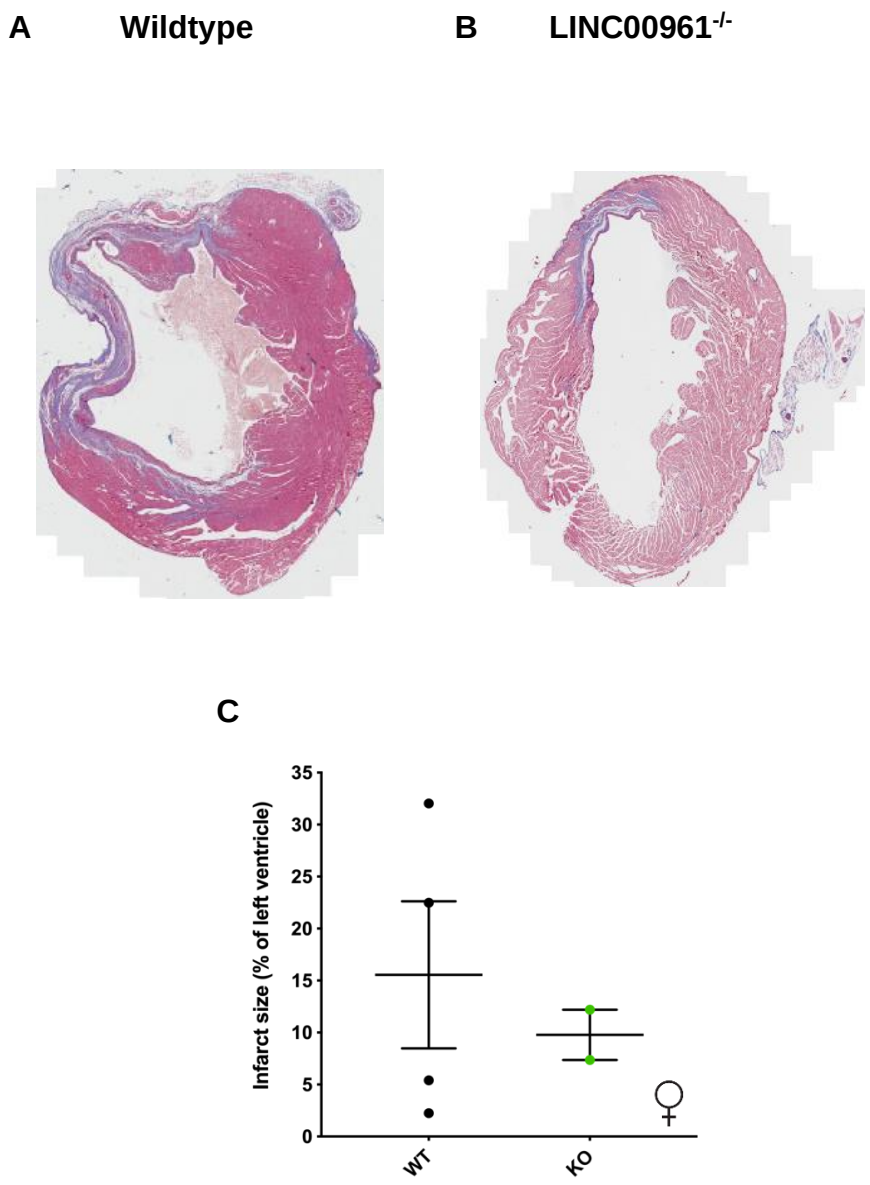

Figure 4.10 Infarct size measurements with Mason's Trichrome.

Representative wildtype (A) and KO (B) left ventricle heart sections stains with Mason's Trichrome showing the infarcted area in blue and healthy heart tissue in red. C) graphical representation of infarct size represented as % of total volume of the left ventricle (within the section). Images taken at 20x objective. N= 4WT, N=2KO, error bars are mean +/- SEM.

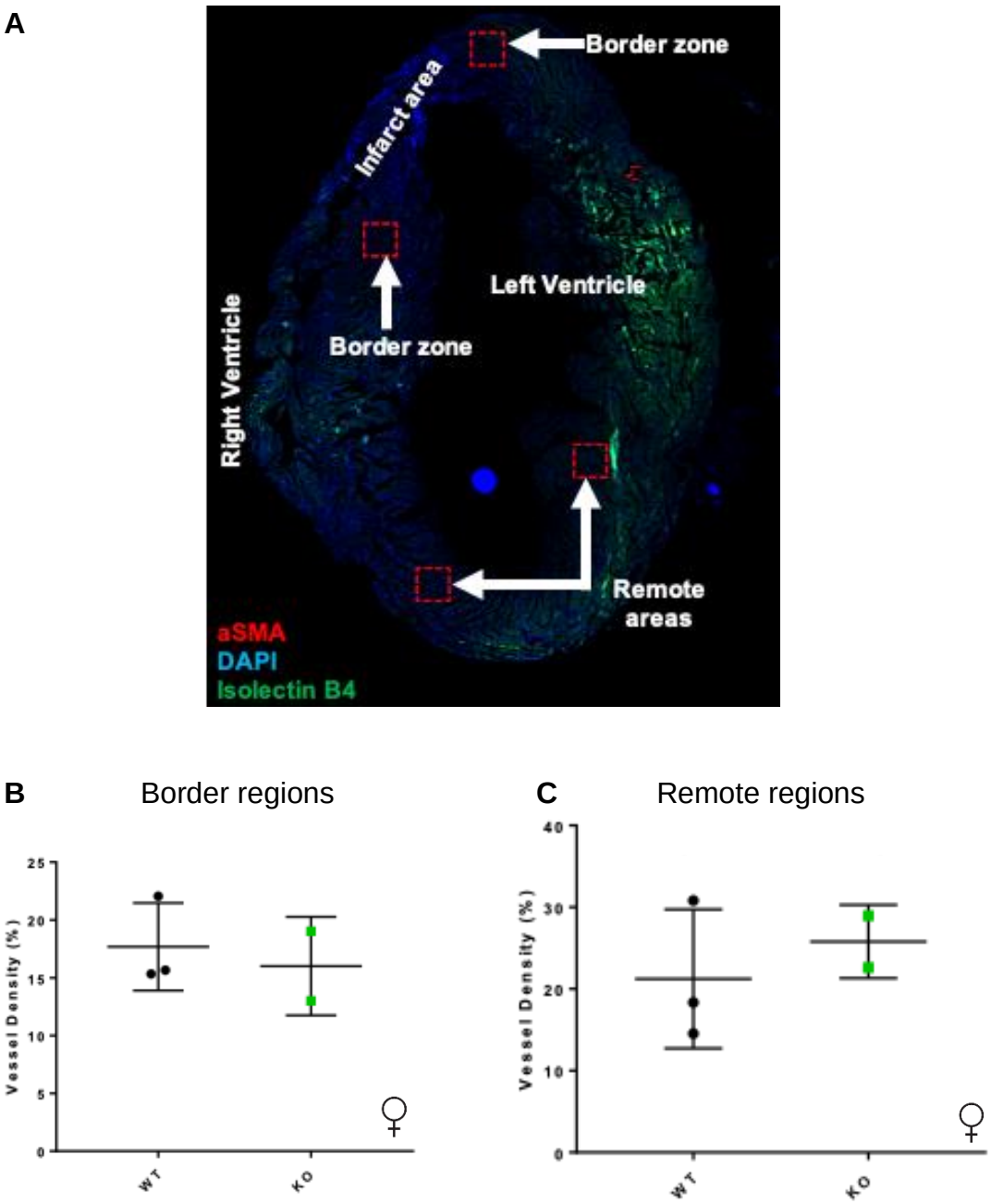

Figure 4.11 Immunohistochemical analysis of the border and remote zones of MI hearts following myocardial infarction.

A) Representative image of a wildtype heart section at 14 days after myocardial infarction. For each heart section 2 areas of equal size were taken from the border region of the infarct and 2 from the remote areas of healthy tissue. These areas were used to analyse the number of capillaries present which is represented in B and C for the border and remote regions. Images taken at 40X objective, 3 sections 50 μm apart were analysed. N=3WT, N=2KO, error bars are mean +/- SEM.

4.6 Conclusions of further experimental work in this Chapter

- LINC00961 is highly expressed in the murine bEND3 cell line.
- In the bEND3 cell line, the LINC00961 transcript is located in both the nucleus and cytoplasm, 38%: 62% respectively.
- LINC00961$^{-/-}$ offspring are viable and appear at the expected 1:4 mendelian ratio.
- Male LINC00961$^{-/-}$ offspring are statistically lighter in weigh, and shorter than their female counterparts.
- Bosy weight and weigh of fat depots do not differ between female wildtype and LINC00961$^{-/-}$ animals at 6 months of age.

4.7 Discussion

This Chapter summarises data demonstrating *in vitro* and *in vivo* evidence of the murine LINC00961 locus' role in EC, identified a novel role for this locus in development and provides the first *in vivo* evidence that this locus may have important implications in regard to MI and cardiovascular health. This Chapter includes peer reviewed published data, additional data regarding murine locus manipulation, and data from preliminary MI experiments which although unfinished show early indications of a role for this locus in MI pathophysiology for future investigation.

4.7.1 Expression and manipulation of the murine LINC00961 locus

Analysis by qRT-PCR showed that of the murine endothelial-like cell lines tested, bEND3 cells expressed LINC00961 at a sufficient level to determine is localisation within the cell and carry out transcript depletion experiments. Fractionation data showed that LINC00961 was 61% cytoplasmic and 38% nuclear (Figure 4.4B) in comparison to HUVECs where this ratio was 40% cytoplasmic and 60% nuclear [254]. These data show that in both human and mouse this transcipt is found almost equally in both compartments. Guo & colleagues (2020) recently established that several lncRNAs which had either sequence conservation, or genomic position conservation between human and mouse, demonstrated remarkable differences in cellular localisation [164]. This is interesting as the localisation of lncRNAs has been linked to their function [154, 155, 164]. LncRNAs are often reported to accumulate in the nucleus indicating roles in gene expression and chromatin organisation [156]. Cytoplasmic lncRNAs contribute to mRNA turnover, stability and translation, protein stability, and sponging of cytosolic molecules [157] [158]. Presence in both compartments could indicate multiple cellular functions.

Realistically, validation of siRNA KD in the mouse endothelial-like cells is incomplete as we only had 1 siRNA which sucessfully depleted the LINC00961 transcript. More assays which look at other endothelial behaviours also should be assessed to fully understand the similarity in role of this locus across species, such as adhesion, migration, and barrier function which were assessed in the HUVECs with LINC00961 KD in the publication in Chapter 3. GapmeR experiments may have been good to carry out in parallel to ensure we achieved KD of the transcripts in the nucleus and to confirm the siRNA KD phenotype. However, we have now established that

LINC00961 locus loss does impact EC behaviour *in vivo*, at least in angiogenesis during HLI recovery.

4.7.2 LINC00961$^{-/-}$ viability and potential infertility

The strong phenotypic effects seen in ECs *in vitro* when LINC00961 is KD gave some cause for concern as to whether LINC00961$^{-/-}$ offspring would be viable if their ECs failed to support a functional vascular system. Despite these concerns' offspring were observed in the expected ratios compared with WT and heterozygous littermates. The data summarised in this Chapter not only shows their viability but through monitoring the offspring from weaning to 9 weeks of age has highlighted the characteristic differences between male and female LINC00961$^{-/-}$ mice and has uncovered a role for LINC00961 in development.

An incidence of mis-genotyped breeders (LINC00961$^{-/-}$) was erroneously set up which yielded no offspring, indicating the KO may not be fecund. However, this may be circumstantial and to determine whether KO mice are fertile, a detailed investigation of their reproductive organs would be required. Several more KO breeders could be set up and allowed chance to breed. A limitation of this approach is the possibility that only one gender of KO mice could be infertile, therefore, a mismatch of genotype breeding pairs could be set up to determine a problem with reproduction in either gender (male KO with a heterozygous female, and vice versa). LINC00961 is highly expressed in the murine testis [232] (refer to Figure 5.1B), however, its role within the testis is unknown. The testes have high lncRNA expression and interestingly, one study identified that ~ 2/3 of all lincRNA were found to be testis specific [308]. One example is the testes associated oncogenic lncRNA THOR which was found to cause defects in zebrafish fertility when genetically deleted [309]. Relevant to mammals; deletion of murine testis-specific long non-coding RNA 1 (Tslrn1) reduced the number of sperm produced [310]; testis specific X-linked (Tsx) deletion caused apoptosis in spermatocytes [311]; and Dmrt1 related gene (Dmr) was found to be required for spermatogonia differentiation [312], validating the role for lncRNAs in male reproduction and highlighting the question of whether LINC00961 could play a role in fertility.

Wu & colleagues identified MiR-223-3p as a direct target of LINC00961 sponging in colon cancer cells and therefore identify LINC00961 as an anti-oncogenic lncRNA as

this miR sponging increased SOX11 expression inhibiting colon cancer migration and invasion [244]. Interestingly, miR-223-3p was also shown to be pro-tumorigenic in the context of testicular germ cell tumours by inhibiting cell apoptosis [313]. As LINC00961 is highly expressed in the testis, it is likely to also sponge miR223-3p in this context, highlighting the possibility for an important anti-tumour effect of LINC00961 in the testis, however, this requires further investigation. In contrast, there is little data currently available regarding LINC00961 expression in the female reproductive system, except for its presence in the human uterus [314] (refer to Figure 5.1C). The study by Wu & colleagues offers a potential interesting role for LINC00961 as the LINC00961 - MiR233-3p - SOX11 axis as they suggest it could also operate in the ovary, as SOX11 upregulation has been reported to be anti-tumorigenic by inhibiting ovarian cancer invasion and proliferation [315]. Unsurprisingly, several other lncRNAs have been identified with functions within the female reproductive organs, for example; loss of lncRNA EphrinB2 associated transcript 1 (Leat1) decreases fertility by reducing expression of its neighbouring gene Ephrin B2 in the developing female genitals in utero [316], and the lncRNA H19 has been shown to be over expressed in endometriosis where it sponges miR let-7, preventing the miR dependent reduction in insulin-like growth factor 1 receptor, increasing endometrial cellular proliferation, thereby affecting the health of the endometrium and subsequently fertility [317]. H19 also has a role in controlling placental growth [318], and high H19 expression has been implicated in cisplatin-resistant ovarian cancer cells as its depletion rescued the cell death response to cisplatin by causing KD of several proteins involved in glutathione metabolism. Interestingly, the same study found LINC00961 was also significantly highly expressed in this drug resistant cancer cell line, although the mechanism behind this and its significance in the cancer were not investigated [233]. To conclude whether LINC00961 has a role in reproduction, and reproductive organ cancers, further investigations are required such as histological analysis with macro and microscopic evaluation of the reproductive organs and further molecular investigation of LINC00961 in cancerous tissues and cell lines.

4.7.3 Comparison of SPAAR$^{-/-}$ and LINC00961$^{-/-}$ strains

Matsumoto & colleagues generated a SPAAR$^{-/-}$ mouse line which differs to the LINC00961$^{-/-}$ used here: It harbours ATG deletions for the SPAAR translational start sites, whilst maintaining expression of the LINC00961 host transcript. Interestingly, they show no difference in KO and WT weights at 8 weeks of age in either gender. Although they only provide animal weight for one time point, this differs to the results we see in the LINC00961$^{-/-}$ line, providing further evidence that SPAAR and LINC00961 have independent functions, although a more thorough characterisation of the SPAAR$^{-/-}$ mouse for comparison between lines would be interesting.

4.7.4 Male LINC00961$^{-/-}$ exhibit signs of potential foetal growth restriction

Male LINC00961$^{-/-}$ juveniles showed differences in body weight, body length, and brain weight, revealing that LINC00961 deletion has somehow affected their normal development. Foetal growth restriction (FGR), also referred to as intrauterine growth restriction, is defined as an abnormal pattern of foetal growth deriving from an event whilst in utero [319]. The retention of a healthy brain weight in the smaller and lighter male LINC00961$^{-/-}$ mice, indicated by their increased brain weight to body weight ratio (refer to Table 1, row 3 in the above manuscript. Brain: body weight) is a feature of asymmetrical FGR; referring to the fact that the growth patterns of some vital organs may continue normally whilst sacrificing the growth patterns of others. In contrast, symmetrical FGR refers to the fact that the entire foetus and internal organs are in proportion as growth of the whole organism is restricted [320]. This brain specific phenotype is referred to as ‘head-sparing’ or ‘brain-sparing’, which is a protective mechanism where cerebral blood flow is increased, thereby the brain preferentially receives oxygenated blood when the foetus is exposed to acute or chronic hypoxia, allowing the brain to develop normally [321-323]. Consequently, the energy reserves of fat deposits suffer as fat deposition is less important at that time [324]. Previously, NEAT1 and H19 are, to the best of our knowledge, the only 2 lncRNAs which have been linked to roles in FGR. NEAT1 is upregulated in human FGR placentas, although its role on FGR remains unclear [325], whilst H19 is significantly lower in human FGR placentas [326]. Zuckerwise & colleagues (2016) were the first to identify a novel lncRNA mechanism in FGR, showing that decreased H19 releases inhibition of miR let-7, resulting in a downregulation in a novel target gene, type III TFG-β receptor.

This dysregulation in a TGF-β pathway leads to a reduction of migration and invasion of extra villous trophoblasts cells [327].

Given the hypothesis that LINC00961 is vital for EC function, and that *in vitro* data showed that LINC00961 loss negatively affects endothelial functions, it is logical to infer that genetic loss of LINC00961 could have negatively affected the endothelium in utero, fundamentally altering blood vessel physiology in the foetuses and their individual placentas, leading to placental dysfunction and ultimately foetal hypoxia. This could then induce the sexually dimorphic, reduced growth and development phenotype we see here which could be due to FGR, although this is speculation which requires further investigation to confirm or deny. In order to test the hypothesis that male LINC00961$^{-/-}$ offspring and their placentas have abnormal vessels and vascular insufficiency causing a lack of oxygen and nutrients to reach the foetus, there are several tools which could be used: Blood oxygen level dependent (BOLD) magnetic resonance imaging (MRI) utilises the fact that deoxyhaemoglobin and oxyhaemoglobin differ in their magnetic properties and has been used to study foetal blood flow in mice, sheep and humans. Cahill & colleagues (2014) used BOLD to show real time changes in the foetal liver and brain blood flow, in response to alterations in oxygen level of air supplied to mothers [322]. Additionally, a recent study by Basak & colleagues (2019) highlighted the use of multispectral optoacoustic tomography as another imagine modality which can be used to determine blood oxygenation in mice non-invasively [328]. Thorough histological analysis of the foetal blood vessels and placenta would be required downstream to blood flow imaging and measurements. Of particular interest would be the number, perfusion, and structure of capillaries and αSMA positive larger vessels, as well as the extent of mural cell coverage of larger vessels. Analysis of the blood vessels in the brain would also be of interest to determine if there is any compromise to the endothelium and the vessels of the brain. In parallel to histology, qRT-PCR, western blot analysis, and in situ hybridisation for known hypoxia response genes and protein expression, such as HIF1α, HIF2α, VEGF-A, would confirm the presence of hypoxia in utero. Not forgetting the analysis of potential LINC00961 downstream interactors, such as miR233-3p.

Given our suspicion that the above post weaning, reduced growth and development phenotype of male KO animals may be due to the absence of the LINC00961 locus causing a FGR or a FGR-like phenomenon, the following sections describe the

implications of FGR to cardiovascular health and explore how the LINC00961 locus may play a role.

FGR has been linked to the development of several medical conditions in adulthood such as hypertension, metabolic syndrome, type 2 diabetes and insulin resistance, obesity, dyslipidaemia, and cardiovascular diseases including pulmonary arterial hypertension and atherosclerosis [329] [320, 330, 331] [28]. This is supported by evidence that male FGR mice have higher cholesterol levels and more advanced atherosclerotic plaque development in adulthood [332]. Skilton & colleagues (2005) determined that babies born after FGR had significant aortic wall thickening at birth. This is an interesting early marker for cardiovascular health, given that atherosclerosis can be detected in the abdominal aorta in early childhood, decades before any symptoms of atherosclerosis appear [333]. Pre-clinical alterations such as this are excellent early markers to identify at risk individuals for continued monitoring, early intervention, and management of risk factors. It would therefore be interesting to carry out ultrasound on the abdominal aortic walls of the LINC00961 line offspring to look for aortic wall thickening in KOs. Histological analysis would determine if there are any alteration in aortic wall thickness in male LINC00961$^{-/-}$mice after birth or in adulthood.

Another example of FGR affecting disease susceptibility in later life is demonstrated by foetal hypoglycaemia in FGR pregnancies. In order to cope with this, the foetus must shift its energy metabolism to conserve energy for survival [334]; this results in a defect in insulin secretion and an alteration in expression of glucose uptake transporter isoforms GLUT1 and GLUT3, allowing tissues to regulate glucose uptake. However, these changes are sustained into adulthood where they can result in a flawed and pathological response to the adult environment and disease burden [331]. Several animal models of FGR with impaired insulin secretion have been shown to express less of the islet β-cell development and differentiation transcription factor *Pdx1* and changes in the epigenetic markers present on its promoter. Interestingly, the human gene has also been found to have altered epigenetic markers in type 2 diabetic patients [335] [331]. Insulin positively regulates mTOR signalling, which in turn influences the amount of GLUT3 in the placenta [336]. Furthermore, mTORC1 has been shown to have a role in nutrient sensing within the placenta, and as we now know, SPAAR has a role in mTORC1 regulation, which may be relevant to the FGR phenotype in LINC00961$^{-/-}$ given that SPAAR is also deleted [337]. Amino acid

concentrations also contribute to insulin secretion and interestingly SPAAR was shown to negatively regulate mTORC1 activation, but only under amino acid supplemented conditions [232]. Therefore, it would be interesting to investigate whether SPAAR$^{-/-}$, and LINC00961$^{-/-}$ mice, do have altered glucose metabolism, and whether this differs between the two strains. Glucose tolerance and insulin tolerance tests would be an easy way to establish any alterations in these parameters. One hypothesis may be that as SPAAR$^{-/-}$ relieves the negative regulation of mTORC1 activity, and despite lower amino acid and glucose concentrations in the FGR foetus, metabolism is unaltered, as one of mTORs many actions it to act as a nutrient sensor within the cell and gate keeper of initiating protein synthesis (when nutrients are plentiful), thus preventing the FGR phenotype. Interestingly, mTOR is a known regulator of GLUT3 (higher affinity GLUT) concentration in the human placenta, which could theoretically be altered downstream of SPAARs interaction with mTOR. There is decreased mTOR expression in FGR, which suggests a possible explanation as to why growth is restricted, considering mTORs role in initiating protein synthesis; we can speculate however that release of mTOR dampening by SPAAR$^{-/-}$ could potentially alleviate this negative effect of reduced mTOR.

Interestingly, the identification of fatty acid synthase (FAS) as a potential binding partner of LINC00961 in our RNA-protein pull down experiment (see supplemental table in publication in Chapter 3) offers another connection between LINC00961 and FGR. Adults who underwent FGR have upregulated FAS, which synthesises long chain fatty acids and is the rate limiting step in lipogenesis [338, 339]. It is likely then, that FAS is upregulated in the LINC00961$^{-/-}$ FGR mice, and LINC00961 may influence this. However, to confirm the presence of upregulated FAS and the speculation of LINC00961 regulation of FAS, mRNA and protein analysis in the mouse adipose tissue would need to be carried out. Collectively, LINC00961 and SPAAR may have independent roles in the FGR phenotype seen in these KO mice, and a summary of their potential interactions is shown in Figure 4.12.

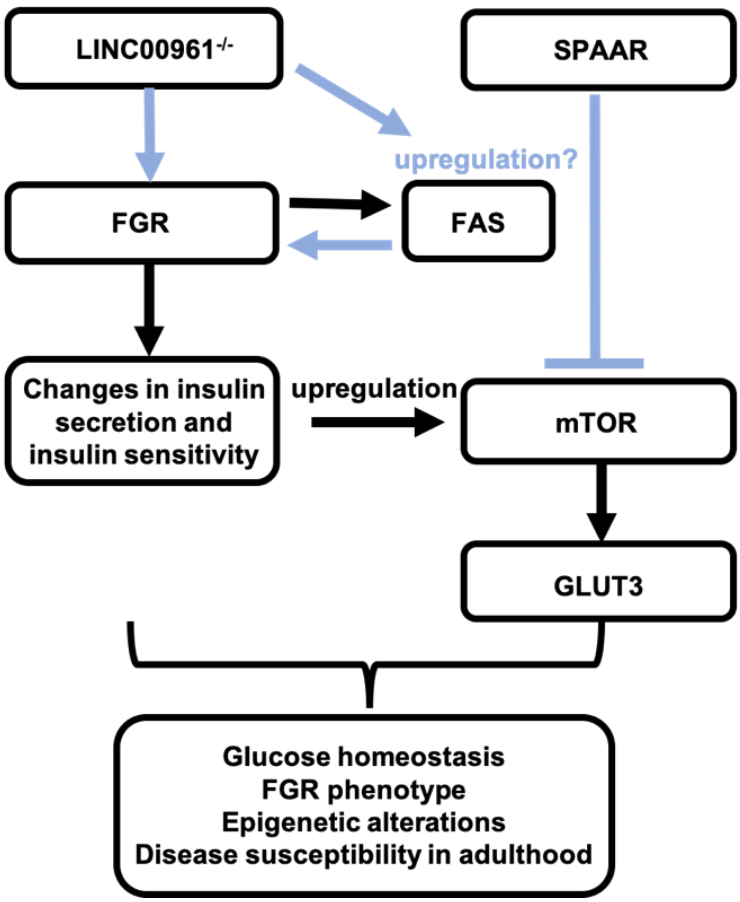

Figure 4.12 Potential mechanisms for the role of LINC00961 and SPAAR in a growth and development restricted phenotype and subsequent disease susceptibility in adulthood.

Blue arrows/lines represent the how the data from this work (and that of Matsumoto & colleagues (2017) regarding SPAARs regulation of mTOR) could compliment a known regulatory pathway in foetal growth restriction and susceptibility to disease in adults who underwent foetal growth restriction. On the schematic, FGR – foetal growth restriction and FAS – fatty acid synthase. [336] [331] [232].

Interestingly, this LINC00961$^{-/-}$ data fits with the observed phenomenon that FGR has a bias towards affecting male offspring [340]. We know that female offspring, even those having undergone FGR, have some protection against developing metabolic and cardiovascular diseases; one theory behind this is that sex-specific epigenetic signatures may be present, affecting the ability for each sex to respond to stress in utero [331]. Related to cardiovascular disease, Zhang and colleagues (2019) found that murine FGR induced via calorie restricting mothers resulted in altered epigenetic markers in the endothelial gene endothelin-1, upregulating its expression in pulmonary vascular ECs and the sperm of male offspring in the f1 and f2 generations. This endothelial upregulation was associated with a susceptibility for pulmonary arterial hypertension and endothelial dysfunction in adulthood for both those generations [28], thus providing further evidence of FGR carrying intergenerational consequences. In conclusion, LINC00961$^{-/-}$ mice may be useful as a novel murine model to study FGR/hypoxia in pregnancy, as chronic hypoxic stress is a major concern in human pregnancies given its high prevalence [323]. The relationship between LINC00961, endothelial dysfunction, and the consequences of FGR on adult disease susceptibility requires further investigation.

4.7.5 Further characterisation of LINC00961$^{-/-}$ blood vessel phenotype

As we are particularly interested in the role of the LINC00961 locus in blood vessel endothelium, further characterisation of the vasculature in this mouse line would be beneficial by investigating the structural integrity and function of their blood vessels throughout body tissues. Histological analysis of the organs would include sectioning tissues and staining for endothelial markers such as CD31, VE-CADHERIN, or using an isolectin b4 infusion to identify capillaries, and co-staining with αSMA to visualise larger vessels. Of interest would be the number of capillaries and larger arterioles, as well as their perfusion (by perfusion of injecting isolectin b4 which would flow through perfused vessels tagging the endothelium, and co-staining the endothelium with an additional marker, thus allowing the visualisation of any capillaries which are not perfused, perhaps due to vessel pruning and regression, or due to instability).

To investigate whether LINC00961$^{-/-}$ offspring have fully functional blood vessels myography could be used to determine whether their arteries can contract and relax efficiently. Myography is a well-established technique used to determine isometric tone in an artery and involves *ex vivo* dissection of vessels of interest and passing a

wire through the lumen, careful not to damage the endothelium, and mounting the wired vessel onto apparatus attached to a force transducer which records changes in force from vessel contraction/relaxation [13]. An advantage of using wire myography is that many different stimuli can be used to induce contraction and relaxation with known mechanisms of action. These can be used to test endothelial dependent vasorelaxation, and endothelial independent vasorelaxation with substrates which act directly on the vessels smooth muscle. For example, acetylcholine is an endothelium dependent vasodilator stimulating the release of endothelial nitric oxide (NO) which then diffuses across to the surrounding smooth muscle cells stimulating relaxation and thus vessel dilation. In contrast, sodium nitroprusside is a NO donor, providing NO to the smooth muscle cells, by-passing the need for endothelial NO release [72]. Myography is an ideal method to compare the contraction/relaxation abilities of arteries between LINC00961$^{-/-}$ and WT mice and can be coupled with blood pressure analysis via tail cuffing, to provide more data on cardiovascular parameters in these mice. Of particular interest, would be to investigate whether there are any endothelial dependent mechanistic differences, considering the high level of endothelial LINC00961 and the negative impacts of LINC00961 depletion on EC behaviour demonstrated *in vitro*. As LINC00961$^{-/-}$ offspring where viable and survived to adulthood without any obvious negative phenotype, there likely is compensatory mechanisms which allow the mice to function with underlying physiologically altered vessels, as shown in the previous chapter.

4.7.6 A link/lncRNA between FGR and body fat?

Here, we assessed the weight of female mice at 6 months of age and found it was not significantly different between genotypes, however, weight differences or lack thereof, do not inform on any underlying changes in adipose biology such as fat metabolism and the relationship between the fat depot and its vascularisation. The size and number of adipocytes, and their metabolic profiles such as expression of lipogenesis genes in may still be altered. This warrants further investigation, particularly the relationship between the fat depot vasculature and its homeostasis, and the scrutiny into whether the metabolic profiles are altered in KOs. It would be interesting to investigate further the adipose tissues of these mice and perhaps incorporate time domain nuclear magnetic resonance (TD-NMR) into our analyses to accurately decipher the proportions lean muscle mass and fat mass.

Importantly, we need to investigate these parameters in LINC00961$^{-/-}$ male mice considering the identification of the FGR phenotype, as at the time of fat depot investigation we were unaware of this phenotype. In fact, macroscopic observations of what appeared to be increased amounts of internal fat at dissection of adult male mice in the HLI study is what initially prompted us to investigate the weight and fat depots. Fat distribution patterns, fat metabolism, body fat proportion, and the use of fat as an energy source differs between the genders. It has been well documented that women store more fat and utilise it for energy during exertion, whereas males are adapted to utilise glucose and amino acid metabolism. These differences are caused by the differences in levels of sex hormones. Oestrogens such as oestradiol facilitate subcutaneous fat deposition and has been shown to increase preadipocyte proliferation. In contrast testosterone increases lipolysis whilst decreasing circulating trigylcerol and lipase activity [341]. This prompted us to choose female mice in attempts to verify any differences of weight and fat deposition in adult mice.

4.8 Conclusion

In conclusion, although the *in vitro* work regarding manipulation of the mouse LINC00961 locus remains incomplete, *in vivo* data supported our hypothesis that the LINC00961 locus is vital for proper EC function. Additionally, we show that male LINC00961$^{-/-}$ mice may be more susceptible to adverse cardiovascular phenotypes, either due to experiencing reduced growth and development post weaning (in males), being a LINC00961$^{-/-}$ in itself and consequently having altered vessel physiology and whatever unknown phenotypes may be present in these mice, or a combination of these factors. When we consider this locus, it is interesting to presume that a similar phenotype could be present in humans, due to the similar phenotype of endothelial dysfunction in human cells *in vitro* and the conservation of this locus and surrounding genes. This data, as well as other studies', indicate that LINC00961 and SPAAR may be key functional molecules not only with regards to novel mechanisms in endothelial dysfunction, but also regulators contributing to post weaning growth, and FGR, and disease susceptibility, which could be investigated for their use in modulating disease. We also show data which indicates towards altered heart functions at an early age, something which would certainly impact the risk factor for developing cardiovascular disease and heart failure in later life. However, this work is incomplete and opens an

interesting avenue which requires a lot of further research to fully understand the role of the LINC00961 locus in cardiovascular development and disease risk.

Chapter 5 Discussion

Research into ischaemic vascular diseases consistently highlights the need to more effectively promote endogenous regeneration to help combat poor revascularisation in patients with CLI and after an MI. The same research also highlights the difficulty in achieving this clinically, despite years of promising pre-clinical therapeutic outcomes. The innate mechanisms that drive endogenous endothelial regeneration remain somewhat unclear and further understanding of endothelial homeostasis and regenerative mechanisms are required to allow us to successfully induce endothelial repair in the adult. LncRNAs represent a novel class of molecules which could be involved in all processes in the body and therefore manipulated and used therapeutically to induce angiogenesis, among other cellular functions. The value of identifying and validating novel lncRNA transcripts to the medical science field is such that several researchers have developed dedicated protocols specifically to streamline the complex process and bioinformatic processing included in analysing RNA-seq datasets, such as the pipeline for lncRNA annotation from RNA-seq data (PLAR) developed in 2015 [342]. As the interest in lncRNA biology has continued to expand, as too have the bioinformatic techniques continued to be improved upon [343].

Here, we are the first to prove that the LINC00961 locus is crucial in maintaining proper endothelial function and that this locus houses a novel pro-angiogenic molecule, SPAAR, and an anti-angiogenic molecule in the LINC00961 lncRNA transcript. We demonstrate for the first time that depletion of the LINC00961 locus in human cells negatively effects endothelial functions, similarly, genetic deletion in the mouse demonstrated reduced appropriate endothelial regeneration in response to injury in the adult, as well as indicating the presence of maladapted vessels in the adult independent of any injury. We identify a role for this locus in development which requires further investigation to understand fully. We show that male KO offspring suffer from a sexually dimorphic, reduced growth and development phenotype post weaning and found evidence to suggest that KO animals may have underlying heart function issues, though this requires further exploration. The following sections discuss further these major conclusions found in the previous Chapters.

5.1 The LINC00961 locus regulates endothelial function across species

By using RNA-seq in ECs differentiated from hESCs, we were able to search for novel EC enriched transcripts which were likely key factors in the control of EC behaviours. In Chapter 3 we report the first *in vitro* evidence of the LINC00961 locus being crucial to the maintenance of proper EC function through the strong phenotypes seen with siRNA and GapmeR depletion in HUVECs. Several other lncRNAs including SENCR [84], MANTIS [171], GAPLINC [11], MALAT-1, and MEG3 [188, 227] have been associated with angiogenesis, however, we were able to demonstrate that LINC00961 depletion also impacted several other ECs functions such as barrier maintenance and adhesion which are vital to retaining healthy blood vessels. The 65% sequence homology between mouse and human LINC00961 homologues further hinted at a vital conserved function of this locus (http://www.ensembl.org/Homo_sapiens/Gene/Summarydb=core;g=ENSG00000235387;r=9:35909483-35937153). We began to explore this hypothesis In Chapter 4 with siRNA KD of the locus in mouse ECs which had a similar, though somewhat muted effect, of inhibiting angiogenesis. Despite the strong negative phenotypes observed with locus depletion, the LINC00961$^{-/-}$ mouse line generated for *in vivo* work was found to be viable - this was a concern as impaired endothelium in the developing embryo could have been fatal. HLI experiments identified that *in vitro* LINC00961 functions do translate *in vivo* and demonstrated an impaired EC angiogenic response to injury in the adult as well as a indicating an underlying issue with vessel physiology as we saw a decrease in the number of larger αSMA positive supporting vessels at baseline. However, we identified an increase in the number of these vessels post injury which demonstrates that the ability for the vessels to undergo arteriogenesis was intact despite the lack of evident angiogenesis. Although it is unknown whether LINC00961 has a role in pericyte mural cells which support all blood vessels, or in SMC which are required for maturation of vessels in arteriogenesis [58], the failure to develop a comparable number of larger vessels in the adductor to wildtype mice is likely due to EC dysfunction which could cause destabilisation and regression of developing vessels and inhibit the required maturation. The dysfunctional ECs may also have signalling differences which could alter their communication or adherence to these important mural cells. To truly understand that cause of this basal vascular phenotype further investigations are required into the expression of the LINC00961 locus in mural cells, and characterise any differences in EC and mural cell interaction in KO animals.

5.2 The antagonistic effects of LINC00961 and SPAAR

Having identified that the LINC00961 locus is crucial to EC function and that depletion and loss of this locus leads to defects in angiogenesis, we sought to dissect the contributions of the LINC00961 transcript and the locus's MP SPAAR to this phenotype. It was important for us to decipher if the locus effects were simply due to SPAAR, which had previously been shown to be important in the mTORC1 pathway [232], however, at the time no functions of the lncRNA itself had been investigated. Depletion of the LINC00961 transcript and knocking out the locus completely were easier to achieve than attempting to deplete or KO either molecule alone. Although ENSEMBL predicts 4 isoforms coming from this locus in human and 2 in mouse, the true number of transcripts in either species remains unknown, therefore, to assess the functions of these molecule independently, we chose to use an over expression approach. In Chapter 3 we provide crucial evidence that overexpression of the LINC00961 transcript, with mutated ATG codons to prevent SPAAR translation, inhibited angiogenesis in a Matrigel© assay, whereas overexpression of SPAAR through the inclusion of only exon 2 produced a pro-angiogenic response on Matrigel©. Overexpression of the whole locus did not have a significant effect on the angiogenesis assay which is logical considering the opposing effects each molecule demonstrated separately. Conceptually, we believe this to be the first known instance of one locus producing 2 molecules with opposing effects on angiogenesis and who likely contribute to the regulation of angiogenesis via the balancing/ switching between transcripts. Further evidence for this hypothesis is demonstrated in Chapter 4 where mass spectrometry analysis determined that confluent unstimulated HUVECs, did not express SPAAR. This was very interesting data for us as it supports our conclusion that SPAAR is pro-angiogenic as ECs are normally senescent, non-proliferative, and non-angiogenic *in vivo* until appropriately stimulated to adapt to changes in their environment. To investigate this further the next step would be to stimulate HUVECs into a pro-angiogenic state for example, by hypoxia or the addition of VEGF, and then repeat the mass spectrometry analysis which we hypothesise would show induction of the SPAAR MP. We have shown consistently that LINC00961 is expressed to a high level in unstimulated HUVECs [254] and in Chapter 5 we show downregulation of LINC00961 in 24 and 48 h of hypoxia in mouse ECs; it would be interesting to include murine EC line hypoxia lysate samples in mass spectrometry analysis to further validate the similarities in expression and function of human and mouse SPAAR, with the hypothesis that mouse ECs do not produce SPAAR unless

under angiogenic stimuli (e.g., hypoxia). Although we do not have our own evidence of LINC00961 downregulation during hypoxia in human cells, Voellenkle & colleagues (2016) previously investigated differential lncRNA expression during 24 and 48 h of hypoxia in HUVECs by RNA-seq and indeed saw a significant reduction in LINC00961 levels by -1.1 log2FC [344] thus supporting our hypothesis.

5.2.1 Possible multiple transcripts and varied expression

Determining that LINC00961 is a bifunctional RNA [345] led us to question the architecture of the locus which contains 2 functional molecules. Given the above hypothesis that LINC00961 transcript and SPAAR are likely expressed in a mutually exclusive manner and under different cellular conditions, the LINC00961 locus likely possesses a mechanistic switch to control transcript isoform expression. There are 2 possible mechanisms of control; mechanism 1, where alternative isoforms are expressed or spliced under certain conditions or mechanism 2, where there is constant transcription of the transcript(s) followed by degradation of the unrequired SPAAR transcript or alternatively, inhibition of SPAAR translation by a factor whose release of inhibition occurs under stimulated conditions. Figure 5.1 shows the 4 predicted isoforms of this locus in human and 2 in mouse from ENSEMBL (https://www.ensembl.org/Homo_sapiens/Gene/Summary?db=core;g=ENSG00000235387;r=9:35909490-35937153, November 2020). This data suggests that SPAAR could be translated from 2 different isoforms in humans, and that SPAAR is produced from the main full length LINC00961 transcript in mouse, not a second, shorter isoform. However, these are predicted isoforms from bioinformatic analyses and further experiments are required to determine the correct annotation of this locus. The work in this thesis used primers which would effectively pick-up multiple transcripts if they existed, as it was impossible to design separate primer sets for the detection of a LINC00961 transcript and SPAAR transcript, given the ambiguity of the locus.

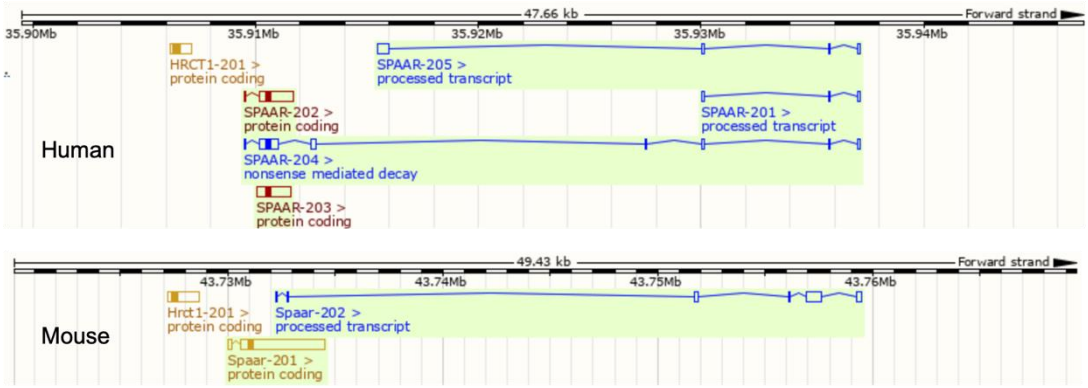

Figure 5.1 ENSEMBL predicted transcripts for the human and mouse LINC00961 loci.

Human predicted transcripts in top panel and mouse predicted transcripts in the bottom panel. Data taken from ENSEMBL November 2020.

The rapid amplification of cDNA ends (RACE) was developed in 1988 to determine the full length of a transcript utilising cDNA synthesis of an RNA transcript and subsequent sequencing PCR amplification [346]. This transcript can then be sequenced to reveal the previously unknown ends of the transcript, this is referred to as RACE-Seq [347]. Anchored RACE, also known as 5' and 3' RACE, refers to the slightly different methods used to detect the ending sequence of a transcript at the 5' and 3' ends respectively. The cDNA made by adding nucleotides to the 5' end of the primer undergoes the addition of a homopolymeric tail by the added enzyme terminal deoxynucleotidyl transferase. By then using PCR with a universal primer recognising this polymeric tail, a transcript is generated with the proper 3' sequence. In contrast, the naturally occurring 3' polyA tail on eukaryotic mRNA is used to amplify the product with its proper 5' end sequence [348]. This technique has been employed to improve annotation of the transcriptome by supplementing the computational predictions of transcript boundaries. The first study to use RACE-seq to clarify the ambiguity of lncRNAs annotations was published in 2016 by Langarde & colleagues (2016) who used 2 rounds of RACE to identify alternative splicing events and over 2500 novel lncRNA transcripts. The authors also provide evidence that lncRNA can range from 1 to 10+ isoforms [347]. When we consider that protein coding genes are estimated to have an average of 9 isoforms [349], and that some lncRNAs have already been shown to have many isoforms, such as the lncRNA CARMN which to date has an estimated 12 isoforms [350], it is logical to consider that many lncRNA may have as many splicing events and isoforms as some protein coding genes. RACE in unstimulated and stimulated HUVECs could be used to determine the number of LINC00961 transcript isoforms in human and mouse which would ultimately aid in the understanding of the control of this locus and the relationship between LINC00961 and SPAAR expression.

5.3 LINC00961 and SPAAR pathways

The literature regarding interactions of LINC00961 and SPAAR is summarised in Figure 5.2 and is supplemented with the interactions discovered in this thesis. In Chapter 3, we show that ERG binds to the LINC00961 promoter at 2 sites approximately 1 Kb apart. While further investigation into what other upstream factors may influence LINC00961 expression was beyond the scope of this thesis, there are

reports in the literature with evidence of regulation of the human LINC00961 locus by LSD1 [236] and STAT1 [247]. Relevant to work here, LSD1 is also known to contribute to the regeneration of muscle by upregulating myogenic transcription factors in satellite cells [351], highlighting that the LSD1 LINC00961 connection may be relevant in the control of SPAAR downregulation during muscle regeneration [232]. Jiang & colleagues (2018) showed that LSD1 did in fact bind to the LINC00961 promoter and decreased its expression in lung epithelial cells [236]. Interestingly, LSD1 has been shown to associate with the ERG super enhancer and furthermore, downregulation of LSD1 by an inhibitor increased ERG expression, representing an interesting connection between LSD1, ERG, and LINC00961.

We were able to validate binding of LINC00961 to Tβ4, however, validation of the SPAAR and Nesprin-1 interaction remains to be carried out. This was beyond the scope of this thesis as we concentrated on validation of the non-coding function of LINC00961, however, this could be validated in a similar approach to LINC00961 and Tβ4 with an antibody against Nesprin-1 and mass spectrometry analysis of the un-crosslinked lysate to identify any SPAAR present which had bound. A limitation of the SPAAR pulldown is that we used an overexpressed HA-tagged SPAAR in order to ensure we could extract the SPAAR complexes, by the HA-tag, for analysis and this artificial environment produced more SPAAR availability, creating less competition for SPAAR and enriching the sample lysate with bias interactions. Never-the-less, the interactions of LINC00961 and SPAAR with actin-binding molecules identified suggests that these interactions are the likely mechanistic pathway by which both molecules elicit their cellular effects, although other interactions with different downstream consequences cannot be ruled out.

As LINC00961 depletion resulted in widespread loss of EC function and that LINC00961 and SPAAR were found to bind to actin-binding proteins, the next step would be to investigate changes to the actin cytoskeleton when LINC00961 and SPAAR are modulated. The actin cytoskeleton is fundamental in controlling cell shape, cell-cell adhesions and cell-matrix adhesions; binding to adheren junction proteins such as VE-Cadherin to regulate barrier function, with dynamic alterations in the actin network being vital for endothelial migration and angiogenesis [6, 352]. Future mechanistic work would therefore focus on investigating actin cytoskeletal dynamics in KD and overexpression conditions to validate that the cytoskeleton is in fact altering with modulation of the LINC00961/SPAAR axis. This can be visualised

by staining the actin cytoskeleton with phalloidin after cell fixation. For these experiments we would hypothesise that the conditional expression of, and overexpression of the pro-angiogenic SPAAR would lead to the presence of actin structures associated with sprouting angiogenesis such as the filipodia and lamellipodia respectively required for sensing a stimulus and providing the motility to migrate the cell in the direction of that stimulus [353]. Pro-angiogenic VEGF exposure for example, has been shown to increase the rate of actin polymerisation in HUVECs, which results in the motility required for migration during sprouting angiogenesis by inducing the formation of contractile actin stress fibres [353], which we expect to be the case with SPAAR expression. In contrast, we expect over expression of the anti-angiogenic LINC00961 to lack the presence of these structures and show more stable junctions, not dissimilar to quiescent ECs.

Interestingly, Wu & colleagues (2019) recently reported that LINC00961 can sponge miR-367 in vascular SMCs, which brings together functions for this locus in 2 interacting cell types involved in atherosclerosis [246](refer to Figure 5.2). Endothelial dysfunction leads to increased permeability of the endothelial barrier and penetration of leukocytes and LDLs into the wall of the artery [2, 29]. Pathological phenotype switching and remodelling of the vascular SMCs into a synthetic phenotype leads to further progression of atherosclerotic lesions [13, 187]. LINC00961 may offer a therapeutic target by targeting multiple key cell types involved in atherosclerosis, however, further investigation is required to fully understand the roles of LINC00961 in ECs, whilst to the best of our knowledge, Wu & colleagues are the first group to investigate this locus in SMCs [246].

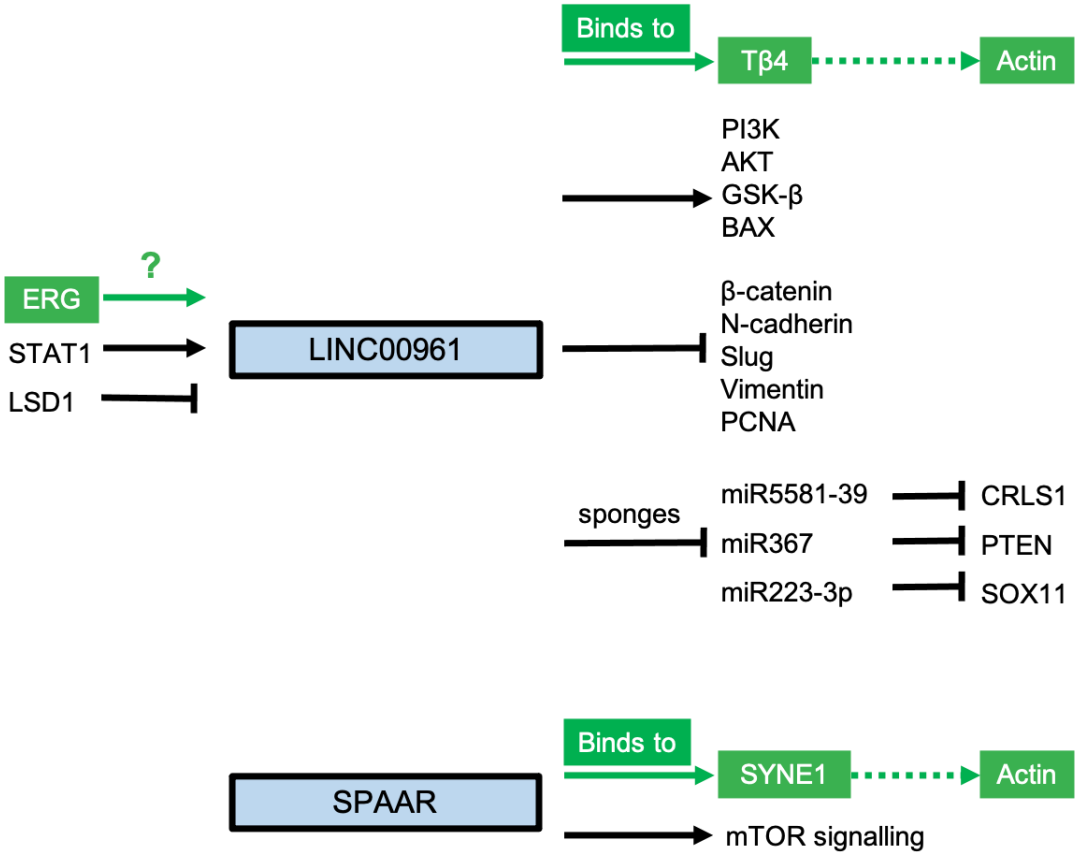

Figure 5.2 Updated summary of LINC00961 and SPAAR interactions.

The data in black was gathered from research in non-small cell lung cancer, tongue squamous cell carcinoma, hepatic cell carcinoma, renal cell carcinoma, glioma, melanoma, colon cancer, gastric cancer, cardiomyocytes following MI, and in skeletal muscle regeneration. Green boxes indicate interactions that have been explored or identified throughout this thesis. Full arrows indicate induction or promotion whilst flat ends indicate inhibition. Punctuated arrows indicate a promotive effect that requires further research into the mechanism. [247] [236] [238] [241] [246] [240] [249] [239] [250] [234] [232].

5.4 Limitations

We must scrutinise the limitations of the work carried out here and consider what alternations to experimental conditions could be made to further understand this locus in future work. Although we identified LINC00961 as a candidate of interest due to its enrichment in ECs, work here and that of others has demonstrated that it is expressed in several other cell types [232] and likely plays essential roles in those cells in a different manner to its actions in ECs. To further explore the role of the LINC00961 locus specifically in ECs, the best approach would be to utilise an endothelial-specific KO mouse line, as the global KO line we used is the largest limitation to this work. This could be achieved by inserting LoxP restriction sites which flank the LINC00961 locus and crossing this line with another which includes Cre-recombinase expression under the control of an endothelial specific marker. This would result in the Cre enzyme produced in endothelial cells removing the DNA of the LINC00961 locus between the LoxP sites and recombining the DNA to create an endothelial-specific KO and retaining LINC00961 locus expression in all other cell types. Considering the implications presented in Chapter 4 that LINC00961 causes a reduction in growth and development in male KO offspring possibly related to FGR, it would be wise to use an inducible Cre expression system, the most common of which is the tamoxifen inducible Cre. Examples of tamoxifen inducible endothelial specific Cre mouse lines includes PDGFβ -iCreER^{T2} [354], and Tie2-cre/ERT2 [355] where PDGFβ and Tie2 are pan-endothelial markers. Utilising an induced Cre is especially important as we are unaware of the full extent of LINC00961 locus loss on foetal development, which may extend beyond the induction of FGR in male KO offspring.

In order to assess the true translatability of this locus to human PAD/CLI and MI we need to ascertain the baseline and diseased modulated levels of LINC00961 in patient samples. Here we lack this data as these samples such as tissue from amputations and MI tissues from deceased patients are difficult to obtain. In relation to this, mice and rats do not naturally develop atherosclerotic disease [356], therefore, mouse and rat models, although excellent for pre-clinical research, have artificial and forced phenotypes which never 100% recapitulate human disease. A next step to consider would be to look at LINC00961 in a large animal model. The pig model of MI is well established and relevant to human physiology as their heart is of a similar size to humans, and pigs are in fact naturally susceptible to atherosclerosis like humans [357], however, to date a pig LINC00961 homologue has not been identified

(ENSEMBL November 2020). As pigs are phylogenetically closer to humans than mice [357] it is likely that LINC00961 is present in pigs but has yet to be identified and annotated.

The final criticism is regarding the approach taken when designing *in vivo* experiments and the lack of power calculations used to determine appropriate N numbers. The final number of animals used in the HLI study was guided by the expertise of Dr Marco Meloni and his experience in conducting HLI studies. In future, any animal studies would benefit from the use of power calculations which are used to define the sample size required to test a hypothesis and answer the scientific question at hand at a desired level of significance, usually 5% ($p<0.05$). This is an important factor of research as too few animals used may lead to incorrectly accepting a null hypothesis, and too many are an unethical use of animals and waste of resources. One example of a power calculation which is applicable to all animal experiments is the following: E = total number of animals – total number of groups, where E should be between 10-20. A value higher than 20 means there are more animals than necessary, whereas less than 10 means that more animals are required to accurately determine if there is any significant difference between groups in the experiment [358].

5.5 Conclusion

In conclusion, there are several major outcomes of the work described in this thesis. We are the first to show that the LINC00961 locus is vital for proper endothelial function, which is translatable *in vivo* to mice. We are the first to report that the LINC00961 transcript itself is a *bona fide* lncRNA, therefore classifying it as a bifunctional RNA due to its ORF which produces the MP SPAAR. We made the novel discovery that LINC00961 and SPAAR have opposing effects on angiogenesis and provide a possible mechanism of action for both molecules in their interactions with actin-binding proteins. We are the first to identify a novel role for this locus in foetal development, with our discovery of male KO offspring mice havinga phenotype of reduced growth and development post weaning. We are also the first to look at the role of this locus in the heart and provide evidence that loss of this locus appears to influence heart function dynamics at an early age, but that this loss also causes susceptibility to larger infarcts in MI. The reduced growth and development phenotype

and the subtle alterations in heart function are of importance to understand further, as these factors certainly influence the risk of cardiovascular disease in later life. Whilst this thesis highlights the importance of not just LINC00961 but of the critical roles of lncRNA in general, further research is necessary to fully understand the role of this locus in human disease and to validate the mechanisms of action for LINC00961 and SPAAR, not only in endothelial dysfunction and the understanding of vessel pathology, but in other cell types and diseases.

References

1. Gisterå, A. and G.K. Hansson, *The immunology of atherosclerosis.* Nature Reviews Nephrology, 2017. **13**(6): p. 368.
2. Leiva, E., et al., *Role of oxidized LDL in atherosclerosis.* Hypercholesterolemia, 2015: p. 55-78.
3. Burke, A.P., et al., *Morphological predictors of arterial remodeling in coronary atherosclerosis.* Circulation, 2002. **105**(3): p. 297-303.
4. Slager, C., et al., *The role of shear stress in the generation of rupture-prone vulnerable plaques.* Nature clinical practice Cardiovascular medicine, 2005. **2**(8): p. 401-407.
5. Falk, E., *Pathogenesis of atherosclerosis.* Journal of the American College of Cardiology, 2006. **47**(8 Supplement): p. C7-C12.
6. VanderLaan, P.A., C.A. Reardon, and G.S. Getz, *Site specificity of atherosclerosis: site-selective responses to atherosclerotic modulators.* Arteriosclerosis, thrombosis, and vascular biology, 2004. **24**(1): p. 12-22.
7. Nakashima, Y., et al., *Distributions of diffuse intimal thickening in human arteries: preferential expression in atherosclerosis-prone arteries from an early age.* Virchows Archiv, 2002. **441**(3): p. 279-288.
8. Limbourg, A., et al., *Evaluation of postnatal arteriogenesis and angiogenesis in a mouse model of hind-limb ischemia.* Nature protocols, 2009. **4**(12): p. 1737.
9. Song, P., et al., *Global, regional, and national prevalence and risk factors for peripheral artery disease in 2015: an updated systematic review and analysis.* The Lancet Global Health, 2019. **7**(8): p. e1020-e1030.
10. Shammas, N.W., *Epidemiology, classification, and modifiable risk factors of peripheral arterial disease.* Vasc Health Risk Manag, 2007. **3**(2): p. 229-34.
11. He, Y., et al., *Long non-coding RNA GAPLINC promotes angiogenesis by regulating miR-211 under hypoxia in human umbilical vein endothelial cells.* Journal of cellular and molecular medicine, 2019. **23**(12): p. 8090-8100.
12. Goodall, R., et al., *Trends in peripheral arterial disease incidence and mortality in EU15+ countries 1990–2017.* European Journal of Preventive Cardiology, 2020: p. 2047487319899626.
13. Stather, P.W., et al., *Differential microRNA expression profiles in peripheral arterial disease.* Circulation: Cardiovascular Genetics, 2013: p. CIRCGENETICS. 113.000053.
14. Morley, R.L., et al., *Peripheral artery disease.* bmj, 2018. **360**: p. j5842.
15. Marso, S.P. and W.R. Hiatt, *Peripheral arterial disease in patients with diabetes.* Journal of the American College of Cardiology, 2006. **47**(5): p. 921-929.
16. Kloos, W., B. Vogel, and E. Blessing, *MiRNAs in peripheral artery disease-something gripping this way comes.* Vasa, 2014. **43**(3): p. 163-170.
17. Shan, K., et al., *Role of long non-coding RNA-RNCR3 in atherosclerosis-related vascular dysfunction.* Cell death & disease, 2016. **7**(6): p. e2248.
18. Chevalier, J., et al., *Obstruction of small arterioles in patients with critical limb ischemia due to partial endothelial-to-mesenchymal transition.* iScience, 2020: p. 101251.
19. Zaman, A., et al., *The role of plaque rupture and thrombosis in coronary artery disease.* Atherosclerosis, 2000. **149**(2): p. 251-266.
20. Figueras, J., et al., *Area at risk and collateral circulation in a first acute myocardial infarction with occluded culprit artery. STEMI vs non-STEMI patients.* International Journal of Cardiology, 2018. **259**: p. 14-19.

21. Johansson, S., et al., *Mortality and morbidity trends after the first year in survivors of acute myocardial infarction: a systematic review.* BMC Cardiovascular Disorders, 2017. **17**(1): p. 53.
22. Alabas, O.A., et al., *Statistics on mortality following acute myocardial infarction in 842 897 Europeans.* Cardiovascular Research, 2020. **116**(1): p. 149-157.
23. Benjamin, E.J., et al., *Heart disease and stroke statistics—2017 update.* 2017.
24. Matsumura, Y., et al., *Intramyocardial injection of a fully synthetic hydrogel attenuates left ventricular remodeling post myocardial infarction.* Biomaterials, 2019. **217**: p. 119289.
25. Buccheri, D., et al., *Understanding and managing in-stent restenosis: a review of clinical data, from pathogenesis to treatment.* Journal of thoracic disease, 2016. **8**(10): p. E1150.
26. Goldman, S., et al., *Long-term patency of saphenous vein and left internal mammary artery grafts after coronary artery bypass surgery: results from a Department of Veterans Affairs Cooperative Study.* Journal of the American College of Cardiology, 2004. **44**(11): p. 2149-2156.
27. Hong, Y.K., et al., *Prox1 is a master control gene in the program specifying lymphatic endothelial cell fate.* Developmental dynamics, 2002. **225**(3): p. 351-357.
28. Zhang, Z., et al., *Intrauterine Growth Restriction Programs Intergenerational Transmission of Pulmonary Arterial Hypertension and Endothelial Dysfunction via Sperm Epigenetic Modifications.* Hypertension, 2019. **74**(5): p. 1160-1171.
29. Toborek, M. and S. Kaiser, *Endothelial cell functions.¶ Relationship to atherogenesis.* Basic research in cardiology, 1999. **94**(5): p. 295-314.
30. Davignon, J. and P. Ganz, *Role of endothelial dysfunction in atherosclerosis.* Circulation, 2004. **109**(23 suppl 1): p. III-27-III-32.
31. Hunting, C., W. Noort, and J. Zwaginga, *Circulating endothelial (progenitor) cells reflect the state of the endothelium: vascular injury, repair and neovascularization.* Vox sanguinis, 2005. **88**(1): p. 1-9.
32. Aird, W.C., *Endothelial cell heterogeneity.* Cold Spring Harbor perspectives in medicine, 2012. **2**(1): p. a006429.
33. Zafar, R., *An insight into pathogenesis of cardiovascular diseases.* Journal of Cardiovascular Diseases & Diagnosis, 2015.
34. Michiels, C., *Endothelial cell functions.* Journal of cellular physiology, 2003. **196**(3): p. 430-443.
35. Ozerdem, U. and W.B. Stallcup, *Early contribution of pericytes to angiogenic sprouting and tube formation.* Angiogenesis, 2003. **6**(3): p. 241-249.
36. Sumpio, B.E., J.T. Riley, and A. Dardik, *Cells in focus: endothelial cell.* The international journal of biochemistry & cell biology, 2002. **34**(12): p. 1508-1512.
37. Otrock, Z.K., et al., *Understanding the biology of angiogenesis: review of the most important molecular mechanisms.* Blood Cells, Molecules, and Diseases, 2007. **39**(2): p. 212-220.
38. Patan, S., *Vasculogenesis and angiogenesis*, in *Angiogenesis in brain tumors*. 2004, Springer. p. 3-32.
39. Cao, R., et al., *Angiogenic synergism, vascular stability and improvement of hind-limb ischemia by a combination of PDGF-BB and FGF-2.* Nature medicine, 2003. **9**(5): p. 604-613.
40. Attwell, D., et al., *What is a pericyte?* Journal of Cerebral Blood Flow & Metabolism, 2016. **36**(2): p. 451-455.

41. Caporali, A., et al., *Contribution of pericyte paracrine regulation of the endothelium to angiogenesis.* Pharmacology & therapeutics, 2017. **171**: p. 56-64.
42. Teichert, M., et al., *Pericyte-expressed Tie2 controls angiogenesis and vessel maturation.* Nature communications, 2017. **8**(1): p. 1-12.
43. Weis, S.M. and D.A. Cheresh, *Pathophysiological consequences of VEGF-induced vascular permeability.* Nature, 2005. **437**(7058): p. 497-504.
44. Carmeliet, P. and R.K. Jain, *Molecular mechanisms and clinical applications of angiogenesis.* Nature, 2011. **473**(7347): p. 298-307.
45. Hirota, K. and G.L. Semenza, *Regulation of angiogenesis by hypoxia-inducible factor 1.* Critical reviews in oncology/hematology, 2006. **59**(1): p. 15-26.
46. Bartoszewski, R., et al., *Primary endothelial cell–specific regulation of hypoxia-inducible factor (HIF)-1 and HIF-2 and their target gene expression profiles during hypoxia.* The FASEB Journal, 2019. **33**(7): p. 7929-7941.
47. Shaw, K., *Environmental cues like hypoxia can trigger gene expression and cancer development.* Nat Educ, 2008. **1**: p. 198.
48. Samanta, D., N.R. Prabhakar, and G.L. Semenza, *Systems biology of oxygen homeostasis.* Wiley Interdisciplinary Reviews: Systems Biology and Medicine, 2017. **9**(4): p. e1382.
49. Downes, N.L., et al., *Differential but complementary HIF1α and HIF2α transcriptional regulation.* Molecular Therapy, 2018. **26**(7): p. 1735-1745.
50. Yoder, M.C., *Human endothelial progenitor cells.* Cold Spring Harbor perspectives in medicine, 2012. **2**(7): p. a006692.
51. Edwards, N., et al., *Endothelial progenitor cells: new targets for therapeutics for inflammatory conditions with high cardiovascular risk.* Frontiers in medicine, 2018. **5**: p. 200.
52. Yoder, M.C., *Is endothelium the origin of endothelial progenitor cells?* Arteriosclerosis, thrombosis, and vascular biology, 2010. **30**(6): p. 1094-1103.
53. Urbich, C. and S. Dimmeler, *Endothelial progenitor cells: characterization and role in vascular biology.* Circulation research, 2004. **95**(4): p. 343-353.
54. Li, M., et al., *Long noncoding RNA/circular noncoding RNA–miRNA–mRNA axes in cardiovascular diseases.* Life sciences, 2019. **233**: p. 116440.
55. Chopra, H., et al., *Insights into endothelial progenitor cells: origin, classification, potentials, and prospects.* Stem cells international, 2018. **2018**.
56. Schmidt-Lucke, C., et al., *Reduced number of circulating endothelial progenitor cells predicts future cardiovascular events: proof of concept for the clinical importance of endogenous vascular repair.* Circulation, 2005. **111**(22): p. 2981-2987.
57. Kumar, D., et al., *Chronic sodium nitrite therapy augments ischemia-induced angiogenesis and arteriogenesis.* Proceedings of the National Academy of Sciences, 2008. **105**(21): p. 7540-7545.
58. Carmeliet, P., *Mechanisms of angiogenesis and arteriogenesis.* Nature medicine, 2000. **6**(4): p. 389-395.
59. Palmer-Kazen, U. and E. Wahlberg, *Arteriogenesis in peripheral arterial disease.* Endothelium, 2003. **10**(4-5): p. 225-232.
60. Annex, B.H., *Therapeutic angiogenesis for critical limb ischaemia.* Nature Reviews Cardiology, 2013. **10**(7): p. 387.
61. Buschmann, I. and W. Schaper, *The pathophysiology of the collateral circulation (arteriogenesis).* The Journal of pathology, 2000. **190**(3): p. 338-342.

62. Lei, Z., et al., *Micro RNA-132/212 family enhances arteriogenesis after hindlimb ischaemia through modulation of the Ras-MAPK pathway.* Journal of cellular and molecular medicine, 2015. **19**(8): p. 1994-2005.
63. Helisch, A. and W. Schaper, *Angiogenesis and arteriogenesis–not yet for prescription.* Zeitschrift für Kardiologie, 2000. **89**(3): p. 239-244.
64. Paszkowiak, J.J. and A. Dardik, *Arterial wall shear stress: observations from the bench to the bedside.* Vascular and endovascular surgery, 2003. **37**(1): p. 47-57.
65. van Oostrom, M.C., et al., *Insights into mechanisms behind arteriogenesis: what does the future hold?* Journal of leukocyte biology, 2008. **84**(6): p. 1379-1391.
66. Scholz, D., et al., *Contribution of arteriogenesis and angiogenesis to postocclusive hindlimb perfusion in mice.* Journal of molecular and cellular cardiology, 2002. **34**(7): p. 775-787.
67. Stabile, E., et al., *Impaired arteriogenic response to acute hindlimb ischemia in CD4-knockout mice.* Circulation, 2003. **108**(2): p. 205-210.
68. Shireman, P.K., *The chemokine system in arteriogenesis and hind limb ischemia.* Journal of vascular surgery, 2007. **45**(6): p. A48-A56.
69. Gandini, R., et al., *Alternative techniques for treatment of complex below-the knee arterial occlusions in diabetic patients with critical limb ischemia.* Cardiovascular and interventional radiology, 2013. **36**(1): p. 75-83.
70. Seiler, C., et al., *The human coronary collateral circulation: development and clinical importance.* European heart journal, 2013. **34**(34): p. 2674-2682.
71. Lupu, I.-E., S. De Val, and N. Smart, *Coronary vessel formation in development and disease: mechanisms and insights for therapy.* Nature Reviews Cardiology, 2020: p. 1-17.
72. Hart, J., *Vascular myography to examine functional responses of isolated blood vessels*, in *Vascular Effects of Hydrogen Sulfide*. 2019, Springer. p. 205-217.
73. Sherman, J.A., et al., *Humoral and cellular factors responsible for coronary collateral formation.* The American journal of cardiology, 2006. **98**(9): p. 1194-1197.
74. Wang, S., et al., *Genetic architecture underlying variation in extent and remodeling of the collateral circulation.* Circulation research, 2010. **107**(4): p. 558-568.
75. Lamblin, N., et al., *A common variant of endothelial nitric oxide synthase (Glu298Asp) is associated with collateral development in patients with chronic coronary occlusions.* BMC cardiovascular disorders, 2005. **5**(1): p. 27.
76. Gulec, S., et al., *Glu298Asp polymorphism of the eNOS gene is associated with coronary collateral development.* Atherosclerosis, 2008. **198**(2): p. 354-359.
77. Resar, J.R., et al., *Hypoxia-inducible factor 1α polymorphism and coronary collaterals in patients with ischemic heart disease.* Chest, 2005. **128**(2): p. 787-791.
78. Liu, Q., et al., *Hypoxia-inducible factor-1α polymorphisms link to coronary artery collateral development and clinical presentation of coronary artery disease.* Biomedical Papers, 2013. **157**(4): p. 340-345.
79. Thomson, J.A., et al., *Embryonic stem cell lines derived from human blastocysts.* science, 1998. **282**(5391): p. 1145-1147.
80. Takahashi, K. and S. Yamanaka, *Induction of pluripotent stem cells from mouse embryonic and adult fibroblast cultures by defined factors.* cell, 2006. **126**(4): p. 663-676.

81. Keller, G., *Embryonic stem cell differentiation: emergence of a new era in biology and medicine.* Genes & development, 2005. **19**(10): p. 1129-1155.
82. Levenberg, S., et al., *Endothelial cells derived from human embryonic stem cells.* Proceedings of the national Academy of Sciences, 2002. **99**(7): p. 4391-4396.
83. McCracken, I.R., et al., *Transcriptional dynamics of pluripotent stem cell-derived endothelial cell differentiation revealed by single-cell RNA sequencing.* European heart journal, 2019.
84. Boulberdaa, M., et al., *A role for the long noncoding RNA SENCR in commitment and function of endothelial cells.* Molecular Therapy, 2016. **24**(5): p. 978-990.
85. MacAskill, M.G., et al., *Robust revascularization in models of limb ischemia using a clinically translatable human stem cell-derived endothelial cell product.* Molecular Therapy, 2018. **26**(7): p. 1669-1684.
86. Paoni, N.F., et al., *Time course of skeletal muscle repair and gene expression following acute hind limb ischemia in mice.* Physiological genomics, 2002. **11**(3): p. 263-272.
87. Monaro, S., S. West, and J. Gullick, *An Integrative Review of Health-Related Quality of Life in Patients with Critical Limb Ischaemia.* Journal of Clinical Nursing, 2016: p. n/a-n/a.
88. Hahn, C. and M.A. Schwartz, *The role of cellular adaptation to mechanical forces in atherosclerosis.* Arteriosclerosis, thrombosis, and vascular biology, 2008. **28**(12): p. 2101-2107.
89. Robless, P., D.P. Mikhailidis, and G.P. Stansby, *Cilostazol for peripheral arterial disease.* Cochrane database of systematic reviews, 2007(1).
90. Choksy, S., et al., *VEGF and VEGF receptor expression in human chronic critical limb ischaemia.* European journal of vascular and endovascular surgery, 2004. **28**(6): p. 660-669.
91. Baumgartner, I., et al., *Constitutive expression of phVEGF165 after intramuscular gene transfer promotes collateral vessel development in patients with critical limb ischemia.* Circulation, 1998. **97**(12): p. 1114-1123.
92. Baumgartner, I., et al., *Lower-extremity edema associated with gene transfer of naked DNA encoding vascular endothelial growth factor.* Annals of internal medicine, 2000. **132**(11): p. 880-884.
93. Yancopoulos, G.D., et al., *Vascular-specific growth factors and blood vessel formation.* Nature, 2000. **407**(6801): p. 242-248.
94. Kusumanto, Y., et al., *Treatment with intramuscular vascular endothelial growth factor gene compared with placebo for patients with diabetes mellitus and critical limb ischemia: a double-blind randomized trial.* Human gene therapy, 2006. **17**(6): p. 683-691.
95. Lawall, H., P. Bramlage, and B. Amann, *Treatment of peripheral arterial disease using stem and progenitor cell therapy.* Journal of vascular surgery, 2011. **53**(2): p. 445-453.
96. Masaki, I., et al., *Angiogenic gene therapy for experimental critical limb ischemia: acceleration of limb loss by overexpression of vascular endothelial growth factor 165 but not of fibroblast growth factor-2.* Circulation research, 2002. **90**(9): p. 966-973.
97. Zhang, J., et al., *Curcumin improves perfusion recovery in experimental peripheral arterial disease by upregulating microRNA-93 expression.* Experimental and therapeutic medicine, 2019. **17**(1): p. 798-802.
98. Couffinhal, T., et al., *Mouse model of angiogenesis.* The American journal of pathology, 1998. **152**(6): p. 1667.

99. Caporali, A., et al., *p75NTR-dependent activation of NF-κB regulates microRNA-503 transcription and pericyte–endothelial crosstalk in diabetes after limb ischaemia.* Nature communications, 2015. **6**: p. 8024.
100. Hellingman, A.A., et al., *Variations in surgical procedures for hind limb ischaemia mouse models result in differences in collateral formation.* European Journal of Vascular and Endovascular Surgery, 2010. **40**(6): p. 796-803.
101. McClung, J.M., et al., *Temporal association between ischemic muscle perfusion recovery and the restoration of muscle contractile function after hindlimb ischemia.* Frontiers in physiology, 2019. **10**: p. 804.
102. Buddeke, J., et al., *Trends in comorbidity in patients hospitalised for cardiovascular disease.* International Journal of Cardiology, 2017. **248**: p. 382-388.
103. Lotfi, S., et al., *Towards a more relevant hind limb model of muscle ischaemia.* Atherosclerosis, 2013. **227**(1): p. 1-8.
104. Dragneva, G., P. Korpisalo, and S. Ylä-Herttuala, *Promoting blood vessel growth in ischemic diseases: challenges in translating preclinical potential into clinical success.* Disease models & mechanisms, 2013. **6**(2): p. 312-322.
105. Smadja, D., J. Silvestre, and B. Levy, *Genic and cellular therapy for peripheral arterial diseases.* Transfusion clinique et biologique: journal de la Societe francaise de transfusion sanguine, 2013. **20**(2): p. 211.
106. Hsieh, P.-L., et al., *Recruitment and therapeutic application of macrophages in skeletal muscles after hind limb ischemia.* Journal of vascular surgery, 2018. **67**(6): p. 1908-1920. e1.
107. Yan, J., et al., *Mesenchymal stem cells as a treatment for peripheral arterial disease: current status and potential impact of type II diabetes on their therapeutic efficacy.* Stem Cell Reviews and Reports, 2013. **9**(3): p. 360-372.
108. Norgren, L., et al., *PLX-PAD Cell Treatment of Critical Limb Ischaemia: Rationale and Design of the PACE Trial.* European Journal of Vascular and Endovascular Surgery, 2019.
109. Pan, T., et al., *Predictors of responders to mononuclear stem cell-based therapeutic angiogenesis for no-option critical limb ischemia.* Stem cell research & therapy, 2019. **10**(1): p. 15.
110. Cagle Jr, S.D. and N. Cooperstein, *Coronary Artery Disease: Diagnosis and Management.* Primary care, 2018. **45**(1): p. 45.
111. Ho, P.M., et al., *Medication nonadherence is associated with a broad range of adverse outcomes in patients with coronary artery disease.* American heart journal, 2008. **155**(4): p. 772-779.
112. Ndrepepa, G., et al., *Impact of therapy with statins, beta-blockers and angiotensin-converting enzyme inhibitors on plasma myeloperoxidase in patients with coronary artery disease.* Clinical Research in Cardiology, 2011. **100**(4): p. 327-333.
113. Oesterle, A., U. Laufs, and J.K. Liao, *Pleiotropic effects of statins on the cardiovascular system.* Circulation research, 2017. **120**(1): p. 229-243.
114. Parviz, Y., et al., *Cellular and molecular approaches to enhance myocardial recovery after myocardial infarction.* Cardiovascular Revascularization Medicine, 2019. **20**(4): p. 351-364.
115. Kranz, A., et al., *Elevation of vascular endothelial growth factor-A serum levels following acute myocardial infarction. Evidence for its origin and functional significance.* Journal of molecular and cellular cardiology, 2000. **32**(1): p. 65-72.

116. Hojo, Y., et al., *Expression of vascular endothelial growth factor in patients with acute myocardial infarction.* Journal of the American College of Cardiology, 2000. **35**(4): p. 968-973.
117. Wang, B., et al., *Targeted delivery of VEGF to treat myocardial infarction*, in *Oxygen Transport to Tissue XXXIV*. 2013, Springer. p. 307-314.
118. Su, H., et al., *Adeno-associated viral vector delivers cardiac-specific and hypoxia-inducible VEGF expression in ischemic mouse hearts.* Proceedings of the National Academy of Sciences, 2004. **101**(46): p. 16280-16285.
119. Hao, X., et al., *Angiogenic and cardiac functional effects of dual gene transfer of VEGF-A165 and PDGF-BB after myocardial infarction.* Biochemical and biophysical research communications, 2004. **322**(1): p. 292-296.
120. Tsang, H., et al., *Large animal models of cardiovascular disease.* Cell biochemistry and function, 2016. **34**(3): p. 113-132.
121. Tao, Z., et al., *Coexpression of VEGF and angiopoietin-1 promotes angiogenesis and cardiomyocyte proliferation reduces apoptosis in porcine myocardial infarction (MI) heart.* Proceedings of the National Academy of Sciences, 2011. **108**(5): p. 2064-2069.
122. Henry, T.D., et al., *The VIVA trial: Vascular endothelial growth factor in Ischemia for Vascular Angiogenesis.* Circulation, 2003. **107**(10): p. 1359-1365.
123. Mendiz, O., et al., *High-Dose Plasmid VEGF Gene Transfer in Patients with Severe Coronary Artery Disease: Final Results of the First Latin American Trial of Gene Therapy in Myocardial Ischemia*. 2011, Am Heart Assoc.
124. Kukuła, K., et al., *Long-term follow-up and safety assessment of angiogenic gene therapy trial VIF-CAD: Transcatheter intramyocardial administration of a bicistronic plasmid expressing VEGF-A165/bFGF cDNA for the treatment of refractory coronary artery disease.* American heart journal, 2019. **215**: p. 78-82.
125. Giacca, M. and S. Zacchigna, *VEGF gene therapy: therapeutic angiogenesis in the clinic and beyond.* Gene therapy, 2012. **19**(6): p. 622-629.
126. Ho-Tin-Noé, B. and J.-B. Michel, *Initiation of angiogenesis in atherosclerosis: smooth muscle cells as mediators of the angiogenic response to atheroma formation.* Trends in cardiovascular medicine, 2011. **21**(7): p. 183-187.
127. Pant, S., A. Deshmukh, and J.L. Mehta, *Angiogenesis in atherosclerosis: an overview*, in *Biochemical Basis and Therapeutic Implications of Angiogenesis*. 2013, Springer. p. 209-224.
128. Zangi, L., et al., *Modified mRNA directs the fate of heart progenitor cells and induces vascular regeneration after myocardial infarction.* Nature biotechnology, 2013. **31**(10): p. 898-907.
129. Gan, L.-M., et al., *Intradermal delivery of modified mRNA encoding VEGF-A in patients with type 2 diabetes.* Nature communications, 2019. **10**(1): p. 1-9.
130. Najjar, S.S., et al., *Intravenous erythropoietin in patients with ST-segment elevation myocardial infarction: REVEAL: a randomized controlled trial.* Jama, 2011. **305**(18): p. 1863-1872.
131. Piepoli, M.F., et al., *Bone marrow cell transplantation improves cardiac, autonomic, and functional indexes in acute anterior myocardial infarction patients (Cardiac Study).* European Journal of Heart Failure, 2010. **12**(2): p. 172-180.
132. Karantalis, V., et al., *Autologous mesenchymal stem cells produce concordant improvements in regional function, tissue perfusion, and fibrotic burden when administered to patients undergoing coronary artery bypass grafting: the Prospective Randomized Study of Mesenchymal Stem Cell*

Therapy in Patients Undergoing Cardiac Surgery (PROMETHEUS) trial. Circulation research, 2014. **114**(8): p. 1302-1310.
133. Choudry, F., et al., *A randomized double-blind control study of early intra-coronary autologous bone marrow cell infusion in acute myocardial infarction: the REGENERATE-AMI clinical trial.* European heart journal, 2016. **37**(3): p. 256-263.
134. Zhou, B. and S.M. Wu, *Reassessment of c-kit in cardiac cells: a complex interplay between expression, fate, and function*. 2018, Am Heart Assoc.
135. Borow, K.M., et al., *Phase 3 DREAM-HF Trial of Mesenchymal Precursor Cells in Chronic Heart Failure: A Review of Biological Plausibility and Implementation of Flexible Clinical Trial Design.* Circulation Research, 2019. **125**(3): p. 265-281.
136. Menasché, P., et al., *Human embryonic stem cell-derived cardiac progenitors for severe heart failure treatment: first clinical case report.* European heart journal, 2015. **36**(30): p. 2011-2017.
137. Traverse, J.H., et al., *First-in-man study of a cardiac extracellular matrix hydrogel in early and late myocardial infarction patients.* JACC: Basic to Translational Science, 2019. **4**(6): p. 659-669.
138. Rodness, J., et al., *VEGF-loaded microsphere patch for local protein delivery to the ischemic heart.* Acta Biomaterialia, 2016. **45**: p. 169-181.
139. Cahill, T.J., R.P. Choudhury, and P.R. Riley, *Heart regeneration and repair after myocardial infarction: translational opportunities for novel therapeutics.* Nature reviews Drug discovery, 2017. **16**(10): p. 699.
140. Gullestad, L., et al., *Intravenous immunoglobulin does not reduce left ventricular remodeling in patients with myocardial dysfunction during hospitalization after acute myocardial infarction.* International journal of cardiology, 2013. **168**(1): p. 212-218.
141. Esteller, M., *Non-coding RNAs in human disease.* Nature Reviews Genetics, 2011. **12**(12): p. 861-874.
142. Ambros, V., *Control of developmental timing in Caenorhabditis elegans.* Current opinion in genetics & development, 2000. **10**(4): p. 428-433.
143. Esquela-Kerscher, A., *The lin-4 microRNA: The ultimate micromanager.* Cell Cycle, 2014. **13**(7): p. 1060-1061.
144. Nelson, P.T., W.X. Wang, and B.W. Rajeev, *MicroRNAs (miRNAs) in neurodegenerative diseases.* Brain pathology, 2008. **18**(1): p. 130-138.
145. Farazi, T.A., et al., *miRNAs in human cancer.* The Journal of pathology, 2011. **223**(2): p. 102-115.
146. Thum, T. and M. Mayr, *Review focus on the role of microRNA in cardiovascular biology and disease*. 2012, Oxford University Press.
147. Azodi, M., et al., *The Missing "lnc" between Genetics and Cardiac Disease.* Non-Coding RNA, 2020. **6**(1): p. 3.
148. Ma, L., et al., *LncBook: a curated knowledgebase of human long non-coding RNAs.* Nucleic acids research, 2019. **47**(D1): p. D128-D134.
149. Lee, H., Z. Zhang, and H.M. Krause, *Long noncoding RNAs and repetitive elements: junk or intimate evolutionary partners?* TRENDS in Genetics, 2019. **35**(12): p. 892-902.
150. Uszczynska-Ratajczak, B., et al., *Towards a complete map of the human long non-coding RNA transcriptome.* Nature Reviews Genetics, 2018. **19**(9): p. 535-548.
151. Ilott, N.E. and C.P. Ponting, *Predicting long non-coding RNAs using RNA sequencing.* Methods, 2013. **63**(1): p. 50-59.
152. Lee, J.T., *Epigenetic regulation by long noncoding RNAs.* Science, 2012. **338**(6113): p. 1435-1439.

153. Azzalin, C.M. and J. Lingner, *Telomere functions grounding on TERRA firma.* Trends in cell biology, 2015. **25**(1): p. 29-36.
154. Goff, L.A., et al., *Spatiotemporal expression and transcriptional perturbations by long noncoding RNAs in the mouse brain.* Proceedings of the National Academy of Sciences, 2015. **112**(22): p. 6855-6862.
155. Derrien, T., et al., *The GENCODE v7 catalog of human long noncoding RNAs: analysis of their gene structure, evolution, and expression.* Genome research, 2012. **22**(9): p. 1775-1789.
156. Xia, C., et al., *Spatial transcriptome profiling by MERFISH reveals subcellular RNA compartmentalization and cell cycle-dependent gene expression.* Proceedings of the National Academy of Sciences, 2019: p. 201912459.
157. Rashid, F., A. Shah, and G. Shan, *Long non-coding RNAs in the cytoplasm.* Genomics, proteomics & bioinformatics, 2016. **14**(2): p. 73-80.
158. Noh, J.H., et al., *Cytoplasmic functions of long noncoding RNAs.* Wiley Interdisciplinary Reviews: RNA, 2018. **9**(3): p. e1471.
159. Wu, L., et al., *Research Progress on Plant Long Non-Coding RNA.* Plants, 2020. **9**(4): p. 408.
160. Trivedi, P.K. and M.H. Asif, *Updates on plant long non-coding RNAs (lncRNAs): the regulatory components.* Plant Cell, Tissue and Organ Culture (PCTOC), 2020: p. 1-11.
161. Parker, S., et al., *Large-scale profiling of noncoding RNA function in yeast.* PLoS genetics, 2018. **14**(3): p. e1007253.
162. Hu, W., J.R. Alvarez-Dominguez, and H.F. Lodish, *Regulation of mammalian cell differentiation by long non-coding RNAs.* EMBO reports, 2012. **13**(11): p. 971-983.
163. Chen, J.-Y., et al., *Emergence, retention and selection: a trilogy of origination for functional de novo proteins from ancestral LncRNAs in primates.* PLoS genetics, 2015. **11**(7): p. e1005391.
164. Guo, C.-J., et al., *Distinct Processing of lncRNAs Contributes to Non-conserved Functions in Stem Cells.* Cell, 2020.
165. Brandes, R.P., J.A. Oo, and M.S. Leisegang, *Thymosin beta-4x LINCs SPAAR to its non-coding function.* Cardiovascular Research, 2020.
166. Wilhelm, D. and P. Bernard, *Non-coding RNA and the reproductive system*. 2016: Springer.
167. Gong, C., et al., *A long non-coding RNA, LncMyoD, regulates skeletal muscle differentiation by blocking IMP2-mediated mRNA translation.* Developmental cell, 2015. **34**(2): p. 181-191.
168. Kotzin, J.J., et al., *The long non-coding RNA Morrbid regulates Bim and short-lived myeloid cell lifespan.* Nature, 2016. **537**(7619): p. 239-243.
169. Yoon, J.-H., K. Abdelmohsen, and M. Gorospe. *Functional interactions among microRNAs and long noncoding RNAs*. in *Seminars in cell & developmental biology*. 2014. Elsevier.
170. Monteiro, J.P., et al., *Endothelial Function and Dysfunction in the Cardiovascular System: The Long Non-Coding Road.* Cardiovascular Research, 2019.
171. Leisegang, M.S., et al., *Long Noncoding RNA MANTIS Facilitates Endothelial Angiogenic Function.* Circulation, 2017: p. CIRCULATIONAHA. 116.026991.
172. West, J.A., et al., *The long noncoding RNAs NEAT1 and MALAT1 bind active chromatin sites.* Molecular cell, 2014. **55**(5): p. 791-802.
173. Zhang, G., et al., *Comprehensive analysis of long noncoding RNA (lncRNA)-chromatin interactions reveals lncRNA functions dependent on binding*

diverse regulatory elements. Journal of Biological Chemistry, 2019. **294**(43): p. 15613-15622.
174. Yu, H.M., et al., *LncRNA NEAT1 promotes the tumorigenesis of colorectal cancer by sponging miR-193a-3p.* Cell proliferation, 2019. **52**(1): p. e12526.
175. Ounzain, S., et al., *CARMEN, a human super enhancer-associated long noncoding RNA controlling cardiac specification, differentiation and homeostasis.* Journal of molecular and cellular cardiology, 2015. **89**: p. 98-112.
176. Elia, L., et al., *The knockout of miR-143 and-145 alters smooth muscle cell maintenance and vascular homeostasis in mice: correlates with human disease.* Cell Death & Differentiation, 2009. **16**(12): p. 1590-1598.
177. Lee, S., et al., *Noncoding RNA NORAD regulates genomic stability by sequestering PUMILIO proteins.* Cell, 2016. **164**(1-2): p. 69-80.
178. Zhang, J., et al., *LncRNA NORAD contributes to colorectal cancer progression by inhibition of miR-202-5p.* Oncology Research Featuring Preclinical and Clinical Cancer Therapeutics, 2018. **26**(9): p. 1411-1418.
179. Makarewich, C.A. and E.N. Olson, *Mining for micropeptides.* Trends in cell biology, 2017. **27**(9): p. 685-696.
180. Guo, B., et al., *Micropeptide CIP 2A-BP encoded by LINC 00665 inhibits triple-negative breast cancer progression.* The EMBO Journal, 2020. **39**(1): p. e102190.
181. Bi, P., et al., *Control of muscle formation by the fusogenic micropeptide myomixer.* Science, 2017. **356**(6335): p. 323-327.
182. Makarewich, C.A., et al., *DWORF: a Novel Cardiac Micropeptide That Enhances SERCA Activity and Cardiomyocyte Contractility.* Circulation Research, 2015. **117**(suppl_1): p. A339-A339.
183. Makarewich, C.A., et al., *The DWORF micropeptide enhances contractility and prevents heart failure in a mouse model of dilated cardiomyopathy.* Elife, 2018. **7**: p. e38319.
184. Wang, L., et al., *The micropeptide LEMP plays an evolutionarily conserved role in myogenesis.* Cell death & disease, 2020. **11**(5): p. 1-12.
185. Bhatta, A., et al., *A Mitochondrial Micropeptide Is Required for Activation of the Nlrp3 Inflammasome.* The Journal of Immunology, 2020. **204**(2): p. 428-437.
186. Grelet, S., et al., *A regulated PNUTS mRNA to lncRNA splice switch mediates EMT and tumour progression.* Nature Cell Biology, 2017. **19**(9): p. 1105-1115.
187. Ballantyne, M.D., et al., *Smooth Muscle Enriched Long Non-Coding RNA (SMILR) Regulates Cell Proliferation.* Circulation, 2016: p. CIRCULATIONAHA. 115.021019.
188. Michalik, K.M., et al., *Long noncoding RNA MALAT1 regulates endothelial cell function and vessel growth.* Circulation research, 2014. **114**(9): p. 1389-1397.
189. Kurian, L., et al., *Identification of novel long noncoding RNAs underlying vertebrate cardiovascular development.* Circulation, 2015. **131**(14): p. 1278-1290.
190. Ounzain, S., et al., *Discovery and functional characterization of cardiovascular long noncoding RNAs.* Journal of Molecular and Cellular Cardiology, 2015. **89**: p. 17-26.
191. Wang, K., et al., *The Long Noncoding RNA CHRF Regulates Cardiac Hypertrophy by Targeting miR-489Novelty and Significance.* Circulation research, 2014. **114**(9): p. 1377-1388.

192. Liu, S.J., et al., *CRISPRi-based genome-scale identification of functional long noncoding RNA loci in human cells.* Science, 2016: p. aah7111.
193. Liu, L., et al., *The H19 long noncoding RNA is a novel negative regulator of cardiomyocyte hypertrophy.* Cardiovascular Research, 2016. **111**(1): p. 56-65.
194. Micheletti, R., et al., *The long noncoding RNA Wisper controls cardiac fibrosis and remodeling.* Science translational medicine, 2017. **9**(395): p. eaai9118.
195. Kumarswamy, R., et al., *The circulating long non-coding RNA LIPCAR predicts survival in heart failure patients.* Circulation research, 2014: p. CIRCRESAHA. 114.303915.
196. Zhu, J., et al., *Expression of lncRNA Novlnc6 in plasma and its clinical correlation with coronary artery disease.* Biomedical Research, 2017. **28**(16).
197. Hennessy, E.J., et al., *The long noncoding RNA CHROME regulates cholesterol homeostasis in primates.* Nature Metabolism, 2018: p. 1.
198. Klattenhoff, C.A., et al., *Braveheart, a long noncoding RNA required for cardiovascular lineage commitment.* Cell, 2013. **152**(3): p. 570-583.
199. Grote, P., et al., *The tissue-specific lncRNA Fendrr is an essential regulator of heart and body wall development in the mouse.* Developmental cell, 2013. **24**(2): p. 206-214.
200. Liu, J., et al., *HBL1 Is a Human Long Noncoding RNA that Modulates Cardiomyocyte Development from Pluripotent Stem Cells by Counteracting MIR1.* Developmental cell, 2017. **42**(4): p. 333-348. e5.
201. Li, K., et al., *A noncoding antisense RNA in tie-1 locus regulates tie-1 function in vivo.* Blood, The Journal of the American Society of Hematology, 2010. **115**(1): p. 133-139.
202. Neumann, P., et al., *The lncRNA GATA6-AS epigenetically regulates endothelial gene expression via interaction with LOXL2.* Nature communications, 2018. **9**(1): p. 237.
203. Yan, B., et al., *lncRNA-MIAT regulates microvascular dysfunction by functioning as a competing endogenous RNA.* Circulation research, 2015. **116**(7): p. 1143-1156.
204. Lai, Y., et al., *HOTAIR functions as a competing endogenous RNA to regulate PTEN expression by inhibiting miR-19 in cardiac hypertrophy.* Molecular and cellular biochemistry, 2017: p. 1-9.
205. Carrion, K., et al., *The long non-coding HOTAIR is modulated by cyclic stretch and WNT/β-CATENIN in human aortic valve cells and is a novel repressor of calcification genes.* PloS one, 2014. **9**(5): p. e96577.
206. Jiang, F., X. Zhou, and J. Huang, *Long non-coding RNA-ROR mediates the reprogramming in cardiac hypertrophy.* PloS one, 2016. **11**(4): p. e0152767.
207. Wang, K., et al., *CARL lncRNA inhibits anoxia-induced mitochondrial fission and apoptosis in cardiomyocytes by impairing miR-539-dependent PHB2 downregulation.* Nature communications, 2014. **5**.
208. Lai, L., et al., *LncRNA KCNQ1OT1 contributes to cardiomyocyte apoptosis by targeting FUS in heart failure.* Experimental and Molecular Pathology, 2020: p. 104480.
209. Zhang, Y., et al., *KCNQ 1 OT 1, HIF 1A-AS 2 and APOA 1-AS are promising novel biomarkers for diagnosis of coronary artery disease.* Clinical and Experimental Pharmacology and Physiology, 2019. **46**(7): p. 635-642.
210. Zhao, R., et al., *Inhibition of long noncoding RNA BDNF-AS rescues cell death and apoptosis in hypoxia/reoxygenation damaged murine cardiomyocyte.* Biochimie, 2017. **138**: p. 43-49.

211. Mahmoud, A.D., et al., *The Human-and Smooth Muscle Cell-Enriched lncRNA SMILR Promotes Proliferation by Regulating Mitotic CENPF mRNA and Drives Cell-Cycle Progression Which Can Be Targeted to Limit Vascular Remodeling.* Circulation research, 2019.
212. Leung, A., et al., *Novel long non-coding RNAs are regulated by angiotensin II in vascular smooth muscle cells.* Circulation research, 2013: p. CIRCRESAHA. 112.300849.
213. Wang, H., R. Qin, and Y. Cheng, *LncRNA-Ang362 promotes pulmonary arterial hypertension by regulating miR-221 and miR-222.* Shock, 2020. **53**(6): p. 723-729.
214. Chen, G., et al., *Lnc-Ang362 is a pro-fibrotic long non-coding RNA promoting cardiac fibrosis after myocardial infarction by suppressing Smad7.* Archives of Biochemistry and Biophysics, 2020: p. 108354.
215. Wu, G., et al., *LincRNA-p21 regulates neointima formation, vascular smooth muscle cell proliferation, apoptosis and atherosclerosis by enhancing p53 activity.* Circulation, 2014: p. CIRCULATIONAHA. 114.011675.
216. Zhao, Y., et al., *Regulation of apoptosis by long non-coding RNA HIF1A-AS1 in VSMCs: implications for TAA pathogenesis.* International journal of clinical and experimental pathology, 2014. **7**(11): p. 7643.
217. Hansson, G.K., *Immune mechanisms in atherosclerosis.* Arteriosclerosis, thrombosis, and vascular biology, 2001. **21**(12): p. 1876-1890.
218. Jung, M., M. Dodsworth, and T. Thum, *Inflammatory cells and their non-coding RNAs as targets for treating myocardial infarction.* Basic Research in Cardiology, 2019. **114**(1): p. 4.
219. Boeckel, J.-N., et al., *Identification and regulation of the long non-coding RNA Heat2 in heart failure.* Journal of molecular and cellular cardiology, 2019. **126**: p. 13-22.
220. Ishii, N., et al., *Identification of a novel non-coding RNA, MIAT, that confers risk of myocardial infarction.* Journal of human genetics, 2006. **51**(12): p. 1087-1099.
221. Gast, M., et al., *Long noncoding RNA NEAT1 modulates immune cell functions and is suppressed in early onset myocardial infarction patients.* Cardiovascular research, 2019. **115**(13): p. 1886-1906.
222. Hung, J., et al., *Novel plaque enriched long noncoding RNA in atherosclerotic macrophage regulation (PELATON).* Arteriosclerosis, thrombosis, and vascular biology, 2020. **40**(3): p. 697-713.
223. Small, E.M., R.J. Frost, and E.N. Olson, *MicroRNAs add a new dimension to cardiovascular disease.* Circulation, 2010. **121**(8): p. 1022-1032.
224. Procházka, V., et al., *The role of miR-126 in critical limb ischemia treatment using adipose-derived stem cell therapeutic factor concentrate and extracellular matrix microparticles.* Medical science monitor: international medical journal of experimental and clinical research, 2018. **24**: p. 511.
225. Cheng, B., et al., *MiR-323b-5p acts as a novel diagnostic biomarker for critical limb ischemia in type 2 diabetic patients.* Scientific reports, 2018. **8**(1): p. 15080.
226. Pérez-Cremades, D., H.S. Cheng, and M.W. Feinberg, *Noncoding RNAs in Critical Limb Ischemia.* Arteriosclerosis, Thrombosis, and Vascular Biology, 2020: p. ATVBAHA. 119.312860.
227. Boon, R.A., et al., *Long Noncoding RNA Meg3 Controls Endothelial Cell Aging and Function.* Journal of the American College of Cardiology, 2016. **68**(23): p. 2589-2591.
228. Liang, H., et al., *LncRNA PFL contributes to cardiac fibrosis by acting as a competing endogenous RNA of let-7d.* Theranostics, 2018. **8**(4): p. 1180.

229. van Heesch, S., et al., *The translational landscape of the human heart.* Cell, 2019.
230. Han, P., et al., *A long noncoding RNA protects the heart from pathological hypertrophy.* Nature, 2014. **514**(7520): p. 102.
231. Wang, Z., et al., *The long noncoding RNA Chaer defines an epigenetic checkpoint in cardiac hypertrophy.* Nature medicine, 2016. **22**(10): p. 1131.
232. Matsumoto, A., et al., *mTORC1 and muscle regeneration are regulated by the LINC00961-encoded SPAR polypeptide.* Nature, 2017. **541**(7636): p. 228.
233. Zheng, Z.-G., et al., *The Essential Role of H19 Contributing to Cisplatin Resistance by Regulating Glutathione Metabolism in High-Grade Serous Ovarian Cancer.* Scientific reports, 2016. **6**.
234. Huang, Z., et al., *Long noncoding RNA LINC00961 inhibits cell proliferation and induces cell apoptosis in human non–small cell lung cancer.* Journal of cellular biochemistry, 2018. **119**(11): p. 9072-9080.
235. Yu, H., et al., *Identification and Validation of Long Noncoding RNA Biomarkers in Human Non–Small-Cell Lung Carcinomas.* Journal of Thoracic Oncology, 2015. **10**(4): p. 645-654.
236. Jiang, B., et al., *Long noncoding RNA LINC00961 inhibits cell invasion and metastasis in human non-small cell lung cancer.* Biomedicine & Pharmacotherapy, 2018. **97**: p. 1311-1318.
237. Liu, J., Y. Xu, and J. Yan, *An 11-lncRNA risk scoring model predicts prognosis of lung squamous cell carcinoma.* European Review for Medical and Pharmacological Sciences, 2020. **24**(10): p. 5456-5464.
238. Yin, J., et al., *Small regulatory polypeptide of amino acid response negatively relates to poor prognosis and controls hepatocellular carcinoma progression via regulating microRNA-5581-3p/human cardiolipin synthase 1.* Journal of cellular physiology, 2019.
239. Chen, D., et al., *LINC00961 restrains cancer progression via modulating epithelial–mesenchymal transition in renal cell carcinoma.* Journal of cellular physiology, 2019. **234**(5): p. 7257-7265.
240. Amini, M.A., et al., *Overexpression of TPT1-AS1 and SAMMSON and down expression of LINC00961 associated with Advanced Grades of Gastric Cancer.* 2020.
241. Mu, X., et al., *Linc00961 inhibits the proliferation and invasion of skin melanoma by targeting the miR-367/PTEN axis.* International journal of oncology, 2019. **55**(3): p. 708-720.
242. Kappelmann-Fenzl, M., et al., *C-Jun drives melanoma progression in PTEN wild type melanoma cells.* Cell death & disease, 2019. **10**(8): p. 1-16.
243. Layeghi, S.M., et al., *Evaluation of the potential role of long non-coding RNA LINC00961 in luminal breast cancer: a case–control and systems biology study.* Cancer Cell International, 2020. **20**(1): p. 1-13.
244. Wu, H., et al., *LINC00961 inhibits the migration and invasion of colon cancer cells by sponging miR-223-3p and targeting SOX11.* Cancer Medicine, 2020.
245. Di Salvo, T.G., et al., *Right ventricular long noncoding RNA expression in human heart failure.* Pulmonary circulation, 2015. **5**(1): p. 135-161.
246. Wu, C., S. Liu, and M. Tang, *Downregulation of linc00961 contributes to promote proliferation and inhibit apoptosis of vascular smooth muscle cell by sponging miR-367 in patients with coronary heart disease.* European review for medical and pharmacological sciences, 2019. **23**(19): p. 8540-8550.
247. Liu, S., et al., *STAT1-avtiviated LINC00961 regulates myocardial infarction by the PI3K/AKT/GSK3β signaling pathway.* Journal of cellular biochemistry, 2019. **120**(8): p. 13226-13236.

248. Arslan, F., et al., *Mesenchymal stem cell-derived exosomes increase ATP levels, decrease oxidative stress and activate PI3K/Akt pathway to enhance myocardial viability and prevent adverse remodeling after myocardial ischemia/reperfusion injury.* Stem cell research, 2013. **10**(3): p. 301-312.
249. Zhang, L., L. Shao, and Y. Hu, *Long noncoding RNA LINC00961 inhibited cell proliferation and invasion through regulating the Wnt/β-catenin signaling pathway in tongue squamous cell carcinoma.* Journal of cellular biochemistry, 2019.
250. LU, X., et al., *Increased expression of long noncoding RNA LINC00961 suppresses glioma metastasis and correlates with favorable prognosis.* European Review for Medical and Pharmacological Sciences, 2018. **22**: p. 4917-4924.
251. Livak, K.J. and T.D. Schmittgen, *Analysis of relative gene expression data using real-time quantitative PCR and the 2− ΔΔCT method.* methods, 2001. **25**(4): p. 402-408.
252. Dufton, N.P., et al., *Dynamic regulation of canonical TGFβ signalling by endothelial transcription factor ERG protects from liver fibrogenesis.* Nature communications, 2017. **8**(1): p. 1-14.
253. Chouchani, E.T., et al., *Ischaemic accumulation of succinate controls reperfusion injury through mitochondrial ROS.* Nature, 2014. **515**(7527): p. 431.
254. Spencer, H.L., et al., *The LINC00961 transcript and its encoded micropeptide, small regulatory polypeptide of amino acid response, regulate endothelial cell function.* Cardiovascular Research, 2020.
255. Birdsey, G.M., et al., *Transcription factor Erg regulates angiogenesis and endothelial apoptosis through VE-cadherin.* Blood, 2008. **111**(7): p. 3498-3506.
256. Shah, A.V., G.M. Birdsey, and A.M. Randi, *Regulation of endothelial homeostasis, vascular development and angiogenesis by the transcription factor ERG.* Vascular pharmacology, 2016. **86**: p. 3-13.
257. Reddy, E., V.N. Rao, and T.S. Papas, *The erg gene: a human gene related to the ets oncogene.* Proceedings of the National Academy of Sciences, 1987. **84**(17): p. 6131-6135.
258. Adamo, P. and M. Ladomery, *The oncogene ERG: a key factor in prostate cancer.* Oncogene, 2016. **35**(4): p. 403-414.
259. Kalna, V., et al., *The transcription factor ERG regulates super-enhancers associated with an endothelial-specific gene expression program.* Circulation research, 2019. **124**(9): p. 1337-1349.
260. Pimanda, J.E., et al., *Endoglin expression in the endothelium is regulated by Fli-1, Erg, and Elf-1 acting on the promoter and a–8-kb enhancer.* Blood, 2006. **107**(12): p. 4737-4745.
261. Shah, A., et al., *The endothelial transcription factor ERG mediates Angiopoietin-1-dependent control of Notch signalling and vascular stability.* Nature communications, 2017. **8**(1): p. 1-16.
262. Zhang, H., et al., *ZO-1 expression is suppressed by GM-CSF via miR-96/ERG in brain microvascular endothelial cells.* Journal of Cerebral Blood Flow & Metabolism, 2018. **38**(5): p. 809-822.
263. Ylipää, A., et al., *Transcriptome sequencing reveals PCAT5 as a novel ERG-regulated long noncoding RNA in prostate cancer.* Cancer research, 2015. **75**(19): p. 4026-4031.
264. Kohvakka, A., et al., *AR and ERG drive the expression of prostate cancer specific long noncoding RNAs.* Oncogene, 2020. **39**(30): p. 5241-5251.

265. Vellingiri, V., et al., *Endothelial specific ERG gene is required for preventing pulmonary vascular complications by regulating sprouting angiogenesis and inflammation.* The FASEB Journal, 2020. **34**(S1): p. 1-1.
266. Martello, A., et al., *Phenotypic miRNA screen identifies miR-26b to promote the growth and survival of endothelial cells.* Molecular Therapy-Nucleic Acids, 2018. **13**: p. 29-43.
267. Zhang, X., et al., *Long Non-Coding RNA Malat1 Regulates Angiogenesis in Hindlimb Ischemia.* International journal of molecular sciences, 2018. **19**(6).
268. Vervoort, V.S., et al., *Splice variants and expression patterns of SHEP1, BCAR3 and NSP1, a gene family involved in integrin and receptor tyrosine kinase signaling.* Gene, 2007. **391**(1-2): p. 161-170.
269. Evrard, C., S. Caron, and P. Rouget, *Functional analysis of the NPDC-1 gene.* Gene, 2004. **343**(1): p. 153-163.
270. Evrard, C. and P. Rouget, *Subcellular localization of neural-specific NPDC-1 protein.* Journal of neuroscience research, 2005. **79**(6): p. 747-755.
271. Villain, G., et al., *MAGP-1 and fibronectin control EGFL 7 functions by driving its deposition into distinct endothelial extracellular matrix locations.* The FEBS Journal, 2018. **285**(23): p. 4394-4412.
272. Richter, A., et al., *EGFL7 mediates BMP9-induced sprouting angiogenesis of endothelial cells derived from human embryonic stem cells.* Stem cell reports, 2019. **12**(6): p. 1250-1259.
273. Hellström, M., et al., *Dll4 signalling through Notch1 regulates formation of tip cells during angiogenesis.* Nature, 2007. **445**(7129): p. 776-780.
274. Usuba, R., et al., *EGFL7 regulates sprouting angiogenesis and endothelial integrity in a human blood vessel model.* Biomaterials, 2019. **197**: p. 305-316.
275. Fish, J.E., et al., *miR-126 regulates angiogenic signaling and vascular integrity.* Developmental cell, 2008. **15**(2): p. 272-284.
276. Zhou, Q., et al., *LncEGFL7OS regulates human angiogenesis by interacting with MAX at the EGFL7/miR-126 locus.* Elife, 2019. **8**: p. e40470.
277. Yu, B., et al., *An integrated hypothesis for miR-126 in vascular disease.* Medical Research Archives, 2020. **8**(5).
278. Sutherland, J.M., et al., *The Musashi family of RNA binding proteins: master regulators of multiple stem cell populations*, in *Transcriptional and Translational Regulation of Stem Cells*. 2013, Springer. p. 233-245.
279. das Chagas, P.F., et al., *Interplay between the RNA binding-protein Musashi and developmental signaling pathways.* The journal of gene medicine, 2020. **22**(1): p. e3136.
280. Nishimoto, Y. and H. Okano, *New insight into cancer therapeutics: induction of differentiation by regulating the Musashi/Numb/Notch pathway.* Cell research, 2010. **20**(10): p. 1083-1085.
281. Horisawa, K., et al., *The Musashi family RNA-binding proteins in stem cells.* Biomolecular concepts, 2010. **1**(1): p. 59-66.
282. de Andrés-Aguayo, L., F. Varas, and T. Graf, *Musashi 2 in hematopoiesis.* Current opinion in hematology, 2012. **19**(4): p. 268-272.
283. MacNicol, M.C., C.E. Cragle, and A.M. MacNicol, *Context-dependent regulation of Musashi-mediated mRNA translation and cell cycle regulation.* Cell Cycle, 2011. **10**(1): p. 39-44.
284. Kudinov, A., et al., *Musashi-2 (MSI2) drives TGFBR1/SMAD3 dependent partial EMT and supports VEGFR2 expression and metastasis of human and mouse NSCLC cells*. 2016, AACR.

285. Wang, Z.-L., et al., *Emerging roles of the long non-coding RNA 01296/microRNA-143-3p/MSI2 axis in development of thyroid cancer.* Bioscience reports, 2019. **39**(11).
286. Zhan, Y., et al., *Long non-coding RNA DANCR promotes malignant phenotypes of bladder cancer cells by modulating the miR-149/MSI2 axis as a ceRNA.* Journal of Experimental & Clinical Cancer Research, 2018. **37**(1): p. 273.
287. Zhan, Y., et al., *Long non-coding RNA SOX2OT promotes the stemness phenotype of bladder cancer cells by modulating SOX2.* Molecular cancer, 2020. **19**(1): p. 25.
288. Kudinov, A.E., et al., *Musashi-2 (MSI2) supports TGF-β signaling and inhibits claudins to promote non-small cell lung cancer (NSCLC) metastasis.* Proceedings of the National Academy of Sciences, 2016. **113**(25): p. 6955-6960.
289. Medina, P.P. and M. Sanchez-Cespedes, *Involvement of the chromatin-remodeling factor BRG1/SMARCA4 in human cancer.* Epigenetics, 2008. **3**(2): p. 64-68.
290. Duim, S.N., M.-J. Goumans, and B.P. Kruithof, *WT1 in cardiac development and disease*, in *Wilms Tumor [Internet]*. 2016, Codon Publications.
291. Vieira, J.M., et al., *BRG1-SWI/SNF-dependent regulation of the Wt1 transcriptional landscape mediates epicardial activity during heart development and disease.* Nature communications, 2017. **8**(1): p. 1-12.
292. Ogley, R., et al., *Wt1 Influences Regenerative Angiogenic Function of the Vascular Endothelium.* Circulation Research, 2017. **121**(suppl_1): p. A370-A370.
293. McCarty, G., O. Awad, and D.M. Loeb, *WT1 protein directly regulates expression of vascular endothelial growth factor and is a mediator of tumor response to hypoxia.* Journal of Biological Chemistry, 2011. **286**(51): p. 43634-43643.
294. Zammit, P.S. *Function of the myogenic regulatory factors Myf5, MyoD, Myogenin and MRF4 in skeletal muscle, satellite cells and regenerative myogenesis*. in *Seminars in cell & developmental biology*. 2017. Elsevier.
295. Lepper, C., T.A. Partridge, and C.-M. Fan, *An absolute requirement for Pax7-positive satellite cells in acute injury-induced skeletal muscle regeneration.* Development, 2011. **138**(17): p. 3639-3646.
296. Sambasivan, R., et al., *Pax7-expressing satellite cells are indispensable for adult skeletal muscle regeneration.* Development, 2011. **138**(17): p. 3647-3656.
297. Zammit, P.S., et al., *Pax7 and myogenic progression in skeletal muscle satellite cells.* Journal of cell science, 2006. **119**(9): p. 1824-1832.
298. Meadows, E., et al., *Myogenin regulates a distinct genetic program in adult muscle stem cells.* Developmental biology, 2008. **322**(2): p. 406-414.
299. Murakami, K., et al., *Human ERG-2 protein is a phosphorylated DNA-binding protein--a distinct member of the ets family.* Oncogene, 1993. **8**(6): p. 1559.
300. Verger, A. and M. Duterque-Coquillaud, *When Ets transcription factors meet their partners.* Bioessays, 2002. **24**(4): p. 362-370.
301. Reiter, F., S. Wienerroither, and A. Stark, *Combinatorial function of transcription factors and cofactors.* Current opinion in genetics & development, 2017. **43**: p. 73-81.
302. Deramaudt, T.B., P. Remy, and P. Stiegler, *Identification of interaction partners for two closely-related members of the ETS protein family, FLI and ERG.* Gene, 2001. **274**(1-2): p. 169-177.

303. Sementchenko, V.I. and D.K. Watson, *Ets target genes: past, present and future.* Oncogene, 2000. **19**(55): p. 6533-6548.
304. Birdsey, G.M., et al., *The transcription factor Erg regulates expression of histone deacetylase 6 and multiple pathways involved in endothelial cell migration and angiogenesis.* Blood, The Journal of the American Society of Hematology, 2012. **119**(3): p. 894-903.
305. Donovan, D., et al., *Comparison of three in vitro human 'angiogenesis' assays with capillaries formed in vivo.* Angiogenesis, 2001. **4**(2): p. 113-121.
306. Cardoso-Moreira, M., et al., *Gene expression across mammalian organ development.* Nature, 2019. **571**(7766): p. 505-509.
307. Chang, J., et al., *Pathology of myocardial infarction.* Diagnostic Histopathology, 2013. **19**(1): p. 7-12.
308. Cabili, M.N., et al., *Integrative annotation of human large intergenic noncoding RNAs reveals global properties and specific subclasses.* Genes & development, 2011. **25**(18): p. 1915-1927.
309. Hosono, Y., et al., *Oncogenic role of THOR, a conserved cancer/testis long non-coding RNA.* Cell, 2017. **171**(7): p. 1559-1572. e20.
310. Wichman, L., et al., *Dynamic expression of long noncoding RNAs reveals their potential roles in spermatogenesis and fertility.* Biology of reproduction, 2017. **97**(2): p. 313-323.
311. Anguera, M.C., et al., *Tsx produces a long noncoding RNA and has general functions in the germline, stem cells, and brain.* PLoS genetics, 2011. **7**(9).
312. Zhang, L., et al., *A novel ncRNA gene from mouse chromosome 5 trans-splices with Dmrt1 on chromosome 19.* Biochemical and biophysical research communications, 2010. **400**(4): p. 696-700.
313. Liu, J., et al., *miR-223-3p regulates cell growth and apoptosis via FBXW7 suggesting an oncogenic role in human testicular germ cell tumors.* International journal of oncology, 2017. **50**(2): p. 356-364.
314. Matsumoto, A., J.G. Clohessy, and P.P. Pandolfi, *SPAR, a lncRNA encoded mTORC1 inhibitor.* Cell Cycle, 2017. **541**(7636): p. 1-2.
315. Fang, G., et al., *MicroRNA-223-3p regulates ovarian cancer cell proliferation and invasion by targeting SOX11 expression.* International journal of molecular sciences, 2017. **18**(6): p. 1208.
316. Mattiske, D., et al., *A novel long non-coding RNA, Leat1, causes reduced anogenital distance and fertility in female mice.* Differentiation, 2020. **112**: p. 1-6.
317. Ghazal, S., et al., *H19 lncRNA alters stromal cell growth via IGF signaling in the endometrium of women with endometriosis.* EMBO molecular medicine, 2015. **7**(8): p. 996-1003.
318. Keniry, A., et al., *The H19 lincRNA is a developmental reservoir of miR-675 that suppresses growth and Igf1r.* Nature cell biology, 2012. **14**(7): p. 659-665.
319. Ergaz, Z., M. Avgil, and A. Ornoy, *Intrauterine growth restriction—etiology and consequences: what do we know about the human situation and experimental animal models?* Reproductive Toxicology, 2005. **20**(3): p. 301-322.
320. Janot, M., et al., *Bilateral uterine vessel ligation as a model of intrauterine growth restriction in mice.* Reproductive biology and endocrinology, 2014. **12**(1): p. 62.
321. Prior, T., et al., *Sex specific differences in fetal middle cerebral artery and umbilical venous Doppler.* PLoS One, 2013. **8**(2).

322. Cahill, L.S., et al., *Brain sparing in fetal mice: BOLD MRI and Doppler ultrasound show blood redistribution during hypoxia.* Journal of Cerebral Blood Flow & Metabolism, 2014. **34**(6): p. 1082-1088.
323. Cahill, L.S., et al., *Fetal brain sparing in a mouse model of chronic maternal hypoxia.* Journal of Cerebral Blood Flow & Metabolism, 2019. **39**(6): p. 1172-1184.
324. Godfrey, K.M., et al., *Fetal liver blood flow distribution: role in human developmental strategy to prioritize fat deposition versus brain development.* PloS one, 2012. **7**(8).
325. Gremlich, S., et al., *The long non-coding RNA NEAT1 is increased in IUGR placentas, leading to potential new hypotheses of IUGR origin/development.* Placenta, 2014. **35**(1): p. 44-49.
326. Koukoura, O., et al., *Hypomethylation along with increased H19 expression in placentas from pregnancies complicated with fetal growth restriction.* Placenta, 2011. **32**(1): p. 51-57.
327. Zuckerwise, L., et al., *H19 long noncoding RNA alters trophoblast cell migration and invasion by regulating TβR3 in placentae with fetal growth restriction.* Oncotarget, 2016. **7**(25): p. 38398.
328. Basak, K., et al., *Non-invasive determination of murine placental and foetal functional parameters with multispectral optoacoustic tomography.* Light: Science & Applications, 2019. **8**(1): p. 1-10.
329. Demicheva, E. and F. Crispi, *Long-term follow-up of intrauterine growth restriction: cardiovascular disorders.* Fetal diagnosis and therapy, 2014. **36**(2): p. 143-153.
330. Salam, R.A., J.K. Das, and Z.A. Bhutta, *Impact of intrauterine growth restriction on long-term health.* Current Opinion in Clinical Nutrition & Metabolic Care, 2014. **17**(3): p. 249-254.
331. Devaskar, S.U. and A. Chu, *Intrauterine growth restriction: hungry for an answer.* Physiology, 2016. **31**(2): p. 131-146.
332. Bhasin, K.K.S., et al., *Maternal low-protein diet or hypercholesterolemia reduces circulating essential amino acids and leads to intrauterine growth restriction.* Diabetes, 2009. **58**(3): p. 559-566.
333. Skilton, M.R., et al., *Aortic wall thickness in newborns with intrauterine growth restriction.* The Lancet, 2005. **365**(9469): p. 1484-1486.
334. Diderholm, B., *Perinatal energy metabolism with reference to IUGR & SGA: studies in pregnant women & newborn infants.* Indian J Med Res, 2009. **130**(5): p. 612-7.
335. Yang, B.T., et al., *Increased DNA methylation and decreased expression of PDX-1 in pancreatic islets from patients with type 2 diabetes.* Molecular endocrinology, 2012. **26**(7): p. 1203-1212.
336. Xu, J., et al., *Regulation of human trophoblast GLUT3 glucose transporter by mammalian target of rapamycin signaling.* International journal of molecular sciences, 2015. **16**(6): p. 13815-13828.
337. Jansson, T., I.L. Aye, and D.C. Goberdhan, *The emerging role of mTORC1 signaling in placental nutrient-sensing.* Placenta, 2012. **33**: p. e23-e29.
338. Desai, M., et al., *Programmed upregulation of adipogenic transcription factors in intrauterine growth-restricted offspring.* Reproductive sciences, 2008. **15**(8): p. 785-796.
339. Sarr, O., K. Yang, and T.R. Regnault, *c.* Journal of pregnancy, 2012. **2012**.
340. Murji, A., et al., *Male sex bias in placental dysfunction.* American Journal of Medical Genetics Part A, 2012. **158**(4): p. 779-783.

341. Power, M.L. and J. Schulkin, *Sex differences in fat storage, fat metabolism, and the health risks from obesity: possible evolutionary origins.* British Journal of Nutrition, 2008. **99**(5): p. 931-940.
342. Hezroni, H., et al., *Principles of long noncoding RNA evolution derived from direct comparison of transcriptomes in 17 species.* Cell reports, 2015. **11**(7): p. 1110-1122.
343. Zhao, Q., et al., *LncPipe: A Nextflow-based pipeline for identification and analysis of long non-coding RNAs from RNA-Seq data.* J Genet Genomics, 2018. **45**(7): p. 399-401.
344. Voellenkle, C., et al., *Implication of Long noncoding RNAs in the endothelial cell response to hypoxia revealed by RNA-sequencing.* Scientific reports, 2016. **6**: p. 24141.
345. Ulveling, D., C. Francastel, and F. Hubé, *When one is better than two: RNA with dual functions.* Biochimie, 2011. **93**(4): p. 633-644.
346. Frohman, M.A., M.K. Dush, and G.R. Martin, *Rapid production of full-length cDNAs from rare transcripts: amplification using a single gene-specific oligonucleotide primer.* Proceedings of the National Academy of Sciences, 1988. **85**(23): p. 8998-9002.
347. Lagarde, J., et al., *Extension of human lncRNA transcripts by RACE coupled with long-read high-throughput sequencing (RACE-Seq).* Nature communications, 2016. **7**(1): p. 1-11.
348. Yeku, O. and M.A. Frohman, *Rapid amplification of cDNA ends (RACE)*, in *RNA*. 2011, Springer. p. 107-122.
349. Nam, J.-W., S.-W. Choi, and B.-H. You, *Incredible RNA: dual functions of coding and noncoding.* Molecules and cells, 2016. **39**(5): p. 367.
350. Vacante, F., et al., *The function of miR-143, miR-145 and the MiR-143 host gene in cardiovascular development and disease.* Vascular Pharmacology, 2019. **112**: p. 24-30.
351. Tosic, M., et al., *Lsd1 regulates skeletal muscle regeneration and directs the fate of satellite cells.* Nature communications, 2018. **9**(1): p. 366.
352. Prasain, N. and T. Stevens, *The actin cytoskeleton in endothelial cell phenotypes.* Microvascular research, 2009. **77**(1): p. 53-63.
353. Lamalice, L., F. Le Boeuf, and J. Huot, *Endothelial cell migration during angiogenesis.* Circulation research, 2007. **100**(6): p. 782-794.
354. Li, Z., et al., *Single-cell transcriptome analyses reveal novel targets modulating cardiac neovascularization by resident endothelial cells following myocardial infarction.* European heart journal, 2019. **40**(30): p. 2507-2520.
355. Payne, S., S. De Val, and A. Neal, *Endothelial-Specific Cre Mouse Models: Is Your Cre CREdibile?* Arteriosclerosis, thrombosis, and vascular biology, 2018. **38**(11): p. 2550-2561.
356. Moghadasian, M.H., *Experimental atherosclerosis: a historical overview.* Life sciences, 2002. **70**(8): p. 855-865.
357. Hamamdzic, D. and R.L. Wilensky, *Porcine models of accelerated coronary atherosclerosis: role of diabetes mellitus and hypercholesterolemia.* Journal of diabetes research, 2013. **2013**.
358. Charan, J. and Kantharia, N.D., 2013. How to calculate sample size in animal studies?. *Journal of pharmacology & pharmacotherapeutics*, *4*(4), p.303.

Appendix

X2 table of P values accessed on 24January 2021 from: https://people.smp.uq.edu.au/YoniNazarathy/stat_models_B_course_spring_07/distributions/chisqtab.pdf

Chi-square Distribution Table

d.f.	.995	.99	.975	.95	.9	.1	.05	.025	.01
1	0.00	0.00	0.00	0.00	0.02	2.71	3.84	5.02	6.63
2	0.01	0.02	0.05	0.10	0.21	4.61	5.99	7.38	9.21
3	0.07	0.11	0.22	0.35	0.58	6.25	7.81	9.35	11.34
4	0.21	0.30	0.48	0.71	1.06	7.78	9.49	11.14	13.28
5	0.41	0.55	0.83	1.15	1.61	9.24	11.07	12.83	15.09
6	0.68	0.87	1.24	1.64	2.20	10.64	12.59	14.45	16.81
7	0.99	1.24	1.69	2.17	2.83	12.02	14.07	16.01	18.48
8	1.34	1.65	2.18	2.73	3.49	13.36	15.51	17.53	20.09
9	1.73	2.09	2.70	3.33	4.17	14.68	16.92	19.02	21.67
10	2.16	2.56	3.25	3.94	4.87	15.99	18.31	20.48	23.21
11	2.60	3.05	3.82	4.57	5.58	17.28	19.68	21.92	24.72
12	3.07	3.57	4.40	5.23	6.30	18.55	21.03	23.34	26.22
13	3.57	4.11	5.01	5.89	7.04	19.81	22.36	24.74	27.69
14	4.07	4.66	5.63	6.57	7.79	21.06	23.68	26.12	29.14
15	4.60	5.23	6.26	7.26	8.55	22.31	25.00	27.49	30.58
16	5.14	5.81	6.91	7.96	9.31	23.54	26.30	28.85	32.00
17	5.70	6.41	7.56	8.67	10.09	24.77	27.59	30.19	33.41
18	6.26	7.01	8.23	9.39	10.86	25.99	28.87	31.53	34.81
19	6.84	7.63	8.91	10.12	11.65	27.20	30.14	32.85	36.19
20	7.43	8.26	9.59	10.85	12.44	28.41	31.41	34.17	37.57
22	8.64	9.54	10.98	12.34	14.04	30.81	33.92	36.78	40.29
24	9.89	10.86	12.40	13.85	15.66	33.20	36.42	39.36	42.98
26	11.16	12.20	13.84	15.38	17.29	35.56	38.89	41.92	45.64
28	12.46	13.56	15.31	16.93	18.94	37.92	41.34	44.46	48.28
30	13.79	14.95	16.79	18.49	20.60	40.26	43.77	46.98	50.89
32	15.13	16.36	18.29	20.07	22.27	42.58	46.19	49.48	53.49
34	16.50	17.79	19.81	21.66	23.95	44.90	48.60	51.97	56.06
38	19.29	20.69	22.88	24.88	27.34	49.51	53.38	56.90	61.16
42	22.14	23.65	26.00	28.14	30.77	54.09	58.12	61.78	66.21
46	25.04	26.66	29.16	31.44	34.22	58.64	62.83	66.62	71.20
50	27.99	29.71	32.36	34.76	37.69	63.17	67.50	71.42	76.15
55	31.73	33.57	36.40	38.96	42.06	68.80	73.31	77.38	82.29
60	35.53	37.48	40.48	43.19	46.46	74.40	79.08	83.30	88.38
65	39.38	41.44	44.60	47.45	50.88	79.97	84.82	89.18	94.42
70	43.28	45.44	48.76	51.74	55.33	85.53	90.53	95.02	100.43
75	47.21	49.48	52.94	56.05	59.79	91.06	96.22	100.84	106.39
80	51.17	53.54	57.15	60.39	64.28	96.58	101.88	106.63	112.33
85	55.17	57.63	61.39	64.75	68.78	102.08	107.52	112.39	118.24
90	59.20	61.75	65.65	69.13	73.29	107.57	113.15	118.14	124.12
95	63.25	65.90	69.92	73.52	77.82	113.04	118.75	123.86	129.97
100	67.33	70.06	74.22	77.93	82.36	118.50	124.34	129.56	135.81